A techno-economic, sustainability and experimental assessment of the direct methanation of biodiesel waste glycerol

Robert White

Submitted in accordance with the requirements for the degree of Doctor of Philosophy as part of the integrated PhD with MSc in Bioenergy

Doctoral Training Centre in Bioenergy, Energy Research Institute, School of Chemical and Process Engineering,

The University of Leeds

October 2018

The candidate confirms that the work submitted is his/her own and that appropriate credit has been given where reference has been made to the work of others.

Acknowledgements

Whilst this PhD has been submitted in my name, it takes a great deal more than one individual to complete a body of work such as this.

Firstly I would like to thank my supervisors, Dr Valerie Dupont and Prof. Timothy Cockerill for their support, guidance and patience throughout the last four years.

I would also like to thank the following from my research group: Oliver Grasham for listening to my ideas and always having the time to have a discussion, Robert Bloom for our chats in the laboratory and Sergio for his help calibrating the micro GC.

My colleagues from the first year and second year of the bioenergy CDT are deserving of my thanks and gratitude and include, in no particular order: Diarmaid Clergy, Andrew Dyer, Gillian Finnerty, Luke Conibear, Hana Mandova, Lee Roberts, Charlotte Stead and Kiran Palmer as well as Jeni Spragg, Charlotte Weaver, Nicola Wood, Daisy Thomas, Iram Razaq, and Ric Birley.

Several members of staff made this work possible and I would like to thank the energy building engineering technicians; Kevin Dyer, Scott Prichard, Gurdev Bogall as well as the lab 1.10 technicians Adrian Cunliffe and Karine Alves Thorne

I would also like to thank the Engineering and Physical Science research council (ESPRC) for my studentship and Freddy from the University of Yucatan, Mexico, for his guidance with life cycle analysis and collaboration.

Someone who should not go unmentioned is my long suffering partner, Emma Johnson. My gratitude for her patience, kindness and love knows no bounds and has been pivotal in the completion of this work, and retention of my sanity.

Finally I would like to thank my family, my mother Ricamor, my father Duncan, and my brother Edward who have made me what I am today.

Abstract

Crude glycerol from biodiesel production is a potential feedstock for energy in many parts of the world. A concept that is yet to be explored is the conversion of glycerol to a methane rich gas known, in this case, as bio-SNG, by taking advantage of steam reforming and methanation reactions in a single reactor. This process is known as direct methanation.

Direct methanation is a type of low temperature steam reforming and is performed at temperatures lower than those commonly used for hydrogen production from organic feedstock. When applied to glycerol, it is termed 'GLT-SR' in this thesis. GLT-SR allows glycerol to be transformed into a gaseous energy vector that can be converted to energy on-site at the biodiesel refinery to offset fossil natural gas usage, for instance, in the energy intensive bean or seed crushing stage.

The present work identifies the feasibility of a GLT-SR process using a design process framework and included process modelling in Aspen Plus, technoeconomic and environmental energy life cycle impacts analysis and laboratory scale experiments using pure glycerol to avoid any unknown impacts of contaminants contained in crude glycerol.

Based on the thermodynamic analysis and process model, the optimum conditions favouring methane production and energy efficiency were 8 atm, with a feed molar steam to carbon ratio of 2.56 and an inlet temperature of 474 K. When compared to natural gas, bio-SNG from soybean based glycerol had the potential to decrease global warming potential with a trade-off of increased eutrophication, terrestrial ecotoxicity and freshwater aquatic ecotoxicity potential. The economic analysis based on biodiesel plants located in the USA, determined that a gas price of USD$6-7 per million BTU was necessary to achieve acceptable rates of return and coincided with the states of Missouri and Arkansas.

A gasification rig was constructed and laboratory experiments confirmed that reducing the temperature were essential to maximising methane production. At steady state roughly 90% of the glycerol was converted to carbon gases with the most effective conditions achieving 66% of the CH_4 conversion at equilibrium at 673 K (400 °C), steam to carbon ratio 2.5, pressure 1 atm and weight hourly space velocity of 0.54 hr^{-1}. Thus current process conditions showed the process was operating away from the desired equilibrium for maximum CH_4. Based on economics and environmental analysis, the process is feasible but would rely on an optimised process to maximise CH_4 production and further trials to determine the impact of glycerol contaminants.

Table of Contents

List of Tables

List of Figures

Abbreviations

100 wt % glycerol	G100
20% biodiesel blend	B20
80 wt % glycerol	G80
Abiotic Depletion Potential	ADP
Abiotic Depletion Potential (fossil fuels)	ADP-FF
Acidification Potential	AP
Anaerobic Digestion	A.D
Autothermal Reforming	ATR
Base equipment cost	BEC
Biological synthetic natural gas	Bio-SNG
Capital expenditure	CAPEX
Carbon Dioxide	CO2
Carbon Monoxide	CO
Chemical Engineering Cost Index	CEPCI
CO2H-	Formate
Engineering procurement and construction cost	EPCC
EROI	Energy return on investment
Eutrophication Potential	EP
Fatty acid methyl ester or biodiesel	FAME
FER	Fossil energy ratio
First of a kind	FOAK
Flue gas recirculation	FGR
Fossil Energy Ratio	FER
Freshwater Aquatic Ecotoxicity Potential	FWAEP
Gas Chromatograph	GC
Global Warming Potential	GWP
Glycerol	$C_3H_8O_3$
Glycerol low temperature steam reforming	GLT-SR
Greenhouse Gases, Regulated Emissions, and Energy use in Transportation Model	GREET
Henry hub	HH
High heating value	HHV
Human Toxicity Potential	HTP

Hydrogen	H_2
Hydrogen sulphide	H_2S
Hydrogenated vegetable oil or renewable diesel	HVO
Hydroxyl	OH
Independent power producer	IPP
Indirect land use change	ILUC
Internal rate of return	IRR
Internal rate of return	IRR
International monetary fund	IMF
International organization for standardisation	ISO
Investor owned utility	IOU
Iron	Fe
kWh	Kilowatt hour
Levelised cost of heat	LCOH
Life cycle analysis	LCA
Low heating value	LHV
Marine Aquatic Ecotoxicity Potential	MAEP
Mass Flow Controller	MFC
Methane	CH_4
Million British thermal units	mmbtu
Million litres	ML
MJ/kg	Mega joules per kilogram
Monte Carlo simulation	MCS
National energy technology laboratory	NETL
Net present value	NPV
Ni	Nickel
nth of a kind	NOAK
Operating expenditure	OPEX
Ozone layer Depletion Potential	ODP
Photochemical Oxidation Potential	POP
Platinum	Pt
Pressure of 1 atm	P1
Pressure of 10 atm	P10
Pressure of 12 atm	P12
Pressure of 30 atm	P30

Pressure of 4 atm	P4
Pressure of 8 atm	P8
Process flow diagram	PFD
Revenue	Rev
Ruthenium	Ru
Silica	Si
Steam to carbon ratio	SC
TASC	Total as spent capital
Terrestrial Ecotoxicity Potential	TEP
Total Organic Carbon	ToC
Total overnight costs	TOC
Total plant cost	TPC
Twigg Scientific and Technical Ltd	TST
U.S energy information administration	eia
United States	US
United states life cycle inventory	USLCI

Nomenclature

a	Cost of the first of a kind unit/plant
A	Sizing factor for equipment in base equipment cost
b	Learning rate exponent
C_p^o	Purchased cost for base equipment conditions
C_{ACC}	Annual capital cost
C_{AOC}	Annual operating cost
C_{BM}	Bare module equipment cost
CCF	Cumulative cash flow
C_f	Cash flow in a particular year
C_g	Total carbon moles in inlet feed glycerol
C_{gas}	Molar flow of carbon contained in outlet gases
$C_{glycerol}$	Molar flow of carbon in the inlet feed of glycerol
C_{GP}	Total carbon moles in gas products
C_{iquid}	Molar flow of carbon contained in liquid condensate
C_{solid}	Molar flow of carbon solid formed on the catalyst bed
$E_{bio\text{-}SNG}$	Energy contained in bio-SNG
$Eq_{\%}$	Equilibrium efficiency
F_{BM}	Pressure and materials adjusted value for equipment
Gm_x	Normalised molar flow per hour of a particular gas component
G_{nx}	Normalised mole fraction of a gas component
G_T	Total value of the summed mole fractions of gases in the product gas before normalisation
G_x	Mole fraction of a gas component prior to normalisation
K	Kelvin
K_1	Constants associated with equipment cost curves at ambient pressure and for carbon steel
K_2	Constants associated with equipment cost curves at ambient pressure and for carbon steel
K_3	Constants associated with equipment cost curves at ambient pressure and for carbon steel
$LHV_{bio\text{-}SNG}$	Low heating value of bio-SNG
L_r	Learning rate
M	Moles
MJ/L	Mega joules per litre
M_r	Relative atomic mass
m_x	Molar flow per hour of a particular gas component, x
N	Number of samples in the set
n	Year of plant investment
P	Pressure

P_c	Production cost
q	Mixture component e.g. glycerol or water
r	Discount rate
R	Gas constant
R	Learning curve exponential factor
RP	Reference parameter
S_c	Scaled cost
SE	Standard error
SP	Scaling parameter
T	Temperature
T_{PL}	Plant life
V	Volume
x	Cumulative number of units
X_{CG}	Conversion to carbon gases
X_x	Conversion to a particular gas component
y	Cost to produce the x^{th} unit
ΔH	Enthalpy
η_{btf}	Biomass to fuel efficiency
P	Density
σ	Standard deviation

Achievements

i. Journal Papers

White, R.; Segundo Navarro-Pineda, F.; Cockerill, T.; Dupont, V.; César Sacramento Rivero, J. Techno-Economic and Life Cycle Impacts Analysis of Direct Methanation of Glycerol to Bio-Synthetic Natural Gas at a Biodiesel Refinery. *Energies* 2019, *12*, 678.

White, R., Dupont, V., Cockerill, T., 2018. Thermodynamic modelling and energy balance of direct methanation of glycerol for Bio-SNG production. Energy Convers. Manag. 160, 354–363. doi:10.1016/j.enconman.2018.01.031

ii. Magazine Articles

White R, Abdul Halim Yun H, Dupont V, Cockerill T. *Direct Catalytic Methanation of Liquid Biomass Wastes.* Gas for Energy Magazine, Selected Reports, 19/10/2017.

iii. Conference Proceedings

White R, Dupont V, Cockerill T. *Thermodynamic and Energy Analysis of Glycerol Low Temperature Steam Reforming for Bio-SNG*, Conference Proceedings, 26th European Biomass Conference and Exhibition, doi: 10.5071/26thEUBCE2018-2BO.6.4.

iv. Conference Oral Presentations

White R, Dupont, V., Cockerill T., *Direct Methanation of Glycerol*, EUBCE, 26th European Biomass Conference and Exhibition, 14 May 2018.

Dupont, V., Yun, H. A. H., **White, R.** & Tande, L. N. High methane conversion efficiency by low temperature steam reforming of bio-feedstock. REGATEC 2017, 4th International Conference on renewable Energy gas Technology, 22-23 May 2017 2017 Pacengo (Verona), Italy. 25-28.

v. Conference Poster Presentations

White R, Dupont V., *Low Temperature Glycerol Steam Reforming for Methane (LT-GSRM),* SUPERGEN, 11-13 December, 2017, Manchester, UK.

White R, Dupont V, Cockerill. T, *Plant Model of Methane Production from Low Temperature Glycerol Steam Reforming*, REGATEC, 22-23 May 2017, Verona, Italy

White R, Dupont, V., *Can Biodiesel Waste Produce a Natural Gas Substitute?*, RSC Early Career Researcher Chemists in Energy Symposium, Royal Society of Chemistry, London, 16 Feb 2016

vi. Prizes

ICHEME water special interest group, first prize, 30th anniversary young process engineer video competition, "*NH_3 recovery and H_2 production at WWTP's".*

Early Career Researcher Chemists in Energy Symposium, third place, poster presentation, *Can Biodiesel Waste Produce a Natural Gas Substitute?*

1 Introduction

1.1 Research Motivation

Significant technology shifts are required if the world is to meet the CO_2 reduction targets associated with less than a 2°C temperature change. In the UK alone, 80% of UK's emissions were associated with energy production from combustion, primarily with fossil fuels as a feedstock. As a consequence of fossil fuel dependency, achieving decarbonisation targets set by the Paris agreement by 2050 will be difficult without changes to current technologies. Crucially, decarbonising heating and cooling, electricity generation and transportation fuels are essential for countries to meet their climate change targets [1].

The reduction of global greenhouse gas (GHG) emissions is a key component of the United Nations framework convention on climate change. Data on the global distribution of CO_2 emissions from combustion of fuels by sector can be seen in Figure 1 where electricity and heat generation make up 42% of overall combustion CO_2 emissions.

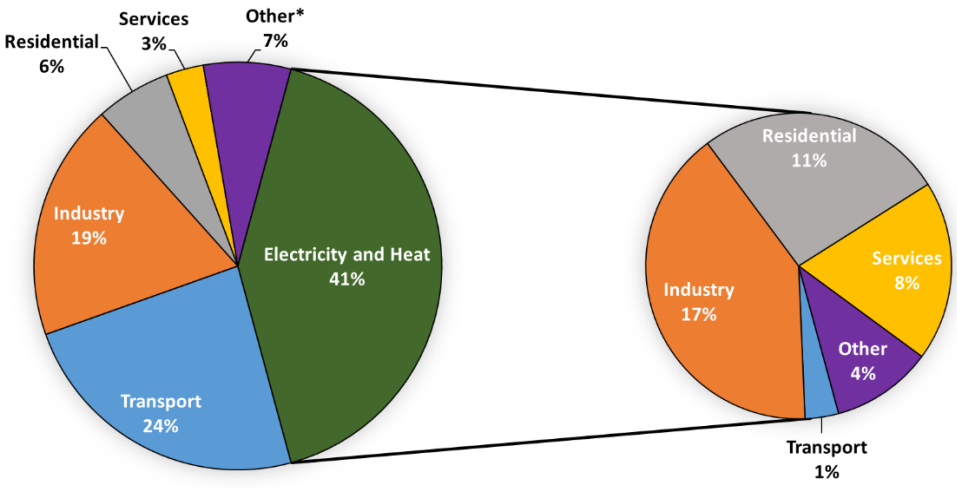

Figure 1. Global CO_2 emissions by sector published by the international energy agency in 2017 based on 2014-2015 data [2]. **Other includes agriculture/forestry, fishing, energy industries other than electricity and heat generation.*

As of today (October 2018), following the Kyoto protocol and the Paris agreement, 181 of the 197 nations have ratified the framework[3]. The central aim of these agreements is for nations to respond to the threat of climate change by preventing the temperature from increasing by 2 degrees Celsius above pre-industrial levels and to pursue efforts to limit the temperature increase even further to 1.5 degrees Celsius. CO_2 emission reduction (decarbonising) is one of the main focus areas due to the large contribution of CO_2 from combustion processes.

Decarbonisation of all sectors represents a significant challenge. To tackle this problem effectively solutions that create simultaneous decarbonisation whilst improving sustainability are desirable and can be discovered by analysing if co-products produced from one sectors decarbonisation method can be utilised in another sector. In this work the focus is on promoting synergy between heat production and transport sectors where a potential waste product from the transport decarbonisation process of biodiesel production could be used to decarbonise heat.

1.1.1 Decarbonising Transport

The transport sector contributes to 25% of global CO_2 emissions. Transport decarbonisation strategies revolve around utilising low carbon energy and improving vehicle efficiency. Examples of low carbon energy that are suitable for transport include: biodiesel, bioethanol, renewable diesel, renewable electricity, and biomethane. These fuels, except for renewable electricity, rely heavily on biomass as a feedstock. In particular, biodiesel is one of the most widely produced low carbon transport fuels.

Replacing fossil diesel with biodiesel

Biodiesel is a renewable transport fuel (biofuel) similar to fossil diesel. Fossil diesel is essential for diesel combustion engines which are the prime mover for freight and domestic transport. Biodiesel can be blended with, and in some cases, serve as a complete substitute for fossil diesel, providing a renewable fuel that has reduced CO_2 emissions. A comparison of different diesels and their characteristics is shown in Table 1.

	Petrodiesel	Biodiesel from oilseed rape	Renewable Diesel (HVO)
Energy MJ L^{-1}	~38.3	~35.0 [4]	34.4
Cetane Number	51+	48-62 [5]	80-100 [6]

Table 1. Comparison of Fossil Diesel, Biodiesel from oilseed rape and Renewable Diesel

The term ‘‘biodiesel’’ defines a ‘‘fuel comprised of mono-alkyl esters of long-chain fatty acids derived from vegetable oils or animal fats, designated ‘‘B100’’ as formulated in the biodiesel standard ASTM D6751, with the European biodiesel standard EN 14214[7] referring to fatty acid methyl esters (FAME) as fuel [6].

First generation biodiesel is produced from edible plant and animal fats whereas second generation biodiesel is produced from wastes such as used cooking oil. Traditional biodiesel is composed of fatty acid methyl esters which are produced during the transesterification reaction as shown in Figure 3. The feedstock for biodiesel depends on what is readily available. North and South America predominantly produce soy bean whereas Europe

produce canola and sunflower oil. Conditions in Asia and the tropics favour the production of palm oil.

Biodiesel accounted for 22% of global annual biofuel production in 2015 and is equivalent to 30.1 billion litres of biodiesel. 94% of this biodiesel was produced by forty countries with the remaining 6% in countries that produced less than 0.1 billion litres of biodiesel per year. Figure 2 describes the distribution of biodiesel production across the world of the top 40 countries. 38% of the 30.1 billion litres was produced within the EU-28 and 37% was produced in North and South America. The top countries in Eurasia consisted of Indonesia, Singapore, Malaysia, and China with 6%, 3.3%, 2.3%, and 1,3% of global production respectively [8]. Roughly 6-8% of the global biodiesel was second generation, produced from waste oils such as waste cooking oil [9].

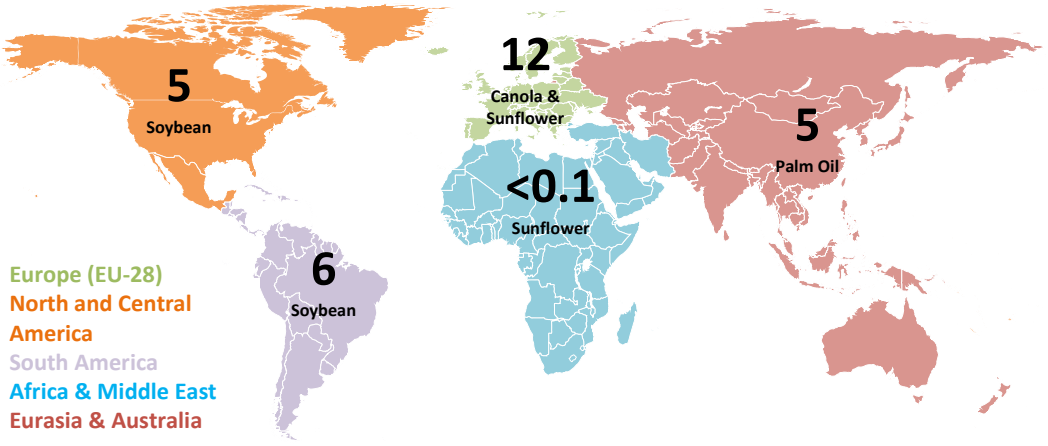

Figure 2. Annual biodiesel production of the major countries (94% of total) by continent with major feedstock [10] *in billion litres from 2015 data* [8].

An extensive documentation of the history of biodiesel has been produced in a work compiled by William Shurtleff and Akiko Aoyagi. Patrick Duffy is recorded as the first person to perform transesterification to produce biodiesel[11]. In 1853 Patrick Duffy succeeded in producing a biodiesel from vegetable oil, four years before a diesel engine was produced. The first use of a "biodiesel" in a diesel engine was recorded as 10 August 1893 whereby peanut oil was combusted [10]. Subsequently, 10 August is internationally known as Biodiesel day. On 31 August 1937, the first account of a patent for a "Procedure for the transformation of vegetable oils for their uses as fuels" was granted to G.Chavanne [12].

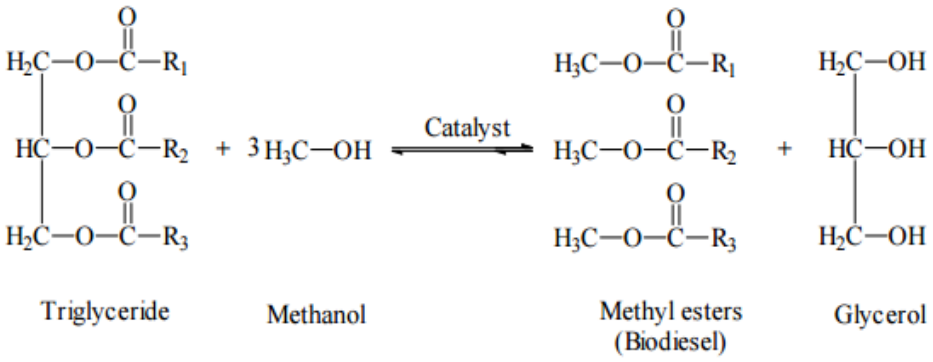

Figure 3. Transesterification reaction to produce biodiesel and glycerol from a triglyceride where R_1-R_3 are long chain hydrocarbons. Typical catalysts include bases such as sodium hydroxide and salts such as sodium chloride.

The transesterification process is a sequence of reversible reactions which break the triglyceride into diglycerides, monoglycerides and glycerol. Each step removes a methyl ester until the triglyceride has been completely broken down into methyl esters and glycerol as shown in figure 4. In this fashion, for every unit of biodiesel produced, 10 wt% of glycerol is also produced.

Within the process of biodiesel production steam is required to generate heat. For soybean biodiesel production in particular, steam is used to liberate the soybean oil from the soybean meal in the crushing process as shown in Figure 4. Currently the steam is generated by combusting natural gas in a furnace and boiler on-site, increasing the fossil energy consumed in the production of biodiesel, reducing its sustainability.

Soybean biodiesel production begins at the agricultural stage whereby soybeans are produced. Once the soybeans are cultivated, they are transported to the biodiesel refinery where the soybean meal and oil are separated using steam in a crushing step. Soybean meal is sold as a by-product, mainly as feed for animals, whilst the soybean oil moves into the biodiesel conversion step, as described in Figure 3. Crude glycerol is produced as a by-product whilst biodiesel is transported to the point of use.

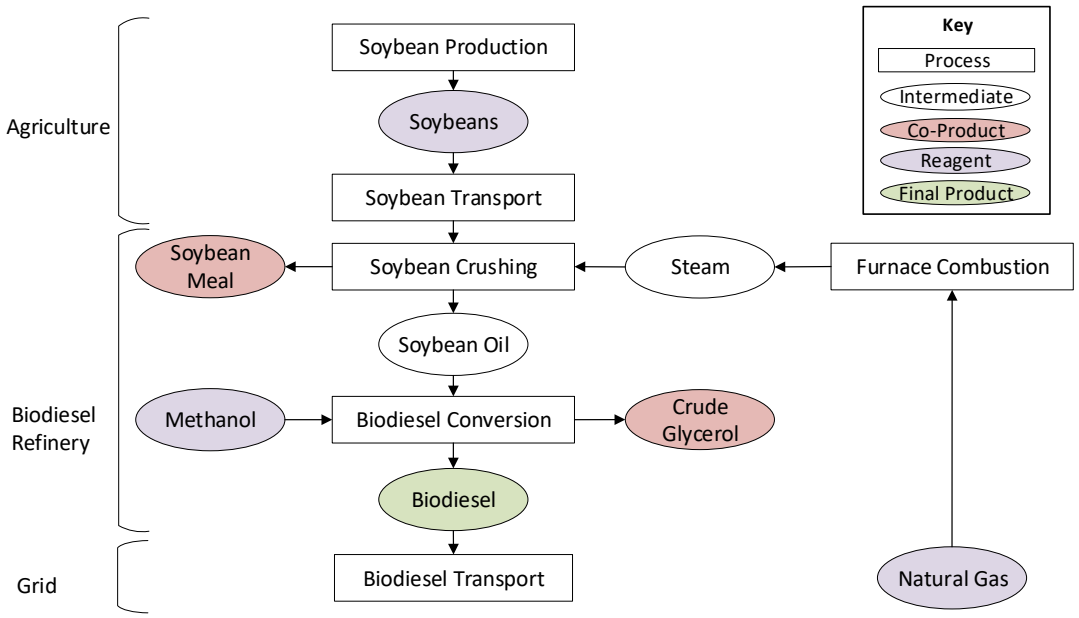

Figure 4. Block flow diagram of the soybean biodiesel production process.

1.1.2 Decarbonising heat

The electricity and heat production sector makes up over a quarter of global CO_2 emissions from combustion. Many countries rely on natural gas to meet their heating, cooling and energy generation demands. Natural gas accounts for roughly twenty two percent of global energy use [13,14] as shown in Figure 5 with nearly a quarter of the world's electricity generated from natural gas and some countries relying on natural gas for up to half of their domestic heating needs[13]. A significant portion of industry, including biodiesel refineries, utilise natural gas for on-site steam production.

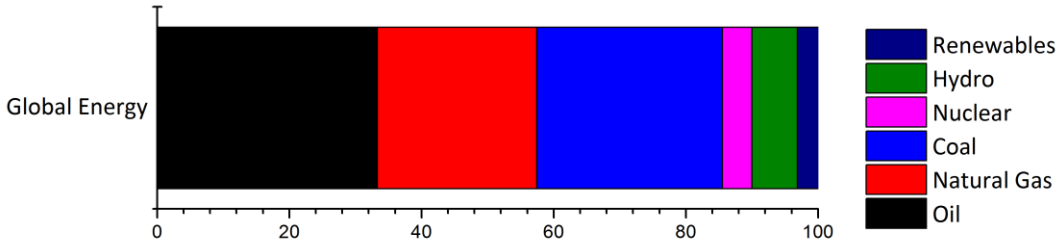

Figure 5. Global energy use by fuel as reported by the BP energy outlook 2017[14].

The high calorific value of natural gas combined with the flexibility of its principle component, methane (CH_4); make natural gas an ideal fuel and feedstock for chemical processes. Natural gas can be used in gas fired boilers for domestic and industrial heating and steam production, as a transport fuel in vehicles that have been appropriately converted

and as a feedstock in steam methane reforming to produce valuable hydrogen (H_2), whilst simultaneously producing lower emissions relative to other fossil fuels such as coal and oil.

Large CO_2 emitters such as China and the USA are interested in moving away from coal and oil fired heat and power generation. As countries become more concerned with CO_2 emissions and pollution, the demand for cleaner energy generating technologies has increased, furthering the demand for natural gas as a transition fuel and eliciting research to convert fossil fuels and biomass into renewable gases [14]. One example is the surge in Shale gas in the USA and China, as well as China's interest in converting coal to synthetic natural gas[15].

Whilst natural gas is a step in the right direction, it cannot be classed as a low carbon renewable fuel, as CO_2 is emitted to the atmosphere at the point of combustion and it is a fossil fuel. At some point in the future, natural gas consumption will need to be reduced causing expensive infrastructure, such as national gas grids and industrial and domestic boilers, to fall into disuse before the end of its lifetime unless an alternative gas can be produced.

1.1.2.1 Renewable and synthetic natural gas

Replacing natural gas with renewable gases is a realistic alternative to natural gas. Producing a renewable gas of similar quality will; facilitate a reduction in carbon emissions whilst requiring minimal change to the current infrastructure, contribute to global CO_2 reduction challenges outlined in the Paris Agreement, utilise and therefore reduce waste, contribute to a circular economy, increase energy security and reduce fossil fuel dependency. Renewable gases can achieve these feats because the feedstock is biomass or a waste.

Examples of renewable gases are biological synthetic natural gas (bio-SNG), biomethane, H_2, biogas and landfill gas. The type of renewable gas is associated with the feedstock as well as the process used to produce it.

Biogas is a product of Anaerobic Digestion (A.D). A.D relies on biological processes from bacteria that produce CH_4 from organic material, known as methanogens, and feedstocks such as; food and drink waste, processing residues, agricultural residues, crops and sewage sludge, provided that the conditions, feedstock ratios and microbes are well adapted. The composition of the gas is usually a 1:1 ratio of CH_4 and CO_2. Biomethane has a methane content greater than 97% and is produced by gas upgrading techniques that purify biogas and remove CO_2. Landfill Gas is the term used to describe the gases that have been captured from decomposing biodegradable waste in landfill sites and is usually the lowest quality gas because of low methane and the high hydrogen sulphide (H_2S) compositions. On the other hand Bio-SNG is produced by the thermochemical method of gasification using biological feedstocks and can be upgraded to similar CH_4 concentrations as biomethane.

In most cases the feedstock for renewable gas is a form of primary biomass. Primary biomass can be defined as contemporary plant matter formed by photosynthetic capture of solar energy which is subsequently processed by the plant into chemical energy and stored that has not been biologically processed. Secondary biomass can be defined as feedstocks that have been processed after photosynthesis such as manure, sewage sludge or bio-refinery effluents. Finally, waste feedstocks such as municipal solid waste and landfill are defined as unwanted or unusable material. Only the sustainable management of such feedstocks with suitable policies will lead to a realisation of the potential for decarbonisation, energy security and circular economy. Cadent predicts that by 2050 over a third of the gas in the natural gas grid in the UK will come from Bio-SNG and 15% from biomethane pending policy and infrastructure investment[16]. The characteristics of different renewable gases, as compared to natural gas from Norway, are described in *Table 10*.

	Units	Norway NG	Landfill Gas	Bio-methane	Biogas from A.D
Methane	Vol-%	87.81	45	>97%	65
Hydrogen	Vol-%	-	0-3	-	0
Hydrocarbons C2+	Vol-%	9.23	0	-	0
Hydrogen Sulphide	ppm	-	0-100	-	0-4000
Carbon Dioxide	Vol-%	2	15-40	-	30-40
Nitrogen	Vol-%	0.96	5-40	-	0.2
Oxygen	Vol-%	-	1	-	
Carbon Monoxide	Vol-%		-	-	-
Ammonia	ppm	-	5	-	100
Water	Vol-%	-	-	-	-
Chlorine (Cl^-)	Mg/Nm^3	-	20-200	-	0-5
HHV_G	MJ/kg	51.0	-	-	-
	MJ/Nm^3	39.8	-	-	-
LHV_G	MJ/kg	46.1	12.3	-	20
	MJ/Nm^3	35.9	16	-	23
Wobbe Index (I_W)	MJ/kg	64.6	-	-	-
	MJ/Nm^3	50.1	18	-	27
Specific Gravity (G_S)	-	0.631	-	-	-
Standard Density	kg/m^3	0.78	-	-	-
Reference		[17]			

Table 2. Comparison of Bio-SNG with Norwegian natural gas, 100% CH_4 and bio-gases. Norway NG contained 87.8% methane, 7.63% ethane, 1.32% propane, 0.24% butane, 0.02% pentane and 0.02% higher than C6 hydrocarbons by mole fraction [18].

In order to substitute natural gas the properties of the substitute must be similar. Biogas, some forms of Bio-SNG and landfill gas are low quality gases that will need to be upgraded by removing components that have no calorific value before they can directly replace natural gas in the grid. However, combustion of low quality gases, such as biogas and landfill gas, at the site of production is possible without upgrading if the gas is created close to or at the point of use, omitting the need for transportation. Utilisation of low quality gases in this way is commonly carried out by farmers who produce biogas from anaerobic digestion, usually though combustion in a combined heat and power engine or boiler, aiding in the decarbonisation of the natural gas grid by reducing natural gas dependency.

1.1.2.2 Synthetic natural gas from fossil fuels

Producing SNG from fossil fuels was popularised in the USA, UK and Germany between the nineteen fifties and nineteen eighties because of a shortage of fossil natural gas and low prices of oil and coal. SNG technologies evolved from initial gasification methods of; coal gas (town gas) from the process of carbonisation of coal in 1618, water gas in 1780 combining combustion and steam reforming, producer gas by partial oxidation of coke in 1839, Mond gas by a combination of partial oxidation and steam reforming of coal in 1889, methanation discovered by Sabatier in 1897 [19] [20], complete gasification with the invention of Lurgi gasifiers in 1927, all of which are covered in extensive detail in CL:AIRE[21].

As natural gas was adopted in the UK and USA after the First World War and the invention of the electric lightbulb reduced the need for gas for lighting, the majority of these gas types became obsolete. Crucially the gasification techniques remained important and are still in use in modern day plants in the form of steam methane reforming to provide the majority of global H_2 and in biomass gasification and coal to SNG processes. Current research trends have moved onto biomass feedstocks due to environmental and sustainability concerns with fossil fuel feedstocks.

The first SNG process was created in the 1970's and converted coal to SNG in a Lurgi gasifier [22] and is shown in Figure 6. This was superseded by the improved Naphtha to SNG process shown in Figure 7 although the only commercialised SNG process was the Great Plains plant in the USA which used coal as a feedstock [23] and is still in operation today (2018). China has renewed their interest in coal to SNG and is determining whether it could be a suitable replacement to coal combustion to reduce pollution and improve efficiency.

In a coal to SNG process the feedstock is gasified with steam (steam gasification) and O_2 at 2.8 MPa (28 bar) and ~1200 ˚C to produce ash and tarry by-products and the raw syngas product. The syngas contains CO, CO_2 and H_2, the concentrations of which are shifted appropriately using the water gas shift reaction (sour shift) and is subsequently purified using a Rectisol scrubber to remove acid gases, sulphides and CO_2. Tar, oils, phenols, NH_3 and H_2O are removed via condensation and stored for steam generation and other impurities. The CO in the gas is methanated by two stage methanation over Ni catalyst at 360˚C with H_2 [23,24]. The product gas from the second methanation reactor is recycled to moderate the temperature of the product gas in the first methanation reactor. A maximum temperature of 450˚C in the product gas is observed from the second reactor and is within the operating range for CRG catalysts [25]. The Naphtha to SNG process is similar, with the improved Naphtha hydrogasification process adding additional de-sulphured feedstock to

the producer gas prior to methanation creating a hydrogen rich environment and reducing the number of methanation stages required as shown in Figure 8.

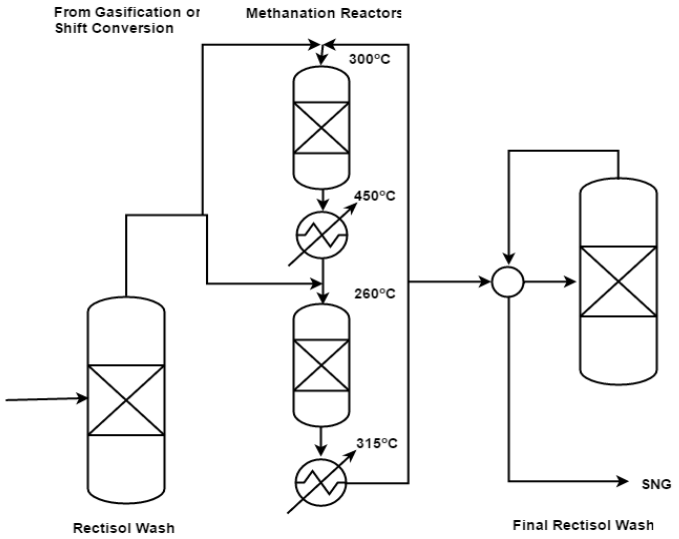

Figure 6. Simplified Lurgi coal-to-SNG process after the coal has been gasified and cleaned.

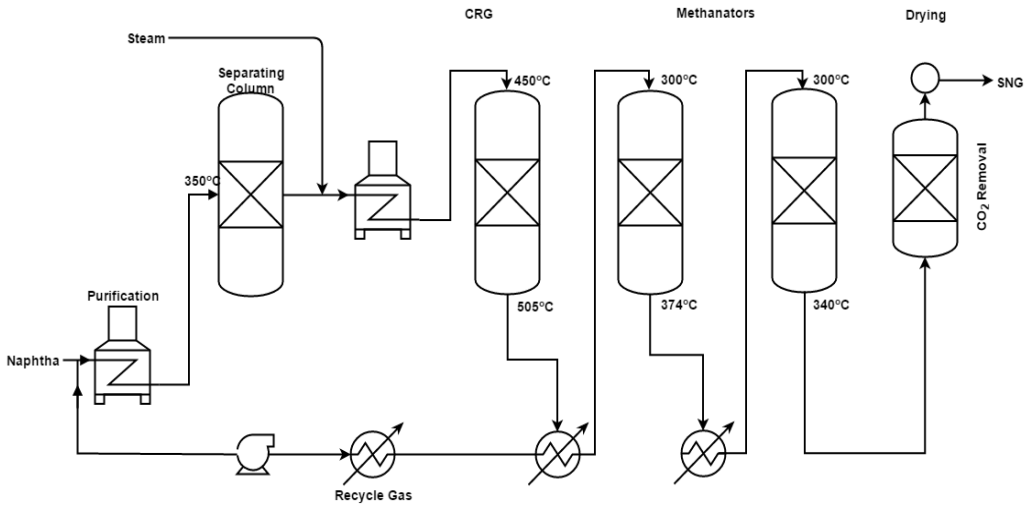

Figure 7. Simplified process diagram for the CRG process with double methanation adapted from the catalyst handbook [25].

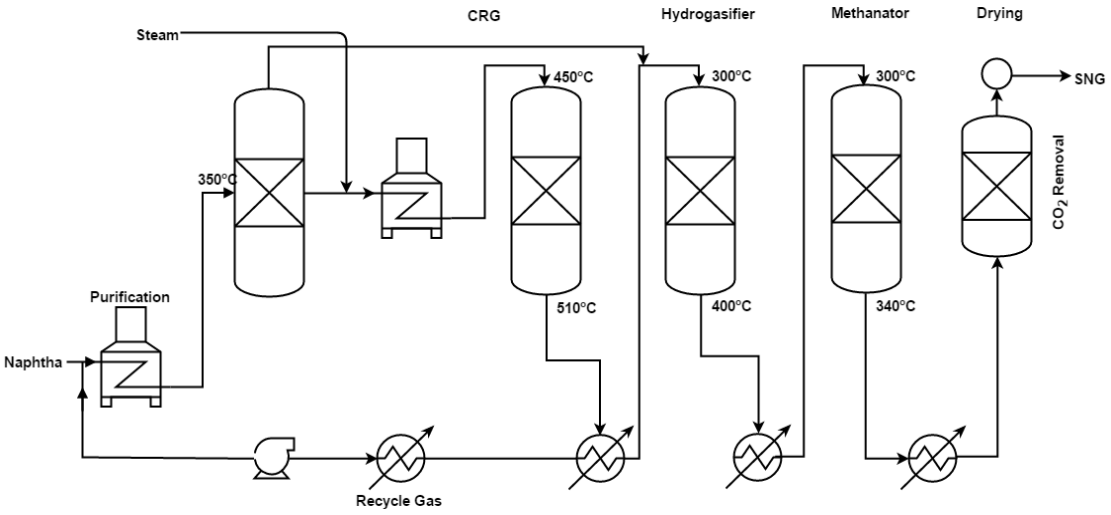

Figure 8. Simplified process diagram for hydrogasification [26,27].

1.1.2.3 Biomass gasification for synthetic natural gas

Research into gasification of Bio-SNG has become more widespread in the last decade. A simple block flow diagram of the steps in biomass gasification is shown in

Figure 9 and differs to the coal and naphtha to SNG processes due to the additional requirements of drying the biomass and adapting to different biomass compositions.

Figure 9. Block flow diagram outlining the primary stages in biomass gasification.

The first step in biomass gasification is pyrolysis and is similar to the coal and naphtha to SNG processes. Process conditions include temperatures in the range of 800-1800 °C combined with a low oxygen (O_2) environment, and the option of adding steam (steam gasification), to prevent combustion. Volatiles are removed producing syngas similar to fossil fuel feedstocks, and leaving behind a carbon rich char. The char can be used as a fuel for the process, accessed via combustion in a separate boiler or can be converted to more gas products during complete gasification. When using biomass as opposed to coal a drying step is added prior to pyrolysis to remove moisture and improve the efficiency of the pyrolysis step.

Depending on the feedstock, the level of syngas cleaning will vary but it is necessary to remove any hydrogen sulphide, tar, thiophenes and other contaminants to maximise the calorific value of the syngas and prevent any reduction in efficiency for the methanation and gas upgrading steps. Syngas contains high concentrations of CO and H_2 which is converted

by the process of methanation into CH_4 using a catalyst. The gas upgrading step includes H_2O and CO_2 removal in separate steps in order to create synthetic natural gas (SNG). Other steps that modify the gasification process that modify the syngas composition or improve conversion to syngas when using different solid or liquid feedstocks include; steam reforming, partial oxidation and complete gasification.

Inherent in any gasification process for high quality SNG is the removal of CO_2. Stripping the gas and capturing the CO_2 is necessary for processing of the syngas into high quality Bio-SNG, similarly to processing of biogas into biomethane. In most cases the CO_2 is vented to the atmosphere as the infrastructure for storage is not available. Consequently gasification provides a platform for carbon capture storage (CCS) systems to combine with bioenergy to generate a renewable gas that produces negative CO_2 emissions, otherwise known as bioenergy carbon capture storage (BECCS). With BECCS the carbon footprint of electricity and gas grids would be reduced, a new sink for atmospheric CO_2 is created, and a new era of net negative CO_2 emission energy generation would begin but this has yet to be implemented in commercial biomass gasification plants.

1.1.2.4 State of biomass to synthetic natural gas technologies

Several institutions have been working with gasification of biomass although not necessarily for the production of SNG. They have paved the way for the world's first commercial biomass to SNG plant known as the GoBiGas plant. Compositions of the product gas prior to methanation from each institutions biomass gasification process are shown in Table 3.

The GoBiGas plant in Sweden was the first commercial solid wood to SNG plant and was completed in 2014. The gasification technology was based on the concept developed at Technical University of Vienna by Prof. Hermann Hofbauer and was proven at the Gussing plant in Austria [28] and is similar to the work carried out at Paul-Scherrer Institute (PSI). At Gussing the product gas was diverted to a methanation reactor developed by PSI, but the technology used in the GoBiGas plant was the TREMP methanation process developed by Haldor Topsoe. A detailed description of the GoBiGas process is reported in the technology review by Kopyscinski [29].

	Coal		Biomass			
	Lurgi (Sasol)	HICOM	ECN	ZSW	PSI	GoBiGas
CO/%	13.0	31.1	<0.1	8.5	15.4	22.5
CO_2/%	15.5	24.7	52.0	12.0	32.4	24
H_2/%	60.1	42.9	2.0	67.5	39.0	39
CH_4/%	10.3	0.1	39.0	12.0	11.9	8.5
Temperature /˚C	270	-	830	700-800	-	850

Table 3. A list of the compositions of syngas gas from each process at the reactor exit (dry) prior to methanation.

The original inspiration for biomass gasifier designs was the Lurgi gasifier and used steam reforming and water gas shift reactions to produce a syngas appropriate for CH_4.

Although it was not used in the final GoBiGas plant, PSI has proven the use of the fast internally circulating fluidised bed (FICFB) gasifier. After a single run through of the PSI methanation step, the CH_4 content increased to ~40% from ~12% with very low concentrations of CO [28,29]. A significant innovation is the gasifier contains two fluidized beds where endothermic gasification with steam takes place in a bubbling bed whilst exothermic combustion occurs in a fast fluidized bed using leftover char. The heated bed material is circulated between the two fluidized beds transporting heat from the exothermal to the endothermal process.

On the other hand ECN have developed an indirect gasifier, tar removal system and methanation process [30]. A detailed report of over 500 hours operation has been released and shows that the ESME methanation system can consistently produce high methane content SNG prior to CO_2 removal with little to no change in catalyst activity over the time period.

What is consistent amongst all SNG processes is that the efficiency of an SNG process is affected by the methane content of the product gas from the gasification or reforming step. If the producer gas has higher methane content prior to methanation, the process efficiency is increased as less CO and CO_2 has to be converted to CH_4. Furthermore, as methanation is exothermic, larger methane content before methanation reduces the overall heat generated. This lowers the amount of heat that needs to be removed allowing more control over the process temperature and a reduction in heat duty required for cooling[31].

The efficiency of the process is also affected by the higher O_2 content and heavy metal content of biomass compared to fossil fuels, removal of different impurities in the product gas, and controlling tar production [29,32].

When gasified, biomass produces gases, tar and char (Equation 1). In most plants the processes of drying, pyrolysis, steam gasification or steam reforming and partial oxidation overlap. Char is easily separated and can be further refined or combusted for heat and power. Tar is a larger problem and can cause mechanical and operation issues if it is not monitored and controlled.

$$Biomass \rightarrow H_{2_{(g)}} + CO_{(g)} + CO_{2_{(g)}} + HC_{(g)} + tar_{(l)} + Char_{(s)} \qquad Equation\ 1$$

Tar is a thick viscous liquid which contains heavy aromatic hydrocarbons and sometimes heavy metals. In addition to the gasification reactions of hydrocarbons tar can be reduced by thermal cracking, steam reforming, dry reforming, carbon formation and partial oxidation represented in equations 14 to 18 respectively[32].

$$pC_nH_x \leftrightarrow qC_mH_y + rH_2 \qquad Equation\ 2$$

$$C_nH_x + mH_2O \leftrightarrow nCO + \left(m + \frac{x}{2}\right)H_2 \qquad Equation\ 3$$

$$C_nH_x + nCO_2 \leftrightarrow 2nCO + \left(m + \frac{x}{2}\right)H_2 \qquad Equation\ 4$$

$$C_nH_x \leftrightarrow nC + \left(\frac{x}{2}\right)H_2 \qquad Equation\ 5$$

$$C_nH_x + (\frac{n}{2})O_2 \leftrightarrow nCO + \left(\frac{x}{2}\right)H_2 \qquad Equation\ 6$$

Where C_nH_x represents tar and C_mH_y is a lighter hydrocarbon than the tar.

When considering glycerol, it is unlikely that tar will form as it is a small/medium chain hydrocarbon ($C_3H_8O_3$) and provides a significant advantage compared to solid biomass gasification. Therefore the area of focus should be optimising the steam reforming and methanation reactions to maximise CH_4 produced.

1.1.2.5 Biodiesel glycerol as a feedstock for decarbonising heat

Research is being carried out into other methods of glycerol utilisation, such as steam reforming for H_2 and conversion to higher value chemicals as shown in Figure 10, but these are far from commercialisation[33]. As these routes include gasification and steam reforming, which have been used to produce syngas and H_2 respectively, there is already

evidence to show that the reagents for conversion to CH_4 by methanation can be produced from glycerol.

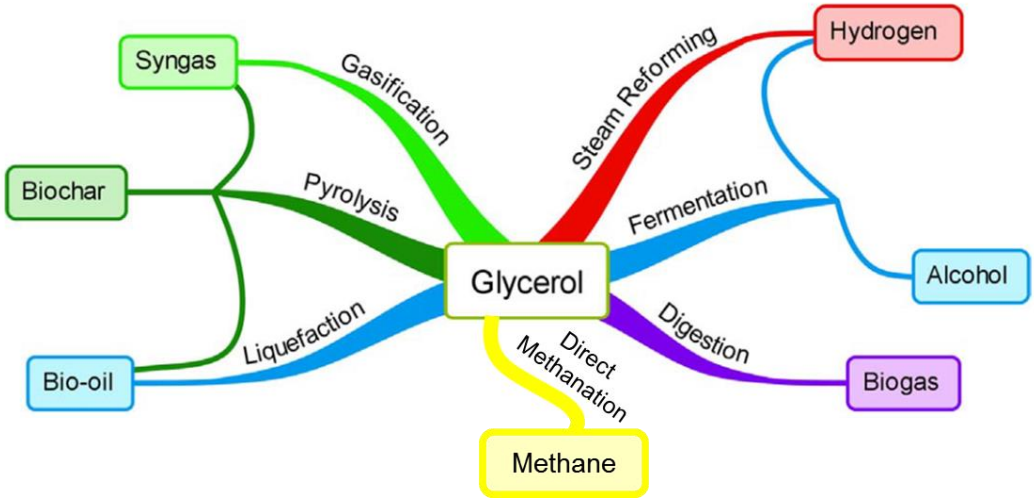

Figure 10. Potential routes for conversion of glycerol into energy vectors with the addition of direct methanation [34]

Extensive review has been carried out on glycerol steam reforming for H_2 by [34,35] but, to this authors knowledge, there has been only one experimental study on direct methanation of glycerol [36] and one published work on the potential of its use in biodiesel refineries [37].

Based on current technologies, for large scale biodiesel refiners to generate value from glycerol they must sell the crude glycerol pre or post purification or convert it to energy. The alternative is to dispose of the glycerol in landfill, affording extra costs to the plant including hazardous waste gate fees, or to give it away for free. At the moment the only commercial methods of using glycerol for energy production on a medium to large scale is incineration, which leads to several hazardous products and pollutants that are stringently controlled by regulations including acrolein. Other small scale uses are available for glycerol such as anaerobic digestion for biogas production, soap production or acting as a dust suppressant but they do not cater for the large scales of excess glycerol currently being produced. Consequently purification and subsequent sale of the pure glycerol remains one of the only profitable routes for glycerol utilisation due to the current low price of glycerol.

However the reason for glycerol's viability as an energy feedstock is also attributed to the value of crude and purified glycerol falling [38–40]. Prior to the rise in biodiesel production in 2003, pure glycerol was valued at \$0.60-\$0.90 lb^{-1} (\$1.32-1.98 kg^{-1}) whereas crude glycerol was \$0.25 lb^{-1} (\$0.55 kg^{-1}). After the expansion, crude glycerol in the USA market began to increase in availability from 2003 onwards, whilst the demand for glycerol remained almost unchanged. As a result, refined glycerol prices dropped by 60% to \$0.30 lb^{-1} (\$0.66 kg^{-1}) and

crude glycerol prices by 80% to \$0.05 lb^{-1} (\$0.11 kg^{-1}) [33,38]. These impacts were felt in the global glycerol market as other countries increased their biodiesel production, promoting the biodiesel industry as the majority supplier of glycerol to the market. A price trend of the spot prices of glycerol over the period 1998-2018 can be seen in Figure 11. A gradual decline can be observed between 1998-2018 for both 99.7% kosher glycerin and 80% crude soap-lye glycerin and shows that glycerol is still a low value product.

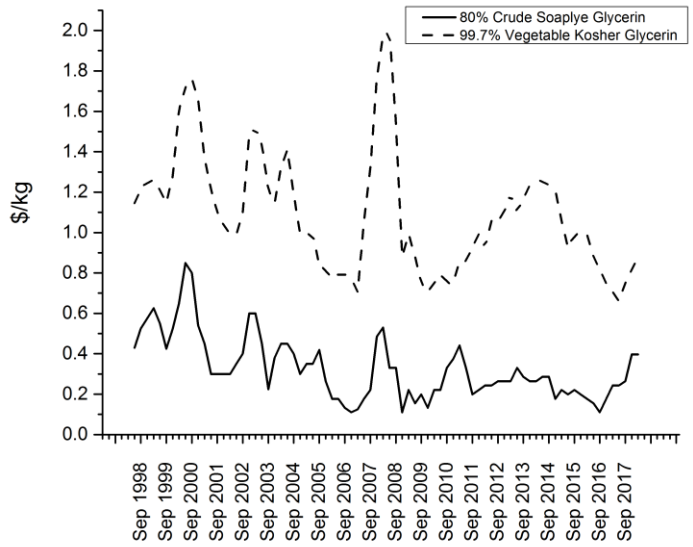

Figure 11. USA spot prices for 99.7% Kosher Glycerin and 80% Crude Soaplye glycerin 1998-2018. Source: Oleoline Ltd [41].

The idea proposed in this work is to convert glycerol into a renewable gas by the process of steam reforming and direct methanation. Direct methanation will minimise the number of process engineering steps required to produce the product gas. The product, known as bio-SNG will be able to supplement the natural gas used to generate steam on-site at the biodiesel refinery. In this case the Bio-SNG would be of low CH_4 purity with the potential to be upgraded or combusted on site at the biodiesel refinery to off-set natural gas dependency and prevent the disposal issues associated with glycerol.

1.1.2.6 Crude vs Pure Glycerol

Glycerol is classified based on its glycerol content or purity as shown in Table 4. Crude glycerol composition varies significantly between biodiesel refining processes where differences in the feedstock, catalyst, filtration and purification methods can be attributed to these variances.

Types of Glycerol	Glycerol Content (%)
Crude	50–90%

Technical	99.5% Technical grade, not certified, mostly >96.0
United States Pharmocopeia	99.5% USP tallow-based
(USP)	99.5% USP vegetable-based
Food Chemical Codex	99.7% USP/FCC-Kosher

Table 4. Grading of glycerol based on origin and percentage glycerol content [42]

A significant challenge will be the impurities contained in the crude form of glycerol which vary depending on the feedstock and the transesterification process. The impurities can range from, but are not limited to: residual transesterification catalyst, biodiesel, fatty acids and soaps methanol, biodiesel, mono and di-glycerides, glycerol oligomers, triacylglycerols and matter organic non glycerol (MONG). Crude glycerol usually contains between 38% and 97% glycerol with the remainder made up of methanol, ash, water and MONG with examples of the composition variation in *Table 5*. [43].

Batch[A]	*Glycerol (%)*	*Moisture (%)*	*Ash (%)*	*Methanol (%)*	*MONG (%)*
B[1]	94.8	2.0	0.0	<0.01	3.2
C[1]	96.5	1.3	0.0	<0.01	1.0
Average	*95.7*	*1.65*	*0.0*	<0.01	*2.1*
F[2]	66.7	0.2	2.9	11.4	18.8
G[2]	64.5	0.0	3.4	13.9	18.1
Average	*65.6*	*0.1*	*3.2*	*12.7*	*18.5*
H[3]	83.4	10.7	1.5	0.2	4.2
I[3]	76.1	11.7	3.5	1.8	6.9
J[3]	74.5	14.3	4.6	0.6	6.7
Average	78.0	12.23	3.2	0.9	5.9

Table 5. Characteristics of crude glycerol from different Australian refinery's processes. [43].

Hu et al. 2012 performed characterisation on the element and composition of several crude glycerol samples. The variance between different soybean samples are shown in Table 6 from different biodiesel plants and processing methods. Without some form of purification, many contaminants will be present in the glycerol reducing the percentage of free glycerol. This has implications for further processing into more valuable products as the impurities may alter conversion percentages e.g. causing catalyst fouling. The majority of biodiesel plants have some form of processing method.

Component (wt %)	CG-SOY1	CG-SOY2	CG-SOY3
Free Glycerol	63.0 ± 0.3	22.9 ± 0.2	33.3 ± 0.1
Methanol	6.2 ± 0.0	10.9 ± 0.2	12.6 ± 0.1
Water	28.7 ± 0.3	18.2 ± 0.1	6.5 ± 0.1
Soap	BDL	26.2 ± 0.2	26.1 ±0.1
FAMES	BDL	21.3 ± 0.2	19.3 ± 0.3
Glycerides	BDL	1.2 ± 0.2	1.6 ± 0.3
FFA's	BDL	1.0 ± 0.1	1.4 ± 0.1
Ash	2.7 ± 0.1	3.0 ± 0.0	2.8 ± 0.1
Total	99.4	102.9	101.8

Table 6. Composition of different soybean glycerol [44]*. Data is shown as an average of three tests and BDL is below the detectable limit.*

As glycerol is a by-product of biodiesel production, the resources required for the purification methods are usually associated with the biodiesel plant and for this work have not been included in the resource costs for the conversion of glycerol to bio-SNG. However understanding the methods may shed light onto contaminants that may be of interest in future simulations.

The most common methods of enhancing the purity of the glycerol include treatments such as; neutralisation, saponification, distillation and vacuum distillation. Usually biodiesel refineries carry out neutralisation as a minimum to remove soaps and catalyst residues from the crude glycerol. A typical process for glycerol purification by neutralisation and saponification is shown in Figure 12 and are usually pre-cursors to methanol removal.

It is in the biodiesel producer's best interest to remove and recycle methanol to prevent the potential negative impacts on public health and the environment, reduce methanol costs, and display willingness to create improved efficiency closed loop processes. Methanol is usually provided in excess in transesterification reactions to generate a high yield of biodiesel. Resultantly, methanol is distributed evenly between the glycerol and methyl ester phase during neutralisation. Vacuum evaporation is the simple and most common process used in biodiesel industries to remove methanol and can also remove water simultaneously. Conditions are usually 50-90 °C for 1-2 hours. Column distillation can also be used and allows a layer of methanol to be removed.

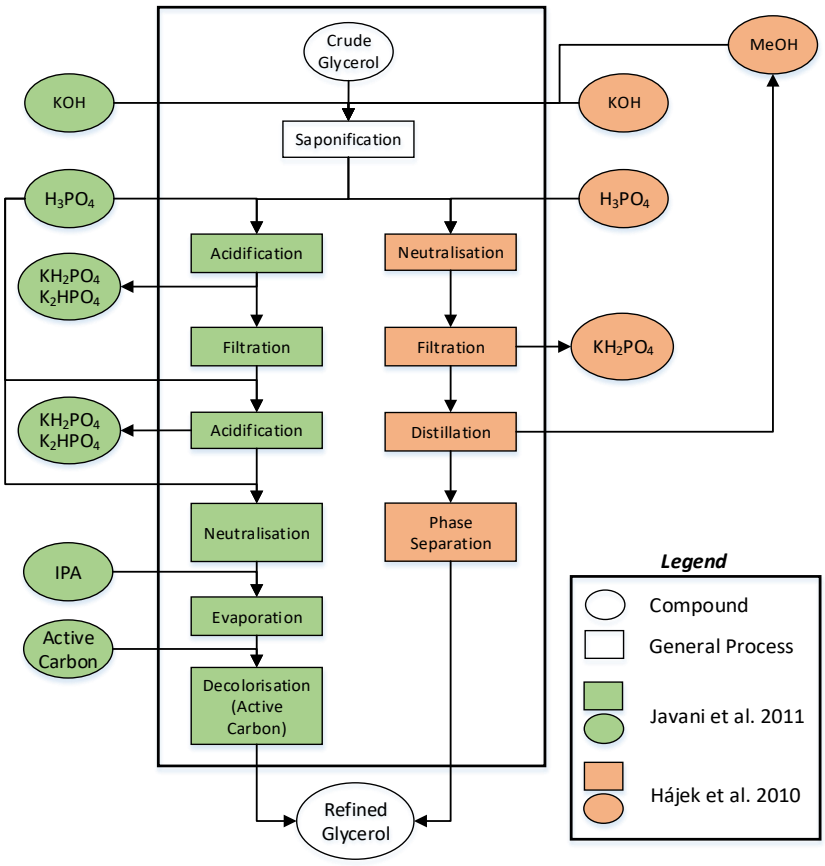

Figure 12. Neutralisation and Saponification processes according to Javani and Hájek [45].

1.1.2.7 Steam reforming and methanation

Steam reforming differs from steam gasification because it converts all of the feedstock into gases by reforming reactions, rather than thermal decomposition reactions. Between 1930 and 1950 Imperial Chemical Industries in the USA developed the technology and method to steam reform hydrocarbons into H_2 for ammonia (NH_3) production. Natural gas was used as a feedstock to produce H_2 via steam reforming, also known as steam methane reforming (SMR) and is shown in Equation 7 [46]. This process is still used today to generate the majority of global H_2.

$$CH_4 + H_2O \xrightarrow[heat]{} CO + 3H_2 \ (\Delta H^0_{298} = -205.2 \text{ kJ mol}^{-1})[47] \qquad \textit{Equation 7}$$

As more refineries were being built due to this discovery, naphtha became a significant by-product from natural gas production. ICI developed a catalyst to reform naphtha at economic steam ratios without carbon formation to produce H_2. The catalytic steam reforming of naphtha is shown in *Equation 8* [48] and was the pre-cursor to the Naphtha to SNG processes.

$$C_nH_n + nH_2O \xrightarrow[heat]{} nCO + \left[\frac{2n+m}{2}\right]H_2 \qquad \textit{Equation 8}$$

Methanation of producer gas from steam reforming is primarily concerned with CO conversion to CH_4 by hydrogenation. Methanators are usually operated at low temperatures and elevated pressures resulting in the forward reaction of the water gas shift, shown in Equation 9, CO methanation, shown in Equation 10, and CO_2 methanation, shown in Equation 11, becoming more thermodynamically favourable than the reverse water gas shift reactions [49].

$CO + H_2O \leftrightarrow CO_2 + H_2$	*(ΔH^0_{298} = -41.2 kJ mol^{-1})*	*Equation 9*
$CO + 3H_2 \leftrightarrow CH_4 + H_2O$	(ΔH_{298} = -206.2 kJ mol^{-1})	*Equation 10*
$CO_2 + 4H_2 \leftrightarrow CH_4 + 2H_2O$	(ΔH_{298} = -165.0 kJ mol^{-1})	*Equation 11*

1.2 Research Justification

For some biodiesel producers, there is no profitable method to process glycerol because of the increased supply and reduced demand. Purification to pure glycerol favours large biodiesel producers with access to capital intensive equipment. Methods of disposal create a significant economic and environmental loss, such as landfill, or cannot accommodate the capacity of glycerol, such as A.D. Other utilisation methods are small scale or are at the research level, such as conversion of glycerol to other chemicals and co-combustion with other fuels whilst some methods rely on a future economy, such as conversion to H_2. If glycerol continues to be low value, an effective solution is to convert the low value glycerol into the renewable gas, bio-SNG, using direct methanation via steam reforming and methanation reactions and combust it for energy to offset fossil fuels in the biodiesel plant.

At present the demand of glycerol is lower than the supply and biodiesel production is forecasted to increase steadily into 2025 by the OECD, as shown in Figure 13, further saturating the glycerol market and maintaining low glycerol prices. Biodiesel is produced globally and focussed in four out of the five areas of the world outlined in Figure 13. Consequently, the issue of surplus glycerol and its lack of a commercial outlet is a global problem which will become more significant as biodiesel production intensifies.

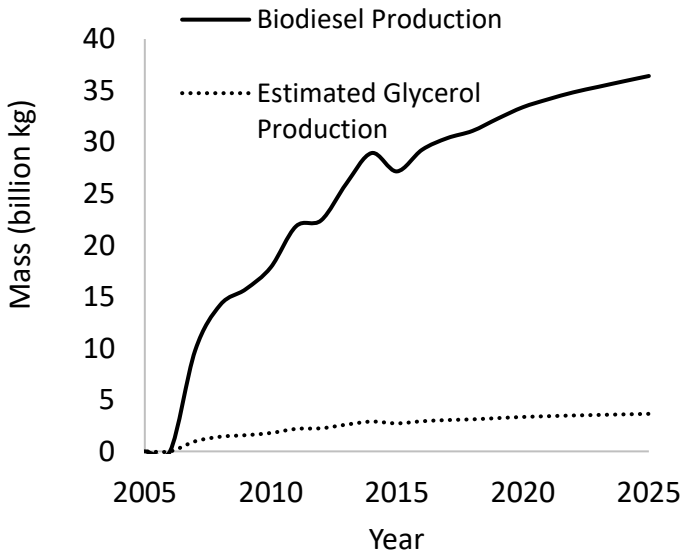

Figure 13. OECD forecast for global biodiesel production, calculated using a density of 0.88 kg L^{-1}. Glycerol production was assumed to be 10% by mass [9].

Not all biodiesel producers have the capital or the available equipment for expensive purification processes on site. Currently the transport and processing costs for post treatment of glycerol in large quantities may be greater than value of the purified glycerol.

Furthermore, traditional methods of disposal such as land fill or incineration pose environmental hazards and additional costs.

Another glycerol utilisation method used commercially is to supplement the biogas produced from A.D plants [50]. This method is limited by the number of A.D plants, the amount of glycerol able to be added to the digester and the time taken to produce the biogas. In response to a consultation paper by OFGEM on whether glycerol is a renewable fuel, Kemble farms who operate an anaerobic digester (A.D) wrote that:

"…there is no better way of disposing of Glycerol safely and environmentally than to use it in AD. It is only possible to use very small quantities of around 3% to enhance anaerobic digestion… Other methods of Glycerol disposal are environmentally dangerous such as in landfill where its effect can be to multiply the production of methane in an uncontrolled way"[51].

This implies that the volumes of glycerol produced will exceed the capacity of A.D and it is not a specific solution to the glycerol problem.

Concerning combustion and incineration, these techniques require specialised burners [52,53] or co-combustion with fossil fuels [54,55] to maintain process efficiency. Crude glycerol is inherently difficult to combust due to high viscosity and high ignition temperatures as well as the contaminants from transesterification. The viscosity hampers pumping; flame spray and pipe flow whereas the high ignition temperature increases the potential to form the toxic substance acrolein. Furthermore, the contaminants create deposits which can reduce the lifetime of the combustion equipment. Conversion of glycerol to a combustible gas will bypass several of these issues although contaminants from transesterification will still be a significant challenge.

1.2.1 Direct methanation of glycerol for Bio-SNG

Usually in gasification, as described in Figure 9, the methanation step takes place after the feedstock has been gasified and cleaned and requires at the very least, one additional reaction vessel. To minimise the steps it would be ideal if the glycerol could be gasified and methanated in one step and one reaction vessel without the need for drying, although this poses challenges. Firstly to take advantage of steam reforming and methanation reactions, the reactants must be in the vapour phase. Therefore, if a liquid reactant is injected into the reactor, there must be enough energy to vaporise the reactants. Additionally the catalyst must be able to convert the reactants into the desired products in a single reactor and catalyst several reactions.

Steam reforming has primarily been applied for H_2 production. Prior to 1917, H_2 had been produced using water-gas generators for the Haber Bosch process. The Haber Bosch process is arguably one of the most important and well established chemical processes of the 20th century as it provided a production pathway for ammonia and therefore fertiliser. Usually steam reforming transforms CH_4 from natural gas into a syngas composed of H_2, CO_2, CO and H_2O. These products are in equilibrium and can be manipulated to increase or decrease the concentration of H_2 by altering process conditions and gas concentrations. Conversion of CO and H_2O into CO_2 and H_2 is known as the water gas shift reaction and can be coupled with methanation to produce CH_4.

By selecting conditions that favour methanation, the glycerol ($C_3H_8O_3$) can be converted to a medium methane content Bio-SNG with the potential for upgrading to a >97% Bio-SNG.

1.2.2 Process Integration in a Soybean Biodiesel Refinery

The direct methanation process would be housed on site next to the biodiesel process. Doing so minimises the transportation and logistical costs and allows the gas to be fed back into the biodiesel refinery to offset natural gas. Benefits would include a reduction in dependence upon grid gas and reduced fossil CO_2 emissions. Some of the Bio-SNG could be used to produce steam for the direct methanation creating a self-sustaining process.

Figure 4 has been modified to include how a direct methanation process could be integrated onto a biodiesel plant, as shown in Figure 14. Rather than crude glycerol being a co-product, it has become an intermediate as it is now processed into Bio-SNG and combined with natural gas in the furnace to produce heat via combustion to raise steam. In this way, the volume of natural gas required to raise steam will be reduced by bio-SNG.

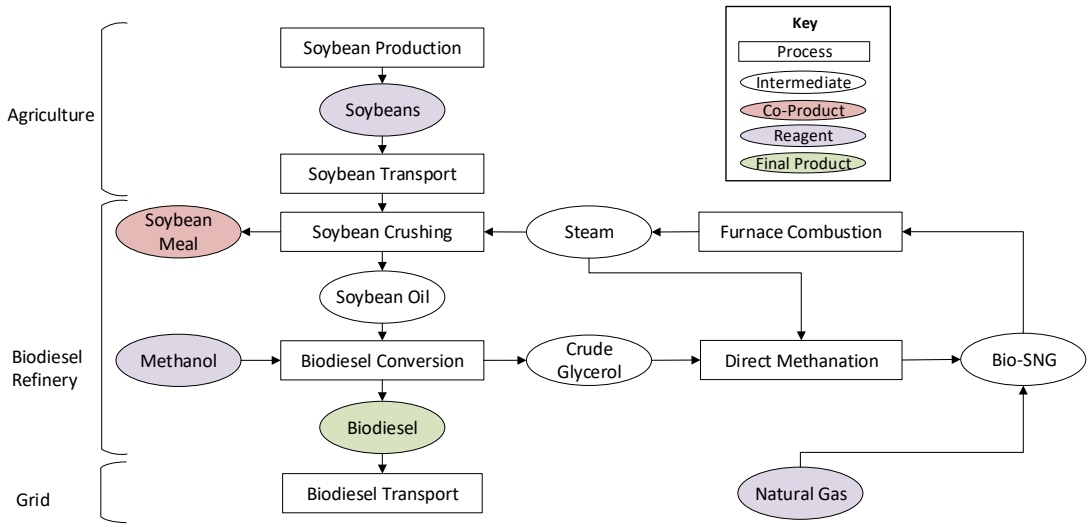

Figure 14. Integration of a low temperature glycerol steam reforming process into a soybean biodiesel refinery.

A soybean biodiesel plant was chosen because steam is already required in the soybean crushing process and data is well documented.

1.3 Research Objectives

The overall aim of the research is to determine the economic, environmental and experimental feasibility of a glycerol direct methanation plant for bio-SNG. The question:

Under what conditions is the direct methanation of glycerol feasible?

Will be answered by completing the research objectives as shown in Table 7. Based on this research question and research aims, six main areas to this project can be identified and include; thermodynamic and process flow sheet modelling, techno-economic and life cycle impacts modelling and construction and optimisation of a laboratory scale gasifier and feasibility discussion.

Chapter	Research Objective
2	Determine the optimum process conditions that would allow the direct conversion of glycerol to a methane rich fuel gas using thermodynamic modelling.
2	Create and optimise a process model of a glycerol direct methanation plant based on thermodynamic modelling with energy and mass flows outputs.
3	Perform a techno-economic analysis of the plant based on the process model.
4	Compare the life cycle impacts of steam generated from glycerol bio-SNG with natural gas based steam.
5	Construct a laboratory scale glycerol gasifier and optimise the process towards maximising CH_4 production.
6	Discuss the feasibility of a glycerol direct methanation.

Table 7. Research objectives by chapter.

Each of the chapters can be read separately although the techno-economic analysis and life cycle impacts analysis in chapter 3 and 4 respectively are dependent on the process model created in Chapter 2.

1.4 Research Challenges and Novelty

Two areas of novelty are addressed in this work using the six main areas as mentioned in 1.3. The first is directly injecting the liquid glycerol and water mixture into the reformer without pre-vaporising it. The second is to methanate the glycerol directly using only one reformer rather than a sequence of methanation reactors. The former permits better control of the exotherms in the reactor which are adverse to reaching the highest methane yields, while the latter achieves process intensification, thus overall both novel features save on capital as well as operating expenditures and ought to ease scaling of the process.

As this is a feasibility study, pure glycerol is used rather than crude glycerol, to avoid the unknown effects of contaminants that would usually be found in crude glycerol. A major challenge in future work will be analysing the impact of contaminants usually found in crude glycerol on the performance of the process such as the influence on carbon formation, conversion rates and selectivity of gas products.

Determining the conditions for thermodynamic and process flow sheet modelling of the low temperature glycerol methanation process required a detailed knowledge of the literature on biomass gasification and steam reforming of glycerol. Usually biomass gasification is employed to produce a high calorific product where the main component is CH_4. On the other hand, steam reforming of glycerol usually produces H_2 as the main product. By combining understandings of both methods, simulations using Aspen Plus V8.8 chemical processing software were performed to verify and fill-in these knowledge gaps, to identify optimum thermodynamic process conditions to maximise CH_4 production.

A more in depth plant design was then carried out, involving heat and resource integration to maximise the energy and CH_4 gained from the process. Detailed information from Aspen Plus was used to determine the heating value of the gas, conversion efficiency and energy intensities. A challenge in optimisation was minimising the energy required to raise steam for the direct methanation process. Any energy savings produced, such as using lower operating temperatures or with less steam, improved the conversion efficiency of glycerol to methane and ultimately improve the feasibility of the process.

In depth analysis of the modelled data, including energy balance and CO_2 emissions, was added to existing life cycle analysis models by creating a new unit process. In doing so, life cycle emissions and energy were calculated and the impact of offsetting natural gas with the renewable fuel gas was predicted. A challenge with this work was ensuring transparency with input data from the life cycle inventory to enable comparison between datasets.

Similarly, energy data from the plant model as well as the sizing of the equipment was used to predict the economic feasibility of a glycerol methanation plant through cost-curve analysis. The main challenge was reducing the uncertainty in sizing and equipment cost estimations as these uncertainties increase the risk of a non-profitable and therefore unfeasible plant.

Laboratory scale tests were carried out using pure glycerol and selected catalysts from the gasification rig that was constructed from the ground up as part of this thesis work. The results from these tests were used to verify the modelled data and determine whether it is possible to directly methanation glycerol using direct liquid injection of glycerol water mixtures. Construction of the rig from the ground up represented a significant challenge as a direct methanation with direct liquid injection rig for glycerol had not been constructed before. During experiments the main challenge was ensuring the carbon produced on the catalyst and in the condensate could be sampled and analysed in tandem with the gaseous carbon.

The final step was to bring these elements of the project together to create an informed decision on the feasibility of glycerol methanation for Bio-SNG and justification for further research.

To meet these objectives a design process framework was used which is commonly applied when creating new engineering solutions to solve design problems for customers or take advantage of new market opportunities.

1.5 Applying the design process to assess the feasibility of the direct methanation of glycerol

The design problem usually has six identifiable steps [56]:

1. Conception and definition.
2. Flowsheet development.
3. Design of equipment.
4. Economic analysis.
5. Life cycle impacts analysis.
6. Optimisation.
7. Reporting.

Due to the growing concerns with environmental damage from human activity, an additional stage was included, and follows the economic analysis. This stage takes the form of life cycle analysis or a sustainability analysis. Additional information such as gCO_2 equivalents were included in the reporting section.

A flow diagram of the design process including the addition of the life cycle analysis step can be seen in Figure 15. The concept involves understanding the needs of the customer. In this case it is that an alternative method of glycerol utilisation is required. The definitions provide a list of constraints and objectives that must be fulfilled such as minimum plant capacity, operating conditions or operating hours. The design concepts are usually created using appropriate chemical engineering design software such as Aspen Plus, as was the case here, or Matlab or gPROMS. From the concepts the performance and fitness for service can be evaluated with further research and development as required. The data outputs from the design concepts can be used to size and cost the plant as well as produce environmental impacts using lifecycle analysis. Optimisation occurs at this stage to allow the design to meet further constraints that the customer or policy dictate with final designs reported to the customer. Later stages involve selecting an appropriate design and constructing the plant but for this work the design process will stop at the reporting stage. The report hopes to provide a solid basis for further work into the glycerol direct methanation process. As more possibilities and constraints are realised there is a need for feedback and re-evaluation whilst research and development underpins the whole process.

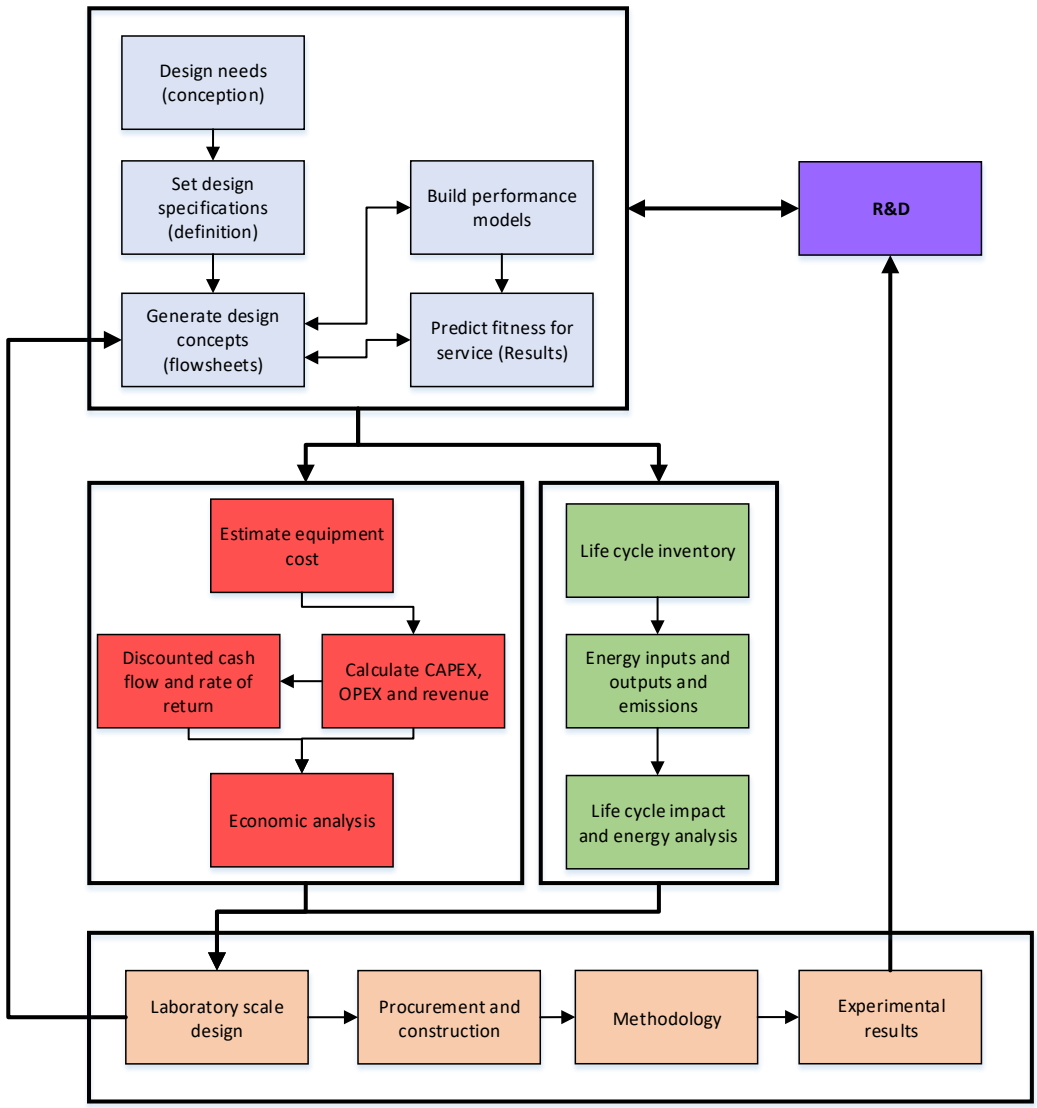

Figure 15. An iterative procedure for the design process adapted from Sinnot [57] *where the process modelling is in blue, economic analysis is in red, environmental analysis is in green and experimental analysis is in orange.*

1.6 System Boundaries

When considering any type of process analysis the system boundaries must be well defined. The system boundary reflects what parts of a process will included in the analysis and allows the results to be compared fairly with other studies and highlights limitations. The system boundaries may need to be expanded to make results more relevant, as will be seen shortly.

For this work the system boundaries for the process simulation, economic analysis and life cycle impact analysis are shown in Figure 16. Process simulation only includes the conversion of glycerol via direct methanation to bio-SNG. On the other hand, the economic analysis includes the conversion of glycerol via direct methanation to bio-SNG followed by combustion in the furnace to produce steam, using natural gas prices as a guideline for

profitability. Finally, the environmental analysis includes the whole biodiesel production chain, as this governs the impacts of the glycerol, as well as conversion to bio-SNG via direct methanation and steam via combustion in a furnace. This shows that all of the analyses are dependent upon the process simulation step.

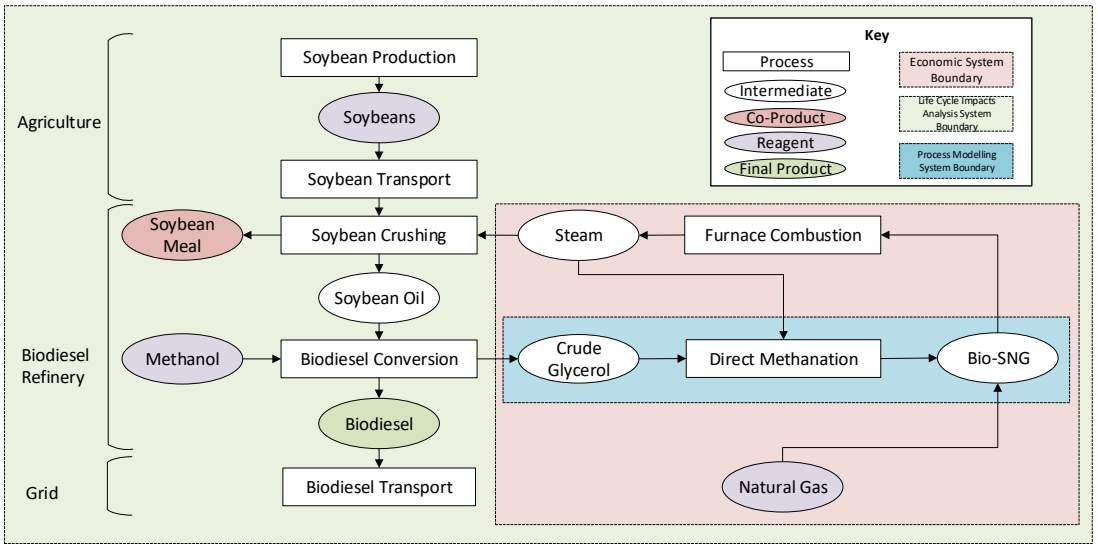

Figure 16. System boundaries for different analysis in the design process

2 Process Simulation

2.1 Introduction

Today, process simulation allows a single engineer to quickly design and optimise a chemical engineering process from a desktop computer. Example simulators for chemical processes include Aspen HYSYS and Aspen Plus, ChemCAD, PRO/II and gPROMS whilst spreadsheet software such as Micrsoft Excel can be adapted for use. Improvements in programming and computing power allow an engineer to depict a biological, chemical, physical or technical process in a process model. An understanding of the physical properties of components, how they interact, thermodynamics and kinetics as well as the mathematical modelling techniques, also known as property methods, permits the transformation of a simple flow sheet to a process model that can generate output data. As several scenarios can be created, the output data can be used to compare each scenario to determine the most effective solution. As a result, process simulation is carried out in the early stages of a design process or before altering plant conditions to approximate the impacts on the procedure before it is implemented in the real world.

The relevant stages of the design process that incorporate direct use of process modelling are highlighted in Figure 17. After the design specifications, or inputs, have been determined by the process modeller and customer, several flowsheet concepts can be designed and then implemented as a performance model within process modelling software. R&D is usually required to determine inputs and what methods to use to manipulate the inputs. Examples include the property method which is the equations used to manipulate the input data and calculate the process model outputs. Once outputs have been acquired comparison with literature or experimental data is necessary for verification. Assumptions will need to be made based on the definition in order to make models fit for service and the limits of the design concepts can be tested. Once scenarios have been deemed satisfactory for the service, the output variables can then be assessed further using economic and environmental analysis. Using these analysis methods will allow the process modeller to determine the optimum process.

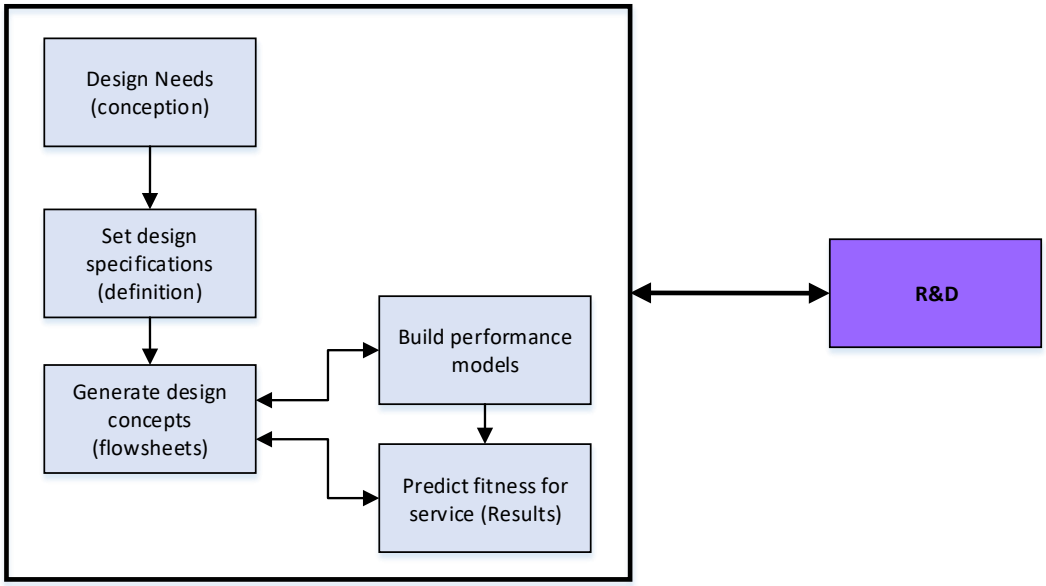

Figure 17. Process modelling steps in the design process.

The optimum process is produced by manipulating input variables in the flow sheet using the process simulation software. Blocks which correspond to different equipment, as designated by the engineer, are connected by streams which can contain energy or material. The mass and energy balances are solved using mathematical equations, usually under steady state conditions rather than dynamic conditions, with assumptions and approximations in order to allow the flow sheet to converge. Engineers can select a property method which defines the equations the flow sheet uses in its calculations. Appropriate property method selection is necessary for accurate results as property methods are specific to certain physical property ranges e.g. temperature and pressure or particular components e.g. electrolytes or solids.

Steady state and dynamic equilibrium

Generally the initial process simulations are of a process at steady state in a closed system, in this case the reactor. A quantity, such as mass flow rate or temperature, is at steady state when it is constant with respect to time whereas a closed system is a vessel that does not exchange any matter with its surroundings.

Process simulations are usually interested in the product outputs when the modelled process is at a dynamic chemical equilibrium.

Equilibrium is a limiting case of a steady state process where the rate of transfer of a quantity in and out of a system is equal to zero and is non-reversible whereas a dynamic equilibrium is a reversible case. For chemical reactions at dynamic equilibrium this means that there are both forward and back reactions that convert the reactants into products and products back

into reactants respectively. Unfortunately it is not possible to achieve a 100% conversion resulting in a mixture of reactants and products being formed. At a steady state dynamic equilibrium, the distribution of these reactants and products is constant with respect to time i.e. the rate of the forward reaction is equal to the rate of the reverse reaction. When process modelling these types of reactions the aim is to determine at what process conditions the equilibrium position can be shifted such that the majority of the desired product is formed. Conditions such as the catalyst, pressure, temperature and concentration affect the equilibrium position and is famously explained by Le Chatelier's principle, proposed by the French Chemist, Henry-Louis Le Chatelier, in 1884:

"When a change is imposed on a system at equilibrium, the equilibrium will shift to counteract the change".

The impact of making changes on a system in dynamic chemical equilibrium is shown in Figure 18.

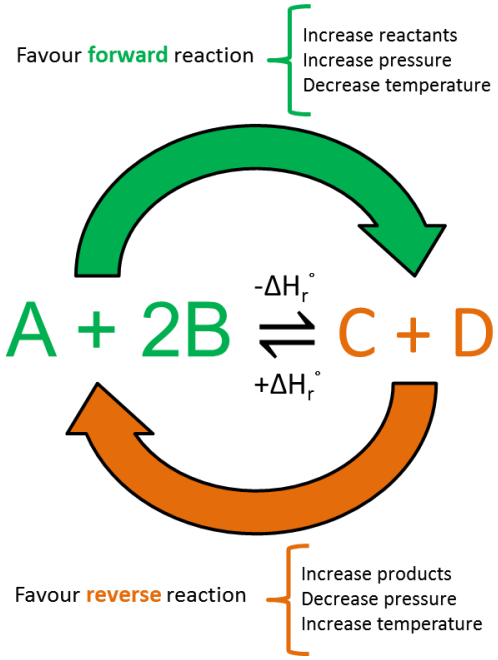

Figure 18. Effects of process conditions on a system at dynamic equilibrium.

By increasing the concentration of the reactants or products the counteraction will be to decrease the reactant or products by favouring the forward or reverse reaction respectively. For pressure, the side with fewer molecules will be favoured when pressure is increased and vice versa. For temperature, the molecules formed as a result of an exothermic reaction will be favoured for a temperature decrease and vice versa. In this way the equilibrium shifts to counteract changes made to a system by a process engineer. On the other hand a catalyst

will seek to improve the rate of reaction of both the forward and reverse reaction to the same extent but does not impact the equilibrium position.

A significant benefit of using process simulation software is minimising risk when implementing changes on a system in dynamic equilibrium. Engineers are able to alter process conditions and equipment in a short time with minimal resources to generate several alternative scenarios for comparison. The most desirable scenario, based on criteria such as energy use or carbon emissions, can be selected without the need to implement all of the processes in real time, thereby saving resources and improving safety in the long term.

Aspen Plus V8.8 was the process simulation software available for this work. There are several examples of process simulations in Aspen Plus to valorise glycerol and the following section is a brief literature review of the work carried out with glycerol in Aspen Plus.

2.2 Literature Review

Several studies have simulated purification of crude glycerol with a subsequent valorisation method. One of the most significant studies was produced by Haas *et al.* 2005 on behalf of the United States department of agriculture and modelled a soybean biodiesel production process with purification of glycerol to 80 wt% In Aspen Plus [58]. Kiss *et al.* 2012 [59] used Aspen Plus to model a novel glycerol separation process to be used in biodiesel refineries. The novel dividing wall column was shown to require 27% less energy and 12% lower investment costs whilst being able to separate methanol, water and glycerol in high purities. Xiao *et al.* 2013 [60] created an Aspen Plus flow sheet for a new glycerol purification process that could refine crude glycerol to 94% and obtained a good match with experiments. Posada *et al.* 2013 [61] produced a flow sheet for the production of 1,3-propanediol from raw glycerol with glycerol purification, fermentation and 1,3-propanediol recovery and purification. Posada *et al.* 2011 [62] produced an aspen process model to first purify crude glycerol to 98% and then convert by fermentation to poly-3-hydroxybutyrate. A further study by Posada *et al*. 2012 [63] analysed the production of a further 9 different chemical products from glycerol to determine which product was most economically valuable.

Aspen Plus has also been used to simulate the conversion of glycerol to other chemicals assuming the glycerol has already been purified. The Aspen Plus simulation environment was used to design and evaluate the performance of an industrial scale glycerol to acrolein conversion plant by Banu *et al.* 2015 [64]. Posada et al. 2013 [61] produced 1,3-propanediol by fermentation whilst Vlysidis *et al.* 2011 [65] investigated the conversion of glycerol to succinic acid by fermentation using additional simulations from MatLab. Vlysidis compared

value of the succinic acid with disposal, distillation and purification of crude glycerol. Bauer and Hulteberg 2014 [66] converted glycerine to isobutanol which could be used as a fuel substitute for fossil gasoline and optimised the process using pinch analysis to maximise the heat energy recycled. Pedersen *et al.* 2017 [67] designed a process based on wood-glycerol co-liquefaction, followed by thermal cracking and hydro-processing to produce gasoline equivalents.

Some studies maximised the energy gained from glycerol conversion by utilising co-products of glycerol conversion for heat and power. Galera *et al.* 2015 simulated the conversion of glycerol to H_2 and power using two scenarios in Aspen Plus, namely autothermal supercritical water reforming and without autothermal operation. They followed this up by conducting a life cycle analysis using the outputs simulated in Aspen Plus [68]. Hunpinyo *et al.* 2016 [69] designed a process that could convert crude glycerol (80-88% wt% free glycerol) into Fischer-Tropsch products using steam reforming where the off gases produced were recycled by co-generation for heat and power to the lower energy costs associated with steam reforming.

Several studies were carried out on reforming or gasification of glycerol with the aim of producing H_2 or syngas. Shuai Wang *et al.* 2017 [70], designed an autothermal reforming process of crude glycerol with *in situ* H_2 separation to determine the effects of H_2 separation on H_2 yield. Liu *et al*. 2013 [71] simulated autothermal reforming of glycerol for syngas over a Pt and Rh/Pt catalyst. Aspen simulations were generated to calculate the equilibrium product composition and determined good agreement between experimental and modelled data. Yang *et al.* 2011 [72] simulated the oxidative steam reforming of glycerol for H_2 production in Aspen Plus to determine the parameters required for autothermal operation and minimising carbon formation. Reddy *et al.* 2016 [73,74] also designed supercritical water gasification of glycerol in Aspen plus but with methanol as an added contaminant to simulate a glycerol stream produced from a biodiesel refinery that did not recover the methanol.

Whilst there have not been any studies showcasing process modelling of a glycerol to CH_4 process there are a number of experimental studies. Schubert et al. 2014 [75] designed and operated a continuous hydrothermal gasification process for the production of syngas from crude glycerol. More recently Imai et al. 2017 [36] carried out the direct synthesis of CH_4 from glycerol. They tested several Ni catalysts with alumina and silica supports at different temperatures and pressures.

From this literature review the following conclusions can be made:

- Aspen Plus is a popular process modelling tool for glycerol valorisation.
- No studies have been carried out in Aspen Plus to convert glycerol to CH_4 either with traditional methods or by direct methanation.
- There are few literature studies on conversion of glycerol to CH_4.
- The majority of studies utilised a steady state chemical dynamic equilibrium with some studies using a minimisation of Gibbs free energy method.
- Popular trends include conversion to chemicals, fuels or heat and power.
- Comparisons between the end product and purification of glycerol have been made.
- Crude glycerol purities varied from 60-88 wt% free glycerol.

2.3 Design Needs

Designing a process revolves around fulfilling a need or requirement. Currently the requirement is that glycerol from biodiesel refineries must be valorised else it will have a negative, low or zero commercial value. The objective of the work in this chapter is to model a process that can create value by converting the glycerol into a medium CH_4 content gas by direct methanation without pre-vaporising the glycerol and water which can be used on site for the generation of heat and steam. The process is a specific form of steam reforming and has been named glycerol low temperature steam reforming (GLT-SR) and is interchangeable with direct methanation.

The gas produced is known as bio-SNG must have the highest CH_4 content possible with a minimum of H_2. The desired method is direct methanation via glycerol steam reforming and methanation without pre-vaporisation. The body of work in the literature on H_2 production from glycerol can be used to inform on the conditions required to produce CH_4 because it will require contrary operating conditions.

As the main product is an energy vector it is integral that the energy cost of the process is minimised to maximise net energy gain. Traditional methanation utilises high and low temperature shift reactors with large amounts of cooling required for each step due to the exothermic nature of methanation. Directly methanating the glycerol reduces the number of stages and takes advantage of the H_2 liberated from the decomposition of glycerol. Maintaining low temperatures will reduce the energy required to heat the reactor and if operated adiabatically will allow the heat generated from exothermic methanation to aid in driving the vaporisation of water and glycerol. This is similar to autothermal reforming but instead of combustion driving the reaction, it is methanation [76,77]. Analysis of the energy will be carried out by calculating the energy efficiency from an energy balance.

Ideally the feedstock would be crude glycerol. Assessments using pure glycerol as a starting point will simplify the process with regards to the effects of crude glycerol contaminants. Determining the contaminants and modelling purification methods to assess the impacts on the process is important for future work but not crucial at this stage of analysis whereby the feasibility at the best case scenario is required although an understanding is necessary and may provide useful information for future work.

2.4 Design Specifications

Design specifications translate the design objective into specific parameters or instructions that can be implemented into a process flow sheet. The design objective is to model a process that can create value by converting the glycerol into a medium CH_4 content gas by direct methanation using steam reforming and methanation reactions without pre-vaporising the glycerol and water which can be used on site for the generation of heat and steam.

Several different scenarios combining each of the different technologies mentioned in the literature review could be proposed and are shown in Figure 19. In this work, the GLT-SR process has been modelled whereby the gas produced is combusted directly to produce heat for steam production on site at the biodiesel refinery. This leaves several combinations of technologies which could be explored in future work and include variations on the feedstock for glycerol production as well as different methods of;

- Glycerol purification such as saponification, vacuum distillation and neutralisation.
- Gas purification such as water, chemical or physical scrubbing.
- Energy generation such as combined heat and power.

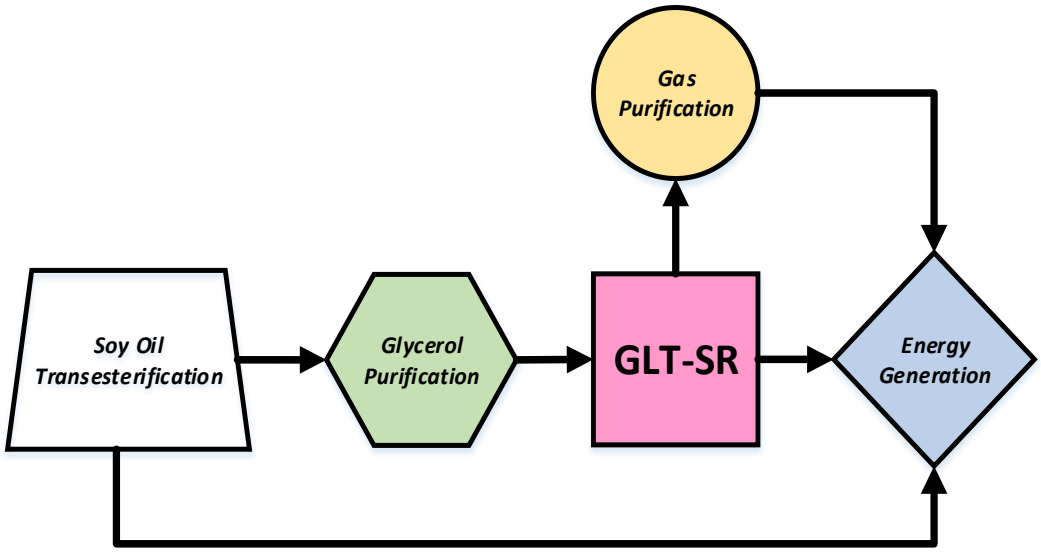

Figure 19. Simplified flow diagram of different processes upstream and downstream of the GLT-SR process.

The focus of this chapter will be designing the GLT-SR process by determining the optimum process conditions by thermodynamic analysis followed by process optimisation using heat integration and calculation of the potential offset of natural gas energy with the GLT-SR Bio-SNG.

2.4.1 Thermodynamics of glycerol low temperature steam reforming (GLT-SR)

Understanding the thermodynamics of GLT-SR will provide us with favourable reaction conditions to produce CH_4. The thermodynamics of a reaction or set of reactions is a method of determining the energy stored in the reaction or products. One of the most common ways of expressing the energy is in terms of Gibbs free energy (Equation 12).

$$\Delta G^o = \Delta H^o - T\Delta S^o \qquad \textit{Equation 12}$$

Where ΔG is change in Gibbs energy, ΔH is change in enthalpy, T is temperature and ΔS is change in entropy.

Gibbs free energy is a measure of the spontaneity of a reaction. If the Gibbs free energy of a reaction is negative, the reaction is spontaneous and more likely to occur where the opposite is true if the Gibbs free energy is positive. Large positive changes in entropy i.e. toward disorder at high temperatures with negative enthalpies i.e. exothermic, tend to be produce the largest negative Gibbs energy and highest spontaneity. Enthalpy and entropy are dependent on pressure and it would incorrect to use an entropy value at one pressure and an enthalpy value of a different pressure. Consequently, enthalpy, entropy and temperature as well as pressure are driving forces behind any chemical reaction as they affect the Gibbs free energy.

Taken on its own, Gibbs free energy is not the only factor which must be considered to determine the likelihood of reactions occurring. When using a Gibbs free energy minimisation method, it assumes the reactions are already at equilibrium, ignoring any kinetic effects, i.e. rate of reaction or mechanistic impacts of a catalyst i.e. selectivity and will inform what the product distribution will be based on the process conditions given. Therefore, Gibbs energy is useful as a guide for the expected products when the reactions and process conditions are known.

The majority of studies on glycerol steam reforming have been produced with H_2 or syngas as the main product. As CH_4 is a competitor to H_2, conditions that do not favour H_2 production usually favour CH_4 production. In addition, carbon formation must be avoided for the maximum production of either H_2 or CH_4. Therefore a review of the literature on the thermodynamics of CH_4 production from glycerol steam reforming and the reactions behind CH_4, H_2 and carbon formation are included.

Glycerol decomposition is one of the potential first steps in a glycerol steam reforming process (*Equation 13*) and yields H_2 and CO. On the other hand, when water is present, steam reforming occurs as in *Equation 14*. Both liberate H_2 and CO as syngas although steam

reforming converts water into additional H_2 and CO via water gas shift (*Equation 15*). By combining steam reforming with CO methanation (*Equation 16*) the theoretical maximum CH_4 able to be produced from glycerol is revealed as glycerol methanation in *Equation 17*.

Equation 18 describes the CO_2 methanation pathway and whilst it is possible, it consumes more H_2 for the same yield of CH_4 and is dependent on the water gas shift reaction for CO_2 production rather than CO. Consequently, less CH_4 would be produced via this pathway and there it would not be the upper theoretical limit. Whether or not methanation occurs after the glycerol steam reforming and water gas shift reactions is dependent upon the process conditions and the catalyst and therefore the ability of the process to reach equilibrium conditions.

Carbon formation in methanation processes can inhibit CH_4 production as it reduces the available carbon and H_2 for CH_4 production and occurs by disproportionation of CO in *Equation 19* (Boudouard reaction) as well as CO and CO_2 hydrogenation in *Equation 20* and *Equation 21*.

Glycerol Decomposition to Syngas

$C_3H_8O_{3(l)} \xrightarrow[heat]{} 4H_2 + 3\mathrm{CO}$ ΔH^0_{298} +338 kJ mol^{-1} *Equation 13*

Glycerol Steam Reforming

$C_3H_8O_{3(l)} + 3H_2O \leftrightarrows 3CO_2 + 7H_2$ ΔH^0_{298} +346 kJ mol^{-1} *Equation 14*

Water Gas Shift

$CO + H_2O \leftrightarrows CO_2 + H_2$ ΔH^0_{298} -41 kJ mol^{-1} *Equation 15*

CO Methanation

$CO + 3H_2 \leftrightarrows CH_4 + H_2O$ ΔH^0_{298} -206 kJ mol^{-1} *Equation 16*

Glycerol Methanation

$C_3H_8O_{3(l)} \rightarrow 1.75CH_4 + 1.25CO_2 + 0.5H_2O$ ΔH^0_{298} -74 kJ mol^{-1} *Equation 17*

CO_2 Methanation

$CO_2 + 4H_2 \leftrightarrows CH_4 + 2H_2O$ ΔH^0_{298} -165 kJ mol^{-1} *Equation 18*

CO Disproportionation (Boudouard)

$2CO \leftrightarrows CO_2 + C$ ΔH^0_{298} -172 kJ mol^{-1} *Equation 19*

CO Hydrogenation

$CO + 2H_2 \leftrightarrows H_2O + C$ ΔH^0_{298} -131 kJ mol^{-1} *Equation 20*

CO_2 Hydrogenation

$CO_2 + 2H_2 \leftrightarrows 2H_2O + C$ ΔH^0_{298} -90 kJ mol^{-1} *Equation 21*

The concept of direct methanation was first recorded by Meyer. H et al. 1976 [78]. In direct methanation equimolar concentrations of CO and H_2 react together in a single step as shown in *Equation 22*. Whilst the stoichiometry is the same as combining the CO methanation and water gas shift, the difference was that CO_2 was produced directly rather than by relying on the water gas shift reaction to produce the required CO from CO_2 for methanation.

Direct Methanation

$2CO + 2H_2 \leftrightarrows CH_4 + CO_2$ ΔH^0_{298} -247 kJ mol^{-1} *Equation 22*

The potential product routes for glycerol steam reforming are shown in Figure 20.

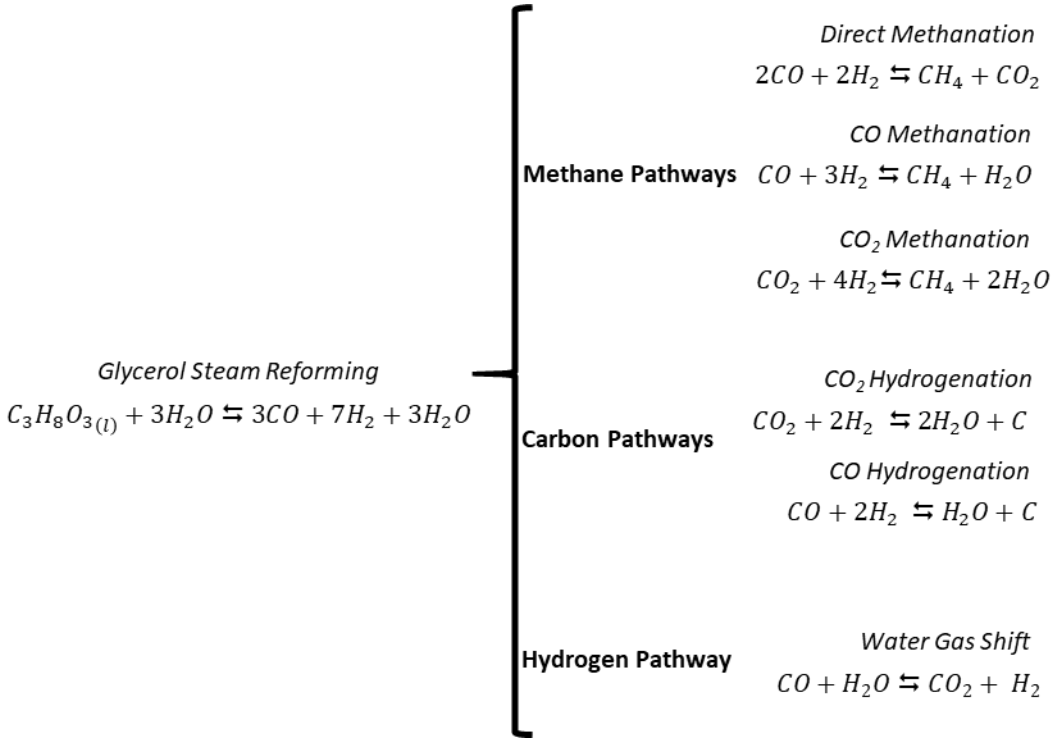

Figure 20. Product routes from glycerol steam reforming.

To maximise methane production, avoiding carbon and hydrogen producing pathways is necessary. To avoid carbon pathways it is advisable to use higher water contents to shift the equilibrium of the hydrogenation reactions to the left. On the other hand, CO and CO_2 methanation reactions would favour reducing the water content, whilst direct methanation would be unaffected. Therefore proceeding via the direct methanation pathway would be most desirable. Thermodynamic studies have been carried out which show that optimising the delicate balance between catalyst and process conditions is necessary to achieve the desired product.

Thermodynamic studies have been carried out for steam reforming of glycerol above 600 K (327 °C) for H_2 production. In accordance with Le Chatelier's principle, increasing the temperature and feed molar steam to carbon ratio (SC) decreases CH_4 production in favour of H_2, whilst increasing pressure favours CH_4. In other words, favouring CH_4 rather than H_2 production requires low steam to carbon ratios and low temperatures with elevated pressures [79–81]. The selectivity towards CH_4 is greater than H_2 at temperatures below 900 K, at pressures greater than 1 atm and an SC above the minimum for negligible solid carbon product but lower than three. When temperatures rise above 950 K, CH_4 is almost inhibited due to steam CH_4 reforming, when operating at 1 bar [81]. Increasing pressure reduces solid carbon up to 850 K but increases solid carbon formation above 850K [80]. In addition to maximising the conversion of glycerol carbon to CH_4, minimising solid carbon formation on the catalyst is integral to prolonging heterogeneous catalyst life and activity in reactors.

When carbon is formed on the catalyst it will block the active sites and reduce catalyst activity and therefore reduce the rate of reactions, increasing the time taken to reach the dynamic chemical equilibrium. Alternatively, carbon formed on the reactor can cause blockages and impede heat transfer.

Catalysts are necessary to maximise conversion and selectivity in steam reforming and methanation processes. Consequently the minimum and maximum operating conditions will be constrained by the catalyst. An example methanation catalyst is the commercial PK-7R low temperature CO methanation catalyst created by Haldor Topsoe is 463 K (190°C) [82]. Experimental work carried out by Adhikari et al. 2007 [83] found that conversion of glycerol to gaseous and liquid products occurred at 100% at 673K over nickel ceria catalysts although most thermodynamic models will assume 100% conversion at temperatures below 673K. Whilst pressure has been shown to favour methanation, pressures to be investigated should be 1-30 atm as this creates only mild stress on the majority of catalysts and prevents them from being damaged [84].

2.4.2 Substitution of energy required for soybean biodiesel production

The purpose of a GLT-SR process is substitute the grid energy demand in the soybean biodiesel plant with Bio-SNG. A soybean biodiesel plant has energy demands in the form of heat and electricity and a comprehensive life cycle energy analysis from soybean cultivation to production of soybean biodiesel has been produced by Pradhan *et al.* 2011 [85].

In this work the major system of a soybean biodiesel plant is separated into five sub-systems; soybean production, soybean transport, soybean crushing, biodiesel conversion and biodiesel transport. The energy demand for these subsystems is shown in Table 8.

	Fossil Energy Use (MJ/L biodiesel)	
Subsystem	Total	Fraction for Biodiesel
Soybean Production	6.0	1.0
Soybean Transport	1.2	0.2
Soybean Crushing	6.3	1.1
Biodiesel Conversion	4.0	3.3
Biodiesel Transport	0.3	0.3
Total	17.8	5.9
Biodiesel Total Energy Output	-	32.7
Fossil Energy Ratio	-	5.5

Table 8. Energy use for biodiesel production with co-product allocation and adjusted with energy efficiency factors adapted from Pradhan et al. *2011* [85].

The energy requirements for each subsystem are separated by energy feedstock e.g. natural gas, and provides a greater understanding of where in the major system energy can be substituted and what type of feedstock can be used to substitute energy. A full breakdown is shown in Table 9.

Subsystem	Life Cycle Energy (MJ/L)	Embodied Energy (MJ/L)
Soybean Production		
Diesel	2.4	2.0
Gasoline	0.9	0.7
LP gas	0.1	0.1
Natural Gas	0.3	0.3
Nitrogen	0.3	0.3
Phosphorus	0.2	0.2
Potassium	0.2	0.2
Lime	0.1	0.1
Seeds	0.5	0.5
Herbicide	0.8	0.8
Insecticide	0.0	0.0
Electricity	0.2	0.2
Soybean Transport	1.2	1.2
Soybean Crushing		
Electricity	1.6	0.8
Natural Gas	4.2	3.9
Hexane	0.5	0.5
Biodiesel Conversion		
Electricity	0.3	0.1
Steam from NG	0.4	0.2
Methanol	3.2	2.2
Sodium Methylate	0.1	0.1
HCl	8.30E-04	0.0
Biodiesel Transport	0.3	0.3
Total	17.8	14.8

Table 9. Breakdown of energy requirements by feedstock of different subsystems in the soybeans biodiesel refinery as calculated from Pradhan [85].

2.4.3 Energy from gas combustion

The method of gaining energy from the Bio-SNG in this work is by directly substituting the natural gas from the soybean biodiesel process for the production of steam. This will involve combustion of the bio-SNG in the same furnace as the furnace used for natural gas combustion with subsequent transfer of the heat via a heat exchanger to the water to raise

steam. The efficiency of the heat transfer from the combusted bio-SNG to the water will be assumed as 90%.

2.4.4 Gas heating value and wobbe Index

To determine the energy or calorific value contained in the Bio-SNG the heating value of the gas components must be calculated. Additionally the Wobbe index is used as a measure of the interchangeability of a gas and is calculated using the high heating value and specific gravity where the specific gravity is a ratio of the density of a substance to the density of a reference substance.

The calorific value was calculated by multiplying the high heating values (HHV) or low heating values (LHV) and mole fraction of the gas components (Equation 23). The heating values were obtained at 1 atm and 15°C. The specific gravity was calculated by dividing the mass of one mole of gas by one mole of air (Equation 24). The Wobbe index was calculated by dividing the HHV by the route square of the specific gravity (Equation 25).

$$\boldsymbol{HHV_G = \sum y_i HHV_i} \qquad \textit{Equation 23}$$

Where HHV_g is the high heating value of the gas, *y* is the mole fraction, *i* is the gas component, and *HHV* is the high heating value of the component. The reference temperature for combustion for heating values is 15°C (60F) and the reference temperature and pressure for standard density and volume for heating value are 15°C and 1 atm.

$$\boldsymbol{G_s = \frac{\sum y_i Mr_i}{\sum y_j Mr_j}} \qquad \textit{Equation 24}$$

Where *y* is the mole fraction, *i* is the gas component, *j* is the air component and *Mr* is the relative atomic mass of the component and G_s is the specific gravity in relation to air.

$$\boldsymbol{l_w = \frac{HHV_g}{(\sqrt{G_s})}} \qquad \textit{Equation 25}$$

Where l_w is the Wobbe Index, HHV_g is the high heating value of the gas and G_s is the specific gravity of the gas in relation to air.

2.5 GLT-SR Flow sheet

A process flow sheet of the GLT-SR plant is shown in

Figure 21 with the corresponding mass flows located in Appendix 1. To check how Aspen calculated the mass flow values, calculations were carried out to identify the energy value in the final composition of the product gas in Equation 23 and showed that Aspen Plus uses the low heating value.

The glycerol inlet feed was calculated based on the mass of glycerol generated from soybean biodiesel production. It was reported that 3,975,000 kg year^{-1} of soybean glycerol could be produced at a ratio of 0.119 kg L^{-1} biodiesel whereby the biodiesel density was taken as 0.8746 kg L^{-1} from the life cycle analysis model GREET [85,86]. Assuming the GLT-SR plant operates for 8000 hours, this led to 497 kg hr^{-1} of glycerol feed.

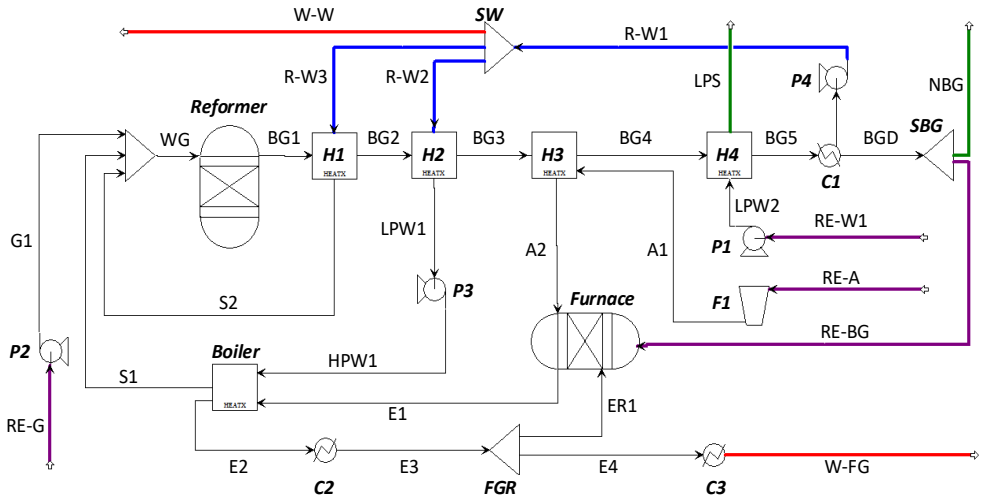

Figure 21. Aspen Plus V8.8 process flow sheet for GLT-SR. Burgundy streams with notation 'RE' are feed inlets, blue streams with notation 'R' are recycled water, red streams with notation 'W' are waste outlets and green streams are product outlets. Italicised and emboldened labels are blocks whereas standard font are streams. A=air, BG=Bio-SNG, BGD=Dry Bio-SNG, C=cooler, E=exhaust, F=fan, FG=flue gas, FGR flue gas recirculation, G=glycerol, H=heat exchanger, HPW=high pressure water, LPW=low pressure water, LPS = low pressure steam, P=pump, S=steam, SBG=splitter Bio-SNG, SW=splitter water, WG=water glycerol.

Glycerol and steam were fed to the adiabatic RGIBBS reformer and converted to gas. The gas was fed through a series of four heat exchangers and 1 condenser. *H1* and *H2* recycled heat to produce steam for use in the reforming process using water that was condensed out of the gas later in *C1*. *H3* pre-heated air for the furnace and *H4* recycled the remaining heat to produce low pressure steam. *C1* removed water from the gas and it was assumed that all the H_2O could be condensed and removed from the gas without the loss of CH_4 or CO_2 in the

condensate. The pressure drop associated with the outlet of any stream passing through a heat exchangers was assumed 10% of the inlet pressure associated with the block.

A fraction of the gas was recirculated to the RGIBBS *furnace* in the stream RE-BG and combusted with 10% excess air. This provided the remaining energy for steam generation in the *Boiler*. The *furnace* was assumed to have a heat transfer efficiency of 90% [87] and was achieved by adding a negative heat duty equal to 10% of the total positive heat duty produced by combustion of Bio-SNG. A fraction of the exhaust was recirculated to the *furnace* by the stream ER1 to maintain an exhaust temperature in E1 of 1315°C (1588 K), with a tolerance of 5°C. The water content in the exhaust was 16.7% mf, which fell within the range of 5.7-19.4% for flue gas recirculation in Liuzzo et al.'s [88] simulations for incineration. A fan was represented by the block F1 and was used to drive the combustion air to the furnace whilst pumps, P1 and P2, were used to circulate glycerol and water. The pumps efficiencies were 29.6% whilst the fan was modelled as an isentropic compressor with 72% efficiency and allowed the power input of the process to be recorded. Aspen plus calculated all heating values by low heating value.

To determine the biomass to fuel (η_{btf}) efficiency of the process, the biomass to fuel efficiency was used as detailed in *Equation 26*, before and after conversion from the gas to heat in a boiler.

$$\eta_{btf} = \frac{LHV_{Bio-SNG}.m_{Bio-SNG}}{LHV_{Glycerol}.m_{Glycerol}} \qquad \textit{Equation 26}$$

Where LHV is the low heating value and m is the mass.

2.6 Results

In the following section the results of each of the flow sheets created in are displayed. In addition the modelled thermodynamics of the direct methanation of glycerol are explored. The results of the flow sheets are discussed in terms of energy and efficiency as individual processes and when combined to produce different scenarios.

2.6.1 Thermodynamics of glycerol steam reforming for CH_4

The change in Gibbs free energy of reactions (ΔG) involved in direct methanation has been plotted in Figure 22.

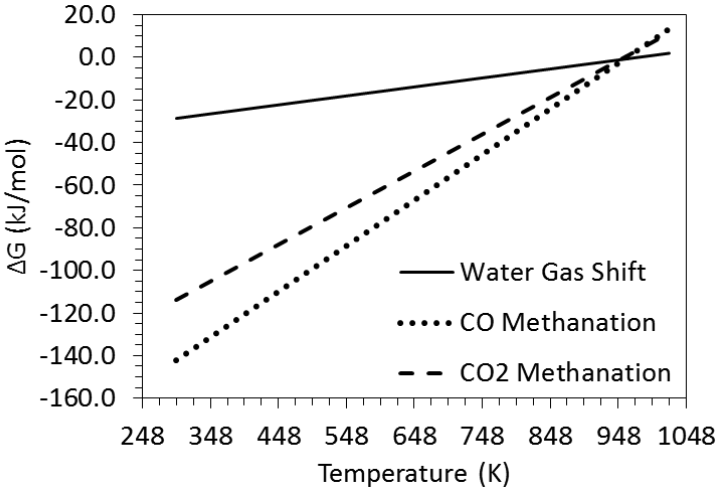

Figure 22. Variation in Gibbs free energy with temperature of the key reactions for direct methanation of glycerol under ideal conditions.

CO methanation had the lowest ΔG until 973K. Both CO and CO_2 methanation had lower ΔG than the water gas shift until 973K. As temperature increased, the rate of increase of the ΔG for both methanation reactions was more significant than that of the water gas shift. Consequently, at lower temperatures, methanation was more thermodynamically favourable than water gas shift, with CO methanation being the strongest. As temperatures increased, both methanation reactions became less favourable whilst water gas shift became stronger in comparison. More H_2 may be formed at equilibrium, consuming CO and reducing availability for CO methanation, but increasing the availability of CO_2 for methanation. This could explain why a reduction in CH_4 was observed experimentally by [36] as they increased the temperature in their direct methanation reactions.

At higher temperatures, the loss of CH_4 was attributed to steam reforming of CH_4 as well as the water gas shift reaction becoming more dominant than methanation. The latter was observed by Dieuzeide et al. [80] by studying reaction contributions.

The water gas shift and methanation reactions are both exothermic but CO and CO_2 methanation reactions have a more negative enthalpy of reaction and Gibbs free energy, when compared to the water gas shift at temperatures below 948 K (675 °C). The speed of the reactions and selectivity of the catalyst will be significant so the spontaneity of the reactions does not necessarily determine the actual distribution of products from glycerol methanation.

2.6.1.1 Isothermal CH_4 and carbon formation

Figure 23 describes the minimum SC required to accomplish zero carbon at equilibrium under isothermal conditions. The minimum SC varied for each temperature within the range of temperatures 400-1000 K (error ±0.01 SC). The condition of zero carbon at equilibrium for Aspen Plus simulations was defined here as less than 1×10^{-5} mol hr^{-1} in the product gas stream. Areas to the left of the curve contained carbon as equilibrium product whereas areas to the right of the curve did not.

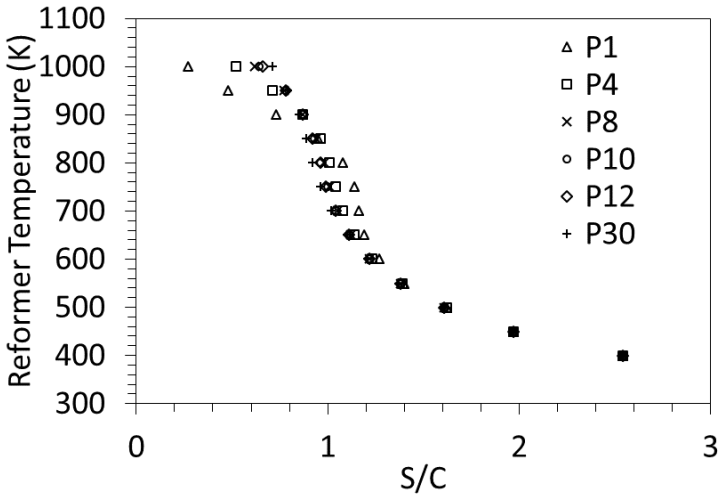

Figure 23. Carbon product boundaries for pressures of 1, 4, 8 and 10 atm (P1-P10) under the IDEAL property method where SC is steam to carbon ratio. Area on the left of the curves indicates solid C as significant equilibrium product.

Starting from 550 K and descending to 400 K all the pressure dependent points for zero carbon converged, indicating that pressure had a minimum effect on the minimum SC for zero carbon formation in this temperature range. At 600 K the points diverged, firstly with P1 (1 atm) and then with P4 (4 atm) at 650K. The largest range occurred at 750 K with P30 (30 atm) requiring an SC of 0.96 and P1 requiring an SC of 1.14. All points except P1 converge again at 900K before diverging again at 950 K. Between 600 K and 800 K increasing pressure reduces the SC required for zero carbon formation. Above 850 K this trend is reversed. Adhikari et al. 2007 [79] reported an SC of at least 1 was required to reduce carbon to zero

at 800 K and 900 K and a SC between 1 and 2 for 700 K and 600 K. The results within Figure 23 fall within these boundaries. Dieuzeide and Amadeo [80] reported reductions in carbon formation at elevated pressures below 900 K and the reverse above 900 K. This manifests in the requirement for smaller SC for zero carbon formation below 900 K at elevated pressures and larger SC above 900 K at elevated pressures.

Figure 24 describes the change in theoretical maximum CH_4 with reformer temperature at different pressures and at the minimum SC ratio for zero carbon. The CH_4 yield is expressed as the percentage ratio of the Aspen Plus calculated equilibrium CH_4 yield to the stoichiometric maximum, according to *Equation 16*.

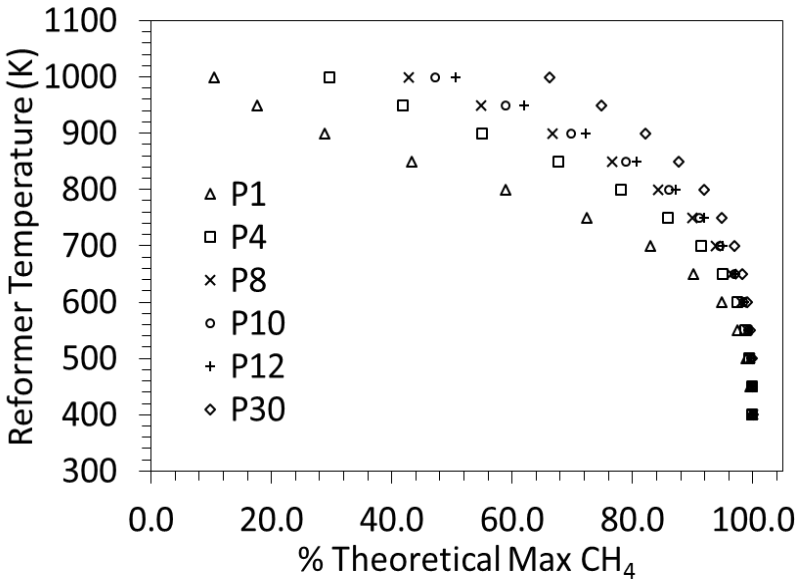

Figure 24. Percentage maximum of theoretical CH_4 yield at the minimum SC for zero carbon formation under the IDEAL property method.

As reformer temperature increased, less of the glycerol converted to CH_4 and more converted to H_2 and CO. Additionally at the minimum SC for zero carbon formation, as expected, the maximum CH_4 was produced as increasing the SC was found to favour H_2 production rather than CH_4 production [79]. Dieuzeide and Amadeo mentioned that the maximum H_2 yield with temperature tended towards higher temperatures at increased pressures [80]. The same was true for CH_4 production. For example, at 1000 K the maximum CH_4 yield under 1 atm was 10%, rising to 30%, 42% and 47%, 50% and 66% for P4, P8, P10, P12, and P30 (4 atm – 30 atm) respectively. Whilst increasing the pressure to 30 atm was significant at 1000 K, less CH_4 yield was gained when observing the pressure effect at low temperatures. This can be seen in Figure 25 which shows more detail in the region of 80-100% of theoretical maximum CH_4 of 1.75 moles per mol of glycerol. Note that 86% of the

theoretical maximum CH_4 yield would correspond to just half the carbon content of the glycerol feed converting to the intended CH_4 product.

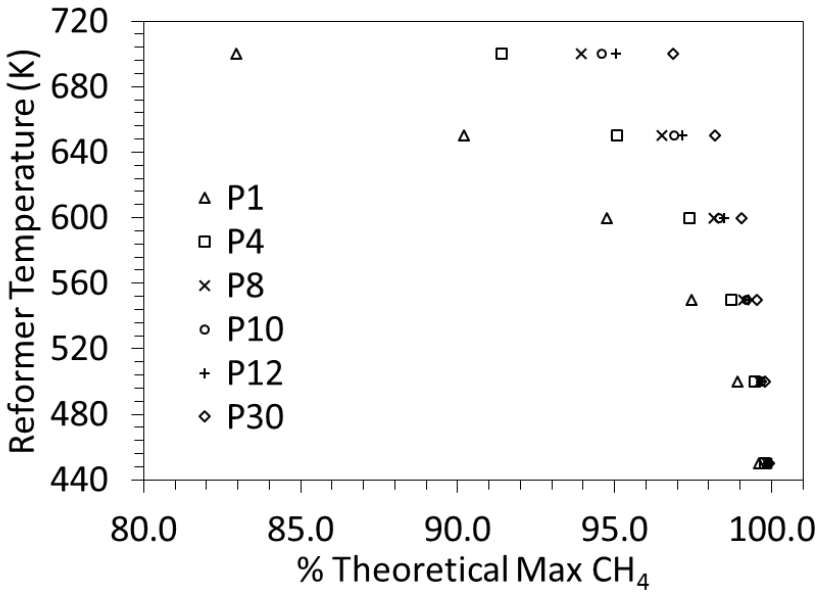

Figure 25. Percentage maximum of theoretical CH_4 yield at the minimum SC for zero carbon formation under the IDEAL property method between 420 and 720K.

At 600 K, increasing the pressure from 1 to 4 atm improved the CH_4 yield by 2.5%, but increasing further to 8, 10, 12 and 30 atm increased the yield an additional 0.8, 0.2, 0.1 and 0.5%. At 600 K, it would be advantageous to increase the reformer pressure to at least 8 atm, but beyond this, increasing pressure to 30 atm only yielded a 0.7% increase of the theoretical maximum CH_4 in addition to the 3.3% by increasing the pressure from 1 to 8 atm. The higher the operating temperature, the more worthwhile it was to increase the pressure to 30 atm to maximise CH_4 yield.

When operating below the temperature range of 500 K, maintaining an operating pressure of 1 atm was sufficient to achieve a yield of 99% of the theoretical maximum CH_4 under ideal conditions. To maintain this yield at 600 K, the pressure would need to increase to 30 atm. This revealed very high sensitivity of the CH_4 yield to temperature and pressure.

A consideration is the minimum temperature for conventional methanation catalysts of 463 K (190°C). Based on the results in Figure 24 and Figure 25, maintaining a reformer temperature within the region of 463-600 K at pressure of 8 atm would be desirable to achieve conditions appropriate for the current generation of commercial methanation catalysts, and a low enough temperature to enable the highest CH_4 yields. From Figure 23, at 600 K an SC of at least 1.2 and at 450 K of at least 2.0 would be required to minimise

carbon equilibrium product and therefore maximise the feed carbon that could be converted to CH_4.

Based on the experimental work by Imai, they found that 673K achieved the highest CH_4 production at 0.3 mPa (3 bar) when compared to 0.1 mPa (1 bar) and 623 K.

2.6.1.2 Property methods sensitivity

The effect of the property method at 1 and 30 atm on the minimum SC for zero carbon product during glycerol steam reforming is shown in Figure 7.

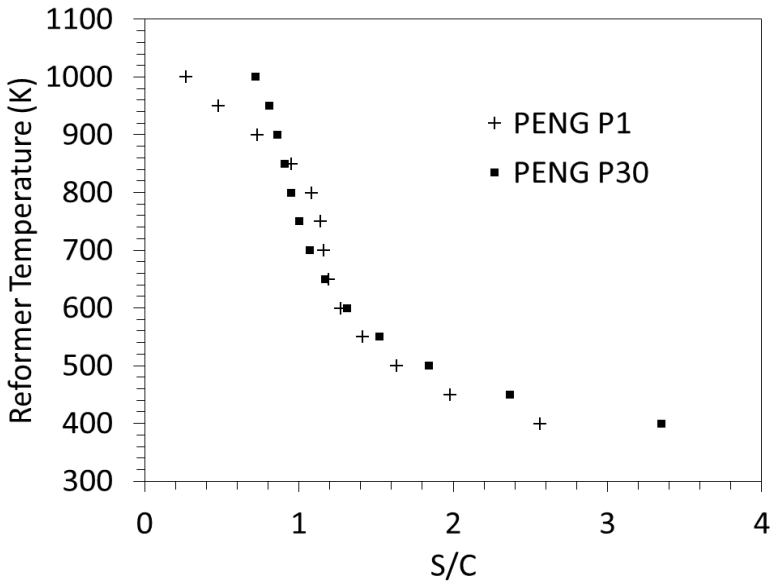

Figure 26. Property method sensitivity for the minimum SC to produce negligible carbon at P1 and P8 for PENG.

Property methods IDEAL, UNIQUAC and NRTL produced identical results where carbon product's sensitivity to SC and reformer temperature was concerned.

Above 650K the choice of property method had a negligible impact on the performance of glycerol steam reforming. At and below 600 K for P1 (1 atm) and 650 K for P30 (30 atm), the points began to diverge away from the ideal for PENG and NRTL-RK. Figure 26 shows the results for PENG at 1 and 30 atm. At 30 atm the SC required for zero carbon was larger than at 1 atm. As temperatures decreased, the SC required to maintain zero carbon also increased. PENG and NRTL-RK property methods went against the IDEAL trend that increasing pressure below 900 K slightly reduced carbon product. The pressure effect was not observed by property methods relying on the ideal properties relationship.

PENG and NRTL-RK do not depend upon the ideal gas law for their vapour phase equation of state calculations whereas IDEAL, UNIQUAC and NRTL do. PENG and NRTL-RK estimated

greater steam to carbon ratios required to produce near zero solid carbon formation at temperatures below 700 K. Based on the results and the method from Carlson [89] the NRTL property method was chosen for the plant design.

There was little to no variance in the CH_4 yield at point of zero carbon when varying property methods. The PENG equation of state method and NRTL-RK activity coefficient method produced the same results as the IDEAL method for predicting CH_4 production by glycerol steam reforming when minimizing Gibbs free energy under constant pressures and temperatures. Experimental data is required to validate the property methods.

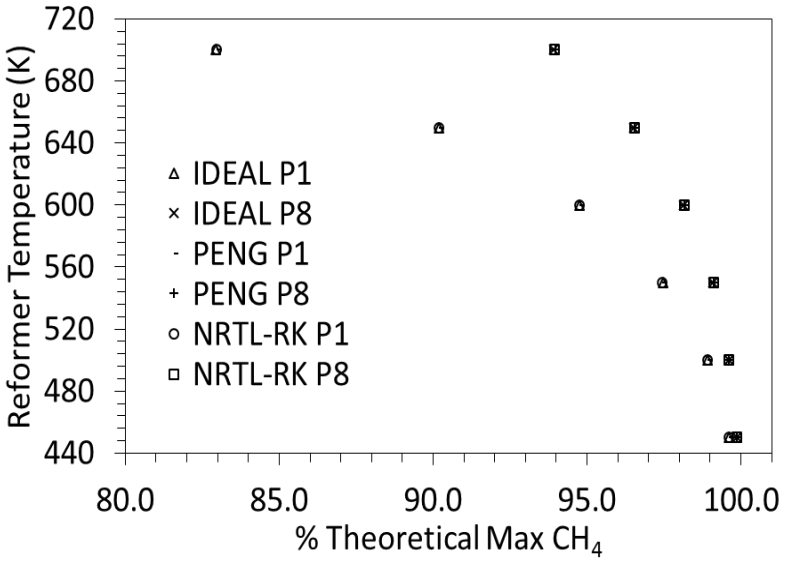

Figure 27. Property method sensitivity for the CH_4 yield expressed as % theoretical maximum CH_4 for P1 (1 atm) and P8 (8 atm)

2.6.1.3 Adiabatic Temperatures and Vapour Fraction

For direct methanation of glycerol, the process is mildly exothermic when compared to CO or CO_2 methanation, designated by the less negative enthalpy change in *Equation 17* when compared to the strongly negative ΔH of *Equation 16* and *Equation 18*. Consequently, the reactor would require cooling to maintain isothermal conditions. In practice, maintaining a constant temperature in a reactor housing exothermic reactions is difficult and requires accurate heat transfer controls. For a mildly exothermic reactor such as one carrying out direct methanation of glycerol, it is more practical and cheaper to operate the reactor without inner cooling, therefore the plant model in this work used adiabatic conditions in the reformer.

The minimum temperature for total vaporisation where the vapour fraction of a water and glycerol mixture is equal to 1 can be calculated in Aspen Plus, using the binary mixing analysis

mode. The results are depicted in Figure 28 at 8 atm. With a SC of 2 the minimum vaporisation temperature was 576 K and SC of 3 required 560 K creating a range of useful temperatures for the minimum vaporisation of 560 to 576 K for any SC in between 2 and 3.

When the minimum temperatures of vaporisation were used in a steam reforming process for CH_4 production in an adiabatic reactor, the outlet reformer temperatures were greater than 700 K. This is above the optimal temperature to achieve maximum CH_4 production and is a result of the exothermic nature of methanation. To reduce the temperature of operation, the temperature of the inlet feed of glycerol and water can be reduced. Consequently, the vapour fraction of the inlet stream will also be below 1 representing a liquid vapour mix of glycerol-water feed. Alternatively generating steam and combining it with glycerol that is below its dew point will have the same effect. As a result, the glycerol will become partially vaporised in the reformer and as methanation takes place, the heat generated is used up to further vaporise the glycerol and prevent temperatures increasing above 700 K. This method of limiting reformer temperatures in exothermic reactors has been used previously in autothermal reforming (ATR). The method has been demonstrated experimentally by Liu et al.[71] using a nebuliser with an initial energy input to initiate partial oxidation and steam reforming and by Rennard et al. [76,77]. In the present process design, instead of the exothermic oxidation reactions driving the endothermic steam reforming, it is the exothermicity of the methanation reaction that is reined in.

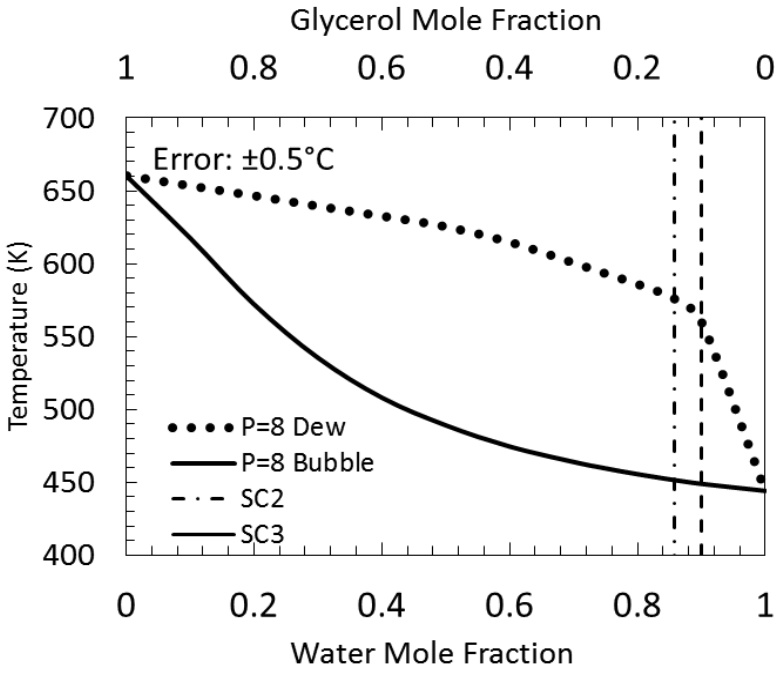

Figure 28. Vapour phase diagram for glycerol water mixtures at 8 atm.

2.6.2 GLT-SR

The potential energy savings associated with the GLT-SR process are described in this section. To calculate the energy in the bio-SNG, the composition of the gas was used which provided the data for energy efficiency calculations.

2.6.2.1 Bio-SNG composition

The composition and characteristics of the simulated Bio-SNG were in between landfill gas and biogas from anaerobic digestion (A.D.) as shown in *Table 10*. As a consequence, Bio-SNG was not suitable for grid injection or as vehicle fuel without further gas upgrading via CO_2 separation. However the Bio-SNG was suitable for combustion on site for heat or in a combined heat and power engine. As the pure glycerol feed contained no H_2S nor silica (Si), combustion of the Bio-SNG will have less corrosive or fouling effects on the machinery than landfill or biogas. On the other hand, this work focuses on pure glycerol as feed. If crude glycerol were used, there would most certainly be an effect on the final composition of the Bio-SNG due to residues from common transesterification catalysts and other contaminants, as shown by studies utilising crude glycerol for syngas production [90].

	Units	Bio-SNG (1 atm, 464 K, SC 2)	Bio-SNG (8 atm, 474 K, SC 2)	Landfill Gas	Biogas from A.D
Methane	Vol-%	41	55	45	65
Hydrogen	Vol-%	21	4	0-3	0
Hydrocarbons C2+	Vol-%	-	-	0	0
Hydrogen Sulphide	ppm	-	-	0-100	0-4000
Carbon Dioxide	Vol-%	38	41	15-40	30-40
Nitrogen	Vol-%	-	-	5-40	0.2
Oxygen	Vol-%	-	-	1	
Carbon Monoxide	Vol-%	0	0	-	-
Ammonia	ppm	-	-	5	100
Water	Vol-%	0	0	-	-
Chlorine (Cl^-)	Mg/Nm^3	-	-	20-200	0-5
HHV_G	MJ/kg	17.9	18.6	-	-
LHV_G	MJ/kg	16.0	16.7	12.3	20
Density	Kg/Nm^3	1.01	1.14	-	-

Table 10. Comparison of Bio-SNG biogas and landfill gas. Landfill gas and Biogas data are taken from Clark et al.[17].

The heating value of Bio-SNG decreased when produced at 1 atm because of the increase in mole fraction of hydrogen. At 8 atm the hydrogen mole fraction is 4% whereas at 1 atm it is 20%. Increased hydrogen content leads to a lower density per Nm^3. Operating at 30 atm produced nearly identical gas composition as 8 atm. To produce a gas with the highest heating value, CH_4 mole fraction and minimum H_2 mole fraction the process should operate at 8 atm.

2.6.2.2 Energy and efficiency

The energy balance of the GLT-SR process to produce Bio-SNG is described in Figure 29. A biomass to fuel efficiency was calculated as 81% before the addition of any Bio-SNG required to raise the steam. When considering the energy required to raise the steam the efficiency decreased to 69%. If the steam at 1.5 atm can be utilised the efficiency before and after the consideration of the required energy to raise steam increases to 94% and 81% respectively. The ability to utilise the steam at 1.5 atm has a significant impact on the efficiency of the process and uses such as space heating or heating requirements in the transesterification process should be found to maximise the energy use from glycerol.

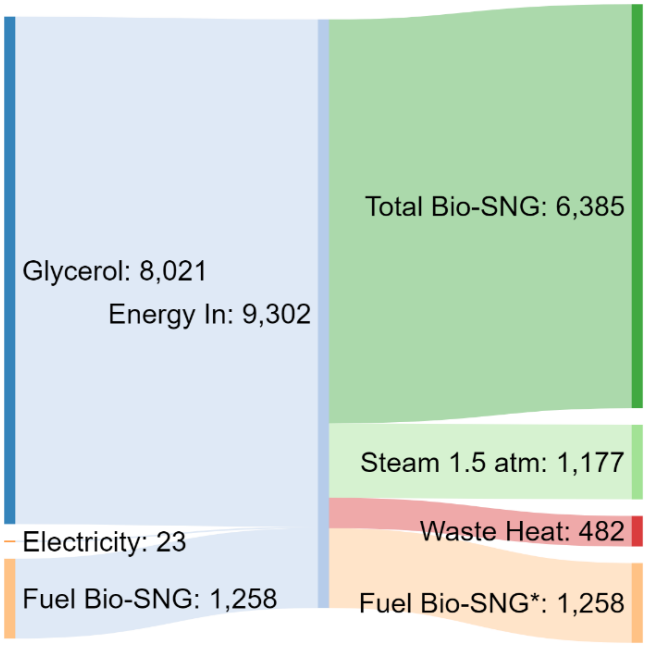

Figure 29. Sankey diagram of the GLT-SR process.

The impact of steam to carbon ratio and pressure on the biomass to fuel efficiency and inlet temperature can be seen in Figure 30. As the SC increased the efficiency was reduced at all pressures. This corresponded to an increase in the energy required to produce steam due to the increased mass of water as SC increased. As more energy was needed, more of the Bio-SNG was re-routed to the furnace, reducing the net Bio-SNG produced and reducing the biomass to fuel efficiency. For a given SC, efficiency increased with increasing pressure, this was related to conditions in the liquid glycerol and saturated steam mixer prior to the reformer. At the higher pressure, the saturated steam temperature at the mixer inlet resulted in the mixer outlet's glycerol/water mixture of vapour fraction lower than 1 with a temperature that exceeded the minimum for catalyst activation (463 K). This temperature became the reformer's inlet temperature, and is shown in the legend of Figure 30 for

pressures 8 and 30 atm (475 K and 536 K). In contrast at 1 atm, the saturated steam temperature at the mixer inlet would have resulted in an outlet mixer temperature lower than the minimum for reformer catalyst activation, thus necessitating an extra heat duty for superheating steam prior to the mixer to reach just above the minimum reformer catalyst temperature, as shown in the legend of Figure 30 1 atm, 464 K). Increasing the pressure above 1 atm improved the efficiency of the process at higher steam to carbon ratios because the product gas contained a great concentration of CH_4. The significance of the improvement diminished above 8 atm as more energy was required to raise the steam.

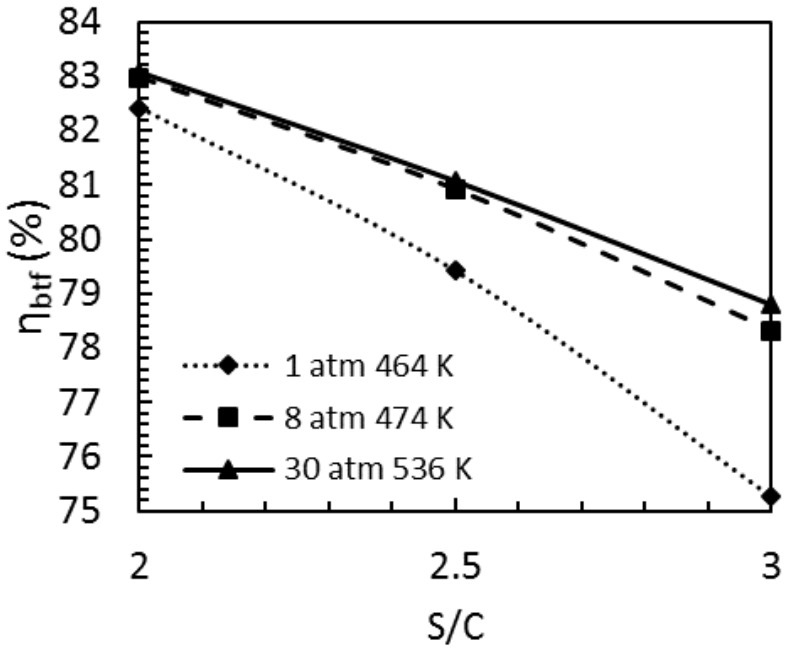

Figure 30. Biomass to fuel efficiency versus steam to carbon ratio at pressures 1-30 atm with reformer inlet temperatures.

The outlet temperature of the reformer as varying with steam to carbon ratio at different pressures is plotted in Figure 31. At higher steam to carbon ratios the outlet reformer temperature reduced.

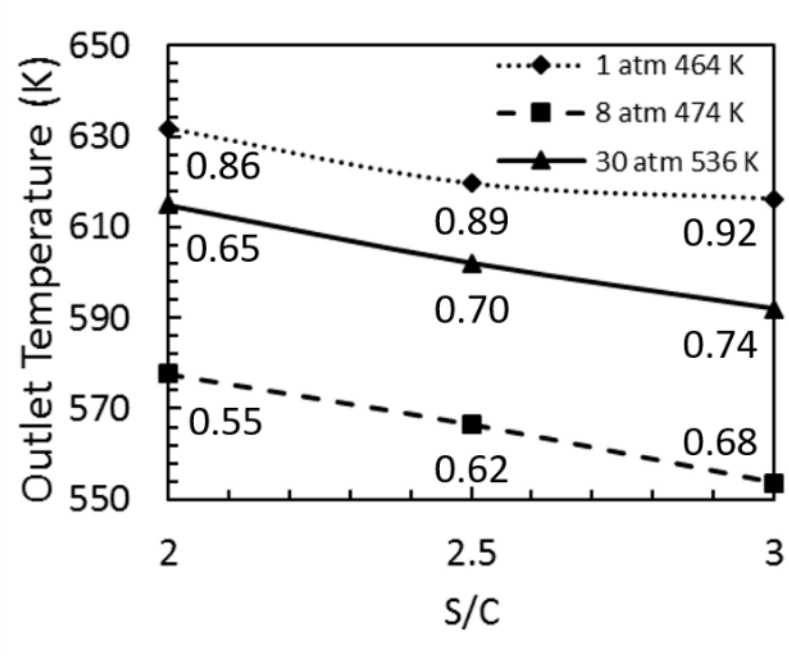

Figure 31. Outlet temperature versus steam to carbon ratio at pressures 1, 8, and 30 atm and change in inlet vapour fraction with SC at different pressures. Vapour fraction at each temperature and SC is noted at each point to two decimal places.

The pressure of 8 atm produced the lowest outlet reformer temperatures whereas 1 atm had the highest outlet reformer temperatures. Increasing the pressure reduced the vapour fraction at the inlet but also increased the inlet reformer temperature as mentioned earlier. The reduced vapour fraction allowed more energy from exothermic reactions to be utilised for vaporising the water and glycerol, reducing the outlet reformer temperature. However, this was mitigated by increasing the inlet temperature to the reformer. For this reason, increasing the pressure from 8 atm to 30 atm increased the outlet reformer temperature even though the inlet vapour fraction at 30 atm was lower.

From this modelled data operating at 8 atm provided the benefits of higher biomass to fuel efficiencies than at 1 atm, via lower increases in temperature at the reformer outlet than 30 atm and achieving the minimum inlet temperature for catalyst operation.

High pressure steam recovery allowed up to 21% of the high-pressure steam to be re-generated from the steam reformer output stream. Flue gas recirculation (FGR) recycled 20% of the exhaust gas to the furnace to maintain an outlet temperature of 1313 °C (1591.15 K). The furnace required 17% of the total Bio-SNG as fuel for the boiler, when the furnace operated at an efficiency of 90% and energy transfer to the steam operated at an overall 81% as calculated. The high and low-pressure steam produced were not superheated. Overall, 1 kg of glycerol produced 0.91 kg total Bio-SNG with a requirement of 1.18kg of non-superheated steam at 8 atm under this GLT-SR process. The net Bio-SNG produced was 0.763

kg hr^{-1} kg^{-1} glycerol as 0.147 kg hr^{-1} Bio-SNG was required for heating the GLT-SR process, assuming a combined boiler and furnace efficiency of 90%.

Decreasing furnace efficiency is expected to occur over time unless it is maintained. The results of a sensitivity analysis to explore the effects of reducing the heat transfer efficiency are shown in Table 11 when Bio-SNG is treated as the product with no further conversion. For every 10% decrease in efficiency for the heat transfer in the furnace and boiler a reduction in η_{th} and η_{btf} of 1.6% occurs. This is equivalent to 126 MJ hr^{-1} of Bio-SNG. This manifests in the increase in Bio-SNG required for the furnace, diverting energy away from the net Bio-SNG which could be used to offset natural gas. Maintaining the heat transfer efficiency through good boiler and furnace maintenance will contribute to maximising the Bio-SNG potential. Additionally, upgrading from an old and less efficient boiler to a more modern and more efficient boiler could increase the net Bio-SNG product from 2 to 9 %.

Furnace efficiency (%)	*Percentage of total Bio-SNG required for Furnace (%)*	*η_{btf} (%)*
100	*16*	*83*
90	*18*	*81*
80	*20*	*79*
70	*21*	*78*
60	*23*	*76*
50	*25*	*74*

Table 11. Effects of decreasing furnace efficiency on required Bio-SNG.

2.6.2.3 Potential energy savings in a soybean biodiesel plant

Based on the life cycle energy data by Pradhan (Table 9) it is possible to determine the natural gas energy that could be offset from the GLT-SR process. The breakdown of natural gas energy requirements is shown in Figure 32 together with the quantity of Bio-SNG that could be produced. In this case it is assumed that the Bio-SNG produced substitutes the natural gas that would be used in the soybean crushing stage of the soybean biodiesel plant. This adheres to the assumption that the Bio-SNG will be used on site with minimal transportation and treatment after it is produced. Whilst natural gas is also required at the cultivation stage, this would require transport from the refinery to the agricultural area, necessitating additional transportation energy requirements and reducing the net gain of energy.

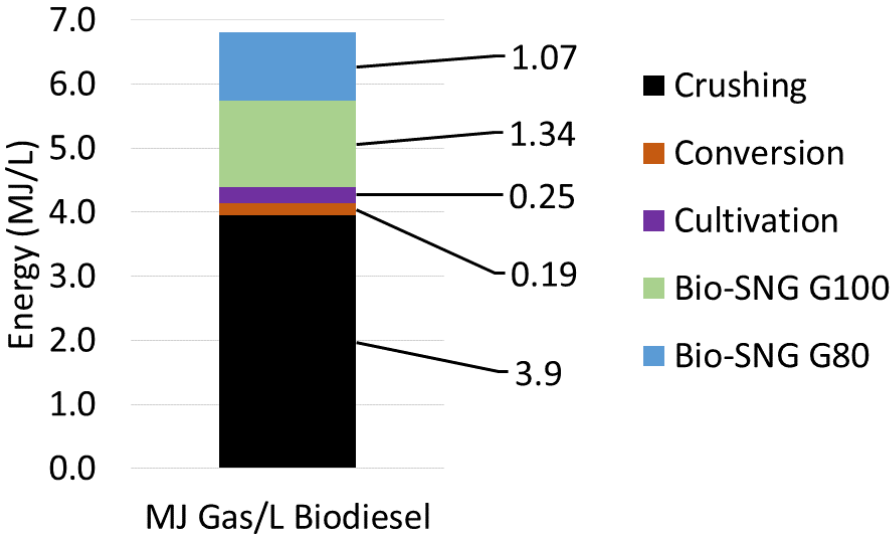

Figure 32. Embodied energy bar chart for the natural gas requirements of different stages in the soybean biodiesel refinery. G100 represents 100 wt % free glycerol whereas G80 represents 80 wt % free glycerol.

Crushing soybeans is the stage where the majority of natural gas is required. Crushing, conversion and cultivation stages required 90%, 4% and 6% of the total natural gas demand in the biodiesel production process respectively for the production of steam. In the crushing subsystem natural gas is combusted to generate steam to crush the soybeans and liberate the soybean oil from the meal and occurs at the biodiesel plant. Therefore, the crushing stage appears to be the most appropriate system for substitution of natural gas with Bio-SNG as the biodiesel refineries will already have a furnace where the bio-SNG could be combined with natural gas. Assuming the same efficiencies as Pradhan for gas conversion to energy, the maximum natural gas that could be substituted would be 30% of the total natural gas requirement (4.4 MJ/L). This value drops to 24% when considering G80 rather than G100 and is based on the assumption that contaminants in the glycerol would not impact the conversion to Bio-SNG. The overall embodied energy that could be substituted in the soybean biodiesel production process is 9.0% and 7.2% for G100 and G80 respectively. Significant factors impacting the net energy are the quality of the glycerol and the level of contaminants, how much glycerol is produced from the refinery and the efficiency of the furnace and boiler when dealing with Bio-SNG in the feed.

2.7 Summary and Brief Conclusions

Based on the design needs it was determined that the thermodynamics of glycerol steam reforming must be analysed. From this analysis, the optimum conditions to produce CH_4 were applied to a process model of a GLT-SR plant. The bio-SNG product was burnt on site in a furnace to prevent energy losses from upgrading further and to utilise the furnace of the biodiesel refinery. The process model can be used as a basis to extend the system boundary include upstream purification methods or downstream gas purification and energy utilisation methods. The net energy gain and factors affecting CH_4 production, and therefore energy efficiency, were determined along with potential energy savings at a soybean biodiesel plant if the GLT-SR process was implemented on site.

The process produces enough bio-SNG to substitute up to 30% of the natural gas requirement of soybean biodiesel, including the energy required to run the process, under ideal conditions with a boiler efficiency of 90%. If the crude glycerol contains roughly 80 wt% free glycerol this value drops to 24%. The quality of crude glycerol will be significant in determining the energy substitution potential as well as a high boiler efficiency to minimise energy losses. The limitation of the work is that it does not account for any contaminants which could increase or decrease the energy in the output bio-SNG such as methanol or from catalyst poisoning respectively and is essentially working at ideal conditions. The product gas composition and energy value will need to be validated against experimental work.

The outputs from the process model can be used in further economic and environmental analysis. The former can use the equipment sizes for capital cost estimations whereas both can apply the material inputs and outputs, the former for operating costs and the latter for environmental impact analysis. The economics will be discussed in Chapter 3 whilst the environmental modelling will be discussed in Chapter 4.

2.7.1 Brief Conclusions

- A process model of a glycerol low temperature steam reforming (GLT-SR) process was successfully modelled in Aspen Plus using pure glycerol.
- Ideal conditions to maximise CH_4 production from glycerol were 8 atm, and 474 K at a steam to carbon ratio of ~2.
- Up to 30% of the natural gas requirement of the biodiesel refinery could be substituted using bio-SNG produced from GLT-SR.
- The impact of using crude glycerol on the process must be considered and investigated.

3 Techno-economic analysis

3.1 Introduction

In this chapter, a technoeconomic analysis is produced in excel based on the equipment sizing outputs from chapter 2's Aspen Plus process model. Technoeconomic analysis is a method of estimating the monetary cost and value of a technology over its lifetime with the main stages from the design process shown in Figure 33.

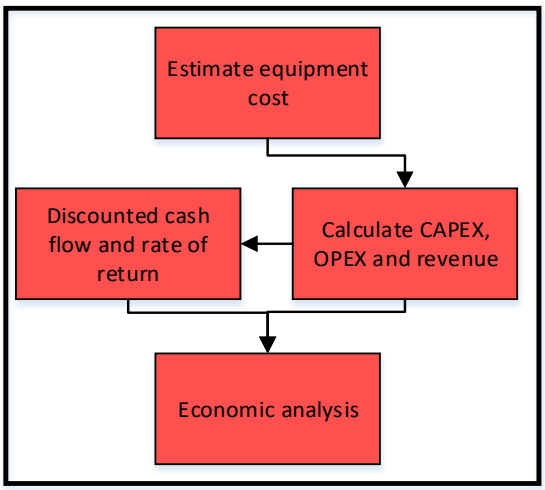

Figure 33. Technoeconomic analysis steps from the design process

Monetary costs involve the expenditure required to setup a plant, known as capital expenditure (CAPEX), as well as the expenditure to operate (OPEX) the plant over the span of its operational lifetime, including construction, start up and shutdown. Monetary value or revenue is assigned based on the value of the main product and any by-products produced. Combining the CAPEX, OPEX and revenue produces distinct composite values that are related to the plant's profitability. Assigning constraints on any of these variables allows a bespoke economic feasibility analysis and if these constraints are met and the outcome is profitable, it can be concluded that under the conditions set, the plant is economically feasible. Consequently assumptions must be made and the results will only apply to each specific scenario. Methods of calculating each of the monetary costs for the GLT-SR plant, the assumptions made in this work, limitations on the method used and the results from the modelling are detailed in this chapter.

3.2 Literature Review and Methodology

As the method used in this work's techno-economic analysis to is a combination of different methods from the literature, the method will be explained in tandem with the literature review.

3.2.1 CAPEX

In general, there are five classes of CAPEX estimation, as shown in Figure 34. As the class decreases from C5 to C1 such that C1 is the highest level of CAPEX estimate, the required effort to prepare such an estimate increases but so does the level of accuracy.

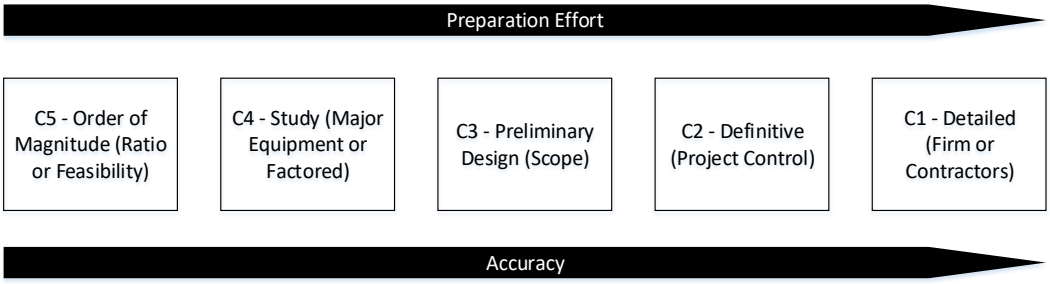

Figure 34. Class of CAPEX estimates indicated by the label C followed by a number as described by Turton [91].

The class of estimate is restricted by what resources are available and what the aim of the estimate is. When designing a new process each of the classes of estimate would be used in sequence. Initially C5 and C4 studies are used to assess the feasibility of different scenarios for the project to provide more definition. Several process alternatives are compared and the least profitable and technically sound are screened out. A C3 study is used to determine a more realistic budget for authorisation or control when applied to the more profitable scenarios. C1 and C2 are produced when the project is well defined with the aim of putting in a bid for the value of CAPEX required. From C1 studies a decision is usually made to scrap or go ahead with the plant. A C5 study would require basing the plant on previous designs and scaling up. As there are no glycerol steam reforming or direct methanation plants a C5 study would have to be based on similar technologies such as steam methane reforming, the most common process of hydrogen production from natural gas.

In this work a C4 Major Equipment study has been produced as only process modelling and initial laboratory scale experimental data is available and plant data from former plants is not available.

The uncertainty associated with each type of estimate is shown in Table 12.

Estimate Class	Project Definition (% project completion)	Methodology	Minimum Uncertainty (%)	Maximum Uncertainty (%)
Class 5	0-2	Stochastic/ Judgement	+24 to -16	+120 to -80
Class 4	1-15	Stochastic	+18 to -12	+72 to -48
Class 3	10-40	Primarily stochastic	-12 to +8	+36 to -24
Class 2	30-70	Primarily Deterministic	+6 to -4	+18 to -12
Class 1	50-100	Deterministic	+6 to -4	

Table 12. Uncertainty associated with different CAPEX estimation classes calculated from Turton [91].

Within the methodology, stochastic is defined as creating a range for the size or cost. Judgement is based on the engineer's previous experience and deterministic i.e. with absolute certainty would be based on real world up to date machinery and parts quotes from companies. Where a method is described as primarily this shows that some stochastic or judgement has been applied where data is not available.

Estimations of CAPEX are made by calculating the cost of the required equipment. Inaccuracies in CAPEX costs usually stem from exclusion of equipment from the estimate or exceeding the sizing limit of the calculated cost curve for the designated piece of equipment. As the project progresses, plant designs evolve and estimates are subject to change. For many estimates, as with this work, the required equipment is designated by a process flow diagram (PFD). Using Aspen Plus, a process flow sheet was produced in chapter 2 and providing the measurements for the equipment based on the mass flow rates of material.

3.2.2 Equipment Cost

Costing equipment based on size can be carried out in three main ways. The first and most accurate is by a price quote from a vendor, the second is based on cost data from previously purchased equipment of the same type. The third type is based on summary graphs or cost curves that are available for different types of equipment. With most academic studies the third method is usually the most available as access to equipment data is limited. Any data obtained by the third method must be time adjusted from the period the data was obtained to the current year using an indexing factor.

Estimation of the purchasing cost of the equipment can be carried out by estimating the size or capacity of the equipment and assuming what material the equipment is constructed from. It is assumed that all of the equipment in the process is constructed of carbon steel.

The size of the equipment is based on Aspen Plus simulations and determined by the flow rates, energy requirements or dimensions for each component.

In this work the equipment module costing technique as described by Turton [91] was used to produce a Major Equipment or Factored estimate. A similar method is described in Sadhukan [92] and Towler [93] as well as Sinnot [57].

$$C_{BM} = C_p^o . F_{BM} \qquad \textit{Equation 27}$$

Where C_{BM} is the bare module equipment cost including the direct and indirect costs for each unit, F_{BM} is the bare module cost factor which accounts for the specific materials of construction, operating pressure and installation costs including: installation materials and labour, freight, insurance and taxes, construction overhead and contractor engineering expenses and C^o_p is the purchased cost for the base conditions of the equipment e.g. ambient pressure and carbon steel.

F_{BM} is calculated by addition of the two constants relevant for the materials and pressure for each piece of equipment. Values for F_{BM} have been calculated for different pieces of equipment in the literature. The equipment in this process operates under 10 bar (10^5 Pa) and as a consequence is not impacted by the pressure factor increasing the simplicity of the calculations.

Cost curves were plotted according to *Equation 28*, where K_1, K_2 and K_3 are constants unique to the cost curve for a specific equipment module at ambient pressure and material carbon steel, and *A* is the size factor relating to the equipment module [91]. Cost curves are limited by what historical data on the size of the equipment is available. Usually the cost curve is accurate within a minimum and maximum size of the equipment.

$$log_{10}C_p^o = K_1 + K_2 log_{10}(A) + K_3 [log_{10}(A)]^2 \qquad \textit{Equation 28}$$

K values and the type of unit for *A* are represented in Table 13 and were taken from Turton *et al.* (2013). The values for *A* were calculated using Aspen Plus.

Equipment	R Value [94]	Unit	Pressure	A	K_1	K_2	K_3
Double Pipe Heat Exchanger	0.01	Area, m^2	8	8.56	3.34	0.27	-0.05
Centrifugal Radial Fan	0.01	Flow, $m^3 s^{-1}$	1.4	0.15	3.54	-0.35	0.45
Furnace FT=1	0.01	Duty, kW	8	500.0	3.07	0.66	0.02
Pump SS centrifugal	0.01	kW	8	0.62	3.39	0.05	0.15
Air Cooler	0.01	Area, m^2	1.4	0.67	4.03	0.23	0.05
Reactor, jacketed agitated	0.04-0.06	Vol, m^3	8	0.15	4.11	0.47	0.00
Catalyst	0.04-0.06	kg	8	-	-	-	-

Table 13. Constants associated with Equation 28 for equipment module cost and R values for learning curves. Catalyst was a defined cost per unit mass.

Cost data for the reference equipment, and therefore the scaled cost data, will only be valid for that year. Costs vary with time; therefore a cost index method must be applied to update the costs that have been taken from previous years, for use in the current cost analysis which is shown in *Equation 29*. In this case *Equation 27* from Towler and Sinnot utilises a CEPCI from 2010 and must be updated using *Equation 29* for the current year. The reactor was chosen as Reactor, jacketed, agitated due to the size restriction of the cost curves in Turton [91]. A non-agitated reactor would be preferred but due to the size (0.15 m^3) the cost curve would not be accurate as the minimum value was 0.5 m^3. On the other hand, the jacketed reactor cost curve was accurate to 0.1 m^3.

$$C_{pr} = C_o \left(\frac{I_{pr}}{I_o}\right) \qquad \textit{Equation 29}$$

Where C_{pr} is the present cost, C_o is the original cost, I_{pr} is the present index value and I_o is the original index value.

The cost indices are published in the literature. For this work, the Chemical Engineering Cost Index (CEPCI) is utilised. Once the cost of equipment has been determined additional engineering costs can be estimated to calculate the final CAPEX value using Lang, Guthrie's [91] or the NETL method [95]. For this work the NETL method was used in a similar way to work carried out by Rotunno et al. [96] by combining the capital cost estimation with cost curve estimations from Turton[91].

The NETL method is described in Figure 35 and has recently been used in publications by Ogidiama [97,98] and produces a final CAPEX value in the form of the total as spent capital (TASC). TASC is composed of the following values as described in Figure 35; total overnight costs (TOC), total plant cost (TPC), engineering procurement and construction cost (EPCC), and the base equipment cost (BEC).

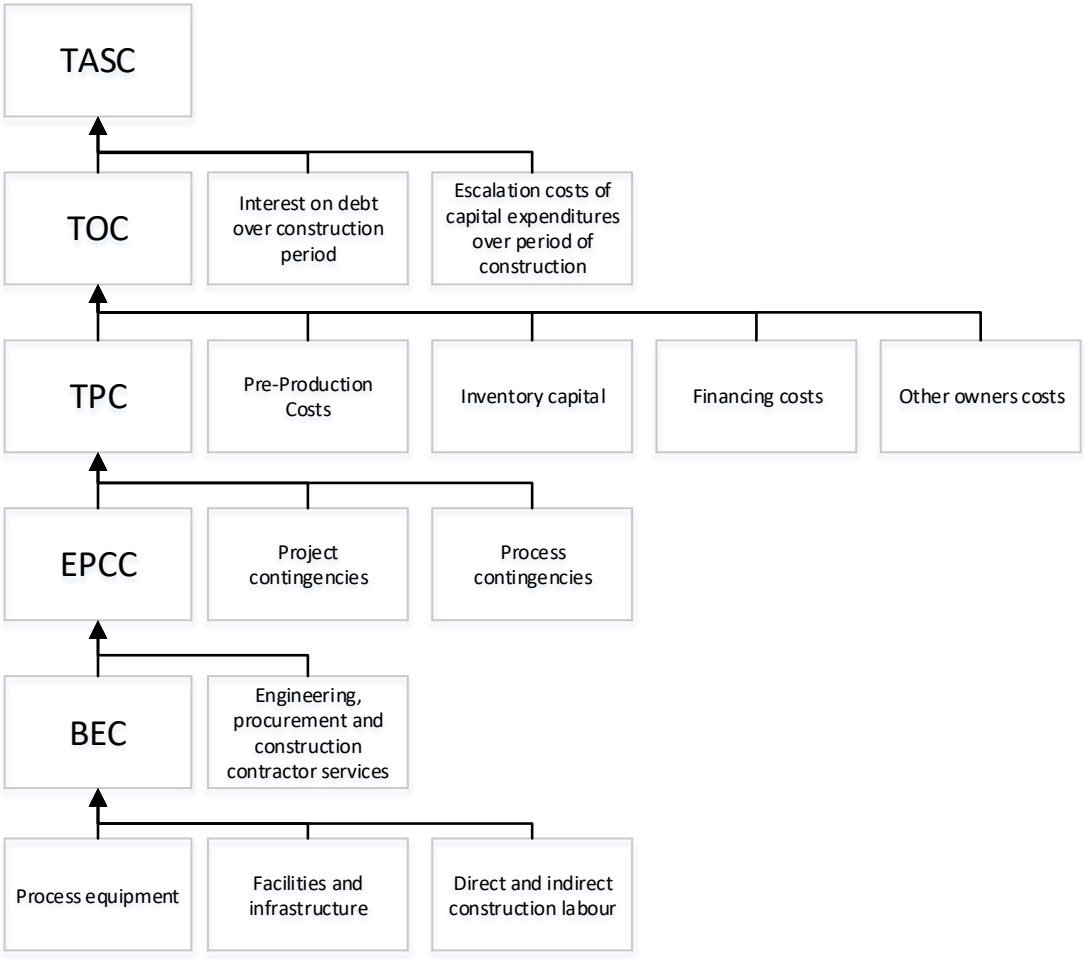

Figure 35. Definitions of the different levels of CAPEX as defined by Gerdes et al [95].

EPCC is estimated as 8-10% of the value of BEC. This includes the cost of site staffing, home office engineering and procurement services as well as field construction management. It

was assumed that as the plant is built on the same land as the biodiesel refinery, there will be no additional land purchase costs.

The TPC is dependent on process and project contingencies which are an estimate of the value of unforeseen or omitted costs. Process contingency costs are based on a percentage of the associated process capital and are applied to a plant based on its current technology status. For a new concept such as GLT-SR, this percentage can be >40% and 30-70% if there is bench scale data. Project contingency is 15-30% of the sum of BEC, EPC fees and process contingency.

TOC refers to costs incurred prior to plant start up or pre-production costs. These costs are estimated at 2% of the TPC. Additionally the cost of six months operating labour of three operators with a salary of $35,000 per year and one month's fuel cost at full capacity. Other pre-production costs were valued each 0.416% of TPC (where one year is worth 5% of the TOC) and included; 1 month maintenance materials at full capacity, 1 month non-fuel consumables at full capacity and 1 month waste disposal. Working capital and royalties are assumed to incur zero cost. Inventory capital accounts for a sixty day supply at full capacity of non-fuel consumables e.g. chemicals and catalysts in addition the cost of spare parts estimated at 0.5% of TPC. Land costs are $3,000 per acre. Financing costs are estimated at 2.7% of the TPC. This estimate contains costs for securing financing including fees and closing costs but not including interest during construction make up this value. Other owner's costs are estimated at 15% of TPC. This does not include risk premiums, transmission interconnection, capital cost taxes or unusual site improvements.

TASC estimates are based on global economic assumptions and a particular finance structure. The global assumptions in this work are the same as the NETL analysis. Finance structures are developed for an investor owned utility (IOU) or independent power producer (IPP) in high and low risk scenarios. Whilst the technology for GLT-SR is not new, the concept, catalyst and potential products have only been modelled, therefore a high risk scenario is adopted as the basis.

Finance Structure	High Risk IOU		Low Risk IOU	
Capital Expenditure Period (years)	3	5	3	5
TASC/TOC multiplier	1.078	1.140	1.075	1.134
Finance Structure	**High Risk IPP**		**Low Risk IPP**	
Capital Expenditure Period (years)	3	5	3	5
TASC/TOC multiplier	1.114	1.211	1.107	1.196

Table 14. Conversion factors from TOC to TASC

3.2.3 OPEX

The annual operating expenditure or cost (C_{AOC}) for a process includes any variable costs required for the plant to operate in a year. For this work the costs considered for OPEX included maintenance, labour, electricity, water. Catalyst has been included as a CAPEX cost rather than OPEX allowing the cost of regenerating or replacing spent catalyst to be incorporated into the maintenance cost. The cost of catalyst was \$20 kg^{-1} and is a conservative estimate based on sale prices at Alibaba [99].

The maintenance cost is calculated as a 3% of the final TASC value. The cost of labour depends on the number of operators required for the GLT-SR plant. It was assumed that as the plant was operating at 8000 hours a year, three separate shifts per day were required to monitor the plant. This would equate to 3 engineers and it was assumed their salaries were \$35,000 per annum. In the sensitivity analysis this value was increased to \$47,000 as a maximum value. It was assumed that other operators of the biodiesel plant will also be able to assist with maintenance and operation.

Due to the recycling ability of the plant and the requirement for small volumes to be pumped, water and costs of natural gas for start-up were near zero and for simplicity assumed to be zero.

Finally, the annual cost of paying back any CAPEX that was borrowed is also factored into the OPEX. Annual cost of CAPEX (C_{ACC}) is defined as the monetary value paid back to the lender and is dependent on the interest rate the loan was lent at, the length of the loan and the original value of the loan. The annual capital cost is the yearly repayment including interest for the capital borrowed in the construction years to build the plant. It was assumed the capital was borrowed and completely spent in the first construction year. The original value of the capital with the added interest is the true value of the capital loan. Using the

excel function PMC the annual repayment can be calculated by setting the length of time over which to repay and the interest rate. Interest is charged on the capital even during plant construction years.

3.2.4 Cumulative cash flow and net present value

Cumulative cash flow (CCF) is the sum of the present and previous year's cash flows. The cash flow (C_f) can be calculated as in *Equation 30*.

$$C_f = Rev - C_{AOC} - C_{ACC} \qquad \textit{Equation 30}$$

Where Rev is revenue, C_{AOC} is annual operating cost and C_{ACC} is annual capital cost.

As capital is expended in the first few years to build the plant, the CCF is negative during the construction phase. Depending on the size of the revenue and OPEX, the CCF will remain negative for a number of years until a cash flow break-even point is reached, known as the payback point. The payback time required to reach this point can determine the minimum lifetime of the plant before a positive cash flow is observed.

CCF does not account for the time value of money. The time value of money assigns higher value to money that is available closer to the present. In other words, money now is worth more than money in the future because present money has earning potential.

This relationship is described in *Equation 31* and converts the present value of money into the future value by applying a discount rate.

$$PV = \frac{FV}{(1+r)^n} \qquad \textit{Equation 31}$$

Where PV is present value or discounted cash flow, FV is future value, *r* is the discount or interest rate and *n* is the number of years of investment. The net present value (NPV) can be calculated by cumulatively summing the discounted cash flow as shown in *Equation 32* .

$$NPV = \sum_{n=0}^{n=T_{PL}} \frac{C_f}{(1+r)^n} \qquad \textit{Equation 32}$$

Whereby C_f is the cash flow in a particular year, *r* is the discount or interest rate and T_{PL} is the plant life.

A positive NPV indicates a profitable venture, a zero NPV indicates the venture breaks even and a negative NPV indicates a venture that produces a loss. The discount rate heavily impacts the NPV and is dependent on the rate of inflation. Standard discount rates of 3%, 7% and 10% have been used by the international energy agency in calculation of the cost of producing electricity from all types of power plants [100].

In addition to the NPV a profitability analysis is essential to determine the feasibility of a project. The payback time and internal rate of return (IRR) are common methods of determining project feasibility. The payback time is the number of operating years required to reach the financial breakeven point. The financial breakeven point occurs when the cumulative cash flow is zero and must include the capital repayments, cost of capital i.e. annual interest on CAPEX, revenue and OPEX.

Internal Rate of Return

The discount rate that creates an *NPV* value of zero at the end of a project is known as the IRR. The IRR is the percentage return that an investor will hope to make on their investment where a larger IRR requires greater profits and therefore more positive cash flows to achieve the zero NPV. The hurdle rate is the minimum IRR that an investor desires before they will invest in a venture. A list of hurdle rates for different energy and heat generating technologies is outlined by Richard Hern [101] and show that for biomass gasification processes the hurdle rate is usually between 10 and 13.2%. The solver function in excel was used to assist in calculating the gas value that was required to achieve the IRR.

3.2.5 Revenue

Revenue is defined as the positive cash flow generated from the sale of the plant product. In this case the revenue is attributed to the Bio-SNG produced from the conversion of glycerol. As the Bio-SNG can offset natural gas, the value of Bio-SNG per unit energy is equated to the value of natural gas. The scenario associated with this work is based in the USA where the history of natural gas spot and industrial price is well documented and varies between each state.

Natural gas spot prices in the USA have experienced several distortions since the early 1990's. Figure 36 displays data on the average price at the Henry Hub in the USA per mmBtu (million Btu, where 1 Btu = 1055 J). Data recorded by the International Monetary Fund (IMF) shows the trend between 1991 and 2017 whereas the U.S energy information administration (eia) reports data from 2016 with forecasts up to 2050. Additionally, the World Bank (WB) reports data from 2014 and forecasts to 2030. The overlap of data from the WB and IMF agrees but deviations occur when natural gas prices are forecasted.

Based on Figure 36, the last 40 years have displayed periods of normal gas supply (1990-2000 and 2008-2017) and scarcity (2000-2008). Increasing domestic shale production was a significant factor in resuming normal gas supply after 2008. Whilst the HH is used as a price marker, the average HH price is not representative of the gas price that industry has paid in

different states. Using April 2017 as an example, the lowest value was \$2.26 $mmBtu^{-1}$ (West Virginia) whilst \$11.62 $mmBtu^{-1}$ (Maryland) was the highest value with an outlier price of \$17.06 $mmBtu^{-1}$ in Hawaii [102]. Comparatively the average USA price was \$4.17 $mmBtu^{-1}$.

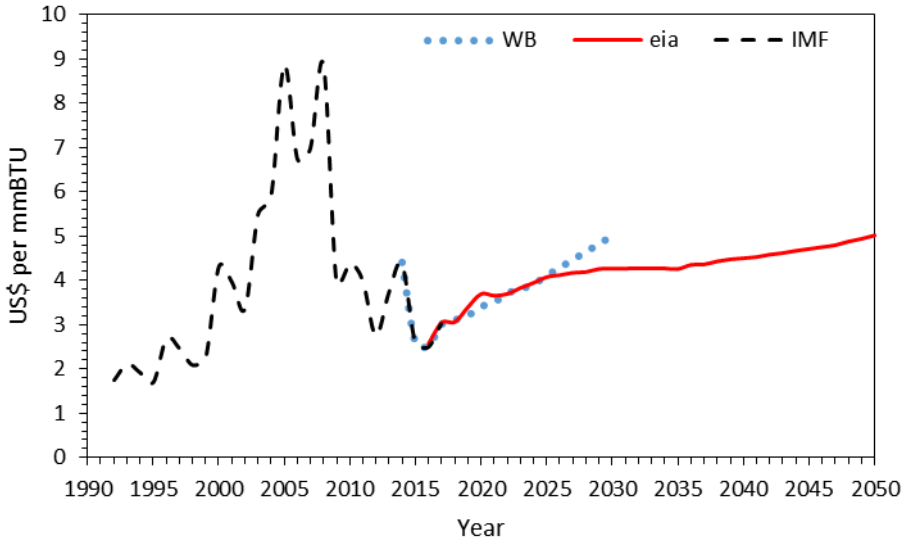

Figure 36. Natural gas price history and future price projections based on the Henry Hub as recorded by the World Bank [103] *(WB), energy information association (eia)* [104] *and the linternational Monetary Fund (IMF)* [105]*. Data from the IMF and eia agrees pre-2017 but only IMF is shown for clarity.*

Spot prices of natural gas give an indicator of the history and present value of natural gas. They are not an indicator of whether investment should be made in natural gas or SNG technologies as it does not account for the investment cost, risk of the venture or future cost of money.

Revenue for different US states

Gas price varies with state. The number of biodiesel refineries in the US also varies with state as does the feedstock that each biodiesel refinery will use. A list of the biodiesel refineries by state and production volume is available from biodieselmagazine and shown in Table 15 [106]. As the focus of this work is on soybean biodiesel, only states containing a plant that exclusively utilise soybean as a feedstock were listed. Missouri contained a significant number of biodiesel refineries and a gas price that was roughly double the Henry Hub (HH) average over the course of 2017 and is an ideal state for a profitable GLT-SR plant. Using the year 2017 data, an average value of the gas price was taken as the static gas price for the discounted cash flow. A range was created for further use by considering the tail ends as three standard deviations away from the mean.

Name	State	City	Capacity (ML)
Delta American Fuel LLC	AR	Helena	40.00
Ag Processing Inc. - Algona	IA	Algona	60.00
Ag Processing Inc. - Sergeant Bluff	IA	Sergeant Bluff	30.00
Cargill Inc. - Iowa Falls	IA	Iowa Falls	56.00
Incobrasa Industries Ltd.	IL	Gilman	32.00
Stepan Co.-Joliet	IL	Joliet	21.00
Louis Dreyfus Agricultural Industries LLC	IN	Claypool	90.00
Owensboro Grain Biodiesel LLC	KY	Owensboro	45.00
Minnesota Soybean Processors	MN	Brewster	30.00
Ag Processing Inc. - St. Joseph	MO	St. Joseph	30.00
Deerfield Energy LLC	MO	Deerfield	30.00
Mid-America Biofuels	MO	Mexico	50.00
Paseo-Cargill Energy LLC	MO	Kansas City	56.00
JNS Biofuels	MS	New Albany	7.50
World Energy Natchez	MS	Natchez	72.00
Cincinnati Renewable Fuels LLC	OH	Cincinnati	60.00

Table 15. Locations of soybean biodiesel plants in the USA

3.2.6 Glycerol Value and Opportunity Cost

Opportunity cost refers to the revenue the plant could have received, but gave up, to take another course of action. The difference in revenue between the default and the alternative is the opportunity cost or benefit if the alternative is less or more lucrative respectively.

In the case of the soybean biodiesel plant, the default choice was to sell crude glycerol. The selling price of crude glycerol at a soybean biodiesel plant in the model produced by Hofstrand was \$0.03 lb^{-1} (\$0.066 kg^{-1}) [107]. This is similar to the range of values of crude glycerol as reported by Johnson *et al.* of \$0.025-0.05 lb^{-1} [38]. Converting glycerol to Bio-SNG changes the market the product is sold in as well as the value associated with glycerol as it is now a feedstock for Bio-SNG. The monetary value that the Bio-SNG can be sold for or the monetary value that is equal to the natural gas that the Bio-SNG can offset becomes the new revenue stream. Depending on the final year revenue, which accounts for the costs associated with running the plant, a comparison can be made between the revenues achieved over the lifetime of the plant for glycerol based Bio-SNG and selling of the crude glycerol. It was assumed that no subsidy was available for the generation of renewable heat in the USA compared to the UK which at the time of this thesis, has the renewable heat incentive.

3.2.7 Production and Levelised Cost

Production cost is the cost incurred by a business or manufacturer when creating a good or service. The annual cost of production for the product Bio-SNG can be calculated by dividing the OPEX by the total units of product per year which, in this case, is energy in the form of Bio-SNG as shown in Equation 33. Overhead costs such as marketing, rent and administration as well as taxes are not included in OPEX for this case.

$$P_c = \frac{C_{ACC} + C_{AOC}}{LHV_{Bio-SNG}} \qquad \textit{Equation 33}$$

Where P_c is production cost, $LHV_{Bio\text{-}SNG}$ is the total energy contained in the Bio-SNG that is produced annually based on lower heating value, C_{ACC} is the annual capital cost and C_{AOC} is the annual the cost of labour, maintenance and electricity.

A similar calculation to the production cost is the levelized cost. Levelised cost mechanisms allow comparison of different methods to generate the same product, in this case heat. It is the average total cost to build and operate a power-generating asset over its lifetime divided by the total energy output of the asset over that lifetime and gives the required cost of the energy at particular discount rates.

Usually levelised costs are calculated for electricity. Significant analysis has been carried out by Lazard and the UK government on levelised cost of electricity and compares conventional generation versus renewables [108,109]. Several authors have advocated for levelised cost of heat because some technologies can utilise heat directly without the need to convert to electricity, reducing the number of stages in energy conversion and improving efficiency [110–112].

Calculation of the levelized cost of heat is carried out according to Equation 34. The direct conversion of the Bio-SNG to heat for use within the biodiesel plant is set at an efficiency of 90%, the same as within the GLT-SR process.

$$LCOH = \sum_{n=0}^{n=T_{PL}} \frac{\frac{C_{ACC} + C_{AOC}}{(1+r)^n}}{\frac{E_{Bio-SNG}}{(1+r)^n}} \qquad \textit{Equation 34}$$

Where C_{ACC} is annual capital cost, C_{AOC} is annual operating cost, r is the discount rate, n is the year, $E_{Bio\text{-}SNG}$ is the energy from Bio-SNG that is converted at an efficiency of 90% (0.9) to heat for steam production and T_{PL} is and plant life in years.

3.2.8 Sensitivity Analysis

A sensitivity analysis can be carried out to determine the robustness of the model to different variable factors. Main outputs of interest are the IRR and LCOH and can be altered by changing the following factors: CAPEX, OPEX, Gas price, Boiler efficiency, free glycerol content, plant load factor, loan interest rate, and loan lend time, electricity cost, labour cost.

3.2.9 Scale and Learning Rate

Many technologies achieve a significant reduction in costs when the plant is scaled up in size. An estimate of the impact of scale on the CAPEX required for larger or smaller plants can be made using *Equation 35* which has been adapted for GLT-SR plants [113].

$$S_c = R_c \left(\frac{SP}{RP}\right)^{Exp} \qquad \textit{Equation 35}$$

Where S_C is the scaled cost, R_C is the reference cost from the reference plant, SP is the scaling parameter, RP is the reference parameter and Exp is the exponent which is specific to each technology or type of plant.

For a GLT-SR plant the reference cost is the calculated BEC or CAPEX. The scaling parameter will be the inlet feed of glycerol for the new plant and the reference parameter will be the input glycerol from the reference plant. Exponents are calculated based on a history of costs for a particular plant or type of equipment and accounts for the economy of scale. Exponents are logarithmically derived and some equations are specific to different technologies. Exponents used in this method have been obtained from NETL [113].

To obtain reasonable results using plant scaling methods, it must be assumed that the technology of both facilities must be the same or very close to the original plant. Likewise, the scaling factor that is applied must be specifically applicable to the range of sizes for the specific technology of facility being analysed. Configuration of the facility, its location, and any unique design and site characteristics must also be considered and will usually require application of cost adjustment factors. If any categories deviate significantly from the original plant, the results can become non-meaningful. To ensure the cost is appropriate to the year, the cost must be time adjusted.

As the number of plants produced increases, the efficiency of creating the plant improves as we gain experience and learn, thereby reducing costs. Calculating the reduction in costs due to the learning rate allows comparison of the required costs for a first of a kind (FOAK) and an n^{th} of a kind (NOAK) plant. It is usual to compare the FOAK with the 5^{th} plant which represents a proven technology.

The assumption is that the cost of new and developing technologies is usually greater at the point of inception and decreases after it has become more developed. Technologies such as GLT-SR fall into this assumption. The trend of a learning curve is described in Equation 36 and allows the determination of the NOAK plant [94].

$$y = ax^{-b} \qquad \textit{Equation 36}$$

Where *y* is the cost or time to produce the x^{th} unit, *a* is the time or cost of the first-of-a-kind unit, *x* is the cumulative number of units, capacity or ratio of capacities and *b* is the learning rate exponent.

The learning rate equation is defined in Equation 37

$$L_R = (1 - 2^{-b}) \qquad \textit{Equation 37}$$

Where L_r is the learning rate and 2^{-b} is defined as the progress ratio.

Solving for the learning rate exponent rearranges the equation to:

$$b = -\log(1 - L_R)/\log(2) \qquad \textit{Equation 38}$$

Based on literature the learning rate varies between 0.06 to 0.01 in intervals of 0.01 where 0.06 is experimental first of a kind and 0.01 is mature (17^{th} plant or greater). These values are displayed in Table 16.

Maturity Level	R-Value
Experimental (FOAK)	0.06
Promising (2^{nd})	0.05
Growing (3^{rd} and 4^{th})	0.04
Proven (5^{th}-8^{th})	0.03
Successful (9^{th} to 16^{th})	0.02
Mature (>17^{th})	0.01

Table 16. R-values for technology learning curves at different maturity levels by number of plant [94].

Several uncertainties plague the use of learning curves when forecasting costs of new energy technologies. The traditional cost curve mentioned in *Equation* 36 creates a straight line on a log-log plot and is the most simple to produce, however it may be the case that the cost of the subsequent plants built after the first increases before any learning benefit is observed. For these cases an S-shaped curve may be more appropriate. Other uncertainties have been well documented by Yeh *et al.* 2012 [114] and include factors such as institutional forgetting and the influence of social, economic and political factors.

3.2.10 Risk and Probability of Success by Monte Carlo Simulation

An important analysis metric is the idea of risk. Up to this point, all of the economic analysis methods describe how to calculate project costs and profitability but do not factor in risk assessment.

In this work, the risk is that the GLT-SR plant will not be profitable and is represented by a negative NPV at the end of the plant lifetime. It is important to quantify risk and uncertainty as the basis for utilising glycerol for bio-SNG that there is a risk that, in the future, crude glycerol will become a waste and incur addition costs. Whilst it is beyond the scope of this work to analyse the risk of glycerol becoming a waste product, it is possible to quantify the risk of a GLT-SR plant being unprofitable by using MCS and confidence internals by standard deviation. Moreover, the worst case and best case scenarios can be determined and what conditions must be met for a high likelihood of a plant becoming profitable and therefore economically feasible.

Monte Carlo simulation (MCS), also known as probability simulation, is a popular method of risk analysis. MCS was credited to Stanislaw Ulam and Nicholas Metropolis in 1939 [115]. Application of MCS is wide reaching. Some examples of areas where risk assessments are necessary include; environmental health and safety [116,117], financial/investment [115,118], time management [119] decision making and impact of uncertainty on LCOE for power generating technologies[120].

The value of MCS is the ability to utilise stochastic variables (having a random probability distribution or pattern that may be analysed statistically but may not be predicted precisely). Thanks to computers it is possible to assign truly random numbers within a designated range. As computing technology has become significantly more powerful in the last few decades, the availability and affordability of computers as well as accessibility of programs able to generate random stochastic values has increased.

Originally risk analysis was conducted using single point estimates (single deterministic values) without any uncertainty. In a discussion by the RAND corporation cost analysis department, using a single point estimates, rather than stochastic values, were deemed to be poor selection indicators when attempting to make an optimal decision in choosing which project to pursue [115,121]. When compared to a single point estimate, MCS allows the selection of a range of values for each variable, allowing a normal distribution to be produced from several iterations. The normal distribution details the probability of reaching the high and low end (tails) of the normal distribution as well as the average value, standard deviation and therefore confidence level of achieving a positive or negative output.

Four main limitations of MCS have been highlighted by Scott Ferson [122] and are as follows;

1. Data intensive and require a significant body of data or assumptions in place of empirical information.
2. Cannot be used to propagate partial ignorance i.e. values and ranges must be defined.
3. Cannot be used to conclude that exceedance risks (likelihood of being exposed a certain scenario) are no larger than a certain level.
4. Cannot be used to solve back calculation problems.

Regarding points one and two, this work makes assumptions when calculating CAPEX and OPEX using a C4 estimate. According to Turton, the C4 estimate, as shown in Figure 34, has an inaccuracy of 4-12 times the inaccuracy of a C1 (best case) estimate. The uncertainty of the C1 estimate is -4% to 6%. Therefore the best case uncertainty range for a C5 estimate is -12% to 18% whereas the worst case uncertainty range is -48% to 72%. This provides the upper and lower bounds for the CAPEX and OPEX variables for the MCS. The third variable, revenue, is based on the historic natural gas price and future projections of gas prices. Point 3 must be considered in discussion whereas point 4 is irrelevant for this work.

Monte Carlo simulations were carried out using gas prices in Missouri. The historical gas price in 2017 was the base case gas price. Projected gas prices for 2030 and 2050 were based on the gas price increase ratio as predicted at the Henry Hub in 2030 and 250, shown in Figure 36. The range of these values along with the minimum and maximum ranges for CAPEX and OPEX are detailed in Table 17. The minimum range was calculated as -12% and 18% of the base case whereas the maximum range was -48% to 72% of the base case, in line with the uncertainties associated with the C4 estimate shown in Table 12. A random number within the range of gas price was selected for each year of operation as the gas price varied considerably between the years. Interest rate, discount rate, length of lend, load factor, boiler efficiency and glycerol purity were kept constant. The variables used for the MCS are detailed in Table 17.

Value	Unit	Base	Min	Max
CAPEX Cost	**M$/year**	-0.054	-0.048	-0.064
CAPEX	M$	-0.4200	-0.3696	-0.4956
Interest	%	5	5	5
Length of Lend	Years	10	10	10
Revenue	**M$**	0.2588	0.2453	0.2723
Load Factor	%	1	1	1
Boiler Eff	%	0.9	0.9	0.9
Glycerol Purity	%	0.8	0.8	0.8
Gas Price 2017	$/mmBtu	6.03	6.36	6.70
Gas Price 2030	$/mmBtu	7.46	7.07	7.85
Gas Price 2050	$/mmBtu	9.09	8.61	9.56
OPEX	**M$/year**	-0.1236	-0.10877	-0.14585
Maintenance	M$/year	-0.0126	-0.01109	-0.01487
Labour	M$/year	-0.105	-0.0924	-0.1239
Electricity	M$/year	-0.006	-0.00528	-0.00708

Table 17. Variables and ranges for Monte Carlo Simulation.

3.3 Economic Analysis Results

3.3.1 BEC and CAPEX

The base equipment cost was calculated using the measurements in the Aspen process flow sheet. The breakdown of costs is displayed in Figure 37.

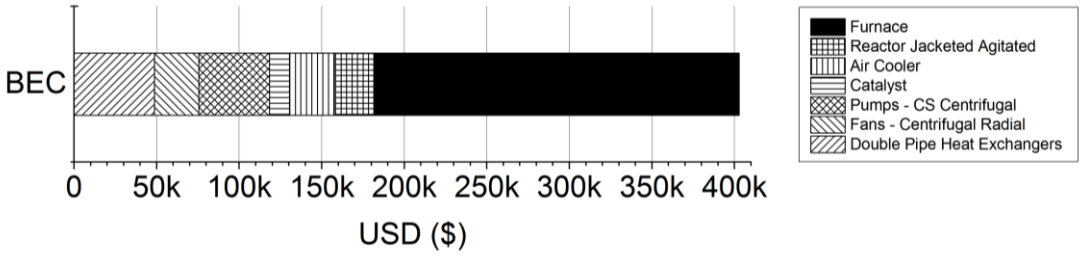

Figure 37. Breakdown of equipment contribution to the Base Equipment Cost.

The total cost including the furnace was $402,735. The major cost was the furnace accounting for 55% of the expenditure and by removing the furnace, the BEC was reduced to $181,423. At a soybean biodiesel plant, a furnace is required to produce steam for soybean crushing. Therefore, the BEC value with the furnace omitted was used in further CAPEX calculations as it was assumed the soybean biodiesel plant would already have a furnace.

The final TASC was calculated using the BEC and is displayed in Table 18.

Factor	Cumulative Minimum ($)	Cumulative Maximum ($)
BEC	181,423	
EPCC	195,937	199,565
TPC	273,405	406,388
TOC	384.536	577,011
TASC	413,376	642,790

Table 18. Cumulative minimum and maximum values for each of the CAPEX components.

Calculating TASC provided a minimum and maximum value depending on the risk associated with the project. Minimum, maximum and average TASCS of $414,530, $642,790, and $528,660 respectively were calculated and the average value was used in the base case which is synonymous with CAPEX. This relates to an investment cost of $0.0014-0.0021 $mmBtu^{-1}\ yr^{-1}$.

The C_{ACC} depends upon the interest rate, length of lend of the loan and the value of the loan. In this case the length of lend was set at 10 years, the annual interest at 5% and the value of

the loan was 80% of the calculated CAPEX, assuming that 20% of the cost could be fronted by the business. For the base case this resulted in a C_{ACC} of \$5,383 yr^{-1}.

3.3.2 OPEX

A breakdown of C_{AOC} is shown in Table 19. The main energy use required for the plant is heat that is generated from utilisation of a portion of the Bio-SNG. The electricity requirement is minimal and results in a process that is close to being self-sustaining. The major contributor to C_{AOC} is the cost of labour where each engineer was paid a salary of \$35,000. The number of engineers or operators required to operate the plant will significantly impact the operating cost of the plant as well as their salaries. Water was assumed to be freely available from a river source and was also recycled in the GLT-SR plant requiring little additional water inlet.

Factor	Annual Cost (\$)
Labour	105,000
Electricity	6,187
Maintenance	15,548

Table 19. Values associated with the C_{AOC}.

3.3.3 Discounted Cash Flow Analysis

The discounted cash flow will depend on many factors which are outlined for a base scenario in Table 20. Utilising the factors for a base case scenario, a cash and discounted cash flow diagram can be created as shown in Figure 38. A discount rate of 10% was used in line with the recommended rate from literature.

The cash flow and NPV are negative for the year -1 because the capital is spent in these years to build the plant and no revenue can be generated. Upon beginning operation the cash flow becomes positive in plant operation year 0 when the plant is working at 67.5% load. The cash flow becomes more positive once the C_{ACC} payments have ceased in plant year 9. Overall the time taken to reach a net zero revenue (payback time) is 10 years from beginning of plant construction.

Variable Description	Value
Glycerol Feed	497 kg hr^{-1}
Glycerol Purity	0.8
Bio-SNG produced (80% glycerol)	4.34 mmBtu hr^{-1}
Bio-SNG to heat conversion efficiency	0.9
Plant Operating Hours	8000 hr yr^{-1}
Plant Load	90%
Plant Construction Time	3 years
Conversion Efficiency of Bio-SNG to Steam	0.9
Plant Lifetime	25 years
Plant Operation years 1,2, 24, 25	40%, 70%, 70%, 40%
Loan Grace Period	0 years
Loan Length	10 years
Loan deposit	20%
Loan annual interest	5%
Discount rate	12%
Catalyst Mass	200 kg
Catalyst Cost	\$60 kg^{-1}
Electricity Cost	\$0.12 kWh
CAPEX	\$528,660
Electricity	51.6 MWh yr^{-1}
Engineer Salary	\$35,000
Labour	\$110,000 yr^{-1}

Table 20. Constants and assumptions used in this work.

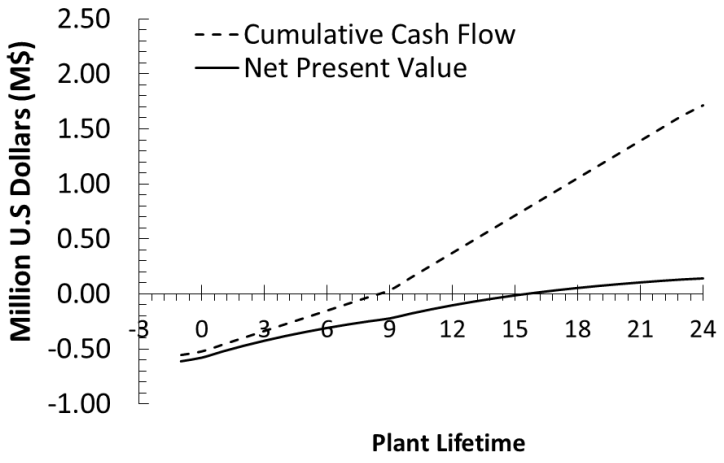

Figure 38. Discounted cash flow diagram for the base case GLT-SR scenario.

To achieve an IRR of 12% the required gas price was \$6.82 $mmBtu^{-1}$ and is near the average gas price in Missouri in 2017. On the other hand for an IRR of 18% the required gas price was \$7.93 $mmBtu^{-1}$ which exceeded the maximum gas price in Missouri in 2017.

3.3.4 Glycerol Value

Figure 39 compares the value of glycerol and required gas price to achieve this value with the achieved IRR. To achieve the same crude glycerol value as that of selling the crude glycerol, an IRR greater than 30% and gas price greater than \$12 $mmBtu^{-1}$ was required. This value is greater than the highest average historical U.S gas price for the period 1990-2018. For this particular plant, 27% could be perceived as the hurdle rate if there is an option to sell the crude glycerol. In the case where glycerol could not be sold and would be consigned as waste, the hurdle rate would be significantly lower. Therefore, a GLT-SR plant would be unfeasible economically if there was the option to sell crude glycerol at the current natural gas prices.

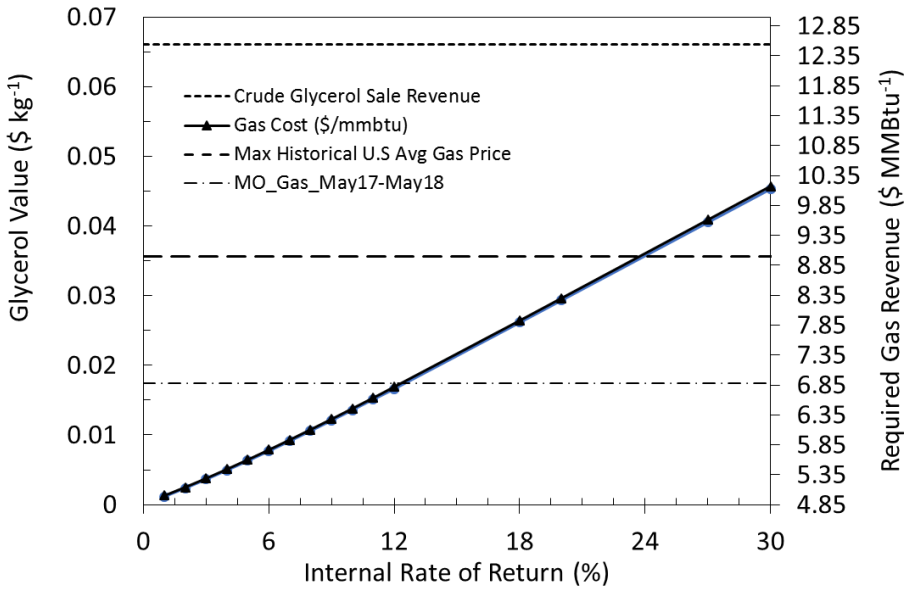

Figure 39. Value of crude glycerol (kg) when converted to Bio-SNG and required gas revenue to achieve each IRR.

In the past natural gas purchase prices in the USA have been as high as \$9 $mmBtu^{-1}$ as shown in Figure 36. Data from 2016-2017 shows that prices have averaged between \$3-4 $mmBtu^{-1}$ at the Henry Hub and predictions forecast a slow and relatively constant increase in the gas price of up to \$5 $mmBtu^{-1}$ by the year 2030 from the World Bank and 2050 by the U.S energy information administration (eia). At these prices the value of the glycerol shown in Figure 39 is less than \$0.01 kg^{-1} and an IRR of <2% would be achieved.

The recommended hurdle rates for biomass conversion technologies were 10-13.2% [101]. To achieve this rate of return, a gas price of \$6-7 $mmBtu^{-1}$ would be necessary. Missouri and Arkansas are states with soybean biodiesel plants that had gas prices in this range during 2017 [102,106]. Although this would create a plant that is economically viable in terms of rate of return, the revenue is still lower than that of simply selling the crude glycerol, although the costs incurred to sell glycerol are not known.

Selling crude glycerol does not require construction of a plant. There are inherent costs such as logistics and staffing that must be accounted for but there is no data available as yet. As the value of glycerol is still larger when sold outright, the opportunity cost is 39.4% if the Bio-SNG is sold at the highest average HH price and 58% if it is sold at the recommended hurdle rate price in Missouri. Based solely on revenue it is plausible that selling crude glycerol rather than converting it to Bio-SNG will generate more revenue.

3.3.5 Levelised Cost of Heat

The levelised cost of heat (LCOH) of Bio-SNG from GLT-SR was calculated and compared against natural gas for heat systems in Figure 40. The range of values associated with the LCOH is attributed to changing the discount rate because the discount rate affects the future monetary cost from the C_{ACC} and C_{AOC} as well as the worth of the energy produced. The minimum value of using a discount rate of 1% coincides with the LCOH of \$5.1 $mmBtu^{-1}$ whereas the maximum value using a discount rate of 30% coincides with an LCOH of 14.2 $mmBtu^{-1}$. It is possible to achieve LCOH that are comparable to utilising natural gas for heat in natural gas for heat boilers in the USA and EU. Reducing the energy output of the plant, either through load factor, glycerol content in the glycerol feed or the conversion efficiency of gas to heat will increase the levelised cost. If the glycerol feedstock were to have a value e.g. had to be purchased, this would increase the LCOH as it would need to be factored in as an operating cost.

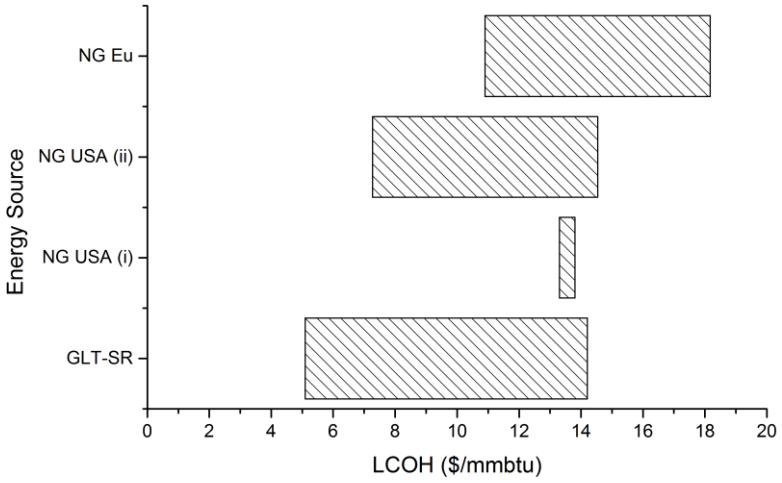

Figure 40. Floating bar graph comparison of LCOH for GLT-SR between different technologies where NG USA (i) is a gas furnace power vent from [110] *and NG USA (ii) and NG EU are from gas heating plants* [123].

Figure 41 displays a tornado diagram and represents the sensitivity of LCOH with each variable. The range for each variable is outlined in Table 21. Aside from the discount rate, as shown in Figure 40, Glycerol content or percentage of glycerol that contains free glycerol, efficiency of gas conversion to heat and CAPEX value were the most significant factors within the range of values tested. Load factor, labour costs and loan interest rates were less significant whilst loan lend time and electricity cost were negligible.

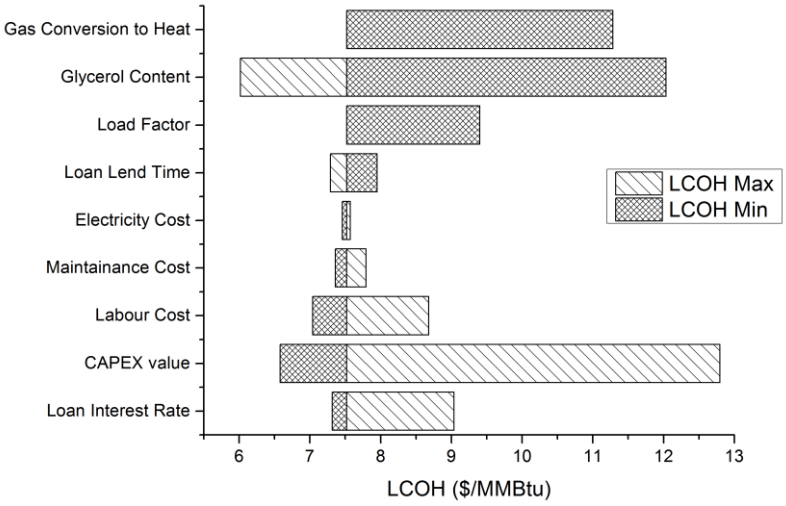

Figure 41. Tornado diagram for a sensitivity analysis on variables influencing the LCOH for the base case scenario with a discount rate of 12%.

Glycerol content had a significant influence as it controls the energy available for conversion to Bio-SNG. It would be unlikely that >99% glycerol (pure glycerol) would be converted to Bio-SNG as pure glycerol is worth significantly more when sold. In addition, to achieve this level of purity significant energy input is required for the processing steps. Usually 50-80 wt% glycerol is produced when methanol is not recovered and has great potential for conversion to Bio-SNG. Lack of purity will increase the levels of contaminants and may lead to less favourable conversion of glycerol to Bio-SNG. In some cases, the contaminants may increase the conversion, for example, methanol contains carbon and H_2 which could be reformed to CH_4. Crude glycerol free glycerol content can vary significantly between processes and refineries and must be considered in energy production projections.

Gas conversion to heat efficiency was also important as a drop of 10% efficiency results in an increase in LCOH by nearly 17%. Maintaining high boiler and heat exchanger efficiency will be necessary to maintain low LCOH which could in turn increase maintenance costs.

Fluctuations in market values such as CAPEX, loan interest rate and cost of labour were important factors that could cause the GLT-SR LCOH to increase above natural gas when higher IRR are desired. Omitting the furnace significantly reduces the CAPEX value and the LCOH, as shown by the maximum CAPEX value which reflects the cost of including the furnace at 1.25 million USD in Figure 37. Utilising the existing furnace at a soybean biodiesel plant is an important measure to reduce the LCOH.

Variable	Minimum	Maximum
Loan Interest Rate (%)	2.5	20
CAPEX value (Million $)	0.4	1.25
Labour Cost (Million $ yr^{-1})	0.09	0.141
Maintenance Cost (Million $ yr^{-1})	0.01	0.025
Loan Lend Time (yrs)	5	15
Electricity Cost ($ yr^{-1})	4000	8000
Load Factor (%)	80	100
Glycerol Feed Content (%)	50	100
Gas Conversion to Heat Efficiency (%)	60	90

Table 21. Variable value ranges for the sensitivity analysis in Figure 41.

There are several criticisms of levelised cost calculations as energy metrics. As levelised costs are inherently simple they ignore the following; distinctions between capital and operational costs, fluctuations in interest rates, risk, environmental impacts of the technology, transmission constraints, additional systems and infrastructure costs. Using a levelised cost alone as a comparison can lead to misleading conclusions. Taken alone it appears that the LCOH using GLT-SR is lower cost than other natural gas methods. However, it is not possible to offset all of the natural gas requirement of the plant and it ignores other potential uses of the glycerol e.g. selling as crude. As seen in Figure 39, selling the glycerol rather than converting it to bio-SNG appears to produce the highest value for the glycerol, which is not shown using LCOH. Furthermore the environmental factors are not considered in LCOH.

3.3.6 Learning Rate

The GLT-SR plant will consist of several different technologies each with their own technology maturity. The different parts of the plant were previously listed in Table 13. Each type of equipment has its own R value as assigned by NETL in their work on technology learning curves [94]. To estimate the L_R value for the plant, an L_R value must be calculated that is representative of mixture of mature and immature technologies. The percentage contribution from equipment section to BEC will be used as a determinant for the plant L_R value. Only the catalyst and reactor have L_R values above 0.01 and make up 19% of the BEC without considering the furnace. Based on the catalyst and reactor L_R values range of 0.04-0.06 for gasifier technology, if 19% of the plant is attributed to an L_R value of this range, the

overall plant L_R value range is 0.015-0.020. The impact of learning rate on the value of BEC is displayed in Figure 42.

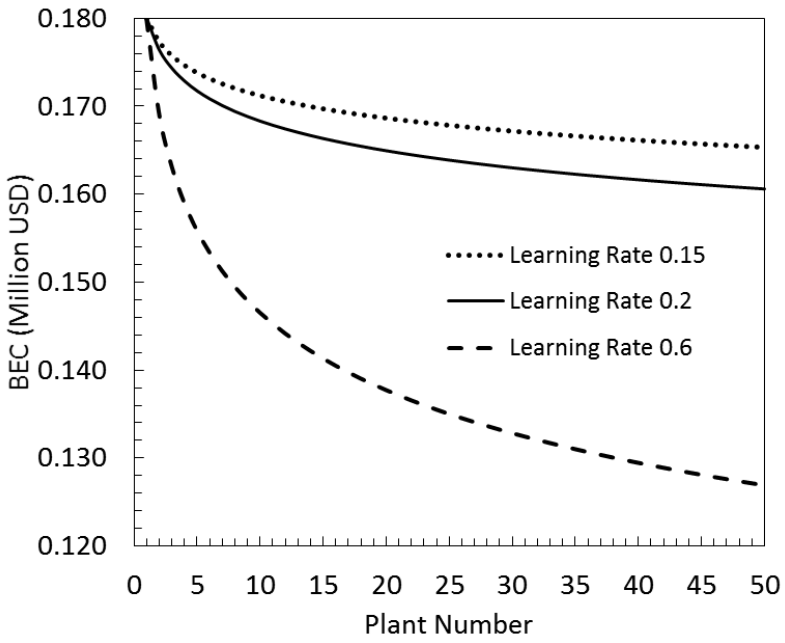

Figure 42. Impact of learning rate on the value of BEC

At the 5th plant the reduction of costs is 3.4% and 4.6% for the learning rate of 0.15 and 0.2 respectively. At plant 25 and 27 the cost reduction doubles to 6.8% and 9.2% for learning rates 0.15 and 0.2 respectively.

The majority of the plants technology is mature because it is based on steam reforming. Consequently the reduction in cost associated with learning on CAPEX due to learning rate could be limited. On the other hand, steam reforming processes for the production of methane have not been carried out under these conditions. Therefore there are optimisation opportunities for the process as well as how to effectively integrate equipment.

When compared to the learning rate of a completely immature technology, at the fifth plant the reduction in BEC is 13.4% and a doubling to 26.8% occurs at plant number 33. The GLT-SR plant BEC value is lower than \$0.2M when applied to a biodiesel refinery that produces 38.6 million litres of biodiesel per year. Based on learning rates of 0.015 and 0.02 the cost reduction at the fifth plant is \$6000 and \$8000 respectively. Overall, relying on cost reductions from technology learning will not significantly impact the CAPEX value for the GLT-SR plant and will have limited impact on the LCOH.

3.3.7 Scale

The effect of increasing or decreasing the scale of the plant on the CAPEX value is shown in Figure 43 and on investment cost per $MJ_{Bio\text{-}SNG}$ in Figure 44. The scaling parameter utilised was the inlet feed of glycerol in tonnes per hour (T hr^{-1}).

The range between exponent (EXP) values 0.45 and 0.7 represents the maximum and minimum CAPEX or investment cost change respectively. The exponent 0.45 is the lowest exponent that can be attributed to a biomass technology whereas 0.7 was the highest exponent found for biomass technologies. The larger exponent implies the technology has higher costs when scaled up but reduced costs when scaled down and is a good representation of more immature technologies or expensive equipment.

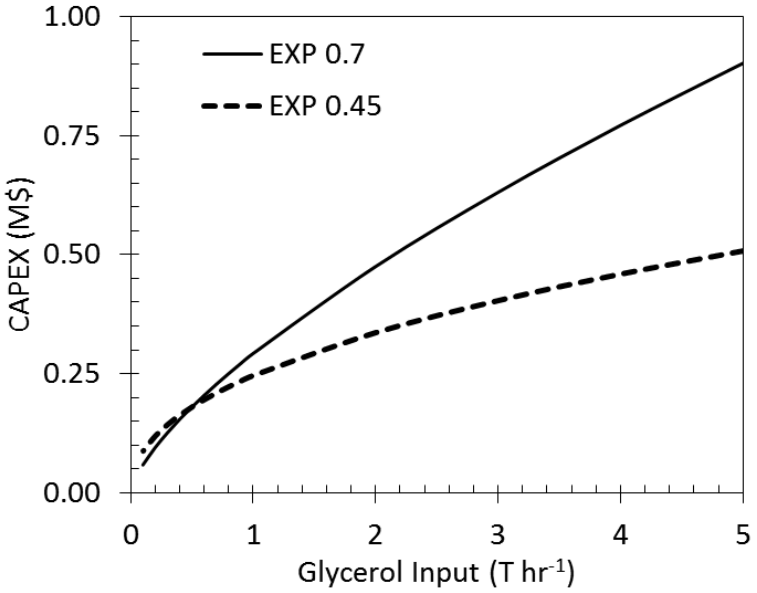

Figure 43. Impact of increasing and decreasing plant scale on CAPEX

Doubling the capacity of the plant results in a significant investment cost reduction. For Exp 0.7 the cost reduces from \$28 MJ^{-1} to \$19 MJ^{-1} and for Exp 0.45 from \$28 MJ^{-1} to \$23 MJ^{-1}. Doubling the inlet feed from 1 to 2 ton hr^{-1} results in less than half of the cost reduction for both exponents. To obtain a glycerol feed of 1 T hr^{-1} a biodiesel plant producing twice as much glycerol as the plant mentioned in Pradhan *et al.* 2011 would be required, producing 76 million litres of biodiesel each year. To the authors knowledge there are currently no biodiesel plants that produce greater than this volume or that solely utilise soybean feedstock for biodiesel at this capacity. Without a several plants being constructed, only projections can be made as to the impact of scale and learning rate on the investment cost.

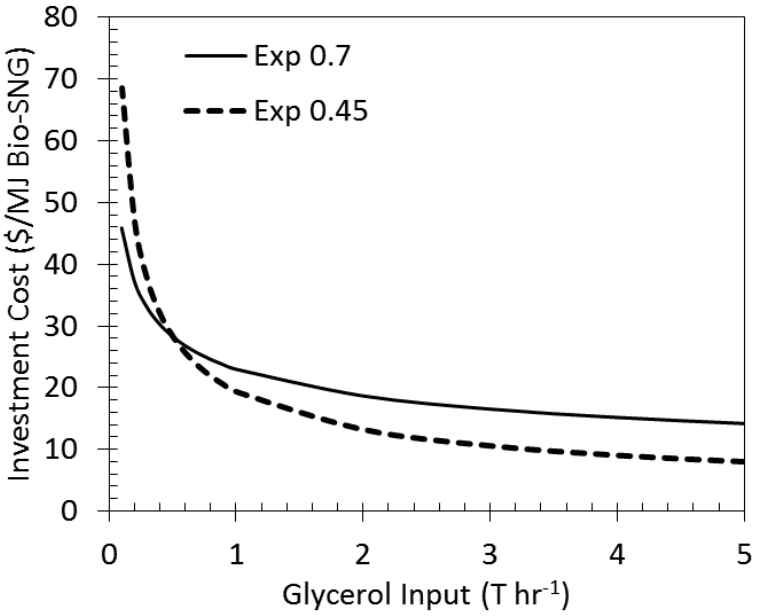

Figure 44. Impact of increasing and decreasing plant scale on investment cost.

3.3.8 Risk and Probability of Success

Histograms containing data from 15,000 iterations are displayed in Figure 45. The minimum and maximum uncertainty ranges for the normal distributions for each year's gas price are overlapped for comparison. The mean, standard deviation, variance, minimum and maximum values are recorded in Table 22.

As the gas price is projected to rise from 2017 to 2050, the normal distribution shifts right towards a more positive NPV. The increase in uncertainty range from the minimum to maximum increases the possibility of more negative NPV's in all cases and is represented by the lower mean, larger range and greater spread of the distribution. Consequently the standard deviation increases for all of the data under the maximum uncertainty. Furthermore the maximum and minimum NPV under the maximum uncertainties increases.

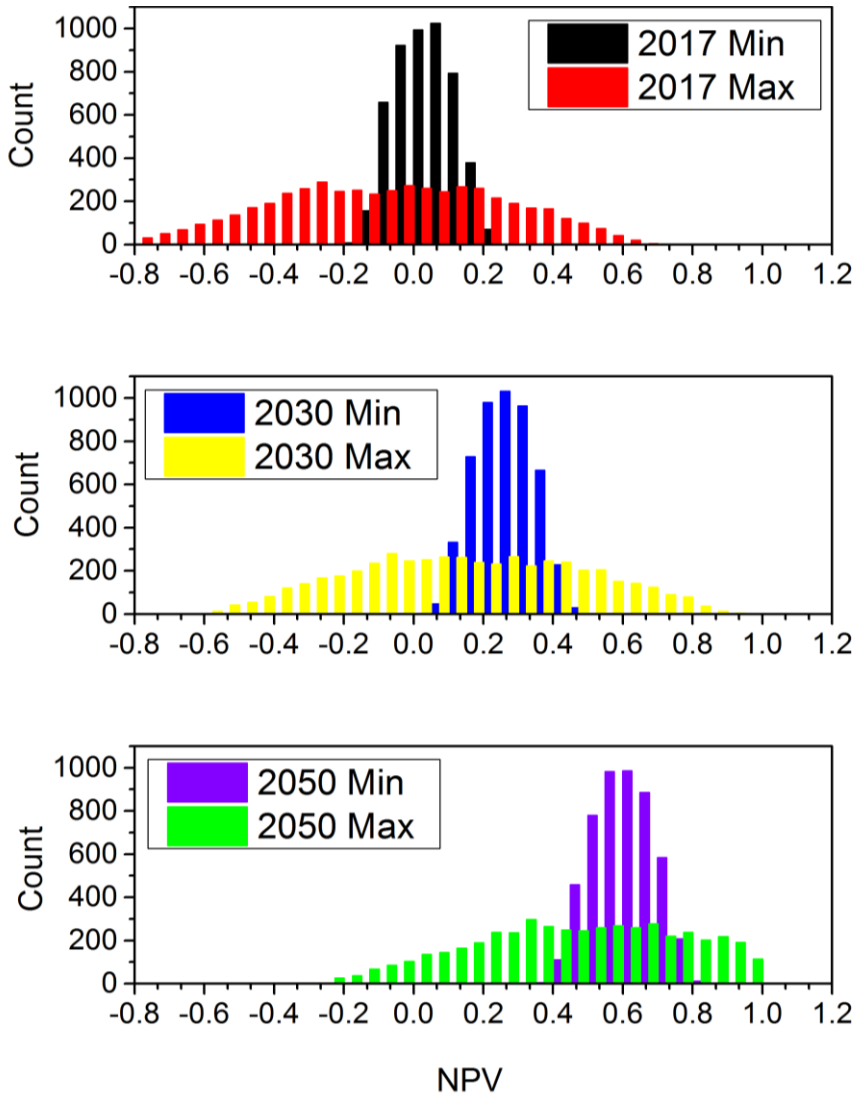

Figure 45. Histograms for the minimum and maximum ranges of CAPEX and OPEX for a Missouri based plant at the historical gas price in 2017 and the projected gas prices in 2030 and 2050 at a discount rate of 18%.

Whilst it is possible to obtain an NPV of zero under the 2017 Missouri gas price, it appears equally likely that a negative NPV will be achieved. Under the minimum uncertainty the normal distribution is centred closely to zero NPV, indicated by a mean of 0.04. Based on a confidence interval of 2 standard deviations (95%) 95% of the NPV values will fall between -0.12 and 0.2 for the minimum uncertainty and -0.71 and 0.57. What's more the worst case scenario is an NPV of -0.17 and -0.84 for the minimum and maximum uncertainty respectively whereas the best case is 0.25 and 0.68 respectively.

At the projected 2030 and 2050 gas prices obtaining a breakeven or positive NPV is more likely. In both cases the mean NPV is positive for both the minimum and maximum uncertainties. Furthermore the minimum NPV for the minimum uncertainty is also positive resulting in 100% confidence that the NPV will be positive under the minimum uncertainty.

This is not the case for the maximum uncertainty where the range of values for the maximum uncertainty conditions in 2030 will be -0.49 to 0.79 and for 2050 will be -0.14 to 1.14 with a 95% confidence interval.

Year	2017		2030		2050	
Uncertainty	Min	Max	Min	Max	Min	Max
Mean	0.04	-0.07	0.27	0.15	0.39	0.50
Standard Deviation	0.08	0.32	0.08	0.32	0.18	0.32
Variance	0.01	0.10	0.01	0.11	0.03	0.10
Minimum	-0.17	-0.84	0.05	-0.59	0.04	-0.26
Maximum	0.25	0.68	0.48	0.92	0.81	1.26

Table 22. Statistic values for the normal distributions of NPV according to each year and the uncertainty level where min is the minimum uncertainty range of -12% to 18% and max is the maximum uncertainty range of -48% to 72%.

MCS gives insight into when the plant should be built. Based on these gas prices, constructing the plant in 2017 would have larger risks as few scenarios predict a zero or positive NPV at a discount rate of 18%. Constructing the plant in 2030 based on forecasted gas prices results in a scenario where we can be highly confident that the plant will generate positive NPVs under the minimum uncertainty. This confidence level increases in the year 2050 where forecasted gas prices are even higher.

If the plant were constructed now, a subsidy of roughly one third the value of the 2017 gas prices would be required to boost the value of the gas to that of 2050 prices and reduce the risk of negative NPVs at 18% IRR. There are few US states that offer a gas price of this magnitude and none that offer this gas price that also have a soybean biodiesel plant. Furthermore there are no subsidies known for renewable heat in the USA. The closest equivalent would be the renewable heat incentive offered in the UK.

Alternatively a lower rate of return could be attained resulting in reduced risk. MCS was carried out at 2017 Missouri gas prices at a discount rate of 0.12 in which is the hurdle rate for biomass gasification technologies [101]. With a 95% confidence under the minimum uncertainty the NPV will be between 0.39 to 0.81. For the maximum uncertainty with a 95% confidence the NPV will occur between -0.55 and 1.18. The worst case scenario for the maximum uncertainty is -0.94 whereas for the minimum uncertainty is -0.11. Reducing the return significantly reduces the risk of negative NPVs for the minimum uncertainty.

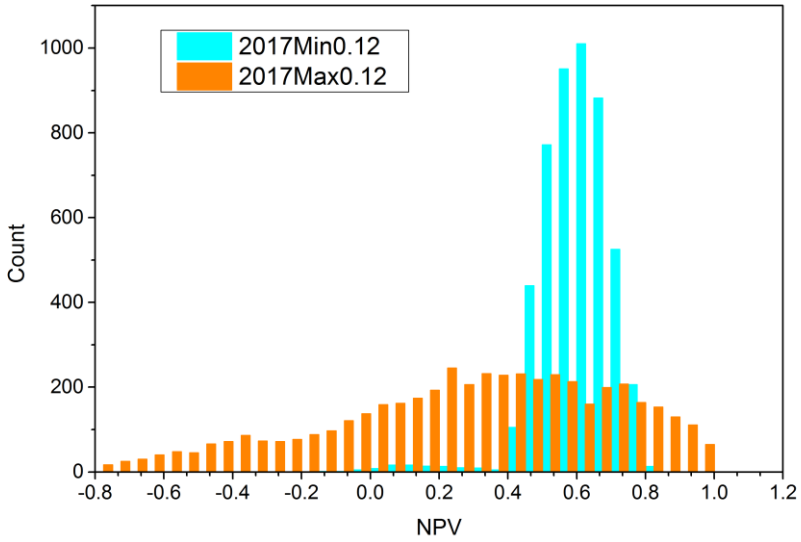

Figure 46. MCS using 2017 gas prices in Missouri and a discount rate of 12%.

Using these uncertainty ranges highlights the issue with the MCS at this level. Increasing the range of uncertainty significantly alters the outlook of the GLT-SR plant. Therefore, it would be beneficial to reduce the uncertainty in calculation before using MCS to predict the viability of an investment. On the other hand, given the high uncertainty, a plant based on conversion of glycerol to bio-SNG for direct use has been shown to have the potential to generate positive NPV's at a discount rate of 18% which exceeds the hurdle rate for a biomass gasification technology.

3.4 Summary

In this chapter the concept of economic feasibility was explored. Outputs from the process model produced in chapter 2 were used to determine the base equipment cost and the CAPEX and OPEX. From these values and projected revenue from the price of gas in the USA, a discounted cash flow and levelised cost of heat was determined. The levelised cost of heat fell within similar costs to traditional natural gas combustion processes both in the European Union and USA. From the discounted cash flow analysis it was possible to analyse the probability of producing a NPV greater than zero with confidence intervals using Monte Carlo Simulation. It was found that several scenarios allow a GLT-SR plant to be feasible and accepting a rate of return of 12%, which is the hurdle rate for biomass gasification technologies, gave a 99.5% chance for a positive NPV under the minimum uncertainty range associated with a C4 study. The projected decrease in plant cost (BEC and CAPEX) due to plant scaling and learning rate was investigated. Finally the value of glycerol when converted to Bio-SNG was concluded as being less than if it could be sold as a crude. If this is not an option then converting the glycerol to Bio-SNG by GLT-SR on site is an economically feasible option to avoid paying fees associated with waste management whilst reducing dependence on fossil-based grid natural gas. Before further decisions are made it is important to reduce uncertainty with further studies to maximise the confidence in a positive NPV being produced.

3.4.1 Discussion of Method Limitations

A major assumption in this work is the natural gas price. The natural gas price was assumed to fall within a range consistent with the previous year (2017). As shown by the historical gas price in Figure 36, there are events which have led to significant price hikes and shortfalls which go against steady trends and may not be predictable, causing problems when building a plant that depends significantly on gas price. Secondly we also assume that the price of natural gas will steadily increase. If the price of natural gas remains the same or decreases, greater subsidy would be required to reduce the risk of negative NPVs. Alternatively a reduced internal rate of return would need to be accepted as shown in Figure 46.

NPV is heavily dependent on the early years of a plants lifetime. The discount on cash flow received in later years becomes more severe over the plants lifetime to account for the time value of cash. This causes sensitivity to the overall NPV at the end of a plants lifetime if an incorrect assumption is made about the length of time required to construct a plant. By reducing the construction time more positive NPVs can be attained at the same conditions

as a plant with longer construction years. This leads to an additional uncertainty and highlights the problem with construction delays.

The discount rate is a major variable for NPV. Adjusting the discount rate significantly impacts the final NPV but in this work it was possible to determine more realistic assumptions of the discount rate by setting the overall NPV to zero, utilising the internal rate of return and coupling it to the gas price. Moreover, MCS attempts to incorporate the idea of variable risk over the lifetime of the project by using a stochastic range for the gas price. It is integral to minimise uncertainties and the first place to do this would be in the estimation of BEC which could be carried out in later studies e.g. C3. As the majority of the technology for steam reforming is available, contacting equipment distributors with sizing measurements would be a reasonable method.

The operating expenditure is dependent on the labour costs. Chemical plant operators in Missouri earn roughly $52,000 per annum whereas chemical engineers average $72,000 if chartered and $62,000 if unchartered in the USA [124]. To improve upon the sensitivity analysis, the labour costs should be increased as currently the maximum pay was $47,000. However, based on *Figure 41*, CAPEX and glycerol purity will still be the dominant factors influencing levelised costs and overall profitability.

3.4.2 Accounting for Environmental Impacts

An important measure that has not been accounted for and is usually overlooked when carrying out economics studies are environmental impacts. Economics studies tend to leave out the environmental impacts as there are no standard metrics which can convert environmental damage, e.g. global warming potential, into an economic value. More recently the concept of carbon pricing or taxation is being researched in a bid to make the 'polluter pay'. One example was the European emissions trading scheme which caps the total level of GHG that a polluter can produce and allows those industries with surplus emissions to sell their extra allowances to larger emitters and creates a market price for carbon emissions by introducing supply and demand. On the other hand a carbon tax sets a direct price on carbon by creating a tax rate for GHG emissions. If the Bio-SNG from GLT-SR has lower carbon emissions than conventional natural gas, there may be future economic benefits that reduce the chance of negative NPVs and improve the feasibility of the plant.

To determine whether a GLT-SR could benefit from pricing or taxation of carbon, an environmental analysis was produced in the form of an environmental impact assessment in the next chapter.

3.4.3 Brief Conclusions

- An average CAPEX cost of $528,660 was calculated using the national energy technologies estimation method and a base equipment cost of $181,423, calculated from cost curve analysis.
- A discounted cash flow analysis was produced for the GLT-SR process in Missouri over a 25-year period using estimated CAPEX, OPEX and revenue from gas costs showing that under certain scenarios it is a profitable venture with 12-18% return.
- The value of crude glycerol using GLT-SR was shown to be roughly $0.02 kg^{-1}, which was less than selling the crude glycerol at $0.06 kg^{-1}.
- Risk analysis by monte carlo simulation identified that accepting a 12% return on investment gives a 95% confidence under the minimum uncertainty that the venture will be profitable.
- Main cost bottlenecks are glycerol purity and CAPEX value

4 Environmental factor assessment

4.1 Introduction

With the advent of climate change and other environmental threats, tools and methods of evaluating the impacts of our actions on the planet have gained popularity. This chapter discusses methods to assess and benchmark these impacts and explains how they can be used to discuss the feasibility of the glycerol to bio-SNG process when compared to the status quo. These types of assessments are broadly termed 'environmental factor assessments' and the main stages from the design process are shown in Figure 47 with the system boundaries in Figure 16.This shows that all of the analyses are dependent upon the process simulation step.

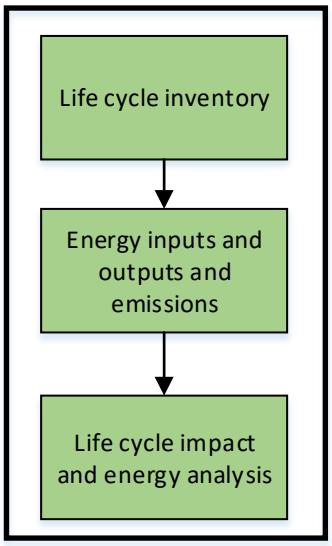

Figure 47. Life cycle assessment steps from the design process.

Environmental factor assessments provide an opportunity for businesses, individuals, governing bodies and policy makers to make informed decisions on technologies and products that reduce the impacts on the environment [125,126]. For example fossil fuels are cheaper to produce than renewable and sustainable alternatives but the trade-off is that fossil fuels are non-renewable and release significant fossil carbon into the atmosphere. On the other hand, renewable biofuels release a significant portion of biogenic carbon back into the atmosphere which is assumed to be sequestered by living biomass. By determining the impacts of biofuel production processes and comparing them to their fossil counterparts, evidence can be produced to guide policy and incentivise environmentally favourable renewable and sustainable energy technologies. Consequently, the impact on the environment is fast becoming one of the determining factors for feasibility of a biofuel

production process. The issue with this assumption is the neglect of timescales. Whilst CO_2 from biomass that is combusted will be sequestered, the time taken for CO_2 to be removed from the atmosphere is dependent on the type and age of biomass that is used to replace the combusted biomass. Furthermore, in the short term, combusting biomass still increases CO_2 and other emissions in the atmosphere, until such time as the CO_2 is sequestered.

A production process can be any route where goods or services are produced where there are required inputs that produce outputs and is usually composed of several unit processes [127]. A unit process as defined by the ISO1404 as the smallest element considered in the life cycle inventory analysis for which input and output data are quantified [128].

Production processes are usually composed of several unit processes. The furthest back that material or energy inputs are calculated from are known as inputs from nature and the system boundary is the point at which the life cycle analysis stops including contributions from unit processes. An example for the production of biodiesel from oilseed rape feedstock is shown in Figure 48. In this case, the life cycle analysis (LCA) focuses on the well to production, ignoring any contributions from the end use unit process of the biodiesel. As the system boundary is somewhat subjective, it is crucial that only LCA's with similar system boundaries can be compared. Once the desired inputs and outputs are quantified, the environmental impact on the environment can be calculated.

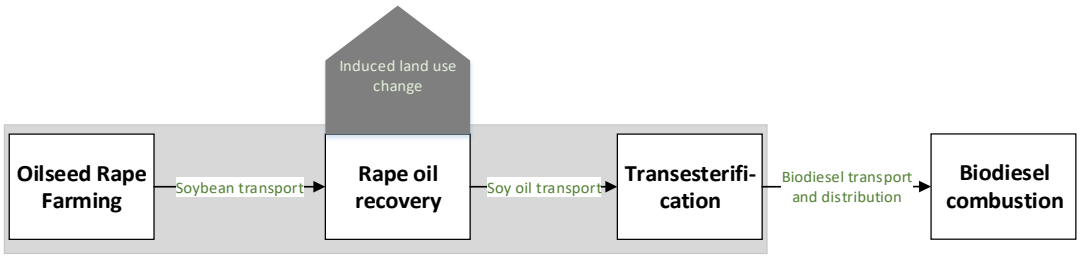

Figure 48. Example of a biodiesel production process displaying individual unit processes for the production of biodiesel from oilseed rape. Unit processes are contained within each box whilst the system boundary is highlighted in grey.

The environmental impacts can be classified into several categories and depend upon the input material streams as well as the type of assessment. Examples of environmental factor assessments include an Environmental Impact Assessment, Strategic Environmental Impact, and Life Cycle Analysis (LCA). LCA includes the environmental impacts derived from the resources used throughout a product's life cycle and includes; production and acquisition, transport, transformation, distribution, use, and waste management including disposal and

recycling of any products. Carrying out an assessment can be as simple as using spreadsheet software or bespoke commercial software and is dependent on the data available [129].

Examples of software that are available for use include the Greenhouse Gases, Regulated Emissions, and Energy use in Transportation Model (GREET) [86], OpenLCA and SimaPro. These examples have a graphical user interface allowing the user to input or import life cycle inventory data, although SimaPro requires a license. Additionally the majority of reference life cycle data is stored in databases which require subscriptions or licensing fees. It is possible to apply any method of LCA when using these softwares as long as data is available and a consistent framework is followed.

4.1.1 LCA Framework

Every LCA begins with a similar method. The framework method for LCA has been strictly documented by the international organization for standardisation (ISO) leading to the ISO 14040 metrics is shown in Figure 49 [127]. Additional details are provided in further international standards 10401, 10402 and 14043 regarding goal and scope definition and inventory analysis, life cycle impact assessment and life cycle interpretation respectively [128,130,131]. The framework consists of defining the goal and scope of the study, including the system boundary and functional unit, before determining what database to use by inventory analysis and then assigning these inputs and outputs to an impact assessment. The system boundary determines which unit processes should be included in the LCA study and is somewhat subjective. The functional unit is a quantitative measure of the functions that the goods or service provide e.g. 1 kWh of electricity. The result of the impacts assessment shows the inputs and outputs (emissions) in relation to the functional unit and system boundary.

As there is no obvious solution to many impact allocation problems, the aforementioned LCA ISO standards leave a large degree of freedom giving the opportunity for multiple ways of interpretation. What is consistent is that, during all of stages, the LCA must be interpreted and changed according to new data and new assumptions.

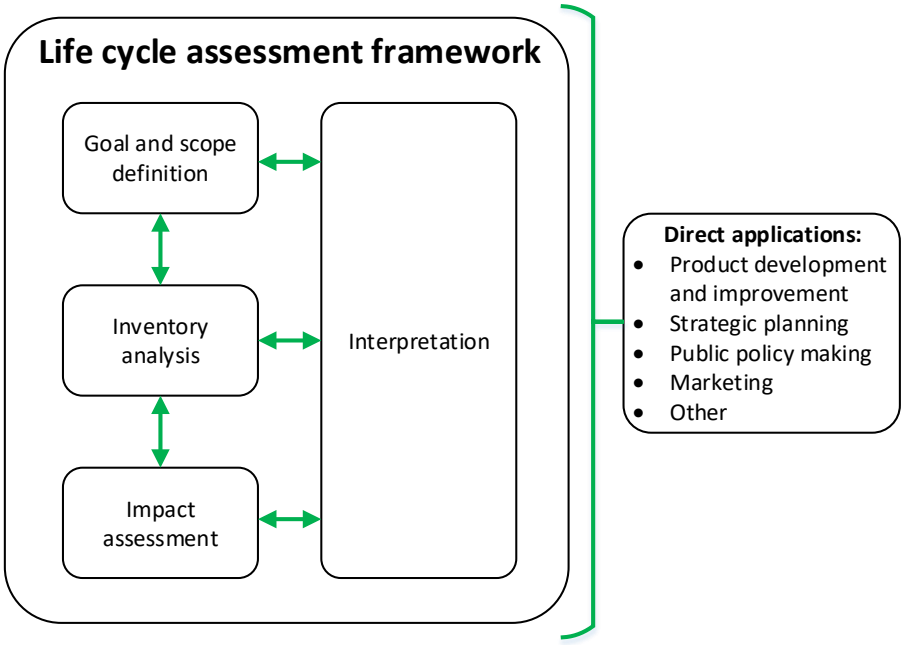

Figure 49. Phases of a life cycle analysis as described by ISO14040.

Developments in LCA from 2009 have been reviewed extensively by Finnveden *et al.* 2009 [132]. Issues and suggestions for improvements and standardisation relative to LCA for biorefineries have been made in the work by Ahlgren *et al*. 2015 [133]. Additionally a book entitled Life-Cycle Assessment in Biorefineries was published in 2017 and covers specifics to do with feedstocks, land use change and products [129]. From these overviews and the ISO standards key areas that must be consistent for comparison and well defined are the goal definition, functional unit, allocation of the biorefinery outputs and biomass feedstock, land use, biogenic carbon and timing of emissions.

Where the usual complications arise and LCAs begin to differ is the approach taken for co-product allocation. Various co-products are produced from processes, especially from biorefineries, and it is important to distinguish how to approach allocating emissions and environmental impacts to each co-product. Moreover, databases such as Ecoinvent, have several different versions of the same data to account for allocation differences based on very diverse approaches.

4.1.2 LCA Approaches

Allocation methods will significantly influence or determine the final results of a life cycle analysis. The allocation method determines how impacts are shared between each of the outputs and usually fall under consequential or physical.

The consequential approach is based on the ability of the by-products to avoid burdens i.e. replace inputs in the process and relies on assumptions on the quality of the by-products

and how much of the input they can replace. The input does not have to be in the same process. To avoid these types of assumptions the physical allocation method can be used.

4.1.3 Physical Allocation

When separating impacts via physical allocation, by-products from the biorefinery must be classified into waste, recyclable material, or marketable co-products. Secondly an allocation key must be defined based on a physical characteristic such as; mass, dry mass, volume, energy content, exergy content, embodied energy (energy input) or economic value. As the choice of the allocation key is subjective, the results may differ significantly and it is often the case that several different keys are used and compared before the most appropriate is chosen.

In the biodiesel process there are often by-products produced. In the case of soybean biodiesel, alongside biodiesel as the main product, the two main by-products are soybean meal from processing of soybeans for oil and glycerol produced during transesterification. When using the consequential method of allocation an assumption must be made about the properties of the by-product and whether it could replace the equivalent product on the market.

On the other hand, physical allocation distributes emissions based on the ratio produced by the allocation key. Using an economic allocation key as an example, if the value of the product biodiesel and glycerol were equal, the emissions would be assigned at a 50:50 ratio. However, if the value of the glycerol was only 1% of the biodiesel, the emissions would be assigned 99:1 with the majority of emissions associated with biodiesel. These allocation keys can be assigned at any point where a by-product is produced.

In the same way energy and mass allocation keys can be assigned. For energy, the ratio depends upon the stored energy within the product. In the case of soybean meal and glycerol this has been measured as the low heating value. For mass the ratio is dependent on quantity of product produced in kg.

For this work the physical allocation method is used with economic value, energy and mass as the allocation keys. The processes involved along with their products is shown in Figure 50, whilst a comparison of allocation methods using values from the USLCI data is shown below and includes mass, energy and economic in Table 23.

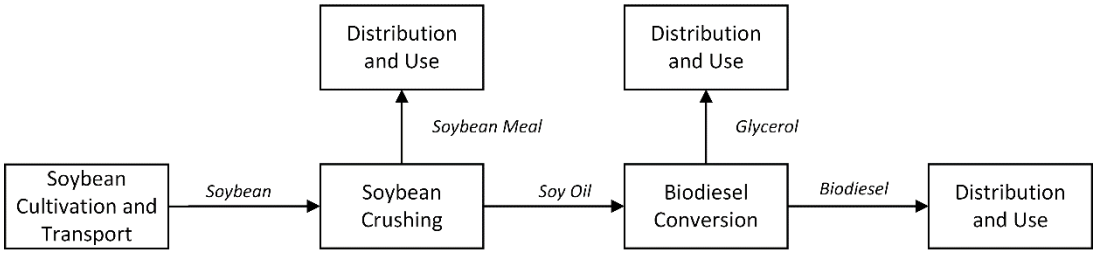

Figure 50. Block flow diagram of soybean biodiesel processes showing products and co-products

Process	Product	Energy (%)	Economic (%)	Mass (%)
Soybean Crushing	Soybean Oil	35.0	38.0	19.5
	Soybean Meal	65.0	62.0	80.5
Transesterification	Soybean Biodiesel	95.4	98.9	89
	Glycerol (0% H_2O)	4.6	1.1	11

Table 23. Distribution of emissions based on energy, price and mass allocations for co-products.

As soybean oil contains less energy, value and mass than the soybean meal, more of the life cycle impacts are associated with the meal in all cases. For the transesterification step, glycerol has the most impacts associated with it on a mass basis, followed by energy and then economic. This is due to the lower energy density and value of the glycerol compared to biodiesel.

4.2 Literature Review

Since 1996 there have been several published papers with the subject of life cycle analysis of soybean biodiesel. The focus of these studies is to compare the life cycle impact factors and fossil energy requirement of soybean biodiesel with fossil diesel and other types of biodiesel from different feedstocks. Prior to the first work in 1996, the USA began utilising biodiesel with no subsidies or tax incentives in 1995 with the first fleet of buses in South Dakota committing to run on B20 (20% biodiesel blend). From here on out, significant evidence was required to determine whether soybean biodiesel was complimentary to, or a viable replacement for fossil diesel before the government could make long term policy decisions. It was not until 1998 that a landmark LCA on soybean biodiesel vs petroleum diesel in U.S urban buses was published [134], coinciding with President Clinton signing executive order 13134, calling for expanded use of bio-based fuels, in the same year[10]. After 1998, subsequent legislation and tax incentives, record high prices of gasoline and LCA reports confirming reductions in GHG emissions and reduced fossil energy use propelled soybean biodiesel into the limelight as a clean, sustainable and home-grown supplementary fuel in the USA.

4.2.1 Life cycle impacts and greenhouse gas (GHG) emissions

Some of the earliest work on biodiesel LCA was carried out in 1996 and 1997 on rapeseed methyl ester. The earliest work was produced in 1996 by Carolin Spirinckx and Dirk Ceuterick on Belgian rapeseed biodiesel using a physical allocation method and was followed by a similar study by Kaltschmitt *et al.* 1997 on German rapeseed biodiesel with a displacement approach. These studies focussed on the life cycle impact factors using a “well to wheel” approach and concluded that biodiesel only surpasses fossil diesel in global warming potential and fossil fuel consumption, because low quantities of fossil fuels are consumed in the biodiesel production chain and rapeseed plants sequester CO_2 during their growth. Eutrophication and photochemical oxidant formation, as well as other airborne emissions such as NO_x, would be increased due to large contributions from fertiliser and other agricultural processes which are not required when producing fossil diesel [135,136]. Both the displacement and allocation methods yielded similar conclusions and set the stage for LCA of soybean biodiesel.

Regarding soybean biodiesel, Sheehan *et al.* 1998 published their well to wheel LCA comparing fossil diesel and soybean biodiesel in urban buses by mass based allocation. Working in partnership with NREL, they determined that biodiesel was a net energy

producer, reduced the life cycle consumption of petroleum as well as CO_2, SO_x, particulates CO emissions and hydrocarbon emissions at the tailpipe but increased NO_x and life cycle hydrocarbon use. MacLean *et al.* 2000 also published a comparison of U.S. soybean biodiesel against fossil diesel but used an economic input-output life cycle analysis from well to wheel. Overall the same conclusions about soybean biodiesel are observed compared to rapeseed biodiesel, where both offered lower GHG emissions, improved sustainability and reduced imported fuel demand compared to fossil diesel, thereby improving energy security. On the other hand, biodiesel from soybeans can only be attractive if there is a demand for the by-products such as soybean meal and glycerol, there is a high demand for the primary product biodiesel and food crops are not diminished in favour of fuel production in the USA [137]. The majority of studies after the year 2000 conclude that utilising soybean biodiesel will reduce GHG emissions when compared to fossil diesel in; Italy [138], the US [86,139–147], China [148,149], Brazil [150,151], Iran [152], Portugal using Brazilian soybean [153], Argentina [154] and Europe [155].

Of these works the earlier studies did not include the impact of indirect land use change (ILUC) on GHG. In the life cycle analysis of biofuels review by McKone they state that one of the grand challenges is understanding and quantifying the impact of land use and land use change [156]. Published works regarding soybean biodiesel and land use change began appearing in 2012 and the majority of inventory data has been updated to include land use change impacts [143,145,146,150,151,153]. Of particular interest is the work by Pradhan who revisited previous LCAs and found that the reduction in GHG's attributed to soybean biodiesel compared to fossil diesel did decrease when land use change was accounted for, but still remained significantly negative [143]. Chen *et al.* 2018 described the most sensitive processes for GHG emissions were; ILUC, farming energy, biodiesel production, and methanol.

Whilst a large focus was placed on reducing GHG emissions and the life cycle impact of global warming potential, several studies emphasised the implications on non-GHG emissions aspects of soybean biodiesel. The trade off when substituting fossil diesel for soybean biodiesel is the significant increase in eutrophication, photochemical oxidant acidification, and human eco-toxicity due to contributions from agricultural processes and materials such as fertiliser and electricity generation [135,136,144,149].

4.2.2 Energy and fossil energy

A plethora of studies are available on how much energy and how much fossil energy is required to produce soybean biodiesel [85,86,138,140,146,148,152]. One way of expressing

the net energy of a fuel is the fossil energy ratio (FER) which is a measure of how much energy is produced per unit of fossil energy input, although Piastrellini describes the net energy as energy return on investment (EROI) [154]. Some studies detail the net energy per hectare but only FER is consistently reported.

Reference	Fossil Energy Ratio (FER)
Chen *et al.* 2018	3.9
Rajaeifar *et al.* 2013	1.97
Pradhan *et al.* 2012	5.5 or 1.84*
Pradhan *et al.* 2009	4.4 or 1.47^
Huo *et al.* 2009	2.08>
Hu *et al.* 2008	1.31
Carraretto *et al.* 2004	2.09
Sheehan *et al.* 1998	3.22

*Table 24. Fossil energy, net energy and EROI values from the literature where appropriate. *calculated from the overall energy requirement as distributed amongst co-products. ^calculated using the same ratio as Pradhan et al. 2012, > calculated from Huo et al. 2009 using fossil energy reduction of 52%.*

From the literature, soybean biodiesel produces a positive net energy compared to the fossil energy input. Chen *et al.* 2018 described the following processes in order of the greatest contribution to energy consumption in soybean biodiesel production; biodiesel production (transesterification), farming and methanol. The net energy will vary with allocation method and LCA approach as well as the input data and whether energy across all of the products is attributed to the soybean or is spread.

4.2.3 LCA Attribution and Analysis methods

Governing bodies and institutions advocate for different physical attributions. The European renewable energy directive insists on energy allocation when concerned with biofuels production [157] whilst the Argonne GREET model has energy allocation as its default allocation method [141]. The Roundtable on Sustainable Biomaterials requires an economic allocation [158] and the Ecoinvent database stores the majority of their data as consequential or mass based allocation [159]. Hybrid attribution methods have been produced in the literature for biodiesel where more than one physical allocation key has been used for different unit processes within the same production process [86,133,142,146]. For example, Huo *et al*. 2008 used two hybrid methods; Hybrid method 1 combines the displacement method for soybean meal and energy value based allocations for energy co-products whilst hybrid method 2 was the same aside from assigning the market based allocation for soybean meal instead of displacement.

The analysis method determines how the outputs of a process are attributed to each life cycle impact. The majority of methods have been reviewed in the white paper by Greendelta [160] and include the commonly used CML baseline, eco-indicator 99 and ReCiPe methods and their derivatives. Each method contains different life cycle life cycle impacts and also looks at the impacts of emissions over different time periods e.g. 20, 50 and 100 years.

The CML baseline method was created by the University of Leiden, Netherlands, and contains the most commonly used life cycle impacts which are; Acidification, climate change, abiotic depletion, ecotoxicity, eutrophication, human toxicity, ozone layer depletion and photochemical oxidation. Using the non-baseline method adds ionising radiation, land use, and odour as additional impacts. These impact indicators are known as mid-point indicators as they focus on single environmental problems whereas endpoint indicators aggregate mid-point indicators to three higher levels. These are; effect on human health, biodiversity and resource scarcity and can be calculated using the Eco-indicator 99 method. The ReCiPe combined Eco-Indicator 99 and CML and provided a method of calculating mid-point and end-point indicators. As mid-point indicators were desired, CML was chosen for this work.

4.2.4 Impact of literature on GLT-SR

From the literature we can conclude that LCA has successfully been used as a tool to convey the benefits and drawbacks of soybean biodiesel. The main environmental benefit is a significant reduction in GHG emissions compared to fossil diesel whereas the energy analysis has determined that soybean biodiesel produces a positive net energy. Fossil energy ratio is a popular metric for determining the net energy. This gives a strong basis that utilising glycerol for bio-SNG will produce similar environmental impacts and fossil energy ratios compared to the fossil equivalent of natural gas but to what extent remains the focus of this work. Moreover, the method of allocation will be integral in impacting both biodiesel and the GLT-SR bio-SNG and economic, energy, mass and hybrid approaches should be used accordingly. As the glycerol will be converted into an energy vector, an energy based allocation appears to be suitable. However, a hybrid version may be more suitable as soybean meal is used as an animal feed and not as an energy vector. If a consequential analysis was adopted, an assumption about the bio-SNG from glycerol is necessary as it will replace some of the natural gas in the system. Finally, fossil energy ratio appears to be an important metric to determine the net energy of a renewable fuel and should be applied here.

4.3 Method

The methodology for this work will follow the ISO14040 standard. The layout of the explanation will consist of the sections mentioned in the life cycle framework (Figure 49).

4.3.1 Goal

The goal of this LCA study is compare the life cycle impacts of conventional natural gas for steam with steam produced from soybean glycerol based bio-SNG. The route is via a direct methanation process that takes advantage of glycerol low temperature steam reforming and produces bio-SNG that can be combusted in a similar way to natural gas. Contributions from resources required to build the infrastructure e.g. iron ore, are not included initially. Comparisons will be made with natural gas to find out whether there is an environmental advantage of utilising glycerol for bio-SNG over fossil natural gas. The intended audience are researchers in the field of steam reforming and methanation as well as engineers and biodiesel refiners to be communicated to by this thesis and any subsequent publications.

4.3.2 Scope

It was assumed that the steam production process using natural gas and bio-SNG was carried out on-site at the biodiesel refinery and there are no additional transport or distribution costs for steam. It was also assumed that the bio-SNG would transfer heat energy at the same efficiency as natural gas. The functional unit selected was 1 kg of steam.

4.3.2.1 System Boundary

The system boundaries for the production of conventional natural gas versus soybean glycerol based bio-SNG are shown in Figure 51. Additional energy requirements for the distribution and end use of the steam are not included.

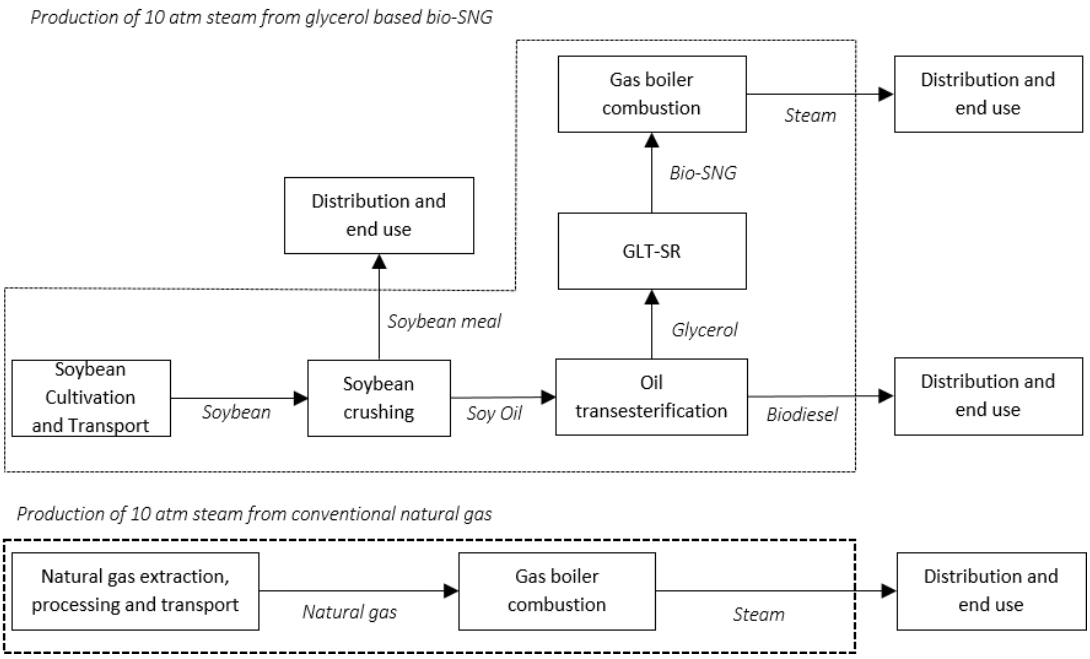

Figure 51. System boundary for the production of steam at 10 atmospheric pressures from conventional natural gas and soybean glycerol via glycerol low temperature steam reforming.

To determine the extent by which the soybean glycerol based bio-SNG can substitute conventional natural gas in a soybean biodiesel refinery, the energy requirement for the production process of soybean biodiesel has been mapped in Figure 52 by unit process.

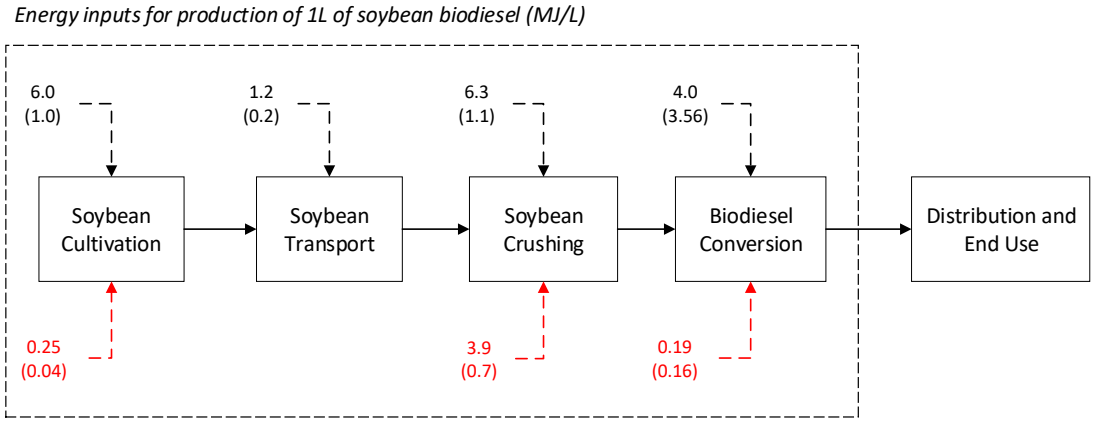

Figure 52. System boundary and energy process flow diagram for a soybean biodiesel plant process. Bracketed values are the share assigned to biodiesel under the mass allocation whilst values in red are the natural gas energy requirements.

The energy data were adapted from Pradhan *et al*. 2012 who used inventory data from the USDA-ARS model and did not describe the end use of biodiesel. All energy values are in MJ L^{-1} biodiesel and the value of 3.56 at biodiesel conversion is modified to the 89% mass allocation in the default USLCI data. The values connected by dashed black lines are total

energy whilst values in brackets are the value of energy that was assigned to biodiesel using only a mass allocation criteria. Finally values in red are natural gas energy contributions to each unit process. Distribution and end use energy requirements are not included.

4.3.2.2 Allocation

In this work, a sensitivity analysis was performed to compare the results under different allocation methods for glycerol: mass, energy, and economic. As a default the USLCI data distributes emissions based on mass for the co-products of soybean meal and glycerol in system 2.

A selling price of \$0.977 kg^{-1} and \$0.066 kg^{-1} [107] was used for biodiesel and crude glycerol, respectively for the economic allocation.

The mass basis allocates 10.7% of the emissions to glycerol as 0.107kg of glycerol was produced for every 1 kg of biodiesel. To determine the mass of glycerol produced per litre of biodiesel a density of soybean biodiesel of 0.885 kg L^{-1} was used [161]. For the calorific energy the calorific value of glycerol was assumed as 16 $MJkg^{-1}$ whereas biodiesel was 39.48 MJ kg^{-1} and [39]. In all cases the natural gas allocation was based on energy as it is a fuel.

4.3.2.3 Environmental Impacts

The potential environmental impacts were assessed using the CML-IA v3.03 World 2000 methodology [162]. The following environmental impacts categories were considered: Abiotic Depletion Potential (ADP), Abiotic Depletion Potential (fossil fuels) (ADP-FF), Global Warming Potential (GWP), Ozone layer Depletion Potential (ODP), Human Toxicity Potential (HTP), Freshwater Aquatic Ecotoxicity Potential (FWAEP), Marine Aquatic Ecotoxicity Potential (MAEP), Terrestrial Ecotoxicity Potential (TEP), Photochemical Oxidation Potential (POP), Acidification Potential (AP), and Eutrophication Potential (EP).

4.3.3 Inventory Analysis

Two data inventories were selected for comparison to determine the environmental impacts of soybean biodiesel using the functional units of 1 kg of biodiesel and 0.12 kg glycerol as well as 1 kg of steam from natural gas. The first is from the USLCI [163] which was used in Pradhan's work [147] and collected by an independent consultancy known as Omnitech International and the second is from the Ecoinvent data base. Both are shown in Figure 53.

		Soybean Biodiesel		*Steam (10 ATM) from NG*	
Impact	*Unit kg^{-1}*	*USLCI*	*Ecoinvent V3.04*	*USLCI*	*Ecoinvent V3.04*
ADP	*kg Sb_{eq}*	N/A	$4.64x10^{-6}$	N/A	$2.13x10^{-8}$

ADP-FF	*MJ*	$8.68x10^{0}$	$1.06x10^{1}$	$3.34x10^{0}$	$1.81x10^{0}$
GWP	*kg* $CO_{2\,eq}$	$6.4x10^{-1}$	$1.06x10^{0}$	$1.92\ x10^{-1}$	$1.08x10^{-1}$
ODP	*kg CFC-11* $_{eq}$	$1.2x10^{-9}$	$1.17x10^{-7}$	$1.07\ x10^{-13}$	$8.34x10^{-9}$
HTP	*kg 1,4-DB* $_{eq}$	$1.9x10^{-1}$	$2.96x10^{-1}$	$5.27\ x10^{-2}$	$1.24x10^{-2}$
FWAEP	*kg 1,4-DB* $_{eq}$	$1.6x10^{-1}$	$2.13x10^{-1}$	$1.88\ x10^{-2}$	$4.77x10^{-3}$
MAEP	*kg 1,4-DB* $_{eq}$	$3.6x10^{2}$	$6.95x10^{2}$	$7.16\ x10^{1}$	$1.71x10^{1}$
TEP	*kg 1,4-DB* $_{eq}$	$8.5x10^{-4}$	$3.37x10^{-3}$	$1.22\ x10^{-5}$	$2.64x10^{-5}$
POP	*kg* $C_2H_{4\,eq}$	$4.6x10^{-4}$	$6.7x10^{-4}$	$8.28\ x10^{-5}$	$2.15x10^{-5}$
AP	*kg* $SO_{2\,eq}$	$4.1x10^{-3}$	$4.61x10^{-4}$	$1.89\ x10^{-3}$	$3.63x10^{-4}$
EP	*kg* $PO_4^{3-}{}_{eq}$	$4.6x10^{-4}$	$2x10^{-3}$	$2.33x10^{-5}$	$2.21x10^{-5}$

Figure 53. Potential environmental impacts of the production of 1 kg of biodiesel and 0.12 kg of glycerol.

In every category the USLCI data has reduced impacts when compared to the Ecoinvent data for soybean biodiesel. The USLCI data contains contributions from 100 unique unit processes whereas the Ecoinvent data contains 10931. The main difference between the two datasets is that the USLCI does not include infrastructure contributions e.g. the steel used to produce the train for transport of the biodiesel. In addition the USLCI data has a zero value for ADP which is calculated based on depletion of non-living natural resources such as iron ore and supports the notion that infrastructure contributions are excluded [164]. ADP-FF has value in the USLCI because of the fossil fuel use in unit processes such as transport. As the infrastructure data is not available for GLT-SR, the USLCI data is more appropriate for comparison using allocation methods.

The USLCI data predicts 0.12 kg of glycerol to be produced per kg of biodiesel as this was taken from OmniTech internationals data. Comparatively Pradhan predicted 0.171 kg kg^{-1} biodiesel [85,147,165] and accounts for the larger contribution of energy to glycerol in their work.

Ozone layer depletion is near zero for both the Ecoinvent and USLCI data. ODP is calculated based on the ability of any emissions to degrade the ozone layer with chlorofluorocarbons as the reference gas[160].

Production of steam was calculated by using a boiler efficiency of 90% and determining the energy required to produce steam. Converting water at a temperature of 15°C to steam at 10 atm and a minimum temperature of 184.65°C required 2.72 MJ kg^{-1}. Accounting for the boiler efficiency increases this value to 3.02 MJ kg^{-1}. It was assumed the natural gas had an LHV of 38.3 MJ m^{-3} according to CAS number 008006-14-2.

4.3.4 Fossil Energy Ratio

As outlined in section 4.2.2, many studies report the fossil energy ratio of biodiesel. Based on each allocation method the magnitude of energy associated with bio-SNG based steam can be calculated by summing the energy values from each unit process that apply to glycerol and bio-SNG based steam. The energy values calculated in Pradhan are altered by their life cycle efficiency factor which is the ratio of the embedded energy to the total energy to produce their life cycle energy. By allocating the life cycle energy inputs to glycerol the fossil energy ratio for glycerol based steam can be calculated.

For soybean cultivation, transport and crushing, the energy values in Pradhan apply to the oil prior to transesterification and can be split into glycerol and biodiesel using the desired allocation ratio. For steam from bio-SNG and natural gas the efficiency of combustion was assumed as 90%. As steam generated in the GLT-SR process is recycled, the only energy input is from electricity. For combustion in the boiler the energy input is calculated as the energy loss due to the boiler efficiency.

4.3.5 Secondary Energy

The USLCI data only includes primary energy inputs. Secondary energy (embodied energy in machinery) was estimated for farm machinery in the soybean cultivation stage as 1.4 MJ L^{-1} soybean biodiesel. Energy for building materials for the crushing and transesterification (conversion) unit processes was estimated as 0.04 MJ L^{-1} and 0.02 MJ L^{-1} respectively [85,166]. It was assumed that the GLT-SR unit process would require the same energy input as the crushing unit process.

4.4 Results and Discussion

The normalized life cycle impacts under mass, economic and energy allocations for bio-SNG based steam and under the default allocation of energy inputs for natural gas are displayed in Figure 54 and express how important the allocation key is.

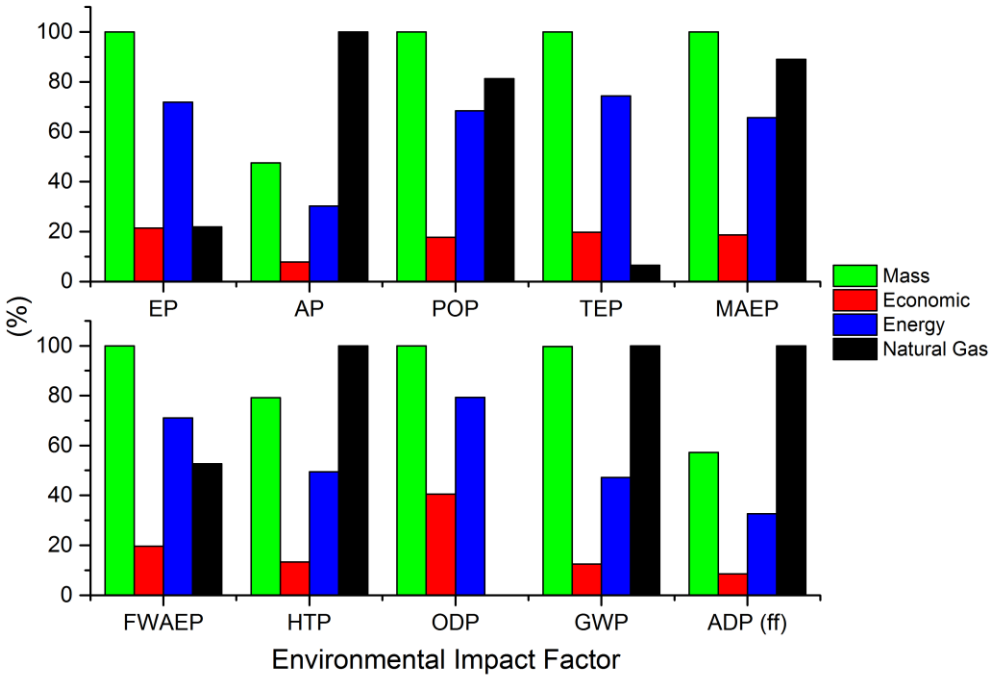

Figure 54. Life Cycle Impact factors of 1kg steam from bio-SNG under mass, economic and energy allocations as well as 1kg steam from natural gas where: EP = Eutrophication Potential, AP = Abiotic Depletion Potential, POP = Photochemical Oxidation Potential, TEP = Terrestrial Ecotoxicity Potential, MAEP = Marine Aquatic Ecotoxicity Potential, FWAEP = Freshwater Aquatic Ecotoxicity Potential, HTP = Human Toxicity Potential, ODP = Ozone layer Depletion Potential, AP = Acidification Potential, GWP = Global Warming Potential, and ADP (ff) = Abiotic Depletion Potential (fossil fuels).

The abiotic depletion is zero for this model because infrastructure is not included. The order of favouring bio-SNG steam in terms of life cycle impacts were the economic allocation, followed by energy and mass. The economic allocation produces the most favourable result for bio-SNG based steam because of the low value of glycerol compared to biodiesel in this work. As the economic value of glycerol fluctuates significantly with scarcity this allocation method may not be favourable. Considering the glycerol is being used for an energy purpose the energy allocation appears more adequate and produces more favourable results than the mass allocation.

Natural gas has reduced impacts against all allocation methods for bio-SNG in TEP, ODP and EP. For EP and TEP this is largely due to the magnitude of agricultural activity required to produce the soybeans for the glycerol base steam. Specifically for EP, high nitrogen and

nitrate, ammonia and phosphate contents in fertilizer provide conditions for plant life such as algae to grow in water courses whilst for TEP, chemicals such as pesticides and heavy metal emissions are important contributors. For ODP the aforementioned chemicals required brominated or fluorinated compounds which have high residence time in the atmosphere.

It is notable that the GWP of bio-SNG steam is the same as NG for the mass allocation and was reduced by roughly 55% and 80% for the energy and economic allocations respectively. According to this energy life cycle impacts analysis, in the worst case no increase in GWP would occur by utilising glycerol for steam. On the other hand improvements on GWP would be seen if an economic or energy allocation were employed in this scenario however these emissions would be allocated onto the biodiesel and soybean meal.

The ADP (ff) is significantly reduced for all allocations pertaining to steam from bio-SNG. This is largely due to the reduced fossil energy required to produce the steam.

In this work the glycerol is being used for energy and gives an argument for the energy allocation. Similarly, soybean meal is used as an animal feed and could also be perceived as an energy carrier. The economic allocation will be most favourable for glycerol-based steam as it has the lowest contribution of emissions at the transesterification stage due to the low value of glycerol. An argument for assigning all the emissions to biodiesel is that it is the primary product of the biodiesel production. Even when all emissions are allocated to biodiesel, it has still been shown to be favourable in terms of global warming potential when compared to fossil diesel in well to wheel analysis[138].

4.4.1 Allocation effects on biodiesel impact factors

A comparison of the change in life cycle impacts for biodiesel under mass, economic and energy allocations can be seen in Figure 55. The mass allocation is the default setting and has the lowest environmental impacts associated with biodiesel whereas the economic allocation has the highest impacts. Biodiesel (and soybean oil) is the most valuable product from the process and will have most of the emissions assigned from the economic allocation. Conversely, the mass allocation assigns more emissions to the co-products than both economic and energy allocations because the mass of the co-products is greater than their subsequent economic and low heating value.

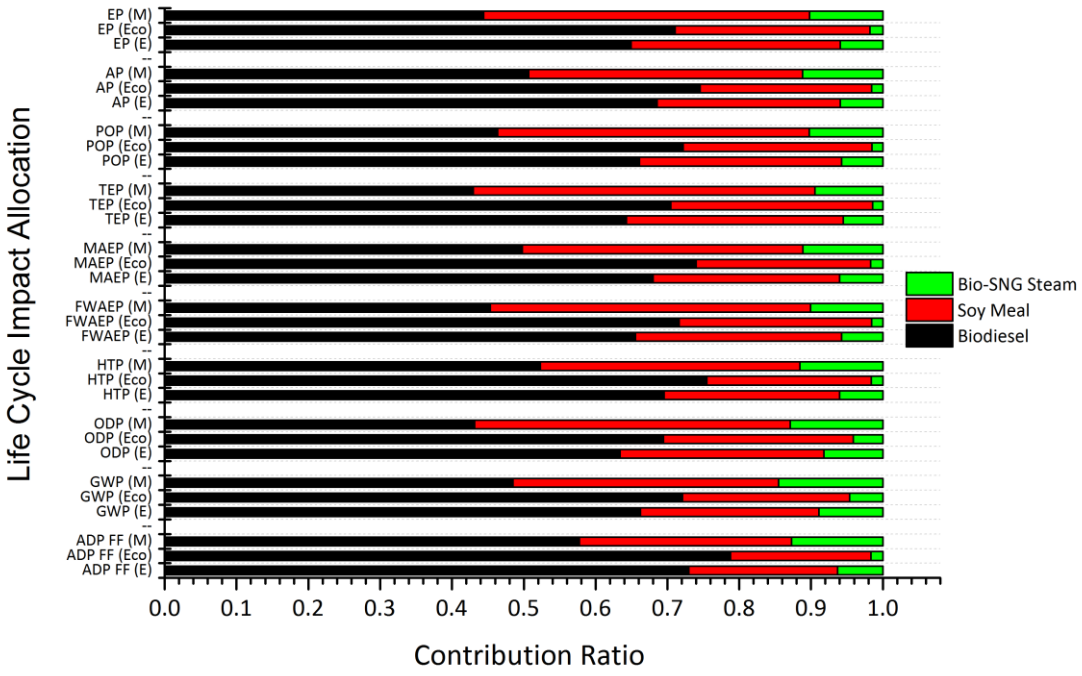

Figure 55. Variation of Life Cycle Impact factors across co-products of soybean biodiesel production with allocation method.

In the USA, the maximum capacity of soybean biodiesel production was recorded as 770 ML y^{-1} (Table 15). Based on the life cycle energy analysis data shown in Table 9, the natural gas requirement per litre of biodiesel was 4.40 MJ and equates to 3385 TJ y^{-1} for all soybean biodiesel plants. If ~24% of the natural gas demand can be substituted by glycerol based bio-SNG, there is potential to save up to 532812 TJ y^{-1} (780,600 MMBtu y^{-1}) of natural gas. This would result in the overall GWP of steam production increasing by 12% under a mass allocation and decreasing by 10% and 2% for economic and energy allocations, respectively.

4.4.2 Fossil Energy Ratio (FER)

The fraction of energy associated with glycerol and steam from glycerol bio-SNG is displayed in the simplified flow diagram in Figure 56. The mass of glycerol for every litre of biodiesel was calculated as 0.106 kg and could be converted into 1.356 MJ of energy or 1.221 MJ of steam with a boiler efficiency of 90%. This gave fossil energy ratios of 1.45, 5.44 and 2.23 for mass, economic and energy allocations respectively. In all cases the FER is greater than 1 which shows that utilising glycerol for conversion to bio-SNG and combusting in a boiler for steam has a positive net energy.

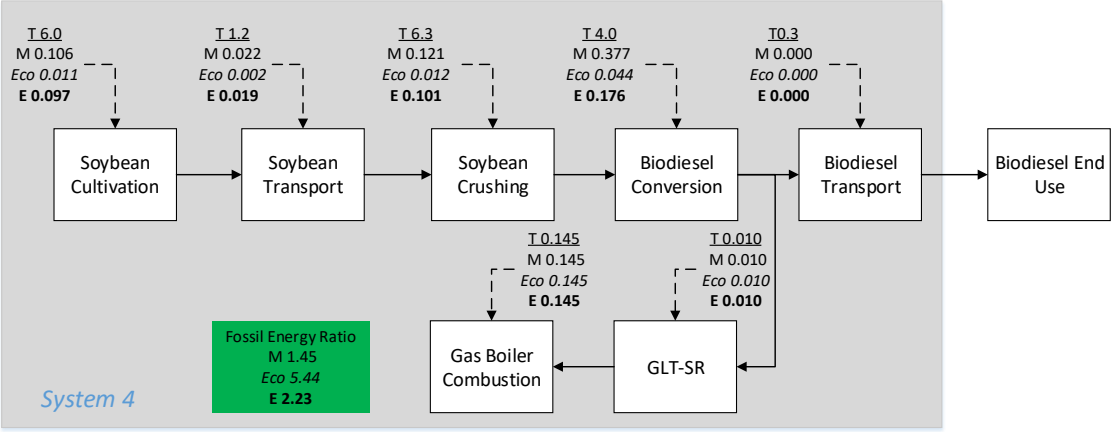

Figure 56. System boundary for system 4 including unit processes specific to combustion of glycerol based bio-SNG. Where T is total energy, M, Eco and E are mass, economic and energy based allocations for glycerol respectively.

The contributions to the energy inputs and FER of glycerol bio-SNG steam are shown Figure 57. The major contributor in all cases is the biodiesel conversion step as the largest sum of energy is associated with biodiesel and glycerol. Energy required for GLT-SR and combustion steps are constant as they are allocated 100% to the glycerol in any case. Overall, the FER is positive for steam produced by GLT-SR with mass allocation being the lowest value.

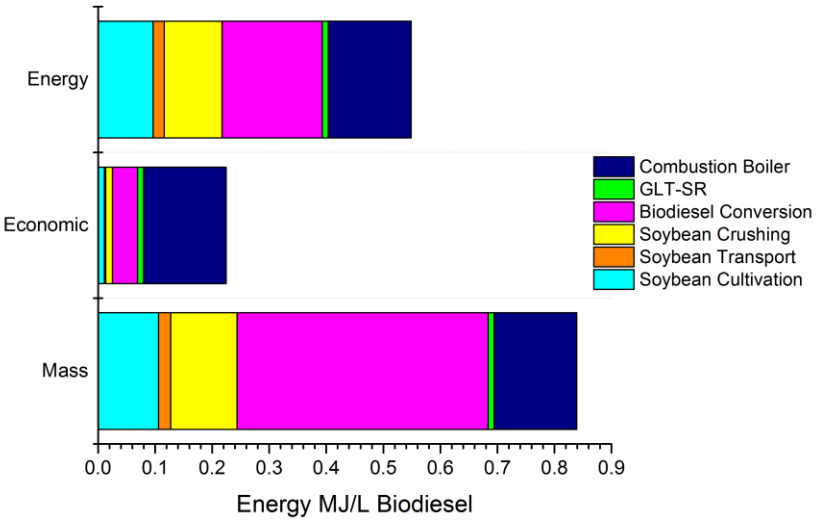

Figure 57. Unit process contributions to fossil energy ratio (FER) by allocation method.

The addition of secondary energy associated with embodied energy in the buildings for each process reduces the FER under all allocations. A reduction in FER of 3%, 2% and 4% for mass, economic and energy respectively resulting in new FER's of 1.42, 5.34 and 2.13 respectively. These values fall within the range of FER in the literature shown in Table 24.

4.5 Summary

An energy life cycle impact analysis based on the energy inputs to produce glycerol based bio-SNG was carried out using data from the US life cycle inventory database. Similarly to biodiesel, global warming potential offset is possible when compared to natural gas based steam but only with the energy and economic allocation and with a trade-off of increased eutrophication, terrestrial ecotoxicity potential and ozone depletion potential due to contributions from the agricultural cultivation of soybeans. Soybean meal and biodiesel were the major products of the process and contained the most emissions. Each allocation method re-distributes the emissions to these co-products and it was found that the economic allocation was most favourable for glycerol steam, with energy next and mass the least favourable, with the reverse true for biodiesel. Considering the glycerol will be utilised as a fuel to produce steam, the energy scenario allocation seems more appropriate and provided a fossil energy ratio of 2.23 or 2.13 when secondary energy is added, resulting in a net positive energy production. In all cases, the fossil energy ratio was positive.

Overall a net positive energy is produced from the conversion of glycerol to bio-SNG based steam with possible reductions for global warming potential when substituting natural gas on an energy basis.

4.5.1 Brief Conclusions

- A life cycle impacts analysis comparing steam production from natural gas and steam production from bio-SNG produced from GLT-SR.
- The GWP of bio-SNG steam is the same as NG for the mass allocation and was reduced by roughly 55% and 80% for the energy and economic allocations respectively.
- A reduction in FER of 3%, 2% and 4% for mass, economic and energy respectively resulting in new FER's of 1.42, 5.34 and 2.13 respectively.
- If all glycerol from U.S soybean biodiesel refineries were utilised for steam, 532,812 TJ y^{-1} could be saved.

5 Experimental Laboratory Scale Gasification

5.1 Introduction

The experimental section is dedicated to the design, assembly, operation and subsequent modification of a liquid glycerol gasification rig for the production of CH_4. Outlined in this chapter are: the methods used to design and operate the rig, a literature review of catalysts and rig designs and methods used to analyse carbon formed in gaseous, liquid and solid products, and the results of experiments. The aim of this section was to operate a laboratory scale liquid biomass gasification rig using glycerol and achieve the greatest conversion to carbon gases, in particular, CH_4, as possible using a $Ni/CaAl_2O_3$ catalyst.

The equilibrium modelling from chapter 2 will act as a guide for the expected gas product distribution. Comparison of the experimental results with the idealised equilibrium results allows determination of how far from the equilibrium the process is operating due to the impact of time which, is not considered when using the Gibbs free energy minimisation model.

The stages in the experimental steps are highlighted in Figure 58.

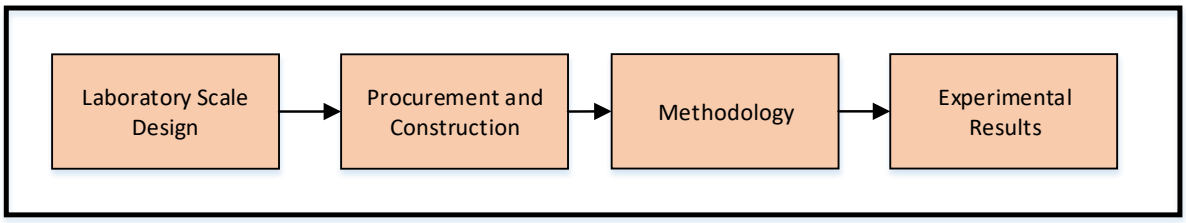

Figure 58. Experimental steps in the design process

5.2 Literature review

Several glycerol gasification rigs have been used in the literature to produce H_2 [83,167–170]. The main differences when working under methanation conditions are the contrary process variables such as low temperatures, high pressures and lower steam to carbon ratios. Consequently many of these gasification systems can be used for methanation with the addition of pressure regulating equipment if higher pressures are desired. In addition at the time of this thesis' work, only one publication had directly injected the liquid in to the reactor, whereas the majority opted for a feed vaporisation step prior to entering the reactor to allow an inlet feed of glycerol and steam to enter the reactor.

5.2.1 Rig Design

To the author's knowledge, there has been one published work on experiments of direct methanation of glycerol [36]. The experiments were conducted at pressures less than 10 bar without a pre vaporisation step, by Imai *et al*. 2017. In Imai's study, a fixed bed reactor of pressurised flow type was used with a combined feed of glycerol and water of 0.06 mL min^{-1} with argon carrier gas at a flow rate of 30 mL min^{-1}. An ice bath condenser cooled the reformate gases before they were captured and sampled using an offline gas chromatograph (GC). Two GCs were used to analyse the gases; CO, CO_2, CH_4 and Ar were analysed with an activated charcoal column whereas H_2 was analysed with an off-line GC with a molecular sieve 5a column. A weight hourly space velocity of 6.7 hr^{-1} was achieved using 0.3g of 355-710 micron pellets of 20 wt% Ni catalyst combined with 1.5 of inert gas in a ratio of 1:5. Reaction temperature, molar feed steam to carbon ratio (SC), pressure and SiO_2 doping percentage were varied although the highest CH_4 production with minimum coke formation occurred at, 673K, 3 atm and 30% SiO_2 doping. By calculation, they used steam to carbon ratios of 1.7, 2.56 and 4, with the former producing the greatest and most consistent amounts of CH_4.

Several works have been carried out under hydrothermal, sub and supercritical conditions but hold less relevance for glycerol methanation at pressures <30 bar. Serrara *et al.* 2014 published work on methanation of the syngas produced by supercritical reforming of glycerol [171] whilst Schubert *et al.* 2014 published work on hydrothermal gasification of glycerol for CH_4 with *in situ* contaminant removal [75]. Tapah *et al.* 2012 processed glycerol under sub and super critical conditions to produce a syngas with up to 14% mole fraction CH_4. Although the primary focus was to produce syngas for energy production, the high energy content of CH_4 would prove to be useful in a mixed gaseous product [172].

A significant number of studies have been documented on the production of H_2 by steam reforming of glycerol and have been covered in several reviews [34,35,173]. Few studies have been carried out below 600°C mainly because at this temperature H_2 is less favoured due to the endothermic nature of the steam reforming reactions.

Based on the literature the minimum requirements for a glycerol gasifier include the following; feedstock reservoir, pump, carrier gas mass flow controller, reactor, catalyst, heat exchanger, condensate catch pot, moisture trap, and gas analyser. Basic setups incorporating these components are detailed in early works on glycerol steam reforming including Czernik *et al.* 2002 [174] Hirai *et al.* 2005 [170] and, Adhikari *et al*. 2007 [83]. Whilst Czernik is one of the earliest works published on glycerol steam reforming, glycerol as a

feedstock for different reforming methods was pioneered by Cortright *et al.* 2002 [168], with their work and subsequent works by their research cohort focussing more specifically on aqueous phase reforming.

Many of the works use off line gas analysis via gas chromatography i.e. the product gas is captured in a gas sample bag and analysed later. The majority of equipment mentioned will have little impact on the reforming of glycerol as long as they are working consistently. For example, the pumping mechanism must be able to deliver consistent flow rates whilst the tube furnace must be able to maintain an observable temperature in the reaction vessel. The condenser must be able to transfer the heat duty from the hot product gases to a cooling fluid, the catch pot must be able to contain any condensate and the moisture trap must be able to remove any additional water before arriving at the gas analyser. Assuming the rig is air tight and the aforementioned components are faultless, the most important determinants of the glycerol reforming reaction will be the reactor vessel and the catalyst.

5.2.2 Catalyst Selection

Catalysts are integral in the glycerol steam reforming process. Under comparable conditions without a catalyst, glycerol will still decompose in a reactor and have low conversion rates to product gases [175]. Catalysts provide greater control over product distribution and selectivity whilst enhancing the conversion of glycerol to desired products by reducing the activation energy, making them essential for the glycerol reforming process due to the variety of potential products, as outlined in Figure 59.

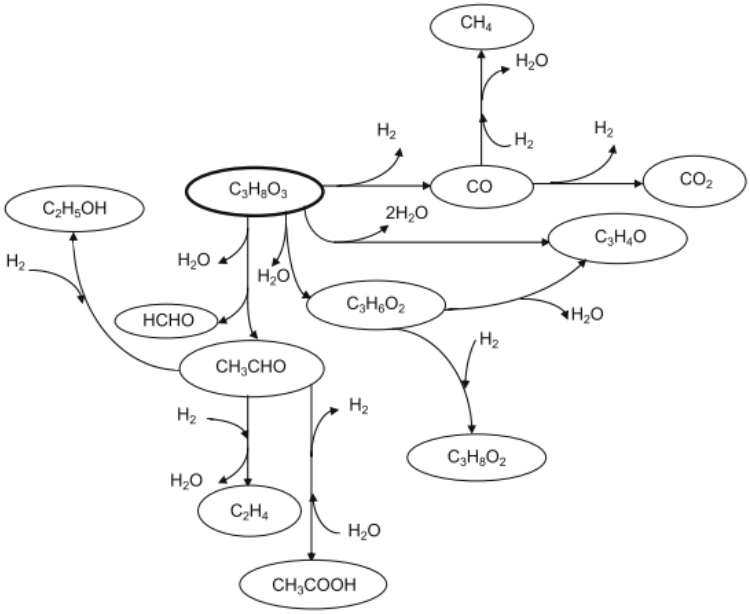

Figure 59. Potential reaction pathways during the glycerol steam reforming process [176].

A catalyst is usually comprised of an active phase and a support. The active phase is usually a transition metal whilst the support can be a variety of materials, from metal oxides to waste fly ash. The majority component of the catalyst is the support but it is the interaction of these two materials that enable the catalyst to provide an alternative reaction pathway that is lower in activation energy than other pathways. Alternative reaction pathways are available because the catalyst allows glycerol to orientate itself in such a way that it can temporarily bond, either through the process of adsorption or chemi-adsorption, requiring less energy to break the glycerol chemical bonds. Consequently the lower activation energy pathway becomes the most favourable out of the potential reaction pathways. How the glycerol interacts with the catalyst is expressed as the mechanism of action and is coupled with kinetic control.

The three important factors that give an understanding of reaction pathways are the thermodynamics, kinetics and mechanism of action. Earlier in chapter 2, the impact of thermodynamics on glycerol steam reforming were explored and predict what operating conditions will be most favourable for CH_4 production. Minimising the steam to carbon ratio and temperature whilst increasing the pressure were shown to favour CH_4 over H_2.

On the other hand, Kinetics determine how fast a chemical reaction will reach equilibrium and brings in the aspect of time. Kinetics are described by the rate of reaction and rate constant k, assuming that enough energy has been supplied to overcome the activation energy.

When a reaction is thermodynamically controlled the more stable of the potential products is dominant. On the other hand, when a reaction is kinetically controlled the product formed from the reaction route that has the lowest activation energy is favoured.

The mechanism of action is the way that the reactants physically interact with the catalyst. Whilst the catalyst is involved in the mechanism it does not act as a reagent or form a product.

The focus of this part of the literature review will be determining what catalysts have been used in the literature, an exploration of the mechanism of GSR and how this can guide direct methanation of glycerol under the conditions discussed in chapter 2.

5.2.2.1 Kinetics of GSR

A substantial review on kinetics and mechanism has been carried out by Silva *et al*. 2015 [173]. The data parameters associated with the kinetics of reactions for glycerol steam reforming are usually fitted to a general power law type equation of the form:

$$GSR = kp_G^a p_W^b \qquad \textit{Equation 39}$$

Where *k* is the reaction rate constant (defined by the Arrhenius equation), p_G and p_W are the partial pressures and whilst *a* and *b* are the reaction orders of glycerol and steam, respectively.

By plotting the natural log of *k* with the inverse of time it is possible to determine the activation energy by inspection of the gradient from the straight line produced. Usually it is difficult to compare different kinetic parameters between literature studies because of the variance in process conditions and catalyst used. On the other hand the activation energy is one of the variables that can be compared across different catalysts as the main role of a catalyst is to reduce the activation energy and favor the kinetics of chemical reactions. Large differences between a catalysts activation energy may show that the rate determining step or reaction mechanism is different. Alternatively other factors, such as the operating parameters, e.g. temperature and different catalyst preparation techniques may also cause stark differences between activation energies.

Regarding the order of reaction, these parameters relate the rate of reaction to the concentration of the reactant but must be determined by experiment. Understanding the order of reaction allows a prediction on the impact of changing the concentration of a reactant on the reaction rate.

The pressure exerted by one gaseous component of a mixture is known as the partial pressure with respect to that particular component. Increasing the partial pressure of a gas in a gaseous reaction mixture may cause a corresponding increase in the rate of reaction.

The formation rates of H_2, CO_2, CO and CH_4 have been often fitted to a power-law expression Equation 39 as well [177–179]. For all cases, the formation rate of CO was shown to be inhibited by steam (negative value of b). Two explanations could be that there is competitive adsorption of steam on the same active sites as the surface precursor for CO production (especially at high steam partial pressures), or because of CO consumption via WGS reaction [179].

For the other gases, positive values of *a* and *b* were obtained, showing that both glycerol and steam positively contribute to H_2, CO2 and CH_4 formation as these products are formed from glycerol decomposition, water gas shift and methanation reactions. In terms of activation energy, H_2, CO_2 and CO formation present similar values (in the range 60–75 kJ mol^{-1}) [178,179] while the formation of CH_4 presents a much higher activation energy (100–120 kJ mol^{-1}) [177–179].

Several reaction mechanisms have been proposed which alter the standard power law rate equation and are mentioned in the review by Silva *et al.* 2015 [173] and are described in 5.2.2.2 however, there has not yet been a consensus on the matter at hand has not been reached yet. As this work is a feasibility study, kinetic parameters will not be obtained from experiment.

5.2.2.2 Mechanism of GSR

Several studies have commented on the mechanism of catalysed glycerol steam reforming [175–178,180–190]. The mechanism varies with the metal centre and support used with the catalyst. Slinn *et al.* 2008 was one of the first to propose that the mechanism was similar to large hydrocarbons over Pt catalysts. This involved dehydrogenation and alpha carbon to carbon cleavage (ΔH=~347 kJ/mol) followed by a final dehydrogenation step [183]. The initial dehydrogenation allows the glycerol to reach the catalyst surface and become adsorbed [175]. Sutar agreed with Slinn and used this mechanism as a basis for a kinetic analysis on glycerol-reforming at low temperature (<500˚C) using a Pt/C catalyst in a fixed bed reactor [187]. Furthermore, Adhikari *et al* agreed with the requirement for C-C bond cleavage[176] when producing H_2 from GSR. The mechanism described by Slinn and Sutar is represented in Figure 60.

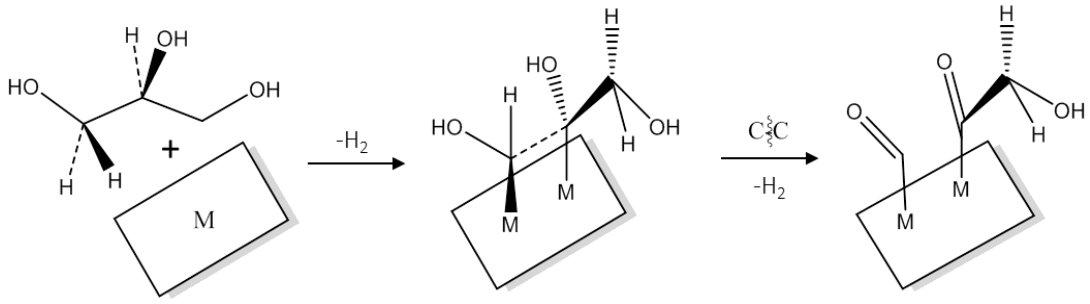

Figure 60. Glycerol adsorption and subsequent reaction with Pt catalysts adapted from Slinn and Sutar.

1. Glycerol dehydrogenates
2. Glycerol chemi-adsorbed onto metal catalyst surface via carbon atoms.
3. Carbon scission between the alpha and a beta carbon with dehydrogenation leaving adsorbed CO.

Using Slinn's mechanism and the work of Byrd *et al.* 2008 [184] on supercritical water glycerol reforming over Ru/Al_2O_3 as a basis, Sundari *et al*. 2012 [189] performed an analysis on Ru catalysts. Byrd proposed a mechanism whereby oxygen atoms from glycerol are adsorbed onto the Ru catalysts rather than carbon atoms. This leads to dehydrogenation and subsequent cleavage of C-C or C-O bonds.

Whether cleavage of a C-C or C-O bond was favoured was determined by Pompeo *et al.* 2011 by studying Ni and Pt catalysts supported on SiO_2. They described two reaction pathways, I and II, represented in Figure 61 and are proposed for Ni, Pt, Ni and Pt/SiO_2 catalysts. Path I relies upon C-O cleavage, dehydrogenation and/or dehydration and can produce CH_4 and

CO_2 whereas path II relies on C-C cleavage via dehydrogenation with no dehydration and does not produce CH_4.

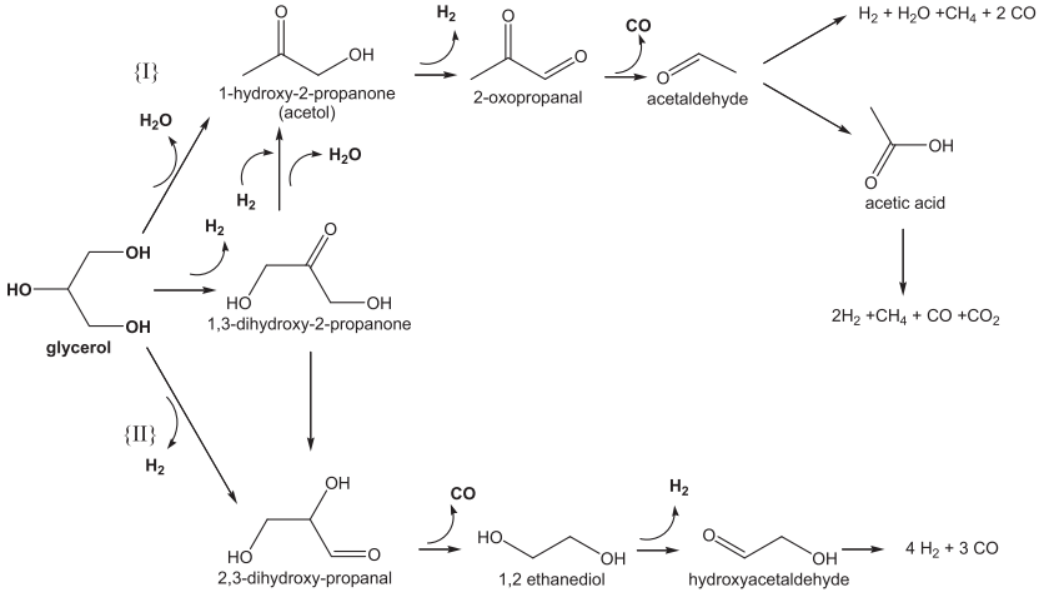

Figure 61. Reported pathways of glycerol steam reforming by Pompeo et al. Pathway I proceeds via C-C cleavage to produce acetol. Pathway II proceeds via C-O cleavage to produce 2,3-dihydroxy-propanal [188,191].

When using platinum catalysts, Pompeo reported that pathway I had a low contribution to their results because of the low concentration of CH_4. The Ni catalysts showed significant differences in the selectivity of gas products as Ni catalyses the water gas shift reaction (WGSR) in order to remove the CO adsorbed on the surface, transforming it into CO_2. In comparison, Sundari found that Ru catalysts favour the first pathway through C-C cleavage because of the product distribution containing more CH_4 than Ni or Pt catalysed reactions. Pompeo's study is significant because it allows for dehydration as well as dehydrogenation, whereas Slinn only mentioned dehydrogenation and did not explain the C-C cleavage step in detail. Furthermore, it provides information on which pathway to favour in order to produce or reduce CH_4 production.

5.2.2.3 Mechanism of Methanation

CO methanation (CO hydrogenation) has been researched more thoroughly than CO_2 methanation and is a combination of the forward WGS and CO methanation. CO methanation is the primary producer of CH_4 from synthesis gas due to the faster rate of adsorption onto catalyst active sites and commercial operating conditions of CO methanation are usually 300˚C and 25 bar.

On the other hand CO_2 methanation is a combination of the reverse WGS and CO_2 methanation. Greater methanation selectivity is achieved through the CO_2 methanation pathway at the cost of more severe operating conditions [192]. Selectively bypassing unwanted reduced products in the catalysis of CO_2 is difficult because it requires an eight-electron process [193]. Sahebdelfar *et al.* 2015 determined that CO_2 methanation in the absence of CO was favoured at lower temperatures and higher pressures and could be carried out with high selectivity below 300˚C with nickel catalysts.

The earliest work on elucidating the mechanism of action was carried out by Sabatier who proposed that hydrogen and pure nickel react to readily produce NiH_2 (a hydride) or with impure nickel to form Ni_2H_2, on the surface of the metal. This acts as a temporary compound and is rapidly dissociated, with the resultant hydrogen given up to any nearby molecules that can use it, whilst at the same time regenerating the metal. In this case, CO and CO_2 for methanation [19,194].

Later work by Vlasenko V.M and Yuzefovich G.E (1969) as well as Vannice M.A (1976) derived a rate equation on the assumption that the rate determining step was the interaction of adsorbed hydrogen atoms with a surface CHOH species [195]. Similarly in 2005 Sehested *et al.* 2005 suggested that instead of a hydride, an intermediate CHxO complex or active carbon intermediate from CO dissociation is formed on the nickel surface[196].

A third method proposed by Wang. Z. specifically for nickel is that nickel inserts into the H_2 via oxidative addition, forming an intermediate that creates a coordination complex with CO detailed in Figure 62 leading on to further transformations as shown below. Carbon deposition is thought to be associated with dehydrogenation at higher temperatures [194].

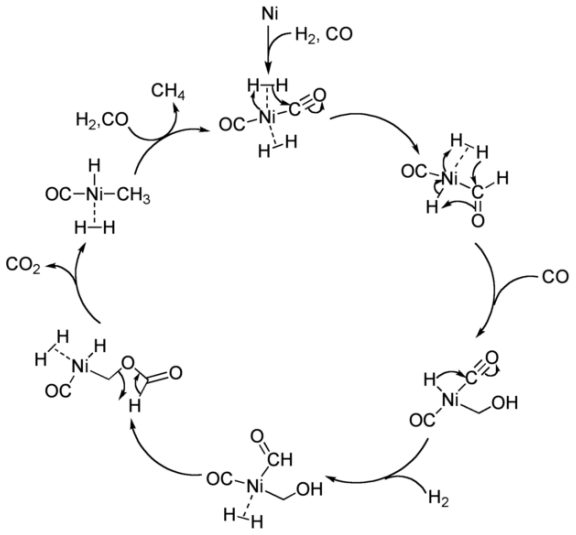

Figure 62. Nickel insertion into H_2 via oxidative reduction leading to a series of transformations as a proposed method of hydrogenation catalysis.

Rönsch *et al.* 2015 and Tada *et al.* 2015 produced a summary of the literature of the fundamentals of methanation and a review on the mechanisms of CO and CO_2 methanation respectively [197,198]. Both agree that the most likely mechanism for CO and CO_2 hydrogenation appears to be that which proceeds via the formation of a surface carbon intermediate on the catalyst metal. This is contrary to the first and second mechanisms proposed earlier. They suggest that the rate determining steps in CO and CO_2 methanation are the dissociation of adsorbed CO to surface carbon and subsequent hydrogenation of surface carbon. In terms of CO and CO_2 mixtures, CO_2 is slower to absorb than CO which may explain the inhibiting effect of CO on CO_2 methanation. Based on this, metal centres that promote CO methanation tend to also support CO_2 methanation.

Specifically for CO_2 hydrogenation in mixed CO and CO_2 conditions, Tada summarises recent studies which have proposed that formate (CO_2H^-) is the carbon intermediate complex in figure 12.

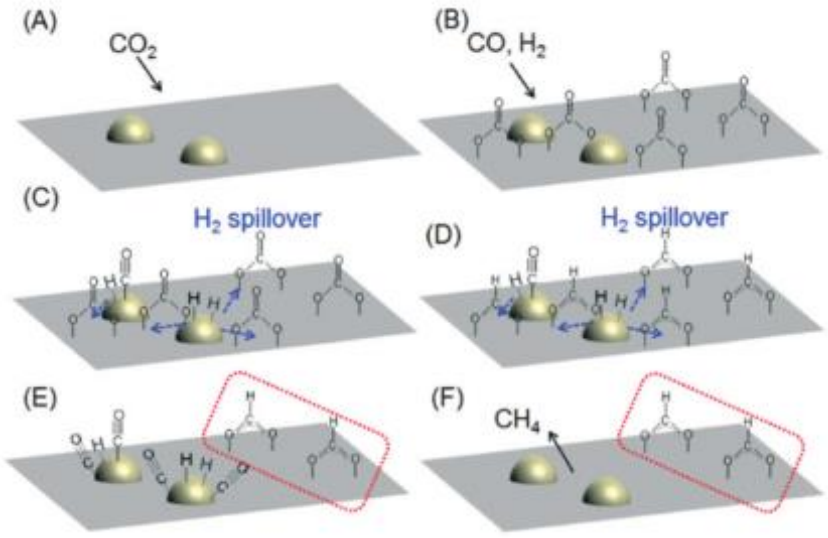

Figure 63. Plausible mechanism of CO_2 mechanism in coexisting CO_2 and CO conditions. reproduced from Tada et al. 2015 [198].

A - CO_2 adsorbed onto the support material

B - Formation of carbonate species on the support by reaction of CO_2 and H_2.

B - CO and H_2 adsorb onto the active metal surface

C - H_2 spill over from this area allows carbonate conversion to formate species.

E -Formate species in contact with the metal are decomposed to CO on the metal-support interface.

F- CO on the metal surface reacts with H_2 to form CH_4.

Rönsch disagrees with Tada about the second stage of the CO_2 mechanism whereas Wu *et al.* agrees with Tada and provides evidence for a formate mechanism[199,200]. All three authors agree that carbonate species are formed initially but Tada and Wu propose carbonate conversion to formate species (figure 12) whilst Rönsch prefers the hydrogenation of the surface carbonate to CH_4, as in CO methanation.

On the other hand, both reviews agree with the literature on CO methanation beginning with CO adsorption and dissociation to surface carbonate. Rönsch goes into detail about this reaction occurring on the step edges of the active metal surface. The following dissociation of CO into adsorbed carbon and oxygen appears to take place on 5-fold coordinated sites of the active metal, where carbon atoms can form several bonds.

In summary several different mechanisms have been proposed in the past with varying levels of agreement. The two most recent mechanisms proposed after surmising the literature both describe the support playing a significant role due to the location of the reactions on

the metal-support interface. Ni catalysts will be active in both CO and CO_2 methanation although CO methanation will be favoured when CO is available due to faster adsorption times compared to CO_2.

5.2.2.4 Ni Catalysts and Supports

By far the most common metal used as an active phase in glycerol steam reforming reactions is Ni due to its relative abundance, reasonable to high activity in the steam reforming reaction and low pricing compared to noble metals. Consequently, much of the research has focussed around Ni due to its economic advantages over more potentially active catalysts such as Pt and Rh. Adhikari *et al.* 2009 [176] and Lin *et al.* 2013[181] have carried out reviews on the catalysis studies for GSR with the former focused on H_2 yield and the latter on H_2 and CO yield. A common factor within their reviews is that the majority of metal centres are supported on or combinations of metal oxides e.g. Al_2O_3. Many metal centres have been shown to be active in steam reforming including; nickel (Ni), Cobalt (Co), Platinum (Pt), Ruthenium (Ru) and Iron (Fe) with several bi-metallic variations available.

The activity of Ni is based on O–H, C–H and C–C dissociation. In order to maintain this activity, it is important to prevent NiO from developing as it is inactive in steam reforming. This requires strong interaction between the support and the metal phase to stabilise the metal centre, or maintaining a steady reducing atmosphere to prevent oxidation of the active Ni for the duration of the reforming process.

The reason for Ni high activity is its capacity to simultaneously assist in two reactions. The first reaction involves elemental Ni in the catalyst assisting in the dissociation of glycerol, thereby producing syngas much like in the Pt catalysts. The second reaction occurs because the $Ni(OH)_2$ or NiOOH species are believed to enhance the movement to equilibrium of WGS. Hydroxyl (OH) groups are able to interact with the CO species absorbed on the neighbouring Ni to produce CO_2 and H_2. The Ni in the first reaction is provided directly by the catalysts. The $Ni(OH)_2$ or NiOOH arises as surface species by interaction of water vapour and elimination of protons either from the support or *in situ* [176].

In comparison to Pt, the barrier for the C–O bond dissociations on the Ni surface to promote methanation is about 2 eV lower than that on the Pt surface[201]. This presents Ni as active towards methanation. Several studies in the literature review have shown CH_4 as a major by-product from GSR using Ni catalysts, even at high temperatures and low pressures where methanation is thermodynamically unfavourable[185].

As there are nearly 400 journal publications (06-08-18) concerning catalysts for glycerol steam reforming, the active phase of Ni was chosen for the literature review due to its popularity, low cost and its availability for this project. To further constrain the literature search, only work that has been carried out in range lower than 600°C was considered.

The supports used for GSR are similar to those used in steam reforming. The best metal oxides create stable interactions with the metal centres and this in turn increases the thermal stability whilst increasing the active site surface area improving catalyst activity. Base metal oxide supports such as CeO_2 and MgO appear to be more effective than acid supports at preventing the formation of CO and CH_4 as by products [198].

For this work a commercial Ni catalyst supported on CaO-Al_2O_3 produced by Twigg Scientific and Technical Ltd (TST) is used. When compared to alumina supports alone, the addition of CaO improves the catalysts resistance to carbon formation due its basic nature. This effect was observed at low temperatures by Lifita Tande in experiments on autothermal reforming of bio-oils [202]. The same catalyst was utilised in the steam reforming of biodiesel by Nahar *et al.* 2015 at temperatures of 650 °C to 850 °C and had comparable performance to Ni-Al catalysts [203].

5.2.2.5 Low Temperature Glycerol Steam Reforming

Xing *et al.* 2015 [204] and Chen *et al.* 2011 [205] published work on low temperature glycerol steam reforming for the purposes of H_2 production. Xing used Ni on three metal oxide supports, Al_2O_3, CeO_2, TiO_2 and MgO with reaction temperatures between 300 and 500˚C and 1 atm and observed CH_4 selectivity <5.4% for all catalysts. Similarly Chen utilised Ni-CeO_2 and Ni-Al_2O_3 at temperatures of 400-600 ˚C but at the pilot scale using catalyst on the kg scale under an SC of 3, pressure of 1 bar and feeding reactants to inert gas ratio of 4:1 using Ni-Al and Ni-Al/CeO_2 catalysts. High conversion of glycerol to products was achieved at >96% with the lowest CH_4:H_2 ratio of 1:3 achieved at 400 °C. Chen found that the experimental data was a good match to the thermodynamic data. If it is possible to reduce the temperature the ratio of CH_4:H_2 could be reduced further. In both cases a pre-vaporisation step was utilised to vaporise the glycerol water mixture prior to entering the reactor.

Imai *et al*. 2017 [36] were able to achieve roughly 70% of equilibrium CH_4 yield at 673K and 3 atm after 5 hours on stream using a WHSV of 6.7 hr^{-1}, an SC of 1.35, with direct methanation of glycerol. However as they reduced the temperature to 623 K, the methane yield was significantly reduced, contrary to the equilibrium modelling carried out in 2.4.1. Moreover, significant deactivation of the catalyst occurred at 623 K becoming worse at 593

K and leading to a CH_4 production of near zero at 5 hours on stream. This is likely due to solid carbon formation on the catalyst as a result of the low SC of 1.35, as this is straddling the boundary between the modelled minimum SC for zero carbon formation discussed in Figure 23.

Rather than using a basic catalyst, they found that a 20 wt% Ni/Al_2O_3 doped with 10% SiO_2 enhanced CH_4 conversion when compared to 20 wt% Ni/Al_2O_3 alone.

5.2.2.6 Favouring Methanation

When considering GLT-SR, combining knowledge of methanation with steam reforming is necessary to choose an ideal catalyst. The following are desirable traits of a GLT-SR catalyst:

- High selectivity for CO and CO_2 methanation
- Low activity for forward water gas shift
- Thermal stability (temperatures below 500°C)
- Pressure stability (up to 30 atm)
- Activity at low temperatures
- Able to withstand handling
- Unreactive to water
- Resist carbon formation at low temperatures by increasing the basicity of the support

Based on the thermodynamic modelling in chapter 2 the process variables to be considered are:

- Pressure greater than atmospheric
- Temperatures lower than 600 K
- Steam to carbon ratio above the minimum to prevent carbon formation.

5.3 Experimental Design

Rig design, procurement and rig construction as well as method and calculations related to data analysis and processing are discussed in this section.

5.3.1 Laboratory Scale Gasifier Design

A scale design is shown in Figure 64 to illustrate the reactor setup. The setup incorporates the need for an additional drying stage in the form of a moisture trap as the condenser cannot remove >99% of the moisture from the gas. The moisture trap removes the majority of the moisture to prevent damage to the micro-GC column, and to ensure any moisture is removed the column, must be conditioned overnight at a temperature of 180 °C with a column temperature of 120 °C.

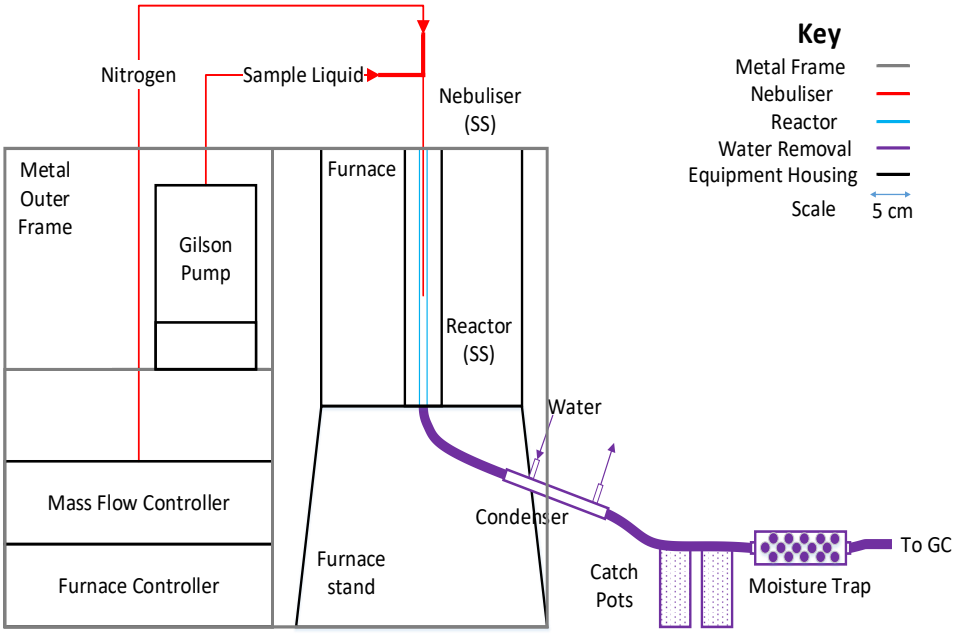

Figure 64. Scale drawing of the rig setup with nebuliser attachment.

The original design incorporated a nebuliser which could create a fine spray by atomising the feed flow with the carrier gas. However, significant inlet pressures of the carrier gas were required to maintain nebuliser and flow rate consistency and was subsequently removed from the system in favour of a 1/16 inch diameter stainless steel inlet tube as shown in Figure 65.

5.3.2 Gasifier Procurement and Construction

The following section describes how the gasifier was constructed and what components and equipment were necessary should replication be desired. The components and basic design were derived from literature papers in 5.2.1.

5.3.2.1 Glycerol Feed and Carrier Gas Inlets

The reactor feed and carrier gas setup is shown in Figure 65. To improve the consistency of the feed delivery a 1/16 inch diameter stainless steel pipe was inlaid into 1/4 inch diameter stainless steel pipe allowing the feed to enter the reactor at the centre. The minimised diameter prevented a fluctuating effect from droplets which would otherwise grow at the end of the larger diameter pipe before falling into the reactor, whilst the extension of the 1/16 inch pipe into the centre of the reactor prevented droplet agglomeration upon their collisions with the reactor walls. Locating the carrier gas above the feed inlet at the horizontal to the T-piece allowed the gas to flow from behind the liquid inlet feed and carry it steadily.

Figure 65. Glycerol feed and gas inlet to reactor.

5.3.2.2 Inlet Sample Fluid Pumping

The pumping mechanism for the rig varies with the required inlet pressure. At atmospheric pressure a syringe pump was used. The desired flow rate is calculated by inputting the diameter of the syringe to the electronic pump whereas the inlet needle can be attached by Swagelok fittings and a luerlock mechanism. Syringes used were ordered from SGE analytical and were gas tight but made of glass with stainless steel fittings and a plastic plunger.

At pressures above atmospheric and up to 5 bar, a peristaltic pump by Gilson was used. Compared to syringe pumps, peristaltic pumps have the ability to pump liquid into a pressurised reactor and prevent liquid backflow. The volume of liquid pumped per unit time

was calculated by using the diameter of the pipe and revolutions per minute, plotted on reference charts provided by Gilson, as shown in Figure 66. The desired flow ranges of 0.100-0.025 ml min^{-1} necessitated the smallest diameter tubing of 0.2 mm.

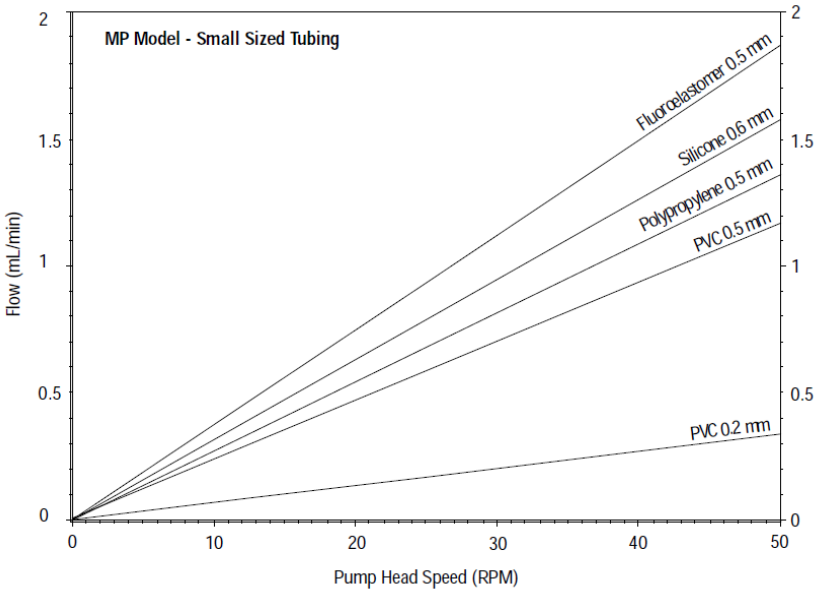

Figure 66. Required Gilson pump head speed (revolutions per minute) for a desired flow rate for each diameter and tubing material [206].

5.3.2.3 Stainless Steel Components

The component connecting pipe, inlet feed tube, reactor, condenser, catch pot and moisture trap were all constructed from stainless steel seamless tubing 316/316L from Swagelok. Dimensions of tubing for particular components are shown in Table 25. The condenser was assembleded together by combining 1/4 Swagelok fittings. The reactor was created by cutting 1 inch outer diameter pipe in half and inlaying with 20 micron stainless steel woven wire mesh across the horizontal to create a platform for the catalyst basket to rest. The pipe was welded back together to complete the reactor. The length of the reactor was 18 inches with an inner diameter of 0.785 inches giving a total volume of 8.27 cubic inches (135.5 cm^3).

Swagelok tube fittings of various sizes along with reducers and T-pieces were used to secure the piping and components together. The catalyst basket was made in a similar way using 120 µm stainless steel mesh to prevent any catalyst or sand from falling through and was outsourced to Oxford Filtration Ltd.

Component	Outer Diameter (inch)
Connecting pipe	1/4
Reactor	1
Inlet feed tube	1/16 fed into 1/8
Gilson inlet feed connection to inlet feed tube	1/8 to 1/16
Condenser	1 inlaid with 1/4 inch
Catch pot	1
Moisture Trap	1/2

Table 25. Rig component tubing and relative dimensions.

5.3.2.4 Catalyst

The nickel supported on calcium aluminate catalyst (Ni/Ca-Al_2O_3), was supplied by Twigg Scientific and Technical Ltd (TST Ltd). For the catalyst to fit into the catalyst basket it was crushed in a mortar and pestle. After crushing and grinding stage the catalyst was sieved in the range of 150-200 µm and 125-150 µm to achieve the desired particle size range. When placing the catalyst in the basket, quartz wool was used as a plug to prevent any catalyst from escaping the basket due to gas mass flow changes during the experiment.

5.3.2.5 Gases and Flow Rate

For gas sampling an Agilent Micro Gas Chromatograph (Micro GC) was connected to the rig after the moisture trap to prevent any moisture reaching the column. Gas chromatography depends upon columns to retain different molecules over time. The affinity of the molecule to the columns stationary phase determines the length of time taken for the molecule to pass through to the detector, otherwise known as retention time. For each column, the retention time of calibrated molecules is distinguishable.

Two columns were present in the Micro GC to analyse different components. The columns used are a HP MoleSieve column in parallel with a CP-PoraPLOT Q (PPQ) column. PPQ columns allow detection of longer chain hydrocarbons and can distinguish between CH_4 and CO_2. The retention times of gaseous molecules pertinent to this work are examined by Wurm *et al.* 2003. A singular combined peak of smaller molecules including H_2, O_2, N_2 and CO occurs with a retention between 1.5 and 1.75 minutes whereas CH_4 is between 1.75 and 2.00 minutes and CO_2 is greater than 2.00 minutes. MS columns can distinguish between H_2 (0.75-1.00), O_2 (1.00-1.20), N_2 (1.20-1.75), CH_4 (2.0-3.0) and CO (>3.0) with all retention times in minutes [207].

Inlet gases kept consistent during operation were Nitrogen (>99%) and H_2 (5% H_2, 95% N_2). Mass flow controllers (MFC) produced by MKS instruments incorporated were used to ensure consistent flow rates and had maximum capacities of 1000 ml min^{-1} for N_2 and 500 ml min^{-1} for H_2. To determine the impact of any pressure drops, blockages or to detect inaccuracies an Agilent technologies AOM1000 flow meter was attached to the output line to read the flow rate of gas.

5.3.2.6 Temperature and Heat Exchange

Temperature maintenance was achieved using an Elite thermal system Ltd vertical tube furnace and thermocouple. The reactor was inserted into the furnace and held using a custom built stainless steel frame. To measure the temperature a type K thermocouple was inserted into the reactor via the Swagelok T-piece. Although the thermocouple was not located in the catalyst bed, it was still possible to determine the inner reactor temperature as the thermocouple was positioned below the catalyst basket. Data capture was provided by Picologger software. To ensure the gases were not hot upon entering the GC and to minimise the moisture content prior to the moisture trap, a cold fluid containing 25% ethylene glycerol and 75% water was circulated through the condenser. A Fischer Scientific 3006S chiller was used to maintain a fluid temperature <1°C to maximise heat exchange.

5.3.3 Experiment Methodology

The main aims of the experimental work are to:

1. Construct a liquid biomass gasification rig.
2. Optimise conversion of glycerol to CH_4 at 673 K using Ni/Ca-Al_2O_3 catalyst.

To determine to what extent the inlet feed of glycerol was converted, a carbon balance was necessary to analyse the amount of carbon in the outlet product gases including CH_4, liquid products (condensate) and solid carbon.

Several factors will influence the distribution of products and conversion of glycerol. These factors are known as process variables, some of which have been described in chapter two. Factors that influence the activity of glycerol conversion to gaseous products are; the nature and mechanism of the catalyst, catalyst particle size, catalyst bed dilution, weight hourly and gas hourly space velocity for the experiment, temperature and pressure in the reformer, molar feed steam to carbon ratio (SC) and reagent residence time.

5.3.3.1 Elemental Balances of outlet product gases using N_2

The Micro GC detected the carbon product gases CO, CH_4, and CO_2 that were produced. It was noted that in some circumstances gases containing larger carbon chains could be formed as shown in previous research[208]. In addition H_2 was a by-product of the process, and N_2 was used in the feed as a carrier gas and the basis of the N_2 Balance to calculate the molar flow rates of gaseous products

As the GC determines the molar fraction of each component in the product gas, knowing the flow rate of N_2 at the inlet allows calculation of the flow rates of the product gases by relation, because N_2 is considered inert in the glycerol methanation and steam reforming reactions.

Firstly the mole fractions were normalised to 100% using Equation 40.

$$G_{nx} = \left({}^{G_x}/_{G_T}\right).100 \qquad \textit{Equation 40}$$

Where G_{nx} is the normalised mole fraction of a particular component, G_x is the mole fraction of a particular gas component before normalisation and G_T is the total value of the summed mole fractions of the gases in the product gas before normalisation.

The flow rate of N_2 was converted from litres per minute to moles per hour using Equation 41.

$$m_{N_2} = {}^{PV}/_{RT} \qquad \textit{Equation 41}$$

Where m_{N2} is the known input molar flow per hour of N_2, P is pressure in pascals, V is volume flow rate in m^3 per hour, R is the gas constant in J K^{-1} mol^{-1} and T is temperature in Kelvin.

Using values obtained for G_{nx} in Equation 40 and m_{N2} in Equation 41 the normalised molar flow for a particular gas component (G_{mx}) can be calculated in Equation 42.

$$G_{mx} = \frac{m_{N_2}}{Gn_{N_2} * Gn_x} \qquad \textit{Equation 42}$$

Where Gn_{N2} is the normalised molar fraction of the product gas of N_2, Gn_x is the normalised molar fraction of a particular gas component, x, in the product gas.

5.3.3.2 Inlet Feed Glycerol Carbon

The moles of carbon in the system depend upon the moles of glycerol in the inlet feed of the water glycerol solution and the flow rate of the pump. In this work two solutions of glycerol were used and will be known as SC3 (steam to carbon ratio of 3) and SC2.5 (steam to carbon ratio of 2.5).

The steam to carbon ratio is the ratio of moles of water to carbon contained in the glycerol when the products are vaporised. As glycerol contains three carbon atoms an SC3 solution would need 9 moles of water whereas SC2.5 would require 7.5 moles of water. Using these mole quantities the desired volume for each solution to be uploaded in the syringe of the feed syringe pump was calculated using equation Equation 43 and the constants in Table 26.

$$V_q = \frac{M_q M_{r_q}}{\rho_q} \qquad \textit{Equation 43}$$

Where V is volume, M is moles, M_r is relative atomic mass, ρ is density and q is the component of the mixture e.g. glycerol.

	Glycerol	Water
Liq Density (g mL^{-1})	1.260	0.998
Relative Atomic Mass (g mol^{-1})	92.094	18

Table 26. Characteristics of glycerol and water.

For every mole of glycerol there are three moles of carbon due to the formula $C_3H_8O_3$.

5.3.3.3 Conversion of glycerol to gaseous carbon

To calculate the glycerol percentage conversion to gases Equation 44 can be used.

$$X_{CG} = \left(\frac{G_{m_{CH4}} + G_{m_{CO}} + G_{m_{CO2}}}{3 * G_{m_{C3H8O3}}}\right) * 100 \qquad \textit{Equation 44}$$

Where X_{CG} is conversion to carbon gases. For every mole of glycerol there are three moles of carbon, the molar flow of glycerol in the inlet feed will vary with the water glycerol mixture.

In the literature it has been noted that not all of the glycerol converts to gases. In some cases, some of the glycerol has been converted to volatiles which subsequently condense into liquid products upon cooling. These condensed volatiles would be removed as a condensate and have been analysed by gas chromatography [83,175]. Examples of liquid products include acetone, acetaldehyde, ethanol, propanol, acetic acid and acrolein, which all contain carbon.

5.3.3.4 Water conversion

Water is added to the system in order to mitigate carbon formation but is not inert. Consequently water can contribute to the formation of H_2 containing product gases due to the water gas shift reaction. Identifying the water conversion is therefore an important parameter which can be used to gauge the extent to which water consuming reactions, the WGSR and SR, or water forming reactions such as methanation have occurred. Water conversion can be calculated in Equation 45 by performing a H_2 balance. H_2 contained in H_2 gas as well as CH_4 can be attributed to both the water and glycerol in the inlet feed. Water conversion [209]. Calculation of water conversion is carried out by the difference between the total H_2 produced and the H_2 input from converted water and glycerol.

$$X_{H2O} = \frac{G_{m_{H2}} + 2\,G_{m_{CH4}} - 0.5r\ * m_{C_3H_8O_3}\ * X_{CG}}{m_{H2O}} \qquad \textit{Equation 45}$$

Where r is the atomic H_2 coefficient in glycerol and X_{H2O} is the water conversion in percent.

Greater conversion of water represents more water being consumed to produce H_2 containing gases. In this case, the three reactions that produce H_2 and CH_4 are glycerol steam reforming (GSR), water gas shift (WGS) and CO methanation (COM) as mentioned in 2.4.1 and are repeated below for convenience.

Glycerol Steam Reforming

$C_3H_8O_{3_{(l)}} + 3H_2O \leftrightarrows 3CO_2 + 7H_2$ ΔH^0_{298} +346 kJ mol^{-1} *Equation 14*

Water Gas Shift

$CO + H_2O \leftrightarrows CO_2 + H_2$ ΔH^0_{298} -41 kJ mol^{-1} *Equation 15*

CO Methanation

$CO + 3H_2 \leftrightarrows CH_4 + H_2O$ ΔH^0_{298} -206 kJ mol^{-1} *Equation 16*

CO_2 Methanation

$CO_2 + 4H_2 \leftrightarrows CH_4 + 2H_2O$ ΔH^0_{298} -165 kJ mol^{-1} *Equation 18*

Both GSR and WGS consume water whilst COM produces water. Therefore, as more CH_4 is produced via COM, water conversion will fall as water is replenished. On the other hand, if GSR and forward WGS are more favoured the water conversion rate will increase.

5.3.3.5 Outlet Carbon in Condensate and Solid Carbon

To account for any carbon that has not been converted to gases it is important to retain the catalyst and condensate over the time on stream. As described by the glycerol reaction pathways in Figure 59 and Figure 61, several intermediate product or alternative pathways are available for glycerol conversion. In most cases these products are liquids e.g. acetaldehyde and will be removed from the gas stream by condensation. Recording the duration of the reaction run (□t) as well as the volume of the condensate collected at the end of the run allows an estimate of the carbon present in the liquid condensate when using total organic carbon (ToC) analysis. Furthermore as the conditions are more susceptible to solid carbon formation, analysis of any solid carbon formed on the catalyst can be carried out by CHNS by taking a sample of the catalyst bed.

5.3.3.6 Carbon Balance

To determine the conversion of glycerol to gaseous products a carbon balance was necessary. The product gases, liquids and solids from the GLT-SR process were all attributed to the feed carbon contained in the glycerol. By summing all of the calculated carbon containing product together for a given duration of operation, an overall total carbon

conversion percentage was calculated, concordant with errors and uncertainty, as shown in Equation 46.

$$C_{glycerol} = C_{gas} + C_{liquid} + C_{solid} \qquad \textit{Equation 46}$$

Where $C_{glycerol}$ is carbon contained in the inlet feed of glycerol for a feed duration □t, and is the maximum carbon in the system, C_{gas} is carbon contained in outlet gases, integrated from the molar rates of C-containing gases over Δt, C_{liquid} is carbon contained in the condensate collected at the end of Δt, and C_{solid} is carbon contained on the catalyst as a result of solid carbon formation over the duration □t. It is important to note that some solid carbon may also be formed in the rig components and will not be able to be accounted for. The carbon balance was then calculated based on a value of □t defined by the time on stream (time interval of glycerol feed pump starting and stopping).

5.3.3.7 Total organic carbon for analysis of solid carbon in condensate

The condensate was analysed using an IL 550 ToC tn produced by HACH. TOC analysers measure the CO_2 formed when organic carbon is oxidized under high temperatures and/or when inorganic carbon is acidified. The condensate was diluted by a factor of ten by adding 1 ml of the condensate to 9 ml of de-ionised water. The concentration of C in the condensate was then re-adjusted to take into accound the dilution and determine C_{liquid}, the molar amount of carbon in the condensates to input into equation 43.

5.3.3.8 CHNS for solid carbon analysis

Carbon contained in the catalyst bed was analysed using the CHNS technique with a Flash 2000 organic elemental analyser by Thermo Scientific. Samples of the catalyst bed were weighed to 10mg ±1 mg in a tin capsule and compressed to remove air. Duplicates of each sample were weighed to within 0.05mg of each other. The tin capsules are combusted in a reactor at 1800°C allowing the sample and container to melt, with the tin promoting flash combustion. Any combustion products are carried by helium to a glass column with oxidation catalyst and finally to a separation column with analysis by a thermal conductivity detector giving outputs in wt% of each element. Chromatographic responses are calibrated against pre-analyzed standards e.g. soil. Using the C wt% and knowing the initial mass of sample collected, the number of moles C on the catalyst (C_{solid}) is then determined to input into the carbon balance equation 43.

5.3.3.9 Errors

Errors for solid and solid carbon in condensate from CHNS and ToC respectively were calculated using the standard error (SE) formula shown in Equation 47. Errors for gaseous carbon were calculated by the variation in N_2 flow rate, as measured by the AOM1000 flowmeter, which was ±1 ml min^{-1}.

$$SE = {}^{\sigma}/_{\sqrt{n}} \qquad \textit{Equation 47}$$

Where σ is the standard deviation and n is the number of samples.

5.3.3.10 Equilibrium Efficiency

The expected equilibrium value was modelled in Aspen Plus V8.8 using a RGIBBS reactor. Under the conditions of minimising Gibbs free energy, the molar flow rate of CH_4 could be calculated. Using measurements from the micro-GC, a comparison of the expected equilibrium value of CH_4 versus the measured value of CH_4 can be made with equation *Equation 48*.

$$Eq\%_{CH4} = \left(\frac{G_{m_{CH_4}}}{Eq_{CH_4}}\right).100 \qquad \textit{Equation 48}$$

Where $Eq\%_{CH4}$ is equilibrium efficiency of CH_4, Gm_{CH4} is the normalised moles of CH_4 as calculated in *Equation 42* and Eq_{CH4} is the expected equilibrium moles of CH_4 predicted by Aspen Plus RGIBBS modelling at the relevant operating conditions.

5.3.3.11 GLT-SR Rig Operation

Rig operation can be split into cleaning and testing. Prior to testing under desired conditions cleaning the rig and removing samples from the previous experiment is necessary for recording purposes and preventing contamination. The following steps comprise the cleaning operation:

1. Remove condensate and record volume then clean catch pot.
2. Remove and replace moisture trap silica beads.
3. Remove spent catalyst bed and replace with fresh catalyst bed.
4. Clean rig prior to catch pot using water and pipe cleaners.
5. Inspect and clean thermocouple.
6. Leak test.

After these steps have been completed the testing phase can begin with testing phase steps detailed in Table 27. During these steps a sampling sequence using the GC software is initiated to determine when purges have been completed e.g. O_2 no longer present on the chromatogram and when reduction is complete i.e. H_2 5% concentration is achieved.

During the finish and N_2 purge step a new conditioning sequence is initiated whilst the previous sampling sequence is finished. The conditioning sequence purges the GC column under the standard conditions and switches to higher temperature for conditioning during the last 2 hours to ensure any moisture has been removed and the column is prepared for the next test.

Action	Temperature (°C)	Time (hours)	Flow Rate (ml min^{-1}
N_2 Purge	25-600	0.5-1.5	500
H_2 Reduction	600	3	350
N_2 Purge	Desired	1.5-2.5	500
Glycerol Feed	Desired	2-3.5	Desired
Finish and N_2 Purge	25-600	5	50

Table 27. Testing phase actions for gasification rig.

5.4 Results and Discussion

The impacts of feed flow rate, temperature, and pressure and weight hourly space velocity on the product gas distribution are described in this section. A carbon balance was produced based on the carbon analysed from the solid deposition on the catalyst, solid carbon in condensate and integration over time of the gaseous carbon in the product gases for a given duration of experiment.

5.4.1 Carbon Balance

The carbon balance of the experiments used for determining the effect of WHSV (Figure 71) and temperature (Figure 72) are shown in Figure 67 with the corresponding operating variables in Table 28. Due to restraints on time these were the only experiments that could analysed.

Figure 71A and Figure 71B had significantly lower than 100% (84.0 and 82.6 respectively). Figure 71C, Figure 72A, Figure 72B and Figure 72/74AC had greater than 98% of the carbon accounted for from gaseous, solid carbon on the catalyst or solid carbon in condensate. Figure 71A and C in particular had large error bars almost twice the value of the other experiments and could be associated with a large disparity between ToC and CHNS samples.

As the temperature is reduced and feed carbon conversion to gases is maintained, the main issue is solid carbon formed on the catalyst as this causes catalyst deactivation. Up to 12% of carbon loss could be associated with solid carbon formation and increased as the WHSV was decreased.

In spite of this, decreasing the WHSV improved glycerol conversion to carbon gases. At higher WHSV more of the carbon was accounted for in the liquid condensate, up to 12%, showing that conversion of glycerol to gases was lower, potentially due to inadequate catalyst active sites or a lack of residence time in the catalyst bed.

At 910 K solid carbon was 4.8% and increased to 7.5% at 793 K and 10.7% at 673 K whilst solid carbon in condensates remained relatively the same. This resulted in a reduction in carbon converted to gases at 673 K of roughly 5.4% and illustrates the increase in carbon deposition as operating conditions become more favourable for methane production.

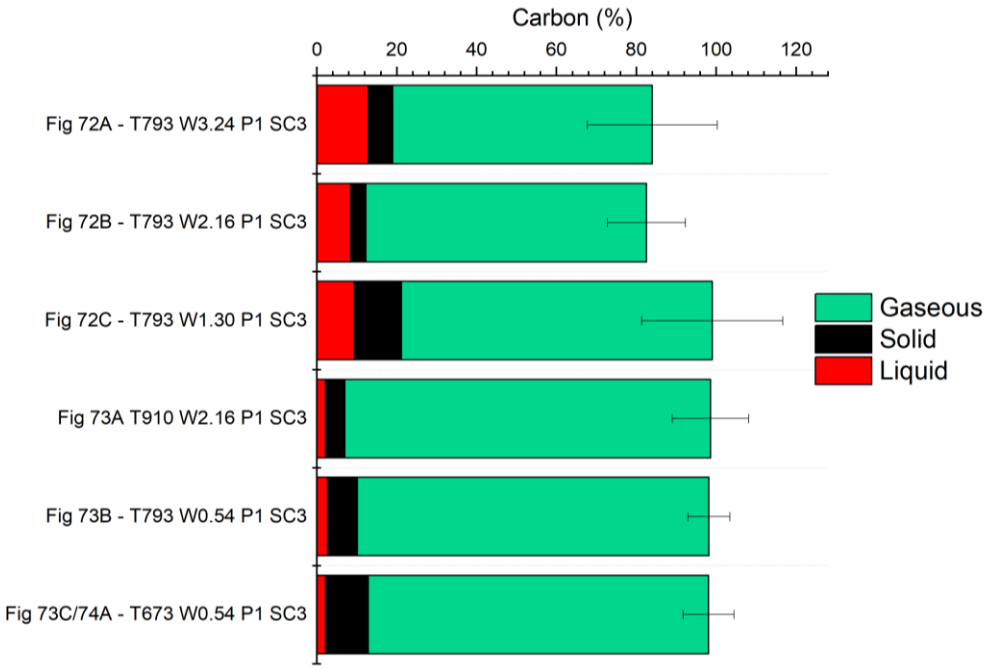

Figure 67. Carbon distribution in the gas, solid and liquid product phases, and carbon balance for experiments in Figure 71 and Figure 72 with corresponding process variables for each experiment displayed in Table 28 where T is temperature in K, W is weight hourly space velocity, P is pressure and SC is steam to carbon ratio.

Figure	*SC*	*Catalyst*	*Particle Size*	*Sand Mass*	*Feed Flow*	*WHSV*	*T*	*N_2 Flow*	*P*
-	-	g	micron	g	ml hr^{-1}	hr^{-1}	K	ml min^{-1}	ATM
Figure 71A	3	2	150-200	9	6.00	3.24	793	69	1
Figure 71B	3	3	150-200	9	6.00	2.16	793	68	1
Figure 71C	3	5	150-200	15	6.00	1.30	793	68	1
Figure 72A	3	3	150-200	9	9.00	2.16	910	105	1
Figure 72B	3	6	150-200	18	3.00	0.54	793	39	1
Figure 72C	3	6	150-200	18	3.00	0.54	673	38	1

Table 28. Process conditions for experiments shown in Figure 67 for the gaseous, solid and solid carbon in condensate balance

Carbon that is unaccounted for may have been deposited on the catalyst basket although this is not known as the basket was not weighed before and after the experiments. Other carbon losses could be attributed to carbon deposition in the reactor as there is a significant distance between the glycerol feed inlet and catalyst bed. Additionally it was noted that carbon deposition occurs on the thermocouple which was discovered during the cleaning process. The accuracy of the CHNS measurement of solid carbon from the catalyst bed is questionable due to the small sample size. Sample sizes of 12 mg are taken from a bed of mass 9-18g where 75% of the bed is sand. Sand would contain much less, if any, deposited

carbon compared to the catalyst and it is difficult to sample the same ratio of catalyst to sand in such small sample sizes.

To improve upon this, the mesh in the reactor that the basket was resting on could be replaced with the correct size to prevent catalyst particles from falling through, eradicating the need for a catalyst basket.

To reduce the errors greater than two samples should be analysed both for CHNS and ToC to provide a greater sample size and reduce the standard deviation.

5.4.2 Glycerol Conversion to Gaseous Carbon

The distribution of gaseous carbon products resulting from the conversion of glycerol is shown in Figure 68 in mols of gas per mol of glycerol carbon, with process conditions in Table 29.

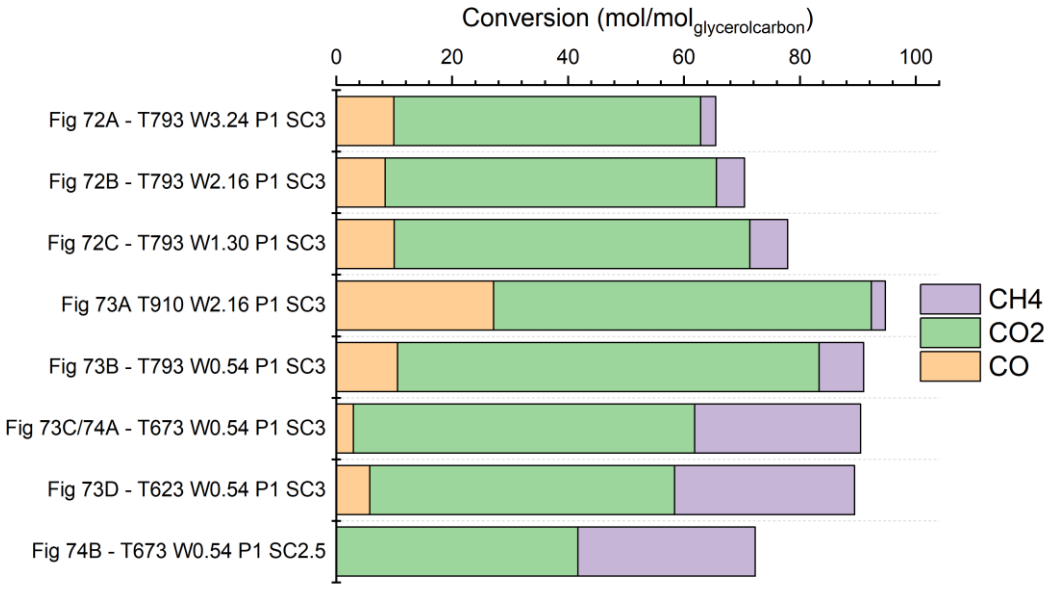

Figure 68. Conversion of glycerol carbon to carbon gases on a molar basis at steady state where T is temperature in K, W is weight hourly space velocity, P is pressure and SC is steam to carbon ratio.

Figure	*SC*	*Catalyst*	*Particle Size*	*Sand Mass*	*Feed Flow*	*WHSV*	*T*	*N_2 Flow*	*P*
-	-	g	micron	g	ml hr^{-1}	hr^{-1}	K	ml min^{-1}	ATM
Figure 71A	3	2	150-200	9	6.00	3.24	793	69	1
Figure 71B	3	3	150-200	9	6.00	2.16	793	68	1
Figure 71C	3	5	150-200	15	6.00	1.30	793	68	1
Figure 72A	3	3	150-200	9	9.00	2.16	910	105	1
Figure 72B	3	6	150-200	18	3.00	0.54	793	39	1
Figure 72C	3	3	150-200	9	1.5	0.54	623	26	1
Figure 72D/ Figure 73A	3	6	150-200	18	3.00	0.56	673	39	1
Figure 73B	2.5	6	150-200	18	3.00	0.56	673	38	1

Table 29. Process conditions for experiments shown in Figure 68 for the conversion of glycerol carbon to gaseous carbon molecules CH_4, CO_2 and CO_2.

The glycerol to carbon conversion based on the gaseous products increases as the weight hourly space velocity is decreased from 3.24 hr^{-1} in Figure 71A to 0.54 hr^{-1} in Figure 72B at the temperature of 793K and pressure 1 atm. The carbon in the gas increase is mainly in the form of CO_2 and CH_4 whilst CO remains constant.

Temperature does not impact the overall total conversion at steady state. At the WHSV of 0.54 hr^{-1} no noticeable change in the total conversion is observed for 793 K, 673 K and 623 K in Figure 72B, Figure 72C/ Figure 73A or Figure 72D respectively. On the other hand, a significant decrease in CO_2 and increase of CH_4 is observed at 673 K and 623 K compared to 793 K. The percentage conversion to CH_4 has increased to 29% and 31% from 8% respectively.

Reducing the SC to 2.5 from 3 had a similar impact on CH_4 conversion as reducing the temperature from 673 K to 623 K without compromising on total carbon conversion. This is likely because H_2 production is more favoured when greater molar ratios of steam are present due to shifting the equilibrium of the water gas shift reaction to the right.

The highest overall conversion to gaseous products was observed at 910 K although a significant quantity of the gas composition is CO due to this temperature favouring H_2 production.

Imai was able to achieve carbon conversions of 41, 81 and 85% at 593 K, 623 K and 673 K respectively using a WHSV of 6.7 hr^{-1} at 1 atmosphere at an on stream time of 5 hrs using a 20 wt% Ni 20% SiO_2 catalyst supported on gamma alumina. Comparatively this work achieved higher carbon conversions, 90% at 673 K and 89% at 623 K respectively but

required a significantly higher WHSV (factor of ten larger). One consideration is the size of the reactor in this case, where

5.4.3 Equilibrium Efficiency

Results from calculating the CH_4 equilibrium efficiency are shown in Figure 69 using the previously calculated equilibrium results in 2.6.1 as the baseline for each set of variables.

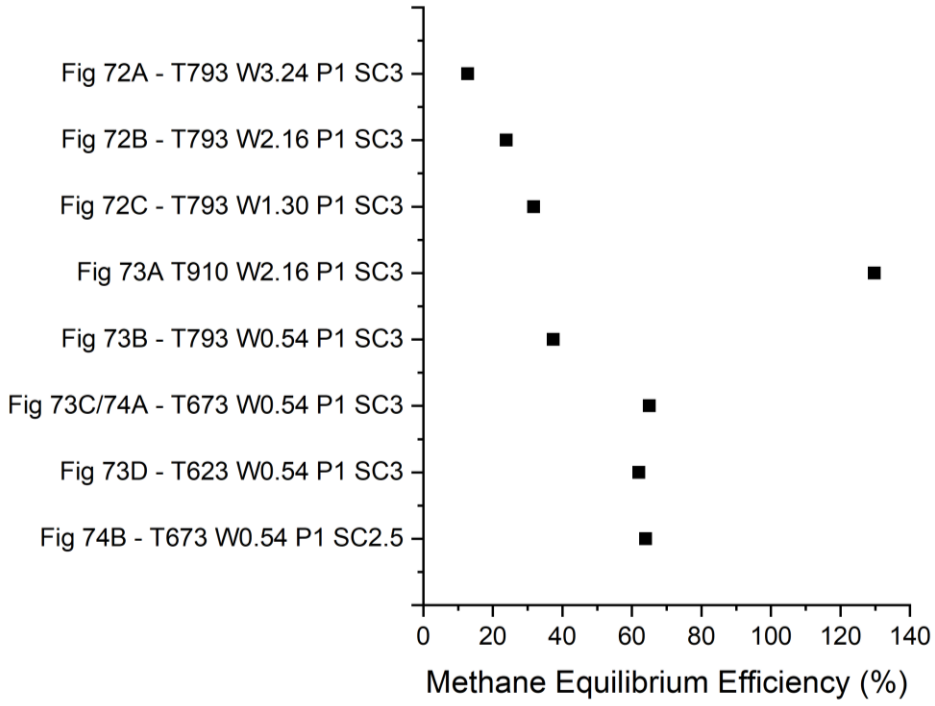

Figure 69. Equilibrium efficiency of experiments in figure 70-72 where T is temperature in K, W is weight hourly space velocity, P is pressure and SC is steam to carbon ratio.

Decreasing the WHSV from 3.24 to 1.3 resulted in a significant increase in equilibrium efficiency at 793 K. This is due to greater overall carbon conversion as discussed in Figure 68, and although the WHSV is doubled at each increment, the increase in CH_4 suffers from diminishing returns. Decreasing the WHSV, by reducing the inlet flow rate or increasing the mass of catalyst or both, increases the likelihood of interaction and time spent in the catalyst bed. As methanation reactions have a larger activation energy, decreasing the WHSV and therefore increasing the residence time will significantly impact the rate of CH_4 production as increasing the residence time allows for reactions to reach equilibrium faster.

As temperature was decreased beyond 793 K and WHSV maintained at 0.54, the equilibrium efficiency rises above 60%. The highest reasonable equilibrium efficiency of 66% is at a temperature of 673 K, WHSV 0.54, P1 and SC of 2.5. At 910 K a 130% equilibrium efficiency is observed for CH_4 and appears to be an outlier.

An important conclusion from these results shows that at 793 K at WHSV of 0.54 and above the process is operating significantly away from equilibrium and is more influenced by kinetic parameters and therefore kinetically controlled under these conditions with the $NiCaAl_2O_3$ catalyst.

As the temperature is reduced to 673 K and 623 K with the WHSV maintained at 0.54, the process is operating closer to equilibrium with higher equilibrium efficiencies above 60%.

5.4.4 Water Conversion

Results for the average calculated inlet feed water conversion to product gases based on the H_2 balance from *Equation 45* are displayed in Figure 70.

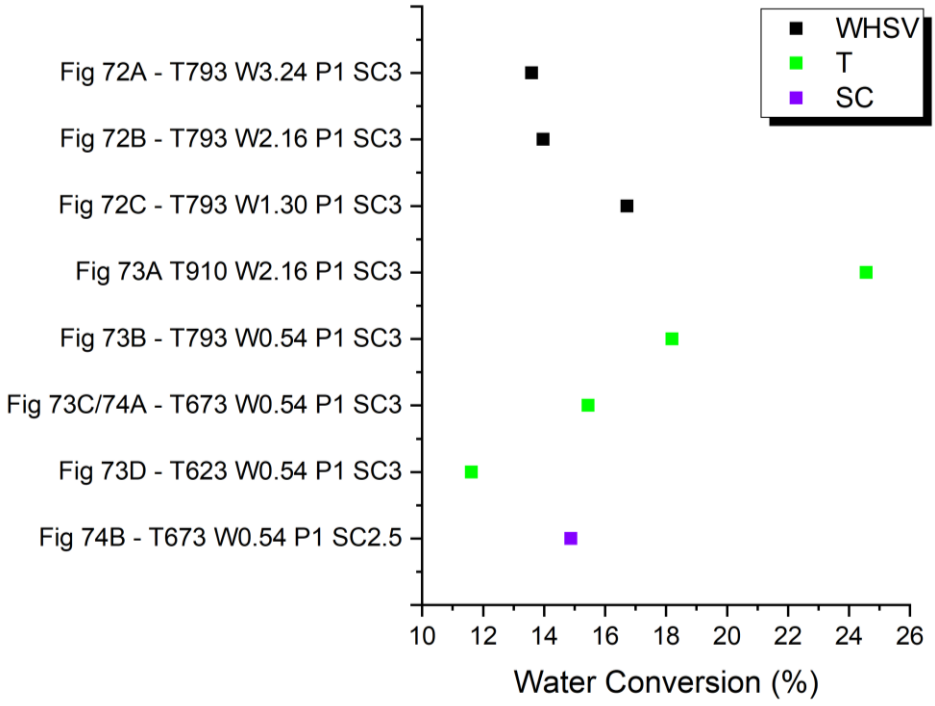

Figure 70. Average water conversion to product gases based on H_2 balance for results used for comparison of the impacts of weight hourly space velocity (WHSV), temperature (T) in Kelvin, and steam to carbon ratio (SC).

At 793 K as the WHSV is reduced the water conversion increases. This shows that the activity of the WGS and GSR increases as WHSV decreases. On the other hand, as the temperature is decreased from 910 K to 623 K, water conversion decreases significantly as methanation conditions become more favourable and the WGS and GSR become less active and COM becomes more active.

None of the water conversion values are negative which shows that there is no net gain in water i.e. water produced at a greater rate than consumed. The theoretical limit of direct methanation, as shown in *Equation 17*, shows that 0.5 moles of H_2O should be produced per mole of glycerol. It is clear that none of the results are close to this limit as they would exhibit a negative water conversion.

Glycerol Autothermal Reforming (direct methanation of glycerol)

$$C_3H_8O_{3(l)} \rightarrow 1.75CH_4 + 1.25CO_2 + 0.5H_2O \qquad \Delta H^0_{298}\ \text{-74 kJ mol}^{-1} \qquad \textit{Equation 17}$$

5.4.5 WHSV Effects on Product Distribution

Results for experiments with different WHSV are shown in Figure 71 with the process variables described in Table 30.

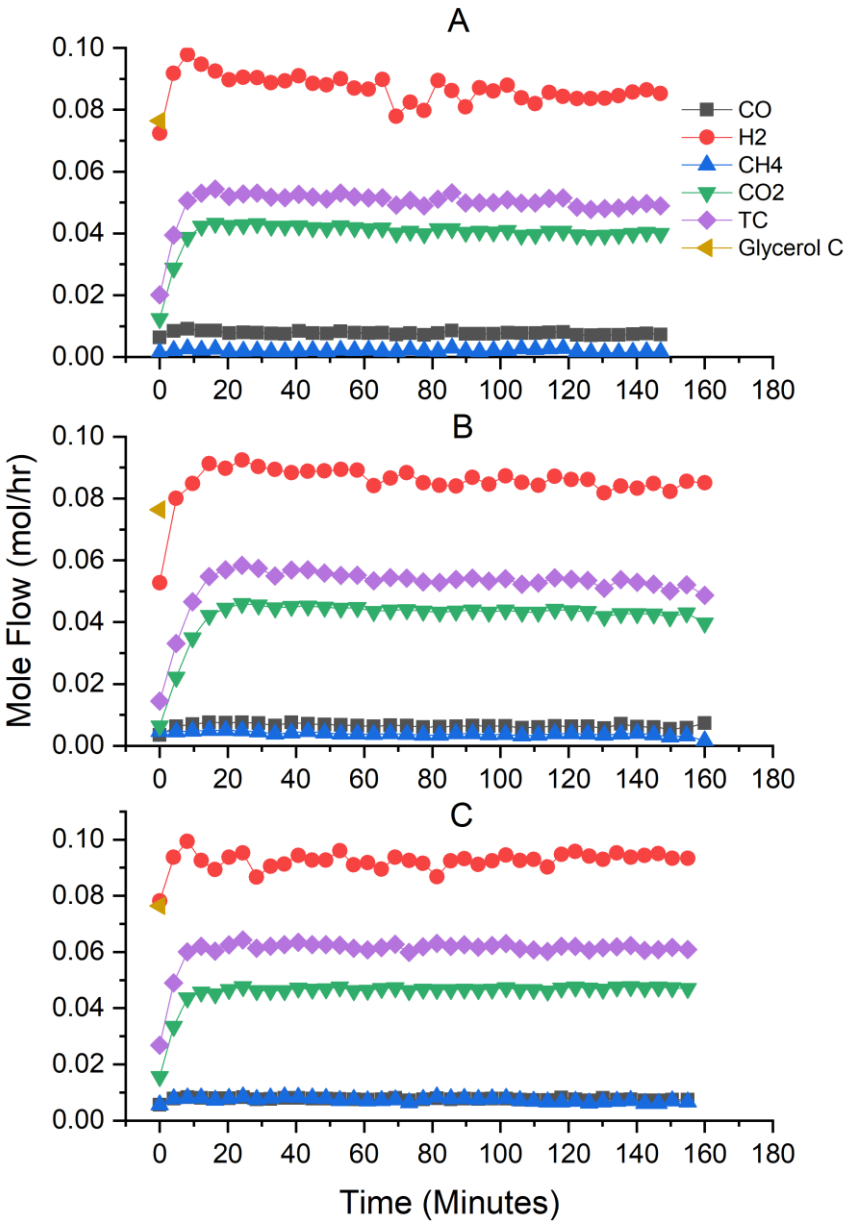

Figure 71. Molar flow rates of product gases from glycerol steam reforming at 793 K and improved WHSV.

Figure	*SC*	*Catalyst*	*Particle Size*	*Sand Mass*	*Feed Flow*	*WHSV*	*T*	*N_2 Flow*	*P*
-	-	g	micron	g	ml hr^{-1}	hr^{-1}	K	ml min^{-1}	ATM
Figure 71A	3	2	150-200	9	6.00	3.24	793	69	1
Figure 71B	3	3	150-200	9	6.00	2.16	793	68	1
Figure 71C	3	5	150-200	15	6.00	1.30	793	68	1

Table 30. Process conditions for WHSV experiments in Figure 71.

Downward trends can be observed in Figure 71A and B for H_2, CO_2 and total carbon indicating that deactivation of the catalyst is occurring within the first 120 minutes of operation. As the WHSV is decreased from 3.24 hr^{-1} to 1.3 hr^{-1}, as shown in Figure 71C, the downward trend is not observed within the first 160 minutes of operation. Based on these results, operating at 793 K required a WHSV close to 1.3 hr^{-1} to prevent early catalyst deactivation and maintain conversion. At 793 K reducing the WHSV also improved the CH_4 production without impeding H_2, reducing CO production and increasing the conversion to carbon gases. The reduction in CO is indicative of methanation, confirmed by the increase in total carbon, although the H_2 concentration does not decrease. This corresponded to greater water conversion and therefore contribution from GSR or WGS, as shown in Figure 70, to make up for the deficit in H_2.

It was found that decreasing the WHSV to 0.56 hr^{-1} did not improve conversion rates at 793 K, but was necessary to maintain conversion rates at 673 K and 623 K. Consequently a WHSV of 0.56 hr^{-1} was chosen for operation at 673 K and 623 K as shown in Figure 72C and 70D. Decreasing further required a significant increase in mass of catalyst or flow rate which was not feasible within the timescale of this project and the accuracy of the pumps. Compared to Imai, it was necessary to decrease the WHSV by a factor of ten, from 6.7 hr^{-1} to achieve comparable conversion rates to carbon gases [36].

5.4.6 Temperature Effects on Product Distribution

Results for experiments at temperatures of 910 K, 793 K, 673 K and 623 K are shown in Figure 72A, Figure 72B, Figure 72C, and Figure 72D respectively.

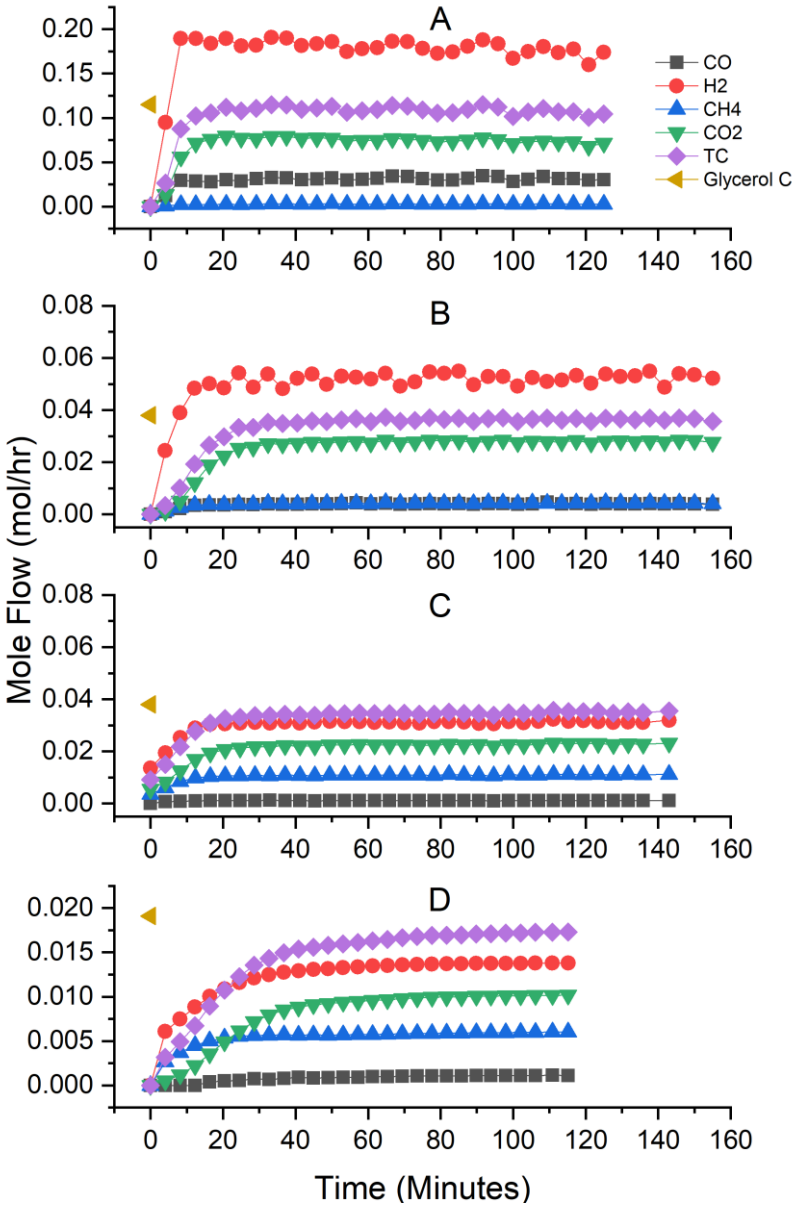

Figure 72. Molar flow rates of product gases from glycerol steam reforming for temperatures between 910 K and 623 K.

Figure	*SC*	*Catalyst*	*Particle Size*	*Sand Mass*	*Feed Flow*	*WHSV*	*T*	*N_2 Flow*	*P*
-	-	g	micron	g	ml hr^{-1}	hr^{-1}	K	ml min^{-1}	ATM
Figure 72A	3	3	150-200	9	9.00	2.16	910	105	1
Figure 72B	3	6	150-200	18	3.00	0.54	793	39	1
Figure 72C	3	6	150-200	18	3.00	0.54	673	38	1
Figure 72D	3	3	150-200	9	1.50	0.54	623	25	1

Table 31. Process conditions for temperature experiments in Figure 72.

The feed flow rate of glycerol and N_2 carrier gas were decreased to prevent the need for large masses of catalyst when operating at low WHSV. Consequently Figure 72A had the largest inlet feed of glycerol at 9 ml hr^{-1} whereas Figure 72D had the smallest inlet feed at 3 ml hr^{-1}.

At all of the temperatures studied, H_2 was the most abundant singular product rather than the desired CH_4. As temperature decreases the molar flow ratio of H_2 to CH_4 was observed to decrease from 20:1, 5:1, 3:1 and 2:1 for 910 K, 793 K, 673 K and 623 K respectively. Therefore in terms of H_2 element distribution, at 623 K the balance was equally split between H_2 and CH_4 showing that the greatest CH_4 production occurred at 623 K. This agrees with the equilibrium modelling results from section 2.6 and coincides with the reduction in water conversion in Figure 70, as the COM reaction is becoming more active in relation to WGS and GSR reactions at temperatures below 973 K. Thermodynamically this is due to COM have a lower Gibbs free energy despite the activation energy of CH_4 formation being greater than CO or H_2. This gives the impression that under these conditions the reaction is still under both kinetic and thermodynamic control.

On the other hand, CO molar flow rate is greatest at 923 K, decreasing at 793 K and is close to zero at 673 K and 623 K. CO is still formed at temperatures above 793 K at a steam to carbon ratio of three from the combination of glycerol decomposition and reverse water gas shift.

As temperature decreases to 793 K from 923 K the ratio of CO to H_2 has slightly decreased from 1:8 to 1:10 but the CH_4 has risen from ~0 to the same as CO. The ratio of total carbon gases to H_2 has increased from 1:2 to 2:3 whilst CH_4 and CO_2 have increased and CO has decreased. This indicates that, although CO is combined with H_2 to produce CH_4, overall more carbon species are being produced. This effect is greater at lower temperatures of 673 K and 623 K where CO is near zero.

5.4.7 Comparison of Experimental data with Imai

A comparison of the normalised experimental data in this work with Imai's work is shown in Table 32.

Unit	Gas	623 K Normalised	623 K Imai	673 K Normalised	673 K Imai
mol/hr	CO	0.003	0.048	0.001	0.000
	CO_2	0.024	0.003	0.027	0.033
	CH_4	0.014	0.009	0.013	0.030
	H_2	0.033	0.044	0.038	0.024

Table 32. Comparison of experimental data in this work with Imai et al. [36]. Conditions for Imai were SC of 1.35, WHSV of 6.7 hr^{-1}, pressure of 1 atm, feed flow rate of 3.6 ml hr^{-1}. Normalised experimental data was calculated by using Imai's inlet flow rate of glycerol as the base line under the conditions of SC 3, WHSV 0.54 hr^{-1}, pressure of 1 atm and feed flow rate of 1.5 ml hr^{-1} at 623 K and 3 ml hr^{-1} at 673 K.

Regarding CH_4 production, this work produced more CH_4 at 623 K, likely due to the higher SC ratio preventing carbon formation and despite 41% less carbon from the glycerol being available for conversion at an SC of 3 compared to 1.2. However at 673 K, this work was less effective at producing CH_4 despite the significantly reduced WHSV of 0.54. In this case, as there was no inhibition of the catalyst activity at SC 1.2 in Imai's work, these conditions were more favourable for methanation, even after accounting for the additional carbon available from glycerol at SC 1.2. Therefore it would important to vary the SC within the range of the minimum SC for zero carbon formation as a further optimisation point whilst monitoring the level of solid carbon deposition on the catalyst.

5.4.8 Steam to Carbon Ratio Effect

The SC was reduced from 3 to 2.5 to determine any impacts on product gas distribution at 673 K, as shown in Figure 73A and B respectively.

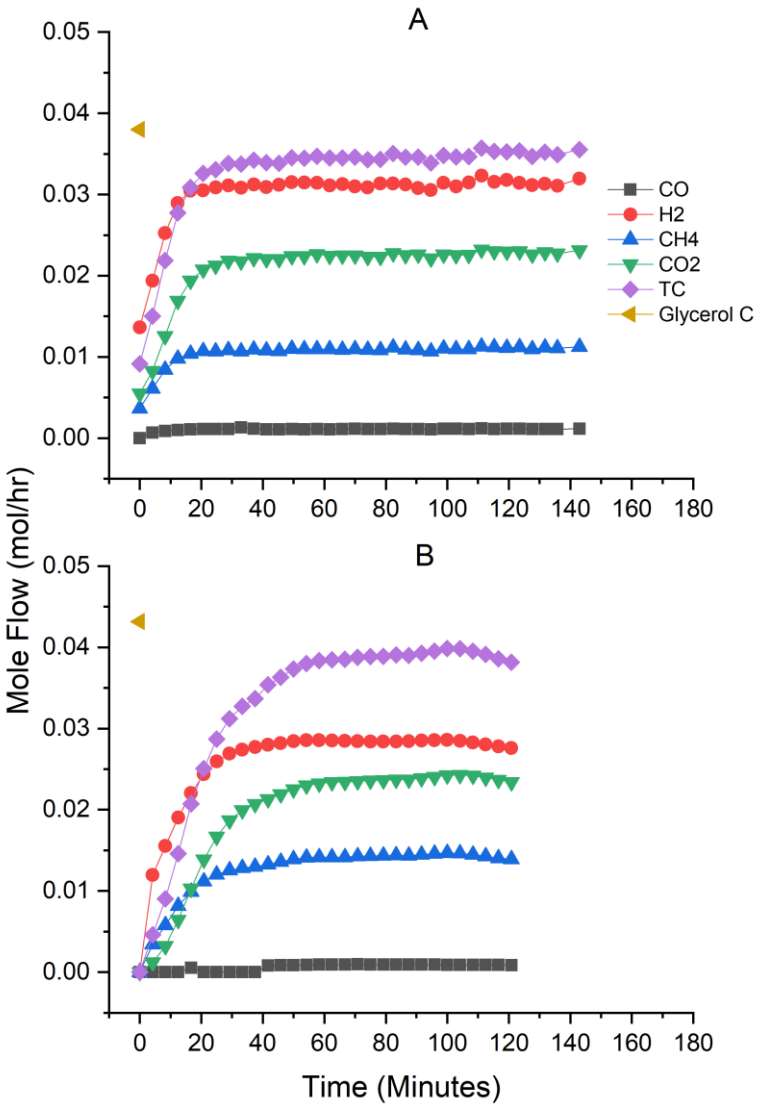

Figure 73. Molar flow rates of product gases from glycerol steam reforming for SC of 3 (A) and 2.5 (B) at 673 K.

Figure	*SC*	*Catalyst*	*Particle Size*	*Sand Mass*	*Feed Flow*	*WHSV*	*T*	*N_2 Flow*	*P*
-	-	g	micron	g	ml hr^{-1}	hr^{-1}	K	ml min^{-1}	ATM
Figure 73A	3	6	150-200	18	3.00	0.56	673	39	1
Figure 73B	2.5	6	150-200	18	3.00	0.56	673	38	1

Table 33. Process conditions for experiments in Figure 73.

At an SC of 3 there was no deactivation of the catalyst observed within the first 140 minutes. For SC of 2.5 the time taken to reach the steady state using H_2 as a reference to 20 minutes from 10 minutes at SC of 3. Moreover, deactivation was observed from 100 minutes into the

process shown by the negative gradient associated with H_2, CO_2, CH_4 and the total carbon gases. On the other hand, an increase in CH_4 production and total carbon gases was observed at an SC of 2.5 prior to deactivation, from 0.011 mol/hr to 0.015 mol/hr due to the increased glycerol carbon in the feed.

Imai *et al.* were able to use an SC of 1.2 at 673 K over 5 hours [36]. Increasing the length of time of the experiment would help determine the severity of the deactivation or if this was an anomaly, as using a lower SC is more favourable for CH_4 production but also solid carbon formation.

5.4.9 Summary

A stainless steel rig was constructed and used to test the efficacy of a commercial powder nickel calcium alumina catalyst for converting pure glycerol to CH_4. For all experiments a steady state conversion was observed. The process conditions varied were temperature and weight hourly space velocity as well as steam to carbon ratio and pressure. Using a WHSV of 0.54, roughly 90% conversion of glycerol to gaseous products at all temperatures was observed. Process variables that yielded the greatest composition of CH_4 in the product gas were temperatures below 673 K, steam to carbon ratio of 2.5 and 3, pressure of 1 atm and 2 atm and a WHSV of 0.54. Between 3-10% of carbon from the inlet feed of glycerol was lost as solid carbon via deposition to the catalyst and solid carbon formation was more prominent at the lower temperatures of 673 K. The greatest equilibrium efficiency for CH_4 of 66% was observed at a temperature of 673 K, SC of 2.5, WHSV of 0.54 and pressure of 1 atm implying that under the conditions used in these experiments, the process was still operating away from the predicted Gibbs free energy minimisation modelled equilibrium.

5.4.10 Brief Conclusions

- A gasification rig for conversion of glycerol to gas products was designed and built.
- A weight hourly space velocity of 0.54, steam to carbon ratio of 2.5 at 623 K and 673 K produced the highest conversion to gases and CH_4, as well as the greatest equilibrium efficiency.
- The process was not operating at equilibrium and required further optimisation, including but not limited to higher pressures.

6 Conclusions and Future Work

In this chapter the case for the feasibility of a direct methanation process for bio-SNG via low temperature glycerol steam reforming (GLT-SR) will be argued based on the overarching conclusions from the work carried in this thesis.

In addition, to what extent the research objectives mentioned in chapter 1 were completed and what future work can be carried out as a result of this thesis is discussed.

6.1 Research objectives

The following research objectives were proposed in table 2 in chapter 1 and what follows is a discussion of the extent to which they were completed:

Determine the optimum process conditions that would allow the conversion of glycerol to a CH_4 rich fuel gas using thermodynamic modelling.

Thermodynamic modelling revealed that the temperatures most suited for CH_4 formation were the lowest possible i.e. closest to the vapour point of the glycerol water solution. Increasing the pressure favoured methanation and the most benefit could be gained by increasing the pressure to 8 atm. The best steam to carbon ratio was the minimum required to prevent solid carbon formation, demonstrating completion of this objective.

Create and optimise a process model of a glycerol direct methanation plant based on thermodynamic modelling with energy and mass flows outputs.

Using Aspen Plus V8.8 a process model with heat integration was created. From this model, it was possible to determine the biomass to fuel efficiency and the potential energy offset when the natural gas at the crushing stage of the biodiesel refinery is substituted for bio-SNG and based on these results this objective was completed.

Perform a techno-economic analysis of the plant based on the process model.

Using Excel, a discounted cash flow analysis model and a Monte Carlo simulation for profitability risk analysis were created. The sizing measurements from the Aspen Plus process model were used to estimate economic values such as the base equipment cost. It was possible to determine the required conditions e.g. gas price, for a profitable venture based on net present value and the risk of the venture becoming unprofitable based on stochastic variables, showing completion of this objective.

Compare the life cycle impacts of steam generated from glycerol bio-SNG with natural gas based steam.

Using SimaPro and the data from the United States life cycle inventory, an energy life cycle impacts analysis comparing steam from glycerol bio-SNG and natural gas was produced. The impact of different allocation keys on the life cycle impacts was compared showing what the trade-offs were of using bio-SNG based steam from glycerol showing that this objective was completed.

Construct a laboratory scale glycerol gasifier and optimise the process towards maximising CH_4 production.

The biomass gasification rig was successfully constructed and tested with conditions that favour CH_4 production from pure glycerol and water solutions without pre-vaporisation. However, the process was not optimised and remains an area for future work. Therefore this objective was only partially completed.

6.2 Feasibility

When discussing feasibility it would be preferable if the answer was a simple yes or no. As with most technologies, this is not the case and the same applies to GLT-SR. Under the conditions used in this thesis, it is possible to determine the feasibility but this does not mean it is applicable to all cases and certainly does not always mean that the process should be used in favour of another. However, it does show that the GLT-SR process is of interest and viable in certain situations and further research should be carried out to reduce the uncertainty around the feasibility. To answer the original question of:

Under what conditions is the direct methanation of glycerol feasible?

The conditions for each area of interest including, process, economics, environment and experimental practicality are discussed.

6.2.1 Process

By converting soybean crude glycerol to bio-SNG it was possible to offset up to 24% of natural gas usage at a soybean biodiesel refinery based in the USA. An ideal process was created where the crude glycerol contained 80% by weight of glycerol and contaminants would have a negligible effect on conversion. Considering the GLT-SR process required steam to be generated on site, energetically the process is feasible as it produces more energy than it requires to operate. Utilising the additional low-pressure steam generated at 1.5 atm would improve the process efficiency and there improve process feasibility. The process will depend upon the ability of the catalyst and process conditions to shift the equilibrium in favour of producing CH_4.

6.2.2 Economics

After calculating the cash flow analysis a scenario where a positive net present value was observed. The hurdle rate of 10-13% for biomass gasification technologies was achieved with a gas price between \$6-7 $mmBtu^{-1}$ and was comparable to the gas prices observed in 2017 in Missouri and Arkansas, both of which have soybean biodiesel plants. Furthermore, from the risk analysis carried out with Monte Carlo simulation, at a 12% internal rate of return it was possible to predict with a 99.5% confidence interval that a positive net present value would be achieved under the minimum uncertainty. This indicates that there is a low risk of producing a negative outcome regarding GLT-SR processes when the gas price has a similar range to 2017 Missouri gas prices and based on the base equipment cost (BEC) calculated in this work. Therefore a GLT-SR process plant could be economically feasible even without subsidies in the state of Missouri.

What remains unclear is the level of uncertainty associated with the BEC estimate which could be improved by carrying out a more in-depth cost estimation study as well as the cost of selling crude glycerol without processing is. Assuming there is a market for crude glycerol, selling crude glycerol outright is more profitable than converting it to bio-SNG. Therefore, GLT-SR is a good option if the glycerol is too low value to make a profit when selling or is consigned to waste. The model generated in this thesis can be adapted to any other geographical situation.

6.2.3 Environmental

Data from the USLCI database combined with different allocation keys was used to determine a life cycle energy impacts assessment. The impacts of bio-SNG compared to natural gas were similar to biodiesel compared to fossil diesel, where there was potential to reduce global warming potential (GWP) at the cost of increased ozone depletion (ODP), eutrophication (EP) and terrestrial ecotoxicity potential (TEP), due to the contributions from agriculture when cultivating soybeans. As the glycerol was now being used for energy instead of being sold on a mass basis, an energy allocation key was more appropriate and had a 55% lower GWP than natural gas whilst in the worst case using a mass allocation had the same. On the other hand, for the energy allocation method, EP, TEP and ODP were 3.5, 20 and 80 times greater respectively than natural gas. Finally, the fossil energy ratio in all allocation cases was greater than one showing that over the life cycle energy investment, bio-SNG is a net producer of energy. Whilst there are trade-offs in terms of environmental impacts, these trade-offs are similar to the case of soybean biodiesel versus fossil diesel and it can be concluded that under certain situations the process of producing bio-SNG can be feasible from the perspective of the environment.

6.2.4 Experimental

A liquid biomass gasification rig was constructed and tested with pure glycerol and water mixtures at temperatures of 623 K to 910 K. At all temperatures, a steady state was achieved with roughly 90% carbon conversion to gases showing that the Ni/Ca-Al_2O_3 catalyst was active in steam reforming and methanation. The main area of carbon loss at temperatures below 673 K was by solid carbon deposition onto the catalyst. The water conversion began to decrease as temperature was reduced clarifying the increase in activity of the methanation reaction. The gas distribution showed that up to 70% of the predicted equilibrium CH_4 and over 100% of the predicted CO and H_2 concentrations were being produced demonstrating that, whilst a steady state was achieved, the current process conditions are not shifting the equilibrium towards maximum CH_4 production.

As there were significant optimisation challenges left, it is not possible to give a definitive answer on experimental feasibility. From an optimistic point of view, if the process could be optimised and over 90% of the predicted equilibrium CH_4 could be produced with minimal catalyst degradation, from a laboratory scale the process would be experimentally feasible. Consequently, the experimental section makes up the bulk of the future work.

Moreover as pure glycerol was used it would not be correct to extrapolate the feasibility of the process to a GLT-SR process with crude glycerol.

6.3 Future Work

6.3.1 Process

Increasing the detail of the process flow diagram is an idea for future work. Currently, simple heat exchanger blocks and an equilibrium Gibbs reactor block are used. To improve upon the heat exchanger network and maximise the heat able to be recovered, pinch analysis could be performed. Doing so will allow greater process optimisation by targeting the most thermodynamically feasible energy targets and modifying energy conditions to maximise heat recycling in the system. Example methods are shown in Pinch Analysis and Process Integration[210] and contains software for ease of calculation.

To improve on the reactor a stoichiometric reactor incorporating reaction kinetics of the process can be used to determine more accurate product distributions. Using detailed heat exchangers will also improve the sizing requirements reducing the uncertainty for the economic analysis. Furthermore, maximising the heat able to be recovered via heat exchangers should be carried out using pinch analysis. Doing so will allow greater process optimisation by targeting the most thermodynamically feasible energy targets and modifying energy conditions. To carry out these improvements, the laboratory scale gasifier needs to be optimised.

6.3.2 Economic

The main challenge is reducing uncertainty in the estimations. To do this, scaling up of the laboratory scale model is required to be able to prepare a C3 –scoping study or better. This hinges on the experimental section where optimisation of the laboratory scale gasifier is required prior to a further scale-up process. In doing so, the uncertainties associated with the base equipment cost can be reduced and create a more precise Monte Carlo simulation to determine the risk of an unprofitable venture.

6.3.3 Environmental

To improve the life cycle impacts analysis the system boundary could be expanded to include depletion of natural resources. A particular focus would be on abiotic depletion as many natural resources are required, for example, the materials used in the construction of the refinery or GLT-SR plant. Determining whether the life cycle impacts are still favourable after expanding the system boundary would require a more detailed life cycle inventory but would give a more definitive comparison between steam production from natural gas and glycerol bio-SNG.

6.3.4 Experimental

Future work in the short term should be focused on optimising the process to achieve maximum conversion to CH_4. This can be achieved by improving the residence time of the reagents in the catalyst bed and improving the yield of CH_4 by investigating lower temperatures combined with elevated pressures. After optimisation, the on-stream time can be increased from 2-3 hours to 3-10 hours to determine at what point the catalyst begins to degrade due to carbon deposition. Further analysis of the catalyst can and therefore the carbon formed can be carried out by transition electron microscopy (TEM) and thermogravimetric analysis (TGA) to understand what form of carbon has been deposited on the catalyst.

The temperature range to be investigated should be 623-673K (350-400°C) initially and then reduced to 573-623 K (300-350°C) depending on the minimum vaporisation point of the glycerol/water feed at an SC of 3. Reducing the SC from 3 is likely to improve the gaseous conversion to CH_4 and bring the process closer to the modelled equilibrium but it will be necessary to monitor the level of carbon deposition on the catalyst.

Once the process is optimised at these temperatures, increasing the pressure above atmospheric should be the next priority. To operate at these pressures back pressure regulators as well as a regulator for the micro-GC may be necessary. A back pressure regulator will allow the system to remain pressurised whilst allowing gas to flow towards the micro-GC.

To remedy this situation an in line back pressure regulator can be purchased from Swagelok in the form of a dome or a needle. Alternatively a back pressure regulator is available as a micro-GC attachment through Agilent.

Improvements to reagent residence time could be achieved by increasing the volume of bed by dilution with the greater mass of sand or inert substance or by increasing the volume of the catalyst using a fibrous support such as catalytic grade Saffil.

A method of sampling the solid carbon in condensate at different intervals could prove useful for more accurate carbon balances. Installing multiple catch pots with a switch will enable the condensate to be captured at a time interval of the operators choosing e.g. after the known lag time has passed and a steady state has been achieved enabling analysis of the condensate at different points on stream as well as over the total on-stream time.

In the long term, once the process is optimised for pure glycerol, crude glycerol should be tested. Doing so will determine the extent to which contaminants impact the conversion,

product distribution and catalyst degradation rate. As the GLT-SR process will need to use crude glycerol to be feasible, this will be the most significant area of research.

6.3.5 Linking Analysis Methods

In this work, each method built upon the process simulation step. The results from the process simulation informed on the experimental work and provided the basis for economic and life cycle impact analysis modelling. Due to the nature of PhD work and the time constraints from learning new techniques, this led to a lack of reciprocity with the methods, when in fact, this may be one of the most powerful ways to gain insights. Enhancing the coherence between the tools used in this work would have been an area to explore.

By using data from the economic analysis the areas which caused the greatest increase to OPEX or CAPEX could be identified. If there are cheaper alternatives available, these could then be substituted into the process simulation to determine any impacts on the final product. Similarly, the largest contributors to the environmental impacts could be identified and replaced or reduced in the same way but with a focus on reducing environmental impacts. Comparisons could be made between economics and environmental benefits to show the cost of reducing impacts and win-win scenarios quantified. In this way environmental and economic analysis can be used as tools to further guide process development at the research and development level, as well as a tool to explore feasibility.

7 Appendix 1

Mass balance for GLT-SR process simulation in Figure 21.

	A1	A2	BG1	BG2	BG3
Mole Flow kmol/hr					
H2O	0.0	0.0	37.2	37.2	37.2
CH4	0.0	0.0	9.3	9.3	9.3
CO2	0.0	0.0	7.0	7.0	7.0
N2	12.0	12.0	0.0	0.0	0.0
O2	3.2	3.2	0.0	0.0	0.0
H2S	0.0	0.0	0.0	0.0	0.0
H2	0.0	0.0	0.7	0.7	0.7
CO	0.0	0.0	0.0	0.0	0.0
GLYCEROL	0.0	0.0	0.0	0.0	0.0
C	0.0	0.0	0.0	0.0	0.0
Mass Flow kg/hr					
H2O	0.0	0.0	669.9	669.9	669.9
CH4	0.0	0.0	149.2	149.2	149.2
CO2	0.0	0.0	306.1	306.1	306.1
N2	335.2	335.2	0.0	0.0	0.0
O2	101.8	101.8	0.0	0.0	0.0
H2S	0.0	0.0	0.0	0.0	0.0
H2	0.0	0.0	1.5	1.5	1.5
CO	0.0	0.0	0.1	0.1	0.1
GLYCEROL	0.0	0.0	0.0	0.0	0.0
C	0.0	0.0	0.0	0.0	0.0
Total Flow kmol/hr	15.1	15.1	54.2	54.2	54.2
Total Flow kg/hr	437.0	437.0	1126.9	1126.9	1126.9
Total Flow cum/hr	318.1	514.0	320.4	258.7	247.2
Temperature C	46.7	140.4	303.3	151.8	145.4
Pressure atm	1.3	1.0	8.0	7.2	6.5
Vapor Frac	1.0	1.0	1.0	1.0	0.9
Liquid Frac	0.0	0.0	0.0	0.0	0.1
Solid Frac	0.0	0.0	0.0	0.0	0.0
Enthalpy MJ/kmol	0.6	3.4	-219.0	-225.3	-230.4
Enthalpy MJ/kg	0.0	0.1	-10.5	-10.8	-11.1
Enthalpy MJ/hr	9.6	51.2	-11864.9	-12208.7	-12481.3
Entropy MJ/kmol-K	0.0	0.0	0.0	0.0	-0.1
Entropy MJ/kg-K	0.0	0.0	0.0	0.0	0.0
Density mol/cc	0.0	0.0	0.0	0.0	0.0
Density gm/cc	0.0	0.0	0.0	0.0	0.0
Average MW	28.9	28.9	20.8	20.8	20.8
Liq Vol 60F cum/hr	0.8	0.8	1.6	1.6	1.6

	BG4	BG5	BGD	COND	E1
Mole Flow kmol/hr					
H2O	37.2	37.2	0.0	37.2	4.7
CH4	9.3	9.3	9.3	0.0	0.0
CO2	7.0	7.0	7.0	0.0	4.0
N2	0.0	0.0	0.0	0.0	17.4
O2	0.0	0.0	0.0	0.0	0.0
H2S	0.0	0.0	0.0	0.0	0.0
H2	0.7	0.7	0.7	0.0	0.0
CO	0.0	0.0	0.0	0.0	0.0
GLYCEROL	0.0	0.0	0.0	0.0	0.0
C	0.0	0.0	0.0	0.0	0.0
Mass Flow kg/hr					
H2O	669.9	669.9	0.0	669.9	84.9
CH4	149.2	149.2	149.2	0.0	0.0
CO2	306.1	306.1	306.1	0.0	174.2
N2	0.0	0.0	0.0	0.0	487.2
O2	0.0	0.0	0.0	0.0	0.1
H2S	0.0	0.0	0.0	0.0	0.0
H2	1.5	1.5	1.5	0.0	0.0
CO	0.1	0.1	0.1	0.0	0.2
GLYCEROL	0.0	0.0	0.0	0.0	0.0
C	0.0	0.0	0.0	0.0	0.0
Total Flow kmol/hr	54.2	54.2	17.0	37.2	26.1
Total Flow kg/hr	1126.9	1126.9	456.9	669.9	746.5
Total Flow cum/hr	267.2	112.5	86.5	0.7	3397.2
Temperature C	141.2	93.5	20.0	20.0	1314.8
Pressure atm	5.8	5.2	4.7	4.7	1.0
Vapor Frac	0.8	0.4	1.0	0.0	1.0
Liquid Frac	0.2	0.6	0.0	1.0	0.0
Solid Frac	0.0	0.0	0.0	0.0	0.0
Enthalpy MJ/kmol	-231.1	-252.8	-202.1	-286.2	-56.1
Enthalpy MJ/kg	-11.1	-12.2	-7.5	-15.9	-2.0
	-	-	-	-	-
Enthalpy MJ/hr	12522.9	13699.4	3434.0	10642.6	1463.7
Entropy MJ/kmol-K	-0.1	-0.1	0.0	-0.2	0.1
Entropy MJ/kg-K	0.0	0.0	0.0	0.0	0.0
Density mol/cc	0.0	0.0	0.0	0.1	0.0
Density gm/cc	0.0	0.0	0.0	1.0	0.0
Average MW	20.8	20.8	26.9	18.0	28.6
Liq Vol 60F cum/hr	1.6	1.6	0.9	0.7	1.2

	E2	E3	ER1	E4	G
Mole Flow kmol/hr					
H2O	4.7	4.7	1.5	3.2	0.0
CH4	0.0	0.0	0.0	0.0	0.0
CO2	4.0	4.0	1.2	2.7	0.0
N2	17.4	17.4	5.4	12.0	0.0
O2	0.0	0.0	0.0	0.0	0.0
H2S	0.0	0.0	0.0	0.0	0.0
H2	0.0	0.0	0.0	0.0	0.0
CO	0.0	0.0	0.0	0.0	0.0
GLYCEROL	0.0	0.0	0.0	0.0	5.4
C	0.0	0.0	0.0	0.0	0.0
Mass Flow kg/hr					
H2O	84.9	84.9	26.5	58.4	0.0
CH4	0.0	0.0	0.0	0.0	0.0
CO2	174.2	174.2	54.3	119.8	0.0
N2	487.2	487.2	152.0	335.2	0.0
O2	0.1	0.1	0.0	0.1	0.0
H2S	0.0	0.0	0.0	0.0	0.0
H2	0.0	0.0	0.0	0.0	0.0
CO	0.2	0.2	0.1	0.1	0.0
GLYCEROL	0.0	0.0	0.0	0.0	499.2
C	0.0	0.0	0.0	0.0	0.0
Total Flow kmol/hr	26.1	26.1	8.1	17.9	5.4
Total Flow kg/hr	746.5	746.5	232.9	513.6	499.2
Total Flow cum/hr	952.7	952.7	297.2	655.5	0.4
Temperature C	172.2	172.2	172.2	172.2	20.9
Pressure atm	1.0	1.0	1.0	1.0	8.0
Vapor Frac	1.0	1.0	1.0	1.0	0.0
Liquid Frac	0.0	0.0	0.0	0.0	1.0
Solid Frac	0.0	0.0	0.0	0.0	0.0
Enthalpy MJ/kmol	-98.8	-98.8	-98.8	-98.8	-668.2
Enthalpy MJ/kg	-3.4	-3.4	-3.4	-3.4	-7.3
	-	-	-	-	-
Enthalpy MJ/hr	2574.8	2574.8	803.3	1771.5	3621.7
Entropy MJ/kmol-K	0.0	0.0	0.0	0.0	-0.6
Entropy MJ/kg-K	0.0	0.0	0.0	0.0	0.0
Density mol/cc	0.0	0.0	0.0	0.0	0.0
Density gm/cc	0.0	0.0	0.0	0.0	1.3
Average MW	28.6	28.6	28.6	28.6	92.1
Liq Vol 60F cum/hr	1.2	1.2	0.4	0.8	0.4

	HPW1	LPS	LPW1	NBG	R-BG
Mole Flow kmol/hr					
H2O	27.9	24.5	24.5	0.0	0.0
CH4	0.0	0.0	0.0	7.7	1.6
CO2	0.0	0.0	0.0	5.8	1.2
N2	0.0	0.0	0.0	0.0	0.0
O2	0.0	0.0	0.0	0.0	0.0
H2S	0.0	0.0	0.0	0.0	0.0
H2	0.0	0.0	0.0	0.6	0.1
CO	0.0	0.0	0.0	0.0	0.0
GLYCEROL	0.0	0.0	0.0	0.0	0.0
C	0.0	0.0	0.0	0.0	0.0
Mass Flow kg/hr					
H2O	502.2	441.4	441.4	0.0	0.0
CH4	0.0	0.0	0.0	124.2	25.0
CO2	0.0	0.0	0.0	254.8	51.3
N2	0.0	0.0	0.0	0.0	0.0
O2	0.0	0.0	0.0	0.0	0.0
H2S	0.0	0.0	0.0	0.0	0.0
H2	0.0	0.0	0.0	1.2	0.2
CO	0.0	0.0	0.0	0.1	0.0
GLYCEROL	0.0	0.0	0.0	0.0	0.0
C	0.0	0.0	0.0	0.0	0.0
Total Flow kmol/hr	27.9	24.5	24.5	14.1	2.9
Total Flow kg/hr	502.2	441.4	441.4	380.3	76.6
Total Flow cum/hr	0.6	515.9	0.4	72.0	14.5
Temperature C	142.1	111.8	10.0	20.0	20.0
Pressure atm	10.0	1.5	1.5	4.7	4.7
Vapor Frac	0.0	1.0	0.0	1.0	1.0
Liquid Frac	1.0	0.0	1.0	0.0	0.0
Solid Frac	0.0	0.0	0.0	0.0	0.0
Enthalpy MJ/kmol	-276.4	-238.9	-286.9	-202.1	-202.1
Enthalpy MJ/kg	-15.3	-13.3	-15.9	-7.5	-7.5
Enthalpy MJ/hr	-7703.8	-5852.6	-7029.1	-2858.1	-575.9
Entropy MJ/kmol-K	-0.1	0.0	-0.2	0.0	0.0
Entropy MJ/kg-K	0.0	0.0	0.0	0.0	0.0
Density mol/cc	0.0	0.0	0.1	0.0	0.0
Density gm/cc	0.9	0.0	1.0	0.0	0.0
Average MW	18.0	18.0	18.0	26.9	26.9
Liq Vol 60F cum/hr	0.5	0.4	0.4	0.8	0.2

	R-W2	R-W3	R-WC	RE-A	RE-G
Mole Flow kmol/hr					
H2O	27.9	7.0	37.2	0.0	0.0
CH4	0.0	0.0	0.0	0.0	0.0
CO2	0.0	0.0	0.0	0.0	0.0
N2	0.0	0.0	0.0	12.0	0.0
O2	0.0	0.0	0.0	3.2	0.0
H2S	0.0	0.0	0.0	0.0	0.0
H2	0.0	0.0	0.0	0.0	0.0
CO	0.0	0.0	0.0	0.0	0.0
GLYCEROL	0.0	0.0	0.0	0.0	5.4
C	0.0	0.0	0.0	0.0	0.0
Mass Flow kg/hr					
H2O	502.2	125.5	669.9	0.0	0.0
CH4	0.0	0.0	0.0	0.0	0.0
CO2	0.0	0.0	0.0	0.0	0.0
N2	0.0	0.0	0.0	335.2	0.0
O2	0.0	0.0	0.0	101.8	0.0
H2S	0.0	0.0	0.0	0.0	0.0
H2	0.0	0.0	0.0	0.0	0.0
CO	0.0	0.0	0.0	0.0	0.0
GLYCEROL	0.0	0.0	0.0	0.0	499.2
C	0.0	0.0	0.0	0.0	0.0
Total Flow kmol/hr	27.9	7.0	37.2	15.1	5.4
Total Flow kg/hr	502.2	125.5	669.9	437.0	499.2
Total Flow cum/hr	0.5	0.1	0.7	364.4	0.4
Temperature C	19.9	19.9	19.9	20.0	20.0
Pressure atm	8.0	8.0	8.0	1.0	1.0
Vapor Frac	0.0	0.0	0.0	1.0	0.0
Liquid Frac	1.0	1.0	1.0	0.0	1.0
Solid Frac	0.0	0.0	0.0	0.0	0.0
Enthalpy MJ/kmol	-286.2	-286.2	-286.2	-0.1	-668.4
Enthalpy MJ/kg	-15.9	-15.9	-15.9	0.0	-7.3
Enthalpy MJ/hr	-7977.0	-1994.2	-10641.9	-2.2	-3622.7
Entropy MJ/kmol-K	-0.2	-0.2	-0.2	0.0	-0.6
Entropy MJ/kg-K	0.0	0.0	0.0	0.0	0.0
Density mol/cc	0.1	0.1	0.1	0.0	0.0
Density gm/cc	1.0	1.0	1.0	0.0	1.3
Average MW	18.0	18.0	18.0	28.9	92.1
Liq Vol 60F cum/hr	0.5	0.1	0.7	0.8	0.4

	RE-W1	S1	STEAM-RE	W-FG	W-W	WG
Mole Flow kmol/hr						
H2O	24.5	27.9	7.0	3.2	2.3	34.8
CH4	0.0	0.0	0.0	0.0	0.0	0.0
CO2	0.0	0.0	0.0	2.7	0.0	0.0
N2	0.0	0.0	0.0	12.0	0.0	0.0
O2	0.0	0.0	0.0	0.0	0.0	0.0
H2S	0.0	0.0	0.0	0.0	0.0	0.0
H2	0.0	0.0	0.0	0.0	0.0	0.0
CO	0.0	0.0	0.0	0.0	0.0	0.0
GLYCEROL	0.0	0.0	0.0	0.0	0.0	5.4
C	0.0	0.0	0.0	0.0	0.0	0.0
Mass Flow kg/hr						
H2O	441.4	502.2	125.5	58.4	42.2	627.7
CH4	0.0	0.0	0.0	0.0	0.0	0.0
CO2	0.0	0.0	0.0	119.8	0.0	0.0
N2	0.0	0.0	0.0	335.2	0.0	0.0
O2	0.0	0.0	0.0	0.1	0.0	0.0
H2S	0.0	0.0	0.0	0.0	0.0	0.0
H2	0.0	0.0	0.0	0.0	0.0	0.0
CO	0.0	0.0	0.0	0.1	0.0	0.0
GLYCEROL	0.0	0.0	0.0	0.0	0.0	499.2
C	0.0	0.0	0.0	0.0	0.0	0.0
Total Flow kmol/hr	24.5	27.9	7.0	17.9	2.3	40.3
Total Flow kg/hr	441.4	502.2	125.5	513.6	42.2	1126.9
Total Flow cum/hr	0.4	103.8	31.7	361.6	0.0	134.0
Temperature C	10.0	180.5	171.0	20.0	19.9	203.2
Pressure atm	1.0	10.0	8.0	1.0	8.0	8.0
Vapor Frac	0.0	1.0	1.0	0.8	0.0	0.7
Liquid Frac	1.0	0.0	0.0	0.2	1.0	0.3
Solid Frac	0.0	0.0	0.0	0.0	0.0	0.0
Enthalpy MJ/kmol	-286.9	-236.5	-236.8	-110.7	-286.2	-294.7
Enthalpy MJ/kg	-15.9	-13.1	-13.1	-3.9	-15.9	-10.5
Enthalpy MJ/hr	-7029.2	-6592.7	1650.5	-1986.3	-670.7	-11864.9
Entropy MJ/kmol-K	-0.2	0.0	0.0	0.0	-0.2	-0.1
Entropy MJ/kg-K	0.0	0.0	0.0	0.0	0.0	0.0
Density mol/cc	0.1	0.0	0.0	0.0	0.1	0.0
Density gm/cc	1.0	0.0	0.0	0.0	1.0	0.0
Average MW	18.0	18.0	18.0	28.6	18.0	28.0
Liq Vol 60F cum/hr	0.4	0.5	0.1	0.8	0.0	1.0

8 References

[1] Saltmarsh J. Decarbonising Energy to Meet Climate Change Targets. 2017.

[2] IEA. CO2 Emissions From Fuel Combustion Highlights. 2017.

[3] United Nations. Kyoto Protocol to the United Nations Framework Convention on Climate Change. 1998.

[4] Alternative Fuels Data Centre. Fuel Properties Comparison 2014. http://www.afdc.energy.gov/fuels/fuel_comparison_chart.pdf (accessed August 11, 2015).

[5] Gerpen J Van. Cetane Number Testing of Biodiesel. Third Liq Fuel Conf "Liquid Fuels Ind Prod from Renew Resour 1996:197–206.

[6] Knothe G. Biodiesel and renewable diesel: A comparison. Prog Energy Combust Sci 2010;36:364–73. doi:10.1016/j.pecs.2009.11.004.

[7] Biofuel Systems Group Ltd. Biodiesel Standards 2013. http://biofuelsystems.com/standards.html (accessed July 14, 2015).

[8] Kristin Seyboth, Sverrisson F, Appavou F, Brown A, Epp B, Leidreiter A, et al. Renewables 2016 Global Status Report. 2016. doi:ISBN 978-3-9818107-0-7.

[9] OECD, FAO. OECD-FAO Agricultural Outlook 2016. 2016. doi:10.1787/19991142.

[10] Knothe G. The History of Vegetable Oil Based Diesel Fuels. Biodiesel Handb. 2nd ed., 2010, p. 405–37. doi:10.1016/B978-1-893997-62-2.50015-2.

[11] Berkley Biodiesel. History of Biodiesel 2019. https://www.berkeleybiodiesel.org/history-biodiesel-fuel-traced.html (accessed June 2, 2019).

[12] Chavanne G. Procédé de Transformation d'Huiles Végétales en Vue de Leur Utilisation comme Carburants. 422,877, 1937.

[13] IEA. Market Report Series: Gas 2017. Mark. Rep. Ser., 2017.

[14] BP. BP Energy Outlook. 2017.

[15] Li H, Yang S, Zhang J, Qian Y. Coal-based synthetic natural gas (SNG) for municipal heating in China: Analysis of haze pollutants and greenhouse gases (GHGs) emissions. J Clean Prod 2016;112:1350–9. doi:10.1016/j.jclepro.2015.04.078.

[16] Parkin D. The future of the gas grid. 2017.

[17] Clark RH. Basic Data On Biogas Composition. 2007. doi:ISBN 978-91-85207-7.

[18] Adelt M, Hoppe M, Montero M, Peureux G. Report on gas composition range in Europe 2010.

[19] Nobelprize.org. “Paul Sabatier - Nobel Lecture: The Method of Direct Hydrogenation by Catalysis”. Nobel Media AB 2014 2014:1. http://www.nobelprize.org/nobel_prizes/chemistry/laureates/1912/sabatier-lecture.html (accessed November 3, 2015).

[20] Sabatier P. Catalysis in Organic Chemistry. 1st ed. London: The Library Press; 1923.

[21] Thomas R. Gasworks Profiles. 2014.

[22] NETL. Lurgi Gasifier 2017. https://www.netl.doe.gov/research/coal/energy-systems/gasification/gasifipedia/lurgi (accessed November 9, 2017).

[23] National Energy Technology Laboratory. SNG from coal: process and commercialization 2015:1. http://www.netl.doe.gov/research/coal/energy-systems/gasification/gasifipedia/great-plains (accessed November 9, 2015).

[24] Jensen J., Poulsen J., Andersen N. From Coal To Clean Energy. 2011.

[25] Dryden IG. The Efficient Use of Energy. 2nd ed. Butterworth-Heinemann; 1985.

[26] Lacey J. CRG-based SNG: principles and process routes. Br Gas Bookl 1971;5:357–474.

[27] Bridger G., Carnell PJ., Davies P, Donald R., Goodman B., Harbord N., et al. Methanation. In: Twigg M V., editor. Catal. Handb. 2nd ed., Billingham: Wolfe Publishing Ltd; 1989, p. 330–57.

[28] Rehling B, Hofbauer H, Rauch R, Aichernig C. BioSNG-process simulation and comparison with first results from a 1-MW demonstration plant. Biomass Convers Biorefinery 2011;1:111–9. doi:10.1007/s13399-011-0013-3.

[29] Kopyscinski J, Schildhauer TJ, Biollaz SM a. Production of synthetic natural gas (SNG) from coal and dry biomass – A technology review from 1950 to 2009. Fuel 2010;89:1763–83. doi:10.1016/j.fuel.2010.01.027.

[30] Rabou L., Almansa Aranda G. 500 hours producing bio- SNG from MILENA gasification using the ESME system ECN System for MEthanation (ESME). ECN 2015:4–5.

[31] Deurwaarder EP, Boerrigter H, Mozaffarian H, van der Drift B. Methanation of MILENA product gas for the production of bio-SNG Exergy analysis of biomass-to-synthetic natural gas (SNG) process via indirect gasification of various biomass feedstock. ECN 2005:17–21.

[32] Sikarwar VS, Zhao M, Clough P, Yao J, Zhong X, Memon MZ, et al. An overview of advances in biomass gasification. Energy Environ Sci 2016;9:2939–77. doi:10.1039/C6EE00935B.

[33] Yang F, Hanna M a, Sun R. Value-added uses for crude glycerol--a byproduct of biodiesel production. Biotechnol Biofuels 2012;5:13. doi:10.1186/1754-6834-5-13.

[34] He Q (Sophia), McNutt J, Yang J. Utilization of the residual glycerol from biodiesel production for renewable energy generation. Renew Sustain Energy Rev 2017;71:63–76. doi:10.1016/j.rser.2016.12.110.

[35] Schwengber CA, Alves HJ, Schaffner RA, da Silva FA, Sequinel R, Bach VR, et al. Overview of glycerol reforming for hydrogen production. Renew Sustain Energy Rev 2016;58:259–66. doi:10.1016/j.rser.2015.12.279.

[36] Imai H, Yamawaki M, Xiaohong L. Direct Synthesis of Methane from Glycerol by Using Silica-modified Nickel Catalyst. Japan Pet Inst 2017;60:311–21. doi:doi.org/10.1627/jpi.60.311.

[37] White R, Dupont V, Cockerill T. Thermodynamic modelling and energy balance of direct methanation of glycerol for Bio-SNG production. Energy Convers Manag 2018;160:354–63. doi:10.1016/j.enconman.2018.01.031.

[38] Johnson D, Taconi K. The glycerin glut: Options for the value-added conversion of crude glycerol resulting from biodiesel production. Environ Prog 2007;26. doi:10.1002/ep.

[39] Ciriminna R, Pina C Della, Rossi M, Pagliaro M. Understanding the glycerol market. Eur J Lipid Sci Technol 2014;116:1432–9. doi:10.1002/ejlt.201400229.

[40] Ayoub M, Abdullah AZ. Critical review on the current scenario and significance of crude glycerol resulting from biodiesel industry towards more sustainable renewable energy industry. Renew Sustain Energy Rev 2012;16:2671–86. doi:10.1016/j.rser.2012.01.054.

[41] Oleoline. Glycerine market report 2017:3–26.

http://www.hbint.com/datas/media/590204fd077a6e381ef1a252/sample-quarterly-glycerine.pdf.

[42] Ardi MS, Aroua MK, Hashim NA. Progress, prospect and challenges in glycerol purification process: A review. Renew Sustain Energy Rev 2015;42:1164–73. doi:10.1016/j.rser.2014.10.091.

[43] Hansen C, Hernandez A, Mullan B. A chemical analysis of samples of crude glycerol from the production of biodiesel in Australia, and the effects of feeding crude glycerol to growing-finishing pigs on. Anim Prod … 2009:154–61.

[44] Hu S, Luo X, Wan C, Li Y. Characterization of crude glycerol from biodiesel plants. J Agric Food Chem 2012;60:5915–21. doi:10.1021/jf3008629.

[45] Javani A, Hasheminejad M, Tahvildari K, Tabatabaei M. High quality potassium phosphate production through step-by-step glycerol purification: A strategy to economize biodiesel production. Bioresour Technol 2012;104:788–90. doi:10.1016/j.biortech.2011.09.134.

[46] U.S Department of Energy. Hydrogen Production: Natural Gas Reforming 2015. http://energy.gov/eere/fuelcells/hydrogen-production-natural-gas-reforming (accessed August 20, 2015).

[47] Nahar G, Dupont V. Hydrogen production from simple alkanes and oxygenated hydrocarbons over ceria–zirconia supported catalysts: Review. Renew Sustain Energy Rev 2014;32:777–96. doi:10.1016/j.rser.2013.12.040.

[48] Bridger G., Carnell PJ., Davies P, Donald R., Goodman B., Harbord N., et al. Catalytic Reforming. In: Twigg M V., editor. Catal. Handb. 2nd ed., Billingham: Wolfe Publishing Ltd; 1989, p. 226–8.

[49] Bridger G., Carnell PJ., Davies P, Donald R., Goodman B., Harbord N., et al. The Water-gas Shift Reaction. In: Twigg M V., editor. Catal. Handb. 2nd ed., Billingham: Wolfe Publishing Ltd; 1989, p. 283–4.

[50] Vlassis T, Stamatelatou K, Antonopoulou G, Lyberatos G. Methane production via anaerobic digestion of glycerol: A comparison of conventional (CSTR) and high-rate (PABR) digesters. J Chem Technol Biotechnol 2013;88:2000–6. doi:10.1002/jctb.4059.

[51] Kemble Farms. Glycerol within the context of the Renewables Obligation A response

to the Consultation paper by OFGEM 2008:2–3.

[52] Bohon MD, Metzger B a., Linak WP, King CJ, Roberts WL. Glycerol combustion and emissions. Proc Combust Inst 2011;33:2717–24. doi:10.1016/j.proci.2010.06.154.

[53] Coronado CR, Carvalho JA, Quispe CA, Sotomonte CR. Ecological efficiency in glycerol combustion. Appl Therm Eng 2014;63:97–104. doi:10.1016/j.applthermaleng.2013.11.004.

[54] Lee BH, Sh L, Bae JS, Choi YC, Jeon CH. Combustion behavior of low-rank coal impregnated with glycerol. Biomass and Bioenergy 2016;87:122–30. doi:10.1016/j.biombioe.2016.02.028.

[55] Bala-Litwiniak A, Radomiak H. Environmental benefits of co-combustion of light fuel oil with waste glycerol. Energy Sources, Part A Recover Util Environ Eff 2016;38:2510–6. doi:10.1080/15567036.2015.1091867.

[56] Ray MS, Johnston DW. Chemical Engineering Design Project - A Case Study Approach. 1989.

[57] Sinnott RK, Towler G. Chemical Engineering Design. Chem Eng Des 2013. doi:10.1002/apj.5500020410.

[58] Haas MJ, McAloon AJ, Yee WC, Foglia TA. A process model to estimate biodiesel production costs. Bioresour Technol 2006;97:671–8. doi:10.1016/j.biortech.2005.03.039.

[59] Kiss AA, Ignat RM. Enhanced methanol recovery and glycerol separation in biodiesel production - DWC makes it happen. Appl Energy 2012;99:146–53. doi:10.1016/j.apenergy.2012.04.019.

[60] Xiao Y, Xiao G, Varma A. A universal procedure for crude glycerol purification from different feedstocks in biodiesel production: Experimental and simulation study. Ind Eng Chem Res 2013;52:14291–6. doi:10.1021/ie402003u.

[61] Posada J, Cardona C, Higuita J, Tamayo J, Pisarenko Y a. Design and economic analysis of the technological scheme for 1, 3-propanediol production from raw glycerol. … Chem Eng 2013;47:239–53. doi:10.1134/S0040579513030093.

[62] Posada J a., Higuita JC, Cardona C a. Optimization on the Use of Crude Glycerol from the Biodiesel Production to Obtain Poly-3-Hydroxybutyrate. World Renew Energy Congr 2011 2011:327–34. doi:10.3384/ecp11057327.

[63] Posada JA, Rincón LE, Cardona CA. Design and analysis of biorefineries based on raw glycerol: Addressing the glycerol problem. Bioresour Technol 2012;111:282–93. doi:10.1016/j.biortech.2012.01.151.

[64] Banu I, Guta G, Bildea CS, Bozga G. Design and performance evaluation of a plant for glycerol conversion to acrolein. Environ Eng Manag J 2015;14:509–17.

[65] Vlysidis A, Binns M, Webb C, Theodoropoulos C. Integrated Biodiesel Plants: Options and Perspectives. Chem Eng Trans 2011;25:827–32. doi:10.3303/CET1125138.

[66] Bauer F, Hulteberg C. Isobutanol from glycerine - A techno-economic evaluation of a new biofuel production process. Appl Energy 2014;122:261–8. doi:10.1016/j.apenergy.2014.02.037.

[67] Pedersen TH, Hansen NH, Pérez OM, Cabezas DEV, Rosendahl LA. Renewable hydrocarbon fuels from hydrothermal liquefaction: A techno-economic analysis. Biofuels, Bioprod Biorefining 2017. doi:10.1002/bbb.1831.

[68] Galera S, Gutiérrez Ortiz FJ. Life cycle assessment of hydrogen and power production by supercritical water reforming of glycerol. Energy Convers Manag 2015;96:637–45. doi:10.1016/j.enconman.2015.03.031.

[69] Hunpinyo P, Narataruksa P. Process simulation and costing study for the FT-liquid fuels production from steam glycerol reforming. Chem Eng Trans 2016;52:241–6. doi:10.3303/CET1652041.

[70] Wang S, Wang Q, Song X, Chen J. Dry autothermal reforming of glycerol with in situ hydrogen separation via thermodynamic evaluation. Int J Hydrogen Energy 2017;42:838–47. doi:10.1016/j.ijhydene.2016.09.103.

[71] Liu Y, Farrauto R, Lawal A. Autothermal Reforming of Glycerol in a Dual Layer Monolith Catalyst. Chem Eng Sci 2013;89:31–9. doi:10.1016/j.ces.2012.11.030.

[72] Yang G, Yu H, Peng F, Wang H, Yang J, Xie D. Thermodynamic analysis of hydrogen generation via oxidative steam reforming of glycerol. Renew Energy 2011;36:2120–7. doi:10.1016/j.renene.2011.01.022.

[73] Reddy SN, Nanda S, Dalai AK, Kozinski JA. Supercritical water gasification of biomass for hydrogen production. Int J Hydrogen Energy 2014;39:6912–26. doi:10.1016/j.ijhydene.2014.02.125.

[74] Reddy SN, Nanda S, Kozinski JA. Supercritical water gasification of glycerol and

methanol mixtures as model waste residues from biodiesel refinery. Chem Eng Res Des 2016;113:17–27. doi:10.1016/j.cherd.2016.07.005.

[75] Schubert M, Mu JB. Continuous Hydrothermal Gasification of Glycerol Mixtures : Autothermal Operation, Simultaneous Salt Recovery, and the Effect of K3PO4 on the Catalytic Gasification. J Supercrit Fluids 2014;95:4–15. doi:10.1016/j.supflu.2014.09.011.

[76] Rennard DC, Kruger JS, Schmidt LD. Autothermal catalytic partial oxidation of glycerol to syngas and to non-equilibrium products. ChemSusChem 2009;2:89–98. doi:10.1002/cssc.200800200.

[77] Rennard DC, Kruger JS, Michael BC, Schmidt LD. Long-time behavior of the catalytic partial oxidation of glycerol in an autothermal reactor. Ind Eng Chem Res 2010;49:8424–32. doi:10.1021/ie100405h.

[78] Meyer H., Hill VL, Flowers A, Happel J, Hnatow M. Direct Methanation - A new Method of Converting Synthesis Gas to Substitute Natural Gas 1976:109–15.

[79] Adhikari S, Fernando S, Gwaltney S, Filipto S, Markbricka R, Steele P, et al. A thermodynamic analysis of hydrogen production by steam reforming of glycerol. Int J Hydrogen Energy 2007;32:2875–80. doi:10.1016/j.ijhydene.2007.03.023.

[80] Dieuzeide ML, Amadeo N. Thermodynamic Analysis of Glycerol Steam Reforming. Chem Eng Technol 2010;33:89–96. doi:10.1002/ceat.200900260.

[81] Chen H, Zhang T, Dou B, Dupont V, Williams P, Ghadiri M, et al. Thermodynamic analyses of adsorption-enhanced steam reforming of glycerol for hydrogen production. Int J Hydrogen Energy 2009;34:7208–22. doi:10.1016/j.ijhydene.2009.06.070.

[82] Haldor Topsoe. PK-7R 2017:1. https://www.topsoe.com/products/pk-7r (accessed December 12, 2017).

[83] Adhikari S, Fernando S, Haryanto A. Production of hydrogen by steam reforming of glycerin over alumina-supported metal catalysts. Catal Today 2007;129:355–64. doi:10.1016/j.cattod.2006.09.038.

[84] Stangeland K, Kalai D, Li H, Yu Z. CO 2 methanation: the effect of catalysts and reaction conditions. Energy Procedia 2017;105:2022–7. doi:10.1016/j.egypro.2017.03.577.

[85] Pradhan A, Shrestha DS, Mcaloon A, Yee W, Haas M, Duffield JA. Energy Life Cycle Assessment of Soybean Biodiesel Revisited. Am Soc Agric Biol Eng 2011;54:1031–9.

[86] Huo H, Wang M, Bloyd C, Putsche V. Life-Cycle Assessment of Energy Use and Greenhouse Gas Emissions of Soybean-Derived Biodiesel and Renewable Fuels. Environ Sci Technol 2009;43:750–6. doi:10.1021/es8011436.

[87] Ashrae. HEATING EQUIPMENT AND COMPONENTS - Boilers. Ashrae Handb. -HVAC Syst. Equip., American Society of Heating, Refrigerating and Air-Conditioning Engineers, 2016; 2016.

[88] Liuzzo G, Verdone N, Bravi M. The benefits of flue gas recirculation in waste incineration. Waste Manag 2007;27:106–16. doi:10.1016/j.wasman.2006.01.002.

[89] Carlson EC. Don't Gamble With Physical Properties. Chem Eng Process 1996:35–46.

[90] Sabio E, Álvarez-Murillo A, González JF, Ledesma B, Román S. Modelling the composition of the gas obtained by steam reforming of glycerine. Energy Convers Manag 2017;146:147–57. doi:10.1016/j.enconman.2017.03.068.

[91] Richard Turton, Richard C. Bailie, Wallace B. Whiting JAS. Analysis, Synthesis and Design of Chemical Processes Third Edition. vol. 53. 2013. doi:10.1017/CBO9781107415324.004.

[92] Sadhukhan J, Siew NG K, Hernandez ME. Economic Analysis. Biorefineries Chem. Process. Des. Integr. Sustain. Anal., John Wiley and Sons; 2014.

[93] Towler G, Sinnott R. Chapter 13 - Equipment Selection, Specification, and Design. Chem Eng Des (Second Ed 2013:557–62. doi:http://dx.doi.org/10.1016/B978-0-08-096659-5.00013-4.

[94] NETL. Technology Learning Curve (FOAK to NOAK) 2013.

[95] Gerdes K, Summers WM, Wimer J. Cost Estimation Methodology for NETL Assessments of Power Plant Performance DOE/NETL-2011/1455 2011:26.

[96] Rotunno P, Lanzini A, Leone P. Energy and economic analysis of a water scrubbing based biogas upgrading process for biomethane injection into the gas grid or use as transportation fuel. Renew Energy 2017;102:417–32. doi:10.1016/j.renene.2016.10.062.

[97] Ogidiama OV, Abu-Zahra MRM, Shamim T. Techno-economic analysis of a poly-

generation solar-assisted chemical looping combustion power plant. Appl Energy 2018;228:724–35. doi:10.1016/j.apenergy.2018.06.091.

[98] Ogidiama OV, Shamim T. Techno-economic evaluation of a chemical looping combustion plant with waste heat utilization. Energy Procedia 2017;142:2990–5. doi:10.1016/j.egypro.2017.12.371.

[99] Alibaba. Alibaba Ni Catalyst Price 2018. https://www.alibaba.com/showroom/nickel-alumina-catalyst.html (accessed October 2, 2018).

[100] Codes AI. Projected Costs of Generating Electricity 2015.

[101] Hern R, Radov D, Carmel A, Spasovska M, Guo J. Electricity Generation Costs and Hurdle Rates Lot 1: Hurdle Rates update for Generation Technologies 2015.

[102] EIA. Natural Gas Industrial Prices by Month 2018. https://www.eia.gov/dnav/ng/ng_pri_sum_a_EPG0_PIN_DMcf_m.htm (accessed February 14, 2018).

[103] World Bank. World Bank Commodities Price Forecast 2017:1–4.

[104] EIA. Henry Hub Natural Gas Spot Price 2017:1. https://www.eia.gov/dnav/ng/hist/rngwhhdm.htm (accessed February 14, 2018).

[105] IMF. Henry Hub Natural Gas Spot price 2017. http://www.imf.org/external/np/res/commod/index.aspx (accessed February 14, 2018).

[106] Biodiesel Magazine. Biodiesel US Plants 2017. http://www.biodieselmagazine.com/plants/listplants/USA/ (accessed April 11, 2018).

[107] Hofstrand D. Tracking biodiesel profitability 2015;13:13–5.

[108] Lazard. Levelised Cost of Energy Analysis. 2017.

[109] BEIS. Electricity Generation Costs. 2016.

[110] Tanton T. Levelized Cost of Energy : Expanding the Menu to Include Direct Use of Natural Gas. 2017.

[111] Beckers KF, Lukawski MZ, Anderson BJ, Moore MC, Tester JW. Levelized costs of electricity and direct-use heat from Enhanced Geothermal Systems. J. Renew. Sustain. Energy, vol. 6, 2014. doi:10.1063/1.4865575.

[112] Nian V, Sun Q, Ma Z, Li H. A Comparative Cost Assessment of Energy Production from Central Heating Plant or Combined Heat and Power Plant. Energy Procedia 2016;104:556–61. doi:10.1016/j.egypro.2016.12.094.

[113] Black J. Capital Cost Methodology. 2013.

[114] Yeh S, Rubin ES. A review of uncertainties in technology experience curves. Energy Econ 2012;34:762–71. doi:10.1016/j.eneco.2011.11.006.

[115] Platon V, Constantinescu A. Monte Carlo Method in Risk Analysis for Investment Projects. Procedia Econ Financ 2014;15:393–400. doi:10.1016/S2212-5671(14)00463-8.

[116] Poulter SR. Monte Carlo Simulation in Environmental Risk Assessment — Science , Policy And Legal Issues. Risk Heal Saf Environ 1998;7:7–26.

[117] Dinis ML, Fiúza A. Using Monte-Carlo Simulation for Risk Assessment: Application to Occupational Exposure during Remediation Works. In: Dimov I, Dimova S, Kolkovska N, editors. Numer. Methods Appl., Berlin, Heidelberg: Springer Berlin Heidelberg; 2011, p. 60–7.

[118] Onofrejová D. Implementation of Monte Carlo Simulation in Investment Decision Making. Int Sci J about Simul 2015:5–8.

[119] Avlijas G. Examining the Value of Monte Carlo Simulation for Project Time Management. Manag Sustain Bus Manag Solut Emerg Econ 2018:1–11. doi:10.7595/management.fon.2018.0004.

[120] Tran TTD, Smith AD. Incorporating performance-based global sensitivity and uncertainty analysis into LCOE calculations for emerging renewable energy technologies. Appl Energy 2018;216:157–71. doi:10.1016/j.apenergy.2018.02.024.

[121] Dienemann PF. Estimating Cost Uncertainty using Monte Carlo Techniques, 1966, p. 61.

[122] Ferson S. What Monte Carlo methods cannot do. Hum Ecol Risk Assess An Int J 1996;2:990–1007. doi:10.1080/10807039609383659.

[123] Gabbrielli R, Castrataro P, Del Medico F, Di Palo M, Lenzo B. Levelized cost of heat for linear Fresnel concentrated solar systems. Energy Procedia 2013;49:1340–9. doi:10.1016/j.egypro.2014.03.143.

[124] ICHEME. Salary Survey. 2019.

[125] Spargo PL. Green Engineering: Environmentally Conscious Design of Chemical Processes By David T. Allen and David R. Shonnard. Prentice Hall PTR: New Jersey. 2002. 552 pp. £51.99. ISBN 0-13-061908-6. Org Process Res Dev 2004;8:1083. doi:10.1021/op049881a.

[126] K. SS. Sustainable development and sustainability metrics. AIChE J 2004;49:1928–32. doi:10.1002/aic.690490802.

[127] International Organization for Standardisation. ISO 14040-Environmental management - Life Cycle Assessment - Principles and Framework. 1997. doi:10.1016/j.ecolind.2011.01.007.

[128] International Organization for Standardization. ISO14041 Environmental management - Life cycle assessment - Goal and scope definition and inventory analysis. vol. 1998. 1998.

[129] Gnansounou E, Pandey A. Life-Cycle Assessment of Biorefineries. 2017. doi:10.1016/B978-0-444-63585-3.00004-8.

[130] International Organization for Standardisation. ISO14042 Environmental management - Life cycle assessment - Life cycle impact assessment. vol. 2000. 2000.

[131] International Organization for Standardization. ISO14043 - Environmental management - Life cycle assessment - Life cycle interpretation. vol. 1999. 1999.

[132] Finnveden G, Hauschild MZ, Ekvall T, Guinée J, Heijungs R, Hellweg S, et al. Recent developments in Life Cycle Assessment. J Environ Manage 2009;91:1–21. doi:10.1016/j.jenvman.2009.06.018.

[133] Ahlgren S. Review of methodological choices in LCA of biorefinery systems - key issues and recommendations. Biofuels, Bioprod Biorefining 2015;6:246–56. doi:10.1002/bbb.

[134] Sheehan J, Camobreco V, Duffield J, Graboski M, Shapouri H. Life Cycle Inventory of Biodiesel and Petroleum Diesel for Use in an Urban Bus A Joint Study Sponsored by. Natl Renew Energy Lab US Dep Energy US Dep Agric 1998:300. doi:10.2172/658310.

[135] Spirinckx C, Ceuterick D. Biodiesel and fossil diesel fuel: Comparative life cycle assessment. Int J Life Cycle Assess 1996;1:127–32. doi:10.1007/BF02978938.

[136] Kaltschmitt M, Reinhardt G a., Stelzer T. Life cycle analysis of biofuels under different environmental aspects. Biomass and Bioenergy 1997;12:121–34. doi:10.1016/S0961-9534(96)00071-2.

[137] MacLean HL, Lave LB, Lankey R, Joshi S. A life-cycle comparison of alternative automobile fuels. J Air Waste Manag Assoc 2000;50:1769–79. doi:(10):1769-79.

[138] Carraretto C, Macor A, Mirandola A, Stoppato A, Tonon S. Biodiesel as alternative fuel: Experimental analysis and energetic evaluations. Energy 2004;29:2195–211. doi:10.1016/j.energy.2004.03.042.

[139] Larson ED. A review of life-cycle analysis studies on liquid biofuel systems for the transport sector. Energy Sustain Dev 2006;10:109–26. doi:10.1016/S0973-0826(08)60536-0.

[140] Yan X, Crookes RJ. Life cycle analysis of energy use and greenhouse gas emissions for road transportation fuels in China. Renew Sustain Energy Rev 2009;13:2505–14. doi:10.1016/j.rser.2009.06.012.

[141] Morais S, Martins AA, Mata TM. Comparison of allocation approaches in soybean biodiesel life cycle assessment. J Energy Inst 2010;83:48–55. doi:10.1179/014426010x12592427712073.

[142] Wang M, Huo H, Arora S. Methods of dealing with co-products of biofuels in life-cycle analysis and consequent results within the U.S. context. Energy Policy 2011;39:5726–36. doi:10.1016/j.enpol.2010.03.052.

[143] Pradhan A, Shrestha DS, Gerpen J Van, Mcaloon A, Yee W, Haas M, et al. Reassessment of Life Cycle Greenhouse Gas Emissions for Soybean Biodiesel. Trans ASABE 2012;55:2257–64. doi:10.13031/2013.42483.

[144] Xue X, Collinge WO, Shrake SO, Bilec MM, Landis AE. Regional life cycle assessment of soybean derived biodiesel for transportation fleets. Energy Policy 2012;48:295–303. doi:10.1016/j.enpol.2012.05.025.

[145] Chang WR, Hwang JJ, Wu W. Environmental impact and sustainability study on biofuels for transportation applications. Renew Sustain Energy Rev 2017;67:277–88. doi:10.1016/j.rser.2016.09.020.

[146] Chen R, Qin Z, Han J, Wang M, Taheripour F, Tyner W, et al. Life cycle energy and greenhouse gas emission effects of biodiesel in the United States with induced land

use change impacts. Bioresour Technol 2018;251:249–58. doi:10.1016/j.biortech.2017.12.031.

[147] A. Pradhan, D. S. Shrestha, A. McAloon, W. Yee, M. Haas, J. A. Duffield. Energy Life-Cycle Assessment of Soybean Biodiesel. 2009.

[148] Hu Z, Tan P, Yan X, Lou D. Life cycle energy, environment and economic assessment of soybean-based biodiesel as an alternative automotive fuel in China. Energy 2008;33:1654–8. doi:10.1016/j.energy.2008.06.004.

[149] Hou J, Zhang P, Yuan X, Zheng Y. Life cycle assessment of biodiesel from soybean, jatropha and microalgae in China conditions. Renew Sustain Energy Rev 2011;15:5081–91. doi:10.1016/j.rser.2011.07.048.

[150] Tsao CC, Campbell JE, Mena-Carrasco M, Spak SN, Carmichael GR, Chen Y. Biofuels that cause land-use change may have much larger non-GHG air quality emissions than fossil fuels. Environ Sci Technol 2012;46:10835–41. doi:10.1021/es301851x.

[151] Esteves VPP, Esteves EMM, Bungenstab DJ, Loebmann DG dos SW, de Castro Victoria D, Vicente LE, et al. Land use change (LUC) analysis and life cycle assessment (LCA) of Brazilian soybean biodiesel. Clean Technol Environ Policy 2016;18:1655–73. doi:10.1007/s10098-016-1161-8.

[152] Rajaeifar MA, Ghobadian B, Safa M, Heidari MD. Energy life-cycle assessment and CO2emissions analysis of soybean-based biodiesel: A case study. J Clean Prod 2014;66:233–41. doi:10.1016/j.jclepro.2013.10.041.

[153] Castanheira ÉG, Grisoli R, Coelho S, Anderi Da Silva G, Freire F. Life-cycle assessment of soybean-based biodiesel in Europe: Comparing grain, oil and biodiesel import from Brazil. J Clean Prod 2015;102:188–201. doi:10.1016/j.jclepro.2015.04.036.

[154] Piastrellini R, Arena AP, Civit B. Energy life-cycle analysis of soybean biodiesel: Effects of tillage and water management. Energy 2017;126:13–20. doi:10.1016/j.energy.2017.03.028.

[155] Racz L, Fozer D, Nagy T, Toth AJ, Haaz E, Tarjani JA, et al. Extensive comparison of biodiesel production alternatives with life cycle, PESTLE and multi-criteria decision analyses. Clean Technol Environ Policy 2018:1–12. doi:10.1007/s10098-018-1527-1.

[156] McKone TE, Nazaroff WW, Berck P, Auffhammer M, Lipman T, Torn MS, et al. Grand challenges for life-cycle assessment of biofuels. Environ Sci Technol 2011;45:1751–6.

doi:10.1021/es103579c.

[157] European Parliament. DIRECTIVE 2009/28/EC OF THE EUROPEAN PARLIAMENT AND OF THE COUNCIL 2009:16–62.

[158] Roundtable on Sustainable Biofuels. RSB GHG Calculation Methodology 2012;01:109. doi:10.1017/CBO9781107415324.004.

[159] Ecoinvent. Ecoinvent 2018. https://www.ecoinvent.org/ (accessed March 8, 2018).

[160] Acero AP, Rodríguez C, Ciroth A. LCIA methods Impact assessment methods in Life Cycle Assessment and their impact categories. GreenDelta 2015:1–23.

[161] Singh SP, Singh D. Biodiesel production through the use of different sources and characterization of oils and their esters as the substitute of diesel: A review. Renew Sustain Energy Rev 2010;14:200–16. doi:10.1016/j.rser.2009.07.017.

[162] Jeroen B. Guinee. Handbook of Lifecycle Assessment: Operational Guide to the ISO Standards. 1st ed. Springer Netherlands; 2002. doi:10.1007/0-306-48055-7.

[163] NREL. U.S Life Cycle Inventory Database n.d. https://www.nrel.gov/lci/ (accessed August 14, 2018).

[164] van Oers L, de Koning A, Guinée JB, Huppes G. Abiotic Resource Depletion in LCA. 2002.

[165] Han J, Elgowainy A, Cai H, Wang M, Farming S. Update to Soybean Farming and Biodiesel Production in GREET TM 2014;2012:1–7.

[166] Hill J, Nelson E, Tilman D, Polasky S, Tiffany D. Environmental, economic, and energetic costs and benefits of biodiesel and ethanol biofuels. Proc Natl Acad Sci 2006;103:11206–10. doi:10.1073/pnas.0604600103.

[167] Adhikari S, Fernando SD, Haryanto A. Hydrogen production from glycerin by steam reforming over nickel catalysts. Renew Energy 2008;33:1097–100. doi:10.1016/j.renene.2007.09.005.

[168] Cortright RD, Davda RR, Dumesic J a. Hydrogen from catalytic reforming of biomass-derived hydrocarbons in liquid water. Nature 2002;418:964–7. doi:10.1038/nature01009.

[169] Czernik S, French R, Feik C, Chornet E. Hydrogen by catalytic steam reforming of liquid byproducts from biomass thermoconversion processes. Ind Eng Chem Res

2002;41:4209–15. doi:10.1021/ie020107q.

[170] Hirai T, Ikenaga NO, Miyake T, Suzuki T. Production of hydrogen by steam reforming of glycerin on ruthenium catalyst. Energy and Fuels 2005;19:1761–2. doi:10.1021/ef050121q.

[171] Serrera A, Guti??rrez Ortiz FJ, Ollero P. Syngas methanation from the supercritical water reforming of glycerol. Energy 2014;76:584–92. doi:10.1016/j.energy.2014.08.056.

[172] Tapah BF, Santos RCD, Leeke GA. Processing of glycerol under sub and supercritical water conditions. Renew Energy 2014;62:353–61. doi:10.1016/j.renene.2013.07.027.

[173] Silva JM, Soria M a., Madeira LM. Challenges and strategies for optimization of glycerol steam reforming process. Renew Sustain Energy Rev 2015;42:1187–213. doi:10.1016/j.rser.2014.10.084.

[174] Czernik S, French R, Feik C, Chornet E. Hydrogen by Catalytic Steam Reforming of Liquid Byproducts from Biomass Thermoconversion Processes. Ind Eng Chem Res 2002;41:4209–15.

[175] Chiodo V, Freni S, Galvagno a., Mondello N, Frusteri F. Catalytic features of Rh and Ni supported catalysts in the steam reforming of glycerol to produce hydrogen. Appl Catal A Gen 2010;381:1–7. doi:10.1016/j.apcata.2010.03.039.

[176] Adhikari S, Fernando SD, Haryanto A. Hydrogen production from glycerol: An update. Energy Convers Manag 2009;50:2600–4. doi:10.1016/j.enconman.2009.06.011.

[177] Cheng CK, Foo SY, Adesina A a. H2-rich synthesis gas production over Co/Al2O3 catalyst via glycerol steam reforming. Catal Commun 2010;12:292–8. doi:10.1016/j.catcom.2010.09.018.

[178] Cheng CK, Foo SY, Adesina A a. Glycerol Steam Reforming over Bimetallic Co-Ni/Al 2 O 3. Ind Eng Chem Res 2010;49:10804–17. doi:10.1021/ie100462t.

[179] Cheng CK, Foo SY, Adesina AA. Steam reforming of glycerol over Ni/Al2O3 catalyst. Catal Today 2011;178:25–33. doi:10.1016/j.cattod.2011.07.011.

[180] Dieuzeide ML, Jobbagy M, Amadeo N. Glycerol steam reforming over Ni/Al2O3 catalysts, modified with Mg(II). Effect of Mg (II) content. Catal Today 2013;213:50–7. doi:10.1016/j.cattod.2013.02.015.

[181] Lin YC. Catalytic valorization of glycerol to hydrogen and syngas. Int J Hydrogen Energy 2013;38:2678–700. doi:10.1016/j.ijhydene.2012.12.079.

[182] Rossetti I, Gallo A, Dal Santo V, Bianchi CL, Nichele V, Signoretto M, et al. Nickel Catalysts Supported Over TiO2 , SiO2 and ZrO2 for the Steam Reforming of Glycerol. ChemCatChem 2013;5:294–306. doi:10.1002/cctc.201200481.

[183] Slinn M, Kendall K, Mallon C, Andrews J. Steam reforming of biodiesel by-product to make renewable hydrogen. Bioresour Technol 2008;99:5851–8. doi:10.1016/j.biortech.2007.10.003.

[184] Byrd a, Pant K, Gupta R. Hydrogen production from glycerol by reforming in supercritical water over Ru/Al2O3 catalyst. Fuel 2008;87:2956–60. doi:10.1016/j.fuel.2008.04.024.

[185] Valliyappan T, Ferdous D, Bakhshi NN, Dalai a. K. Production of hydrogen and syngas via steam gasification of glycerol in a fixed-bed reactor. Top Catal 2008;49:59–67. doi:10.1007/s11244-008-9062-7.

[186] Adhikari S, Fernando SD, Haryanto A. Kinetics and reactor modeling of hydrogen production from glycerol via steam reforming process over Ni/CeO2 catalysts. Chem Eng Technol 2009;32:541–7. doi:10.1002/ceat.200800462.

[187] Sutar PN, Vaidya PD, Rodrigues AE. Glycerol-reforming kinetics using a Pt/C catalyst. Chem Eng Technol 2010;33:1645–9. doi:10.1002/ceat.201000055.

[188] Pompeo F, Santori GF, Nichio NN. Hydrogen production by glycerol steam reforming with Pt/SiO2 and Ni/SiO2 catalysts. Catal Today 2011;172:183–8. doi:10.1016/j.cattod.2011.05.001.

[189] Sundari R, Vaidya PD. Reaction Kinetics of Glycerol Steam Reforming Using a Ru/Al2O3 Catalyst. Energy Fuels 2012;26:4295–4204. doi:10.1021/ef300658n.

[190] Nichele V, Signoretto M, Menegazzo F, Gallo A, Dal Santo V, Cruciani G, et al. Glycerol steam reforming for hydrogen production: Design of Ni supported catalysts. Appl Catal B Environ 2012;111–112:225–32. doi:10.1016/j.apcatb.2011.10.003.

[191] Pompeo F, Santori G, Nichio NN. Hydrogen and/or syngas from steam reforming of glycerol. Study of platinum catalysts. Int J Hydrogen Energy 2010;35:8912–20. doi:10.1016/j.ijhydene.2010.06.011.

[192] Gao J, Wang Y, Ping Y, Hu D, Xu G, Gu F, et al. A thermodynamic analysis of

methanation reactions of carbon oxides for the production of synthetic natural gas. RSC Adv 2012;2:2358. doi:10.1039/c2ra00632d.

[193] Sahebdelfar S, Takht Ravanchi M. Carbon dioxide utilization for methane production: A thermodynamic analysis. J Pet Sci Eng 2015;134:14–22. doi:10.1016/j.petrol.2015.07.015.

[194] Wang Z. Sabatier-Senderens Reduction. 2010.

[195] Vlasenko VM, Yuzefovich GE. Mechanism of the Catalytic Hydrogenation of Oxides of Carbon to Methane. Russ Chem Rev 1969;38:728.

[196] Sehested J, Dahl S, Jacobsen J, Rostrup-Nielsen JR. Methanation of CO over nickel: Mechanism and kinetics at high H2/CO ratios. J Phys Chem B 2005;109:2432–8. doi:10.1021/jp040239s.

[197] Rönsch S, Schneider J, Matthischke S, Schlüter M, Götz M, Lefebvre J, et al. Review on methanation – From fundamentals to current projects. Fuel 2015;166:276–96. doi:10.1016/j.fuel.2015.10.111.

[198] Tada S, Kikuchi R. Mechanistic Study and Catalyst Development for Selective Carbon Monoxide Methanation. Catal Sci Technol 2015;5:3061–70. doi:10.1039/C5CY00150A.

[199] Wu HC, Chang YC, Wu JH, Lin JH, Lin IK, Chen CS. Methanation of CO 2 and reverse water gas shift reactions on Ni/SiO 2 catalysts: the influence of particle size on selectivity and reaction pathway. Catal Sci Technol 2015;5:4154–63. doi:10.1039/C5CY00667H.

[200] Wu HC, Chang YC, Wu JH, Lin JH, Lin IK, Chen CS. Methanation of CO2 and Reverse Water Gas Shift Reactions on Ni/SiO2 Catalysts: The Influence of Particle Size on Selectivity and Reaction Pathway. Catal Sci Technol 2015;5:4154–63. doi:10.1039/C5CY00667H.

[201] Tran NH, Kannangara GSK. Conversion of glycerol to hydrogen rich gas. Chem Soc Rev 2013;42:9454–79. doi:10.1039/c3cs60227c.

[202] Tande LN. Autothermal reforming of bio-oil model compounds. University of Leeds, 2018.

[203] Nahar G, Dupont V, Twigg M V., Dvininov E. Feasibility of hydrogen production from steam reforming of biodiesel (FAME) feedstock on Ni-supported catalysts. Appl Catal

B Environ 2015;168–169:228–42. doi:10.1016/j.apcatb.2014.12.036.

[204] Xing Z, Zhang SUO, Wei L, Ming JIN. 负载 Ni 催化剂上低温甘油蒸汽重整制氢. J Fuel Chem Technol 2015;43:684–91.

[205] Chen H, Ding Y, Cong NT, Dou B, Dupont V, Ghadiri M, et al. A comparative study on hydrogen production from steam-glycerol reforming: Thermodynamics and experimental. Renew Energy 2011;36:779–88. doi:10.1016/j.renene.2010.07.026.

[206] Gilson. Gilson Minipuls3 2003. http://www.gilsonuk.com/minipuls-3.html (accessed September 12, 2018).

[207] Wurm DB, Sun K, Winniford WL. Analysis of low levels of oxygen, carbon monoxide, and carbon dioxide in polyolefin feed streams using a pulsed discharge detector and two PLOT columns. J Chromatogr Sci 2003;41:545–9.

[208] Adhikari S, Fernando S, Haryanto A. A Comparative Thermodynamic and Experimental Analysis on Hydrogen Production by Steam Reforming of Glycerin. Energy Fuels 2007:2306–10.

[209] Omoniyi OA, Dupont V. Chemical looping steam reforming of acetic acid in a packed bed reactor. Appl Catal B Environ 2018;226:258–68. doi:10.1016/j.apcatb.2017.12.027.

[210] Kemp I. Pinch Analysis and Process Integration. 2006. doi:10.1016/B978-0-7506-8260-2.X5001-9.